

Process systems analysis of reversible Solid Oxide Cell (rSOC) reactors for electricity storage and sector coupling

A thesis accepted by the Faculty of Energy-, Process- and Bio-Engineering of the University of Stuttgart in partial fulfillment of the requirements for the degree of Doctor of Engineering Sciences (Dr.-Ing.)

by
Srikanth Santhanam
born in Chennai, India

Main referee: Prof. Dr. rer. nat. K. Andreas Friedrich
Co-referee: Dr. P.V. Aravind

Date of defence 20.11.2018

Institute of Energy Storage
University of Stuttgart

2018



Abstract

The challenges of climate change and global warming necessitates a move towards a renewable energy powered society. Certain critical technical challenges must be overcome for a successful transition to a renewable energy powered society. The renewable energy is intermittent and largely depends on the climate, weather, day, season and the energy demand also varies with time. This requires a need for an energy storage and management system to match the supply and demand. Different technologies and conversion techniques exist for electrical energy storage such as thermal, chemical, electrochemical and mechanical. Chemical energy storage is attractive due to its higher energy storage capacity and storage duration. Additionally, in moving towards a renewable energy powered society, electrical energy becomes the prime mover. Hence, alternate synthesis routes have to be established for industrial chemicals and fuels that are currently produced from fossil fuels. Therefore, by converting electrical energy to chemical form in large scale, solves the issue of energy storage and provides a synthesis route for chemical production. Such systems facilitate coupling electricity storage industry and chemical process industry.

Electrochemical reactor systems can address the above challenges. Particularly noteworthy here are reversible solid oxide cells (rSOC) systems, which can be operated at temperatures above 600 °C in a highly efficient manner in electrolysis or fuel cell mode. The reversible Solid Oxide Cell (rSOC) reactor systems can efficiently operate as an electrolysis system to convert electrical energy to chemical energy during storage mode. This process is known as the Power to Chemicals mode. When electrical energy is required, rSOC systems can operate as a fuel cell system to convert chemical energy back to electrical energy. This operation mode is referred to as Chemicals to Power mode. Within this thesis, it is shown that roundtrip electricity storage efficiencies of 60 % can be reached with currently available reactor technology. Hence, an rSOC reactor system

can form an efficient energy conversion system for energy storage and sector coupling. In this thesis, a process engineering study of an rSOC system for energy storage and sector coupling using a commercially available reactor was performed. The thesis aims to provide a roadmap for attaining a highly efficient rSOC system that is feasible with commercial reactors in the near future. A scientific approach for process system engineering of rSOC system or electrochemical reactor system was developed. The proposed approach was applied for investigating different configurations of rSOC systems for selected applications. The scientific utilises theoretical, experimental and modelling tools in three steps.

In the first step, the fundamentals of thermodynamics and electrochemical reactors were used to identify the target efficiencies and key thermodynamic parameters affecting system performance. The ideal performance was evaluated by assuming an ideal reactor with no electrochemical losses. This represents the theoretical maximum value that can be achieved by an ideal system. Limits to ideal system performance and possible opportunities to increase the theoretical limit such as thermal management were identified. The theoretical limits were determined for H-O (hydrogen-oxygen) and H-C-O (hydrogen-carbon-oxygen) reaction chemistries. It is shown that ideal roundtrip efficiencies are limited to 70 % for both H-O and H-C-O systems at 1 bar. This is increased to around 80 % and 90 % for H-O and H-C-O systems respectively at 30 bar. This limit is due to their reaction thermodynamics. The ideal roundtrip efficiencies can be increased to almost 100 % by storing the heat produced by the reactor during the fuel cell operation to utilise it for the heat required by the reactor during the electrolysis operation. Therefore, thermal management is one of the key requirements to achieve a high system performance and a heat storage based thermal management system is proposed. Next, a commercially available rSOC reactor based on electrolyte supported cell design was experimentally characterised and its performance is mapped in both operation modes. The reactor performance was incorporated to the ideal system. The target efficiencies in the vicinity of 55 % and 60 % at 1 bar and 30 bar respectively, at current density of 2500 A/m^2 were determined for an rSOC system with a thermal management concept using heat storage. This represents the system performance target for a detailed process system which also includes the balance of plant (BoP) components such as pumps, blowers and heat exchangers.

In a second step, based on experimental results, mathematical models for the simulation of the commercially available reactor were developed for detailed process system engineering simulations. A zero dimensional model and a one dimensional model were developed. The zero dimensional is required for detailed process system simulations. Different system architectures are developed and their performance were computed considering the requirements of the rSOC reactor and BoP components. The experimentally validated one dimensional model was used to obtain characteristic reactor temperature and effective losses required for the black box model as well as ensuring the operability of the system. A hydrogen based rSOC system and a methane based rSOC system were developed. The hydrogen based rSOC system was developed purely as electrical energy

storage system. The methane (or hydrocarbon) based system was developed for electrical energy storage and sector coupling purposes. In the final step, system operability was verified using the one dimensional model. For the different system operation points, the detailed reactor model was used to identify critical operation of the reactor which could lead to eventual failure of the reactor. The system operation points were then systematically determined in order to attain feasible operation of the reactor. The second and third steps are an iterative process.

Using second and third step, a hydrogen based rSOC system for electrical storage and methane based rSOC system for electrical storage and sector coupling were investigated. For the hydrogen based rSOC system, a system roundtrip efficiency of 52 % and 53 % at 1 bar and 25 bar respectively can be achieved. System performance at 1 bar is close to the target efficiency defined in step 1 whereas the system efficiency at 25 bar is far from the target efficiency at 25 bar defined in step 1. This deviation for the pressurised system was due to parasitic effect of BoP components. Examination of the methane-based rSOC system showed the same effect of operating pressure on the achievable efficiency. Since electrolysis operation at elevated pressure favours the formation of methane, the pressure operation for use in the sector coupling should still be considered. Hence, for the methane based rSOC system for sector coupling application, a pressurised operation is considered. The methane based rSOC system for sector coupling application achieves a roundtrip efficiency of 53 % at 25 bar. Increased pressure generally allows higher target efficiencies, hence, solutions to minimise the difference between ideal system and detailed process system are demonstrated in this work. This requires an increase in system complexity, for example using gas storage under pressure or large number of heat exchangers, in order to achieve roundtrip efficiency close to target efficiency. For all the systems, the heat storage thermal management is shown to play a crucial role in achieving high system performance using the commercially available and future rSOC reactor.



Zusammenfassung

Die Herausforderungen des Klimawandels und der Erderwärmung zeigen die Notwendigkeit einer Wende hin zu einer mit Erneuerbaren Energien versorgten Gesellschaft auf. Für einen erfolgreichen Übergang müssen konkrete technische Herausforderungen bewältigt werden. Die Verfügbarkeit von erneuerbar bereitgestellter Energie hängt weitgehend von Klima, Wetter, Tages- und Jahreszeit ab. Da auch der Energiebedarf mit der Zeit variiert, entsteht die Notwendigkeit für Energiespeicher- und -managementsysteme, die Angebot und Nachfrage aufeinander abstimmen. Es existiert eine Vielzahl verschiedener Wandlungstechnologien mit denen elektrische Energie thermisch, chemisch, elektrochemisch und mechanisch gespeichert werden kann. Energiespeicherung in chemischer Form ist aufgrund der hohen Energiespeicherkapazität und -daueräußerst attraktiv. Darüber hinaus wird elektrische Energie in einer mit Erneuerbarer Energie versorgten Welt eine zentrale Rolle einnehmen. Es steht eine mögliche Elektrifizierung der Chemischen Industrie an, die alternative Syntheserouten für Chemikalien und Brennstoffe, die derzeit auf fossilem Weg bereitgestellt werden, erfordert. Großskalige Wandlung von elektrischer in chemische Energie löst die Frage der Energiespeicherung und bietet mit der Sektorkopplung neue Synthesewege für die Produktion von Chemikalien und Brennstoffen.

Systeme mit elektrochemischen Reaktoren als Kernkomponente sind in der Lage die genannten Herausforderungen zu bewältigen. Hier sind insbesondere reversible Oxidkeramische Reaktoren (engl.: reversible Solid Oxide Cells, rSOC) zu nennen, die bei Temperaturen über 600 °C hocheffizient im Elektrolyse- oder Brennstoffzellenmodus betrieben werden können. Im Speichermodus wandeln rSOC-Systeme elektrische Energie durch Elektrolyse in chemische Energie. Dieser Prozess wird auch "Power to Fuels" genannt. Wird elektrische Energie benötigt, können rSOC-Systeme im Brennstoffzellenmodus betrieben werden, um chemische zurück in elektrische Energie zu wandeln.

Dieser Betriebsmodus wird auch "Chemicals-to-Power" genannt. In dieser Arbeit wird aufgezeigt, dass schon mit derzeit verfügbarer Technologie eine Stromspeicherung mit Wirkungsgraden von bis zu 60 % erreicht werden kann. Somit können rSOC-Systeme einen signifikanten Beitrag zur Energiespeicherung und Sektorkopplung leisten. In dieser Arbeit wurde eine verfahrenstechnische Untersuchung von rSOC-Systemen zur Energiespeicherung und Sektorkopplung unter Verwendung von kommerziell erhältlichen rSOC-Reaktoren durchgeführt. Ziel der Arbeit ist es, eine Roadmap für hocheffiziente rSOC-Systeme zu entwickeln, die in naher Zukunft mit kommerziell verfügbaren Reaktoren realisierbar sind. Diese wissenschaftliche Aufgabenstellung wurde mit einem systemverfahrenstechnischen Ansatz bearbeitet. Mit den Methoden der Systemverfahrenstechnik werden verschiedene Konfigurationen von rSOC-Systemen für ausgewählte Anwendungen untersucht. Der methodische Ansatz verwendet theoretische, experimentelle und Modellierungswerkzeuge in drei Schritten.

Im ersten Schritt wurden die Grundlagen der Thermodynamik und der elektrochemischen Reaktoren genutzt, um die Zielwirkungsgrade zu bestimmen und die thermodynamischen Schlüsselparameter zu identifizieren, die jene beeinflussen. Ein ideales System ohne elektrochemische Verluste wurde betrachtet. Damit wurden temperatur-, druck- und umsatzabhängige theoretische Maximalwirkungsgrade für H-O- (Wasserstoff-Sauerstoff) und H-C-O-Systeme (Wasserstoff-Kohlenstoff-Sauerstoff) Systeme bestimmt. Möglichkeiten zur Erhöhung dieser theoretischen Grenzen, wie z. B. das Wärmemanagement, wurden identifiziert. Es wurde gezeigt, dass ideale Speicherwirkungsgrade für H-O- und H-C-O-Systeme bei 1 bar auf 70 % begrenzt sind. Eine Erhöhung des Drucks auf 30 bar erhöht die idealen Speicherwirkungsgrade für H-O- bzw. H-C-O-Systeme auf etwa 80 % bzw. 90 %. Diese Grenzen sind auf die Thermodynamik der beteiligten Reaktionen zurückzuführen. Die idealen Wirkungsgrade können jedoch auch nahezu 100 % erreichen. Dazu muss die vom rSOC-Reaktor während des Brennstoffzellenbetriebs erzeugte thermische Energie zwischengespeichert und dem Reaktor im Elektrolysebetrieb zur Verfügung gestellt werden. Wärmespeicherung und -management sind daher Schlüsselvoraussetzungen für hohe Speicherwirkungsgrade. Wärmespeicherungs- und -managementsysteme werden detailliert und dargelegt. Zur Überprüfung der mit realen Komponenten erreichbaren Wirkungsgrade wurde ein kommerziell erhältlicher rSOC-Reaktor mit elektrolytgestützten Zellen experimentell charakterisiert. Der ideale Reaktor wurde mit den so gewonnenen Betriebscharakteristiken parametrisiert und die mit einem solchen Reaktor erreichbaren Speicherwirkungsgrade berechnet. Es können Wirkungsgrade von 55 % und 60 % bei 1 bar bzw. 30 bar bei einer Stromdichte von 2500 A/m^2 für rSOC-Systeme mit Wärmespeicher erreicht werden. Mit diesen maximalen Wirkungsgraden sind die Zielwirkungsgrade für den zweiten Schritt, detaillierte verfahrenstechnische Prozesssimulationen bestimmt, die auch die Balance-of-Plant-Komponenten (BoP) wie Pumpen, Gebläse und Wärmeübertrager umfassen.

Im zweiten Schritt wurden basierend auf experimentellen Ergebnissen mathematische Modelle für die Simulation des kommerziell verfügbaren Reaktors in detaillierten verfahrenstechnischen Prozesssimulationen entwickelt. Ein nulldimensionales Modell

wurde für die detaillierte verfahrenstechnische Prozesssimulation benötigt. Damit können unterschiedliche Systemarchitekturen entwickelt und unter Berücksichtigung der Anforderungen des rSOC-Reaktors sowie der BoP-Komponenten untersucht werden. Ein eindimensionales Reaktormodell wurde entwickelt und experimentell validiert, um die charakteristische Reaktortemperatur und die effektiven Reaktorverluste für das nulldimensionale Modell zu bestimmen. Konkret wurden nun ein wasserstoffbasiertes rSOC-System und ein methanbasiertes rSOC-System für verschiedene Anwendungen entwickelt. Das wasserstoffbasierte rSOC-System dient ausschließlich der Stromspeicherung. Das methanbasierte (bzw. kohlenwasserstoffbasierte) System wurde für die Stromspeicherung und Sektorkopplung entwickelt. Im dritten und letzten Schritt wurde zur Überprüfung der sicheren Betreibbarkeit des rSOC-Reaktors erneut das eindimensionale Modell eingesetzt. Verschiedene Systembetriebspunkte und deren Betriebsparameter wurden dem detaillierten Reaktormodell zugeführt. So konnten für den Reaktor kritische Betriebsbereiche identifiziert werden, die zu einem eventuellen Ausfall führen könnten. Die Systembetriebspunkte wurden dann gezielt geändert, um einen sicheren Betrieb des Reaktors zu ermöglichen. Die Ausführung der Schritte zwei und drei ist hierbei iterativ ausgelegt.

Mit den Schritten zwei und Schritt drei wurden ein wasserstoffbasiertes rSOC-System für die Stromspeicherung und ein methanbasiertes rSOC-System Stromspeicherung und Sektorkopplung entwickelt und untersucht. Für das wasserstoffbasierte rSOC-System können Speicherwirkungsgrade von 52 % bzw. 53 % bei 1 bar bzw. 25 bar erreicht werden. Der bei 1 bar erreichbare Wirkungsgrad liegt nahe am im ersten Schritt definierten Zielwirkungsgrad, während der bei 25 bar erreichbare weit von dem im ersten Schritt definierten Zielwirkungsgrad entfernt ist. Diese Differenz entsteht aufgrund des parasitären Verbrauchs der notwendigen BoP-Komponenten. Die Untersuchung des methanbasierten rSOC-Systems zeigte denselben Effekt des Betriebsdrucks auf den erreichbaren Wirkungsgrad. Da Elektrolysebetrieb bei erhöhtem Druck die Methanentstehung begünstigt, sollte der Druckbetrieb zur Anwendung in der Sektorkopplung dennoch in Betracht gezogen werden. Das methanbasierte rSOC-System kann bei 25 bar einen Wirkungsgrad von 53 % erreichen. Da erhöhter Druck generell höhere Zielwirkungsgrade zulässt, werden Lösungen zur Minimierung der Differenz zwischen idealem System und detailliertem verfahrenstechnischem System in der Arbeit aufgezeigt. Dies beinhaltet eine Erhöhung der Systemkomplexität u.a. durch Gasspeicherung unter Betriebsdruck und eine größere Anzahl von Wärmeübertragern. Es wird aufgezeigt, dass für alle Systeme, seien sie mit kommerziell oder zukünftig verfügbaren rSOC-Reaktoren ausgestattet, die systemintegrierte Speicherung von thermischer Energie und eine entscheidende Rolle für hohe Speicherwirkungsgrade spielt.



Dedication and acknowledgements

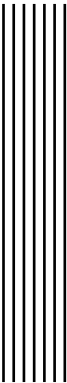
I would like to thank Prof. K. Andreas Friedrich for providing me with the opportunity to pursue my research interest with Electrochemical Energy Technology department within the Institute of Engineering Thermodynamics at DLR, Stuttgart. It is my duty to acknowledge the important role of Prof Friedrich. The research performed within the scope of this thesis is based on a simple idea I proposed to Prof Friedrich. I would like to specially thank him for affording me the patience and time to develop concrete research proposal. It is significant in a day and age where time is a luxury. Finally, I would like to extend my gratitude to him for agreeing to be my Doctor Father and supervise me in pursuit of my Doctorate.

Next, I would like express my sincere gratitude to Dr. Marc P. Heddrich. Marc, was my 2nd supervisor, who assisted me and guided me during my thesis on a day to day basis. He has been crucial in my career development as a scientist. By working with him closely, I learnt the intricacies of scientific approach to process engineering. He helped me to become a better scientist and process engineer. Apart from the professional aspect, he assisted in my personal development during the last 3.5 years and helped me through difficult times during my PhD. Once more, I would like to express my sincere gratitude to Dr. Marc P. Heddrich.

Next, I would like to thank my teammates; Marc Riedel, Christian Schengelberger, Dr. Moritz Henke, Mike Steilen and Marius Tomberg for the fruitful discussions and constructive criticisms. I wish to specially thank Marc Riedel for providing me with high quality experimental results which were crucial for the success of this work. I would also like to thank my students Pegah Mottaghizadeh and Sanchit Gupta for their high quality work and contribution to this research.

Finally, the thesis would not have been possible without the support of my family. I wish to express my sincere gratitude for their unwavering support and positivity. They have been crucial in this pursuit and in achieving my goal.

Don't be too proud of the technological terror that you have created, the ability (Technology) to destroy a planet is insignificant next to the power of the force (Nature)



Author's declaration

I declare that the work in this dissertation was carried out in accordance with the requirements of the University's Regulations and Code of Practice for Research Degree Programmes and that it has not been submitted for any other academic award. Except where indicated by specific reference in the text, the work is the candidate's own work. Work done in collaboration with, or with the assistance of, others, is indicated as such. Any views expressed in the dissertation are those of the author.

SIGNED: DATE:

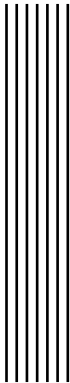


Table of Contents

	Page
List of Tables	xvii
List of Figures	xix
List of Symbols	xxiii
List of Acronyms	xxix
1 Introduction	1
1.1 Energy storage and sector coupling	1
1.2 Vision	2
1.3 Thesis structure	4
2 Scientific motivation	7
2.1 Current state of the art	7
2.2 Scientific gap	9
2.3 Motivation	10
2.4 Scientific approach	12
3 Thermodynamics of electrochemical reactors	15
3.1 Thermodynamics of SOC electrochemical reactor	15
3.1.1 Introduction to SOC electrochemical reactors	16

TABLE OF CONTENTS

3.1.2	Ideal work and Ideal voltage of SOC reactor	19
3.1.3	Lost work in electrochemical reactor	26
3.2	Thermodynamics of rSOC systems	27
3.2.1	rSOC system concepts	27
3.2.2	rSOC systems based on H-O chemistry	33
3.2.3	rSOC systems based on H-C-O chemistry	38
3.3	Results and discussion	43
4	Analysis of commercial rSOC reactors and roundtrip efficiency	47
4.1	rSOC electrochemical reactors	47
4.1.1	Functional Layers and Materials	48
4.1.2	Electrochemical loss mechanisms	50
4.1.3	Current State of the Art	53
4.2	Experimental study of commercial rSOC reactor	54
4.2.1	Experimental methods	54
4.2.2	rSOC reactor experimental analysis	57
4.2.3	Analysis of experimental results	58
4.2.4	Phenomenological ASR model	66
4.3	rSOC system round trip efficiency using commercial rSOC reactor	67
4.3.1	System description	68
4.3.2	Results and Discussion	70
4.4	Summary	74
4.4.1	Commerical rSOC reactor performance	75
4.4.2	rSOC system performance using commercial reactor	75
5	SOC reactor modeling	77
5.1	Literature Review	77
5.2	1-D rSOC model	79
5.2.1	Modelling paradigm, assumptions and subsystems	79
5.2.2	Fuel and air chamber	81
5.2.3	Membrane-Electode-Assembly	85
5.2.4	Interconnects	89
5.2.5	Modelica implementation	89
5.2.6	Results and experimental validation	91
5.2.7	Error discussion and uncertainties	96
5.3	0-D model for process system analysis	97

5.3.1	Thermodynamic model	98
5.3.2	Electrochemical model	98
5.3.3	Aspen implementation	100
5.4	Summary	101
6	Process system analysis	103
6.1	rSOC process system description	104
6.1.1	Process system assumptions	104
6.1.2	Thermal energy storage	105
6.1.3	Downstream processes	108
6.1.4	Balance of plant components and heat recovery unit	108
6.1.5	Perfomance indicators	109
6.2	Closed system architecture for electricity storage	111
6.2.1	Model descripton	111
6.2.2	Results and discussion	115
6.3	Hydrocarbon based rSOC system for sector coupling	127
6.3.1	Model descripton	128
6.3.2	Results and discussion	135
6.4	Summary	143
7	Conlusion and future work	147
7.1	Future work	151
	Bibliography	155
A	Appendix A: Thermodynamic fundamentals	181
A.1	Thermodynamic fundamentals for chemical process systems	181
A.1.1	Laws of thermodynamics	182
A.1.2	Thermodynamic functions	186
A.2	Exergy Analysis in chemical reaction systems	191
A.2.1	Exergy Analysis	192
A.2.2	Maximum work and lost work in chemical processes	195
B	Appendix B: Gas Diffusion model	199
B.1	Gas diffusion model	199
B.1.1	Effective diffusion coefficients	201

TABLE OF CONTENTS

C	Appendix C: Aspen implementation of 0-D model	203
C.1	SOFC operation mode	203
C.2	SOEC operation mode	204
D	Appendix D: Hydrogen based closed architecture rSOC system - performance and thermodynamic stream data	209
D.1	Detailed process flow diagram	209
D.2	Performance data	212
D.3	Thermodynamic stream data for non-pressurised hydrogen based closed system	212
D.4	Thermodynamic stream data for pressurised hydrogen based closed system	223
E	Appendix E: Methane based gas grid connected rSOC system- performance and thermodynamic stream data	235
E.1	Detailed process flow diagram	235
E.2	Performance data	238
E.3	Thermodynamic stream data for gas grid connected methane based open system	238
E.4	Thermodynamic stream data for gas grid connected methane based open system at 1500 A/m ²	249



List of Tables

TABLE	Page
2.1 Technology readiness level of SOC cells, reactors and systems	9
5.1 Convective heat transfer coefficients for SOC reactor	85
5.2 Commercial rSOC reactor properties	91
5.3 Input parameters to 1-D model for rSOC reactor	92
5.4 Fitting parameters for rSOC stack 1-D model	93
6.1 Summary of suitable PCM for rSOC latent heat storage	107
6.2 Input parameters for BoP components and heat exchanger units	109
6.3 Operation parameters for hydrogen based rSOC system at 1 bar	115
6.4 System performance of hydrogen based closed architecture rSOC system at 1 bar	117
6.5 System performance for hydrogen based rSOC system at 25 bar	122
6.6 Operation parameters for methane based gas grid connected rSOC system at 25 bar	134
6.7 System performance of methane based gas grid connected rSOC system . . .	135
6.8 Gas composition of rSOC product streams during SOFC operation	137
6.9 Gas composition of rSOC product streams during SOEC operation	141
7.1 Summarised conclusion of system architectures	152
B.1 Binary coefficients of gases at reference condition	201

LIST OF TABLES

C.1	Aspen Component list in SOFC mode	204
C.2	Aspen Component list in SOEC mode	206
D.1	System performance of hydrogen based closed architecture rSOC system at 1 bar	212
D.2	Thermodynamic stream data for closed hydrogen based system at 1 bar	213
D.3	Gas compositions of streams for closed hydrogen based system at 1 bar	218
D.4	Thermodynamic stream data for closed hydrogen based system at 25 bar	224
D.5	Gas compositions of streams for closed hydrogen based system at 25 bar	229
E.1	System performance of methane based gas grid connected rSOC system	238
E.2	Thermodynamic stream data for gas grid connected methane based system at 2500 A/m ²	239
E.3	Gas compositions of streams for gas grid connected methane based system at 2500 A/m ²	244
E.4	Thermodynamic stream data for gas grid connected methane based system at 1500 A/m ²	250
E.5	Gas compositions of streams for gas grid connected methane based system at 1500 A/m ²	255



List of Figures

FIGURE	Page
1.1 Future energy network based on rSOC electrochemical reactor	3
3.1 SOC reactor process	17
3.2 Thermodynamic description of electrochemical reactor system	20
3.3 A simple rSOC system concept	28
3.4 A simple rSOC system concept with heat storage integration for thermal management	32
3.5 Thermodynamics of an H ₂ -H ₂ O system	34
3.6 Theoretical limit of roundtrip efficiency of H-O system with no heat storage .	35
3.7 Theoretical limit of roundtrip efficiency for H-O system with heat storage . .	36
3.8 Theoretical limit of heat ratio for H-O system system with heat storage . . .	37
3.9 Roundtrip efficiency for an H-C-O system versus temperature with no heat storage.	40
3.10 Methane composition at the out of rSOC reactor in SOEC	42
3.11 Summary of ideal roundtrip efficiency of different rSOC system concepts . . .	44
4.1 Electrolyte materials for intermediate temperature SOC.	49
4.2 Electrochemical loss mechanism in an SOC reactor	51
4.3 Schematic diagram of commercial SOC reactor	54
4.4 Schematic layout of experimental facility.	57
4.5 U(i) characterisation curves of rSOC reactor in SOFC mode	59

LIST OF FIGURES

4.6	Variation of ASR with characteristic reactor temperature	60
4.7	Impact of pressure on rSOC reactor measurements in SOFC mode	62
4.8	Variation of polarisation losses due to pressure at reactant conversion of 55 %	63
4.9	Variation of polarisation losses due to pressure at reactant conversion of 85 %	64
4.10	Variation of polarisation losses due to reactant conversion	65
4.11	Phenomenological ASR model comparison with experimental results	67
4.12	U(i) characteristic curve measured compared with the model calculations . .	68
4.13	Comparison of roundtrip efficiency of commercial rSOC reactor versus Ideal rSOC reactor system	70
4.14	Heat ratio of rSOC system with heat storage with commercial rSOC reactor .	71
4.15	Impact of temperature difference on roundtrip efficiency of rSOC system with heat storage	72
4.16	Impact of temperature difference on heat ratio of rSOC system with heat storage	73
4.17	Impact of current density on roundtrip efficiency of rSOC system with heat storage	74
4.18	Summary of roundtrip efficiencies of rSOC system	75
5.1	Schematic of single repeat unit of SOC reactor	80
5.2	Implementation of 1-D rSOC model in Modelica	90
5.3	Model validation of 1-D model with steady state SOFC measurements	93
5.4	1-D model validation with SOFC dynamic measurements.	94
5.5	Model validation of 1-D model with dynamic SOEC measurements	96
5.6	0D SOC model algorithm	101
6.1	Simplified process flow diagram of an hydrogen based closed rSOC system architecture	112
6.2	Sankey diagram of energy flows in hydrogen based closed architecture rSOC system at 1 bar	116
6.3	Variation of temperature, ideal voltage and losses in SRU for H ₂ based system at 1 bar	119
6.4	Sankey diagram of energy flows in hydrogen based closed architecture rSOC system at 25 bar	121
6.5	Variation of temperature, ideal voltage and losses in SRU for H ₂ based system at 25 bar	124
6.6	Efficiency of hydrogen based closed rSOC system architecture	126

6.7	Heat ratio of hydrogen based closed rSOC system architecture	127
6.8	Process flow diagram of a methane based gas grid connected rSOC system architecture	129
6.9	Sankey diagram of energy flows in methane based gas grid connected rSOC system at 25 bar	136
6.10	Variation of temperature, ideal voltage and losses in SRU for methane based gas grid connected rSOC system at 25 bar	138
6.11	Efficiency of the methane based gas grid connected rSOC system at different current densities	142
6.12	Heat ratio of methane based gas grid connected rSOC system architecture .	143
6.13	Summary of achievable roundtrip efficiency of the different rSOC system architecture	144
6.14	Summary of ζ of different rSOC system architecture	146
A.1	Schematic representation of a open thermodynamic system	193
C.1	SOFC sub model of 0-D rSOC model	205
C.2	SOEC sub model of 0-D rSOC model	207
D.1	Extended process flow diagram of hydrogen based closed grid system in SOFC mode.	210
D.2	Extended process flow diagram of hydrogen based closed grid system in SOEC mode.	211
E.1	Extended process flow diagram of methane based gas grid connected system in SOFC mode.	236
E.2	Extended process flow diagram of methane based gas grid connected system in SOEC mode.	237



List of Symbols

Latin Letters

Symbol	Description	Unit
A	Effective area of reactor or catalyst	m^2
ASR_{Ω}	Ohmic component of ASR	$\Omega \text{ m}^2$
ASR	Area specific resistance of the reactor	$\Omega \text{ m}^2$
b	Width of the reactor	m
c	Specific heat capacity	$\text{J}/(\text{kg K})$
c_p	Specific heat capacity of component at constant pressure	$\text{J}/(\text{kg K})$
E	Energy	J
e	Specific internal energy	J/mol or J/kg
E_{act}	Activation energy	J/mol
Ex	Exergy	J
ex	specific exergy	J/kg or J/mol
F	Faradays constant = 96484 C/mol	C/mol
G	Gibbs function of thermodynamic system	J
g	Specific Gibbs function of thermodynamic system	J/mol or J/kg
H	Enthalpy	J
h	Specific enthalpy	J/mol or J/kg

LIST OF SYMBOLS

Symbol	Description	Unit
j	Current density of SOC reactor	A/m ²
j_0	Exchange current density of the electrode	A/m ²
k^-	Velocity of reverse direction of a reaction	mol/(s m ² bar)
k^+	Velocity of forward direction of a reaction	mol/(s m ² bar)
l	Length of the reactor	m
\dot{m}	mass flow rate of matter	kg/s
M	Molecular weight	kg/mol
\dot{n}	molar of flow rate	mol/s
p	Pressure	Pa or bar
Q	Heat	J
R	Universal gas constant	J/mol K
r	Rate of reaction j	mol/m ² s
S	Entropy	J/K
s	Specific entropy	J/(kg K) or J/(mol K)
T	Temperature	K
t	Time	s
U	Internal Energy	J
U	Voltage	V
V	Volume	m ³
\dot{W}	Work rate or Power	W
W	Work	J
x	Mole fraction of a substance in gas mixture	1
Z	Height of the flow channel	m
z	electron valence of charge carrier	

Greek Letters

Symbol	Description	Unit
α	Convective heat transfer coefficient	W/(m ² K)
β	Symmetry factor of the electrode reactions	
χ	Conversion ratio or Utilisation of reactant in a reaction	
Δ	Operator representing a change in quantity	
δ	Thickness of function layers	m

Symbol	Description	Unit
ϵ	Specific emissivity of a material or medium	
η_{RT}	Roundtrip efficiency defined as ratio of energy produced in SOFC mode to energy consumed in SOEC mode	1
γ	Pre exponential or frequency factor of the electrode	A/m^2
κ	Equilibrium constant of a reaction	
λ	Thermal conductivity of functional layer	$W/(m K)$
μ	Chemical potential	J/mol or J/kg
ξ	Extent of reaction	mol/s or mol
ν	Stoichiometric coefficient of chemical species in a reaction	
Φ	Represents the value of electric power or heat normalised by dividing by the chemical power	1
Π	Entropy generation due to irreversibility in processes	J/K
ρ	Density of functional layer	kg/m^3
σ	Conductivity of functional layers	S/m
σ_{\circ}	Conductivity of functional layers at reference condition	S/m
θ	Heat ratio defined as the heat required in SOEC mode by heat produced in SOFC mode	1
ν	Dynamic viscosity of the gas flow	$kg m/s^2$

Superscripts

Symbol	Description	Unit
a	Air side	
\circ	Indicates a quantity at standard conditions ie $p = 1.10135 \cdot 10^5 Pa$ and temperature of 25 °C	
f	Fuel side	
hs	Denotes heat storage medium	

LIST OF SYMBOLS

Symbol	Description	Unit
$'$	Denotes a quantity entering control volume	
ic	Interconnect	
mea	Membrane electrolyte electrode assembly	
$''$	Denotes a quantity leaving control volume	
TPB	Triple phase boundary	

Subscripts

Symbol	Description	Unit
a	Air side	
ae	Air electrode	
C	Indicates carbon atom	
$conv$	Convection heat transfer	
cv	control volume	
hor	Electrochemical hydrogen oxidation reaction	
$cond$	Conductive heat transfer	
$cond$	Interconnect	
e^-	Indicates electrons	
ec	Indicates electrolysis mode	
f	Fuel side	
fc	Indicates fuel cell mode	
fe	Fuel electrode	
hs	Heat storage	
j	Reaction index in a system of n chemical reactions	
KE	Kinetic Energy	
mea	Membrane electrolyte electrode assembly	
H	Indicates hydrogen atom	
O	Indicates oxygen atom	
PE	Potential Energy	
ref	Reference condition	
rxn	Reaction	
rad	Radiative heat transfer	
rev	Reversible or ideal condition	

Symbol	Description	Unit
<i>se</i>	Solid electrolyte	
<i>smr</i>	Reverse steam methane reform reaction	
<i>soc</i>	rSOC reactor	
<i>sys</i>	system	
<i>wgs</i>	Reverse water gas shift reaction	



List of Acronyms

- ASC - Anode Supported Cell
- ASR - Area Specific Resistance
- BoP - Balance of Plant
- CAES - Compressed air energy storage
- CGO - Ceria doped Gadolinium
- CSTR - Continuously Stirred Tank Reactor
- EES - Electrical Energy Storage
- EIS - Electrochemical Impedance Spectroscopy
- EOO - Equation based object oriented
- ESC - Electrolyte Supported Cell
- GDC - Gadolinium doped ceria
- HHV - Higher Heating Value
- LHV - Lower Heating Value
- LSCF - Lanthanum strontium cobalt ferrate
- OCV - Open Circuit Voltage

LIST OF ACRONYMS

- PCM - Phase Change Materials
- PFR - Plug Flow Reactor
- PtG - Power to Gas
- PtL - Power to Liquid
- PtX - Power to Chemicals
- PtP - Power to Power
- MEA - Membrane Electrode Assembly
- MIEC - Mixed Ionic Electronic Conductivity
- rSOC - reversible Solid Oxide Cell
- SOC - Solid Oxide Cell
- SOFC - Solid Oxide Fuel Cell
- SOEC - Solid Oxide Electrolysis Cell
- SRU - Single Repeating Unit
- STCR - Steam to Carbon Ratio
- TRL - Technology Readiness Level
- XtP - Chemical/Fuel to Power
- YSZ - Yttria Stabilised Zirconia



1 Introduction

In this chapter, a brief introduction to the research topic is provided. The societal driving forces behind the research topic are addressed in section 1.1. A vision of the future energy system landscape using the reversible Solid Oxide Cell (rSOC) technology is rendered in section 1.2. An overview of the thesis structure is provided in section 1.3.

1.1 Energy storage and sector coupling

Efficient and effective energy storage and management systems are required for a successful transition to a renewable energy powered society. Higher penetration of renewable energy sources in the energy mix raises new challenges. The renewable energy sources such as wind and solar are intermittent in nature. Their production varies with time and natural conditions. On the other hand, the energy demand for a society is also time varying. Hence, energy management and storage systems are required to ensure a stable electrical energy grid and continuous supply to meet the demand [1–4]. Electrical energy can be stored in the form of mechanical energy, thermal energy and chemical energy. Different technologies for storing electrical energy in one of these forms either exist or are being developed. Examples of these concepts are pumped hydro storage (mechanical), compressed air energy storage (mechanical), batteries (electrochemical), pump heat storage (thermal) etc. An overview of these concepts highlighting their

advantages and disadvantages can be found in the literature [5–8]. Storing electrical energy in form of chemical energy is very attractive and beneficial due to high storage capacity [8–10]. In this concept, during energy storage mode, the electrical energy is converted to chemical energy form. This is commonly referred to as Power to Gas (PtG) or Power to Liquid (PtL) process or also batteries (batteries are chemical energy in solid form). When required the chemical fuel can then be converted back to electrical energy and is referred to as the Chemical/Fuel to Power (XtP) process. The Power to Chemicals (PtX) process is enabled by technologies such as electrolysis. The XtP process can be achieved using fuel cells, gas turbines, conventional power plants etc. Additionally, by moving towards a decarbonised society driven by renewable energy where electrical energy becomes a prime mover, new pathways are needed to produce essential chemical energy and important industrial chemicals [10, 11]. Hydrogen, methane, syngas (CO , H_2), methanol and ammonia are proposed as possible candidates. These chemicals are of high industrial value. Hydrogen, methane and reformed syngas are major commodity chemicals for various chemical synthesis. Hence, this provides an opportunity to couple energy storage industry with chemical synthesis industry sector.

1.2 Vision

An rSOC electrochemical reactor system can address the challenges raised in section 1.1. Fuel cell systems and electrolysis systems in combination can form an effective energy storage system [12–14]. A Solid Oxide Cell (SOC) reactor can operate as both fuel cell and electrolysis cell. This bidirectional functionality of an SOC reactor enables us to have a unitised reactor and system for energy storage and sector coupling. A schematic of a future energy network based on rSOC reactors is rendered in the Figure 1.1.

During the energy storage mode electricity is converted to fuel such as hydrogen or hydrocarbons (PtX) through electrolysis and during discharge mode the fuel can be used to produce power (XtP) via fuel cell operation. An SOC reactor can efficiently operate in PtX mode as an electrolysis cell and in XtP mode as a fuel cell. They have the potential to show significantly lower electrochemical losses than any other fuel cell/electrolysis technology [15–18]. When the electrical energy supply from the renewable energy sources is higher than the demand, the system operates as a PtX system. The rSOC reactor operates in the Solid Oxide Electrolysis Cell (SOEC) mode. Water (and carbon dioxide) is reduced to hydrogen (and carbon monoxide). The electrical energy is supplied to the

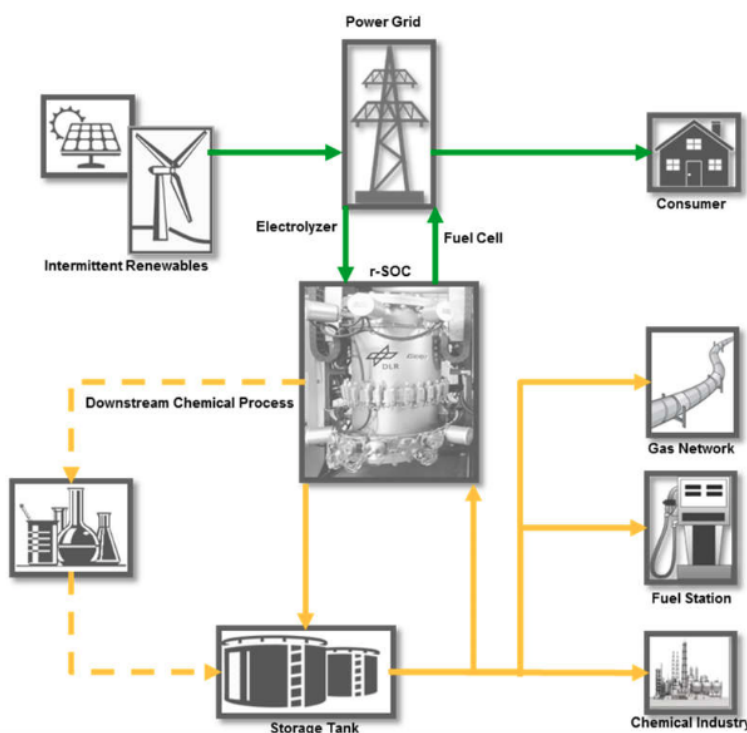


FIGURE 1.1. Future energy network based on rSOC electrochemical reactor.

rSOC reactor in SOEC mode to promote the electrolysis reaction. Thereby the electrical energy is stored as chemical energy in hydrogen and carbon monoxide. The hydrogen or syngas produced during the SOEC process can be processed to higher hydrocarbons by appropriate downstream processes. When the energy demand is greater than renewable energy production, the system shifts to XtP mode. The rSOC reactor operates in the Solid Oxide Fuel Cell (SOFC) mode. Hydrogen, hydrocarbons (methane, methanol etc.) and syngas are supplied to the system as fuels. Electrical energy is produced by the reactor which is fed to the electrical energy grid.

Two broad system architectures can be established depending on its interactions with other industries. The rSOC system can be a *closed boundary system* or an *open boundary system*. In a *closed boundary system*, the rSOC system does not interact with other industries and acts purely as an energy storage system. The chemical energy is not transferred across its boundaries. The fuel produced during the SOEC process is stored in fuel tanks. Likewise, the product gases from the SOFC, which are the reactants for the SOEC process is stored in exhaust gas tanks. The closed boundary rSOC system

can be based on the reaction chemistry of either H – O elements or H – C – O elements. In an *open boundary system*, the chemical energy is exchanged across its boundaries. The fuel or chemical produced during the SOEC process is not necessarily stored within the system boundaries but also supplied to other process industries. The rSOC system interacts with other chemical industries, hydrogen refuelling infrastructure etc. The hydrogen or syngas produced during the SOEC operation can be supplied to chemical industries as feedstocks or converted to industrial chemicals such as ethylene and ammonia in appropriate downstream process. During the SOFC process, the fuel can be obtained from external sources such as natural gas grid, hydrocarbons from chemical industries, ammonia etc. Therefore an *open boundary system* acts as an energy storage system and couples energy storage industry with other process industries.

To summarise, the following points act as societal drivers for research and development of an rSOC process system for energy storage and sector coupling.

1. Higher energy storage capacity in form of chemical energy.
2. Ability to integrate energy storage industry with other process industries.
3. Reduced capital cost of having one system for both PtX and XtP process.

1.3 Thesis structure

The thesis is divided into 7 major chapters followed by an appendix section. The contents are divided in a structured manner for easy understanding. Each chapter briefly introduces the scientific concepts pertaining to the chapter followed by the results and discussion section. A brief overview of the chapters is given below.

Chapter 1 A brief introduction and societal drivers behind the research topic are provided in this section.

Chapter 2 The state of the art of the technology is described. The scientific gap is addressed and accordingly the scientific motivation for the thesis is ascertained. Research questions that are answered by the thesis are listed. The scientific approach undertaken to answer the questions is highlighted.

Chapter 3 The thermodynamic fundamentals and theory of electrochemical reactors is reviewed. Thermodynamic limits to roundtrip efficiencies for different rSOC concepts are discussed.

Chapter 4 A commercial rSOC reactor is analysed. Target system performance of an rSOC system based on a commercial reactor are evaluated.

Chapter 5 Development of a one dimensional and zero dimensional rSOC reactor is addressed. The reactor models are used for process system development and analysis.

Chapter 6 Process analyses of different rSOC system architectures are performed. Closed boundary and open boundary rSOC systems are analysed and performance quantified.

Chapter 7 The final conclusions of the thesis is presented here. The key results of the research are summarised. The chapter is concluded with a list of follow up research activities to continue the research presented in this thesis.



2

Scientific motivation

The scientific motivation behind the thesis is discussed in this chapter. The current state of the art of the rSOC technology is listed in the section 2.1. A brief overview of the scientific research in the field of SOC reactors and the gap in scientific research is addressed in section 2.2. The section on scientific gap lays the foundation for the scientific motivation behind the thesis which is presented in the section 2.3. In this section, the research questions that would be answered by the thesis are raised. Finally, the scientific approach undertaken to answer the research questions is detailed in the section 2.4.

2.1 Current state of the art

SOC are a type of electrochemical reactors which can convert chemical energy directly to electrical energy and vice versa. They consist of a solid ceramic electrolyte membrane, an anode and cathode electrodes. The electrode-electrolyte-electrode assembly separates two chambers commonly referred to as the fuel chamber and air chamber. In the fuel chamber, fuel is supplied and air/oxygen is supplied to the air chamber. The electrolyte allows transport of oxygen ions only and electrons are transported via external circuit. By this transport mechanism, electrochemical reactions are made possible. When chemical energy is converted to electrical energy, the process is called as the fuel cell process. For an SOC electrochemical reactor producing electrical energy is called as the SOFC.

When electrical energy is converted to chemical energy form, the process is referred to as electrolysis process and the reactor is referred to as SOEC.

The commercial development of SOC reactor has been taking place since the early 1990s. Initially, SOC reactors were predominantly developed for SOFC operation. They are optimised for either SOFC or SOEC operation mode. SOC reactors based on the Electrolyte Supported Cell (ESC) and Fuel Electrode Supported cells commonly referred to as Anode Supported Cell (ASC) designs have been developed for both the SOFC and the SOEC operation. The SOC reactors are designed to be modular. It is composed of many singular units commonly referred to as SOC single cells or a Single Repeating Unit (SRU). The SOC single cells are used in the laboratory for research and development purposes for the optimisation of the cell materials, manufacturing, design etc. One SRU does not have sufficient power capacity to meet the commercial demands. Hence, they are stacked together to form a SOC reactor for the required power capacity. SOC reactors can further be combined together to form a SOC reactor module. The SOC reactor modules are generally in the power range of 25 kW electric to 250 kW electric. The SOC reactors or the SOC reactor modules, based on the applications, are combined with the necessary Balance of Plant (BoP) components to build either a SOFC or SOEC system.

The development of SOC reactors optimised for SOFC operation is further ahead in comparison to SOC reactors for SOEC operation. The SOFC reactors are commercially available with suppliers available in the US (Bloom Energy [19], FuelCell Energy [20]), Europe (SolidPower [21], sunfire [22], Convion [23], elcogen [24] etc.) and in Asia (Kyocera [25], Aisin [26], Mitsubishi [27, 28] etc). Now, the SOFC reactor modules in power ranges of 30 kW - 250 kW are available commercially. The commercial availability of the SOC reactors for SOEC operation is lower than for SOFC operation. The SOC cells, SOC reactors and SOC systems are at different stages of Technology Readiness Level (TRL). The TRL of SOC cells, SOC reactors and systems are given in the Table 2.1

The development of rSOC reactors for bidirectional operation in both SOFC and SOEC is in the early stages. Research and development activities are being performed to optimise the materials for bidirectional operation of the rSOC reactor [29, 30]. At the time of writing this PhD thesis, there is only one commercially available rSOC reactor available in the market. The commercial rSOC reactor is based on the planar ESC stack design [22]. A prototype rSOC system based on H_2/H_2O reaction was built

TABLE 2.1. Technology readiness level of SOC cells, reactors and systems in 2017

Technology	TRL	Description
SOC cells	2-8	Research and development of next generation cells to commercially available cells
SOFC reactors	8-9	Commercially available
SOEC reactors	6-8	Prototype demonstration to commercial viability.
rSOC reactors	3-6	Research phase and early demonstration stage
SOFC systems	4-9	Demonstration of large systems and commercially available combined heat and power units
SOEC systems	4-6	Demonstration and prototype stage
rSOC systems	2-4	Research and early demonstration stage.

and demonstrated by Boeing and sunfire. The system achieved a roundtrip efficiency of 30 % [31].

2.2 Scientific gap

The scientific work performed in the field of SOC electrochemical reactor systems is by far dominated by SOFC systems. Tremendous knowledge has been produced in the field of SOFC systems ranging from dynamic operation [32–43], system optimisation [44–52] and SOFC hybrid and integrated systems [53–64]. Process engineering research is also proceeding at a rapid pace for SOEC systems. The quantity of scientific content produced is still lower when compared to SOFC systems. Steady state process system analysis for SOEC systems have been reported in literature. The studies were performed in the context of PtX where 'X' can be either a gas (such as hydrogen, methane etc.) or liquid (such as methanol, dimethyl ether, Fischer-Tropsch liquid etc.) [65–73]. Few of the studies focussed on developing SOEC systems with endothermic operation of the SOEC reactor with nuclear or solar thermal as high temperature heat source [73–76]. In the reported literature, the process systems were developed and optimised for either an SOEC or an SOFC process.

The SOC reactor can operate in both SOEC and SOFC mode. The rSOC systems are still in early research phase. Research activities are largely focussed on materials, cells and optimisation of rSOC reactor for bidirectional operation. theoretical studies have

been performed on rSOC system. The integration of the rSOC model to the AC power network was initially investigated by Roscoe et al. [77]. A hydrogen based storage system for varying renewable energy supply pattern was studied by Kasai et al. [78]. More recently, Wendel et al. [79] and Monti et al. [80] presented a conceptual rSOC system based on carbonaceous reactions. In the reported literatures, the rSOC systems were considered mainly as energy storage systems but not for sector coupling.

Analysing over 200 SOC system journal publications, close to 80 % of the publications were related to the SOFC systems. Around 15 % of the publications dealt with SOEC systems. Finally, close to 5 % were related to rSOC system studies. To achieve the industrialisation of rSOC system for energy storage and sector coupling, a significant scientific gap should be filled .

2.3 Motivation

The primary motivation for the current research is to bridge the scientific gap identified in the section 2.2. In order to achieve an efficient system, several technical challenges have to be met. An SOC reactor can efficiently operate in PtX mode as an electrolysis cell and in XtP mode as a fuel cell. Thermal management is essential for a highly efficient rSOC system. In the fuel cell mode, the r-SOC reactor is highly exothermic whereas in electrolysis mode it can range from highly endothermic over thermoneutral to highly exothermic operation depending on current density. Endothermically operating the rSOC reactor during the SOEC process can result in improved efficiency. Several options for heat management have been proposed to fulfil the requirement of thermally self-sustained operation including exothermic fuel cell mode and possible highly endothermic electrolysis. Bierschenk et al. showed that by coupling an exothermic chemical reaction such as methanation with endothermic electrolysis reaction within the SOC reactor a thermal balance can be achieved [81]. By this method, a thermoneutral or even exothermic operation of SOC reactor in electrolysis mode can be achieved at otherwise same conditions. The same strategy for thermal management was adopted in literature to achieve a self sustaining rSOC system [82–84]. The method proposed raises considerable engineering challenges. Thermodynamically, the exothermic methanation reaction require a combination of lower reaction temperatures in range of 400 °C - 650 °C and/or higher pressures up to 30 bar [85]. Hence, this requires development of SOC reactors with low electrochemical losses at those reaction temperatures capable of operating at

high pressures. Low and intermediate temperature rSOC reactors are in early stages of research and development phase and far from commercialisation. Meanwhile, the commercially available SOC reactors are based on ESC or ASC design and operate at temperatures of 700 °C - 900 °C [26]. The research aims to develop an rSOC system with a feasible thermal management system based on a commercially available rSOC reactor for energy storage and sector coupling.

The secondary motivation of the research relates to the scientific method adopted for process system analysis of SOC electrochemical reactor systems. Typically, a black box approach is used for the SOC reactor model for the system analysis. This can lead to erroneous results and unrealistic operation conditions which can be detrimental to reactor lifetime. Additionally, reactor performances based on single cells experimental results are utilised to predict the system behaviour. Unfortunately, the single cell reactor performances cannot be translated to a SOC stack module performances. This leads to overestimation of system performance. Hence, the secondary motivation of the research is to propose a scientific approach for process system analysis of SOC reactor systems. The approach is adopted for the development and analysis of the rSOC system.

Research question

The motivation can be summarised by the following scientific questions which would be addressed within this thesis.

1. What are the feasible roundtrip efficiencies of an rSOC system based on a commercially available reactor for energy storage and sector coupling?
2. How far is the achieved system performance from the theoretical performance limit? What are the major factors limiting the system performance?
3. How significant is the thermal management system in realising an efficient rSOC system?
4. How can a thermal management system be implemented for the rSOC system using a commercial rSOC reactor?
5. What are the impacts of BoP components on the system performance and system architecture?

6. What is the promising architecture to achieve an efficient rSOC system for energy storage and sector coupling?
7. How can the rSOC reactor model for process system analysis be improved while maintaining the simplicity required for a process system analysis?
8. How can we ensure the system operation point is within the safe operation region of the reactor?

2.4 Scientific approach

To answer the above research questions, a three step scientific approach was adopted. The scientific approach encompasses the different aspects of process engineering in order to arrive at a realisable rSOC system. Theoretical, experimental and modelling tools were utilised with this study.

In the first step, the target efficiencies and key thermodynamic state parameters affecting the system performance were identified. The target efficiencies were set out considering the fundamentals of thermodynamics and electrochemical reactors. An ideal performance was illustrated by assuming an ideal reactor with no electrochemical losses. The ideal performances and efficiencies represent the theoretical maximum value that can be achieved by an ideal system. The ideal performances and efficiencies were evaluated for different reaction chemistries. Thermodynamic reasoning for a thermal management system will be highlighted. A commercially available electrochemical reactor was experimentally characterised and its performance was quantified. The reactor performance was then fed to the ideal system model to determine the maximum efficiency that can be achieved with the given reactor. This is purely dependent on the reactor performance. It represents the system performance target that the process engineering should aim for. The difference between the ideal performance, dictated purely by thermodynamics, and the system performance target for the given reactor technology describes the state of the art of the rSOC reactor.

In the second step, mathematical models of the rSOC reactor were developed. Two reactor models were developed. A one dimensional reactor model for detailed analysis of the reactor and a zero dimensional black box model for system analysis were developed. The one dimensional reactor model was validated against experimental results. The

zero dimensional black box model was used for system simulations. Different system architectures were established considering the boundary conditions of the rSOC reactor and the other BoP components. The one dimensional model was used to obtain the input parameters such as the effective reactor temperature and effective losses for the zero dimensional model. The system performances were quantified for different operation points. The difference between system performance targets defined in the previous step and the system performance obtained from the detailed process engineering model represents the system losses. Sources of entropy generation were identified.

In the final step, the feasibility of the system was evaluated using the detailed one dimensional model. The one dimensional model was used to identify operation points resulting in unrealistic or dangerous operation of the reactor. This could lead to failure of the reactor and possible system failure. The system operation points were altered accordingly in order to achieve safe operation of the rSOC reactor. An iterative process between step two and step three was performed and the results of step 2 already include the iteration. At the end of this step, the feasible system operation points and architectures were developed and its performances quantified.

The Aspen plus chemical process engineering software suite was utilised for process system modelling. The one dimensional reactor model was developed using Dymola based on the Modelica language.



3 Thermodynamics of electrochemical reactors

In this chapter, the thermodynamic fundamental and theoretical concepts required to develop an electrochemical process system are introduced. The thermodynamics governing the processes occurring in an electrochemical reactor are provided in section 3.1. In this section, a thermodynamic relation for the electric work produced or consumed by an electrochemical reactor is established and a relation for ideal voltage is provided. A theoretical analysis of an ideal rSOC system is presented in section 3.2. Two important reaction mechanisms for rSOC processes are considered for an rSOC system. The need for thermal management and its benefits are analysed. Finally, limits to ideal roundtrip efficiency of an rSOC system using an ideal rSOC reactor are discussed. A summary of it is provided in section 3.3

3.1 Thermodynamics of SOC electrochemical reactor

In this section, a brief introduction to SOC electrochemical reactors is provided. The advantages and disadvantages are highlighted in section 3.1.1. Thermodynamic of electrochemical reactors are introduced in following section 3.1.2. The calculation of ideal work produced by the SOC reactor or supplied to the SOC reactor is explained. A thermodynamic formulation of ideal voltage is provided using the first and second law of thermodynamics. Finally, the brief description on entropy generation and lost work in an

electrochemical reactor is described in 3.1.3.

3.1.1 Introduction to SOC electrochemical reactors

A reversible process is an ideal process with no entropy generation and for a real process minimising entropy generation is a requirement for achieving an efficient process. Chemical reactors are inherently thermodynamically irreversible and produce entropy. Thereby resulting in high exergy losses. The losses can be reduced by employing an electrochemical reactor to perform the reaction. In an electrochemical reactor, the work extraction process is in form of electrical work. The chemical energy is directly converted to electrical work and vice versa. In a chemical reaction, the chemical bonds are broken and reconfigured. During this process of reconfiguration, electrons are produced and consumed. By forcing the electrons to go through an external circuit before recombination, an electric current is generated and hence electric work is produced. For this to occur, the reactants should be spatially separated to prevent them from reacting spontaneously. The separation can be achieved by using an electrolyte. The electrolyte only allows for the transfer of ions (either positively or negatively charged) but not electrons. Two electrodes, a cathode and anode are required to complete the process. At the anode, the electrons are produced and flow out through the external circuit. This is the region for electrochemical oxidation reactions. The second electrode, the cathode, consumes the electrons flowing into the electrode from the external circuit. At the cathode electrochemical reduction reactions occur. The ions, either cation or anion depending on the electrolyte, are transported from one electrode to the other, where the reaction is completed and electroneutrality is maintained. Therefore, by such mechanism, the rate of reaction is coupled to electric work. When the external circuit is open (no load condition), electron flow is stopped, hence no work is produced. Without the flow of electrons out of the anode and electrons flow into the cathode, ion transport via electrolyte stops and hence the reaction does not proceed. Therefore, the rate of transport of ions, electrons and the chemical reaction rate is coupled to the rate of work extraction [86]. The electrolyte can be a solid or a liquid electrolyte. Different types of electrolyte are available based on their ion conduction properties. An extended overview is provided in [86–88]. In this work, an oxide ion conducting solid electrolyte is employed. Hence, the following discussions will be centred on oxygen ion conducting solid membrane reactor, also known as SOC reactor.

In a SOC electrochemical reactor, a ceramic membrane is used as an electrolyte. The electrolyte permits transport of the oxygen ion (O^{2-}) which is the charge carrier

3.1. THERMODYNAMICS OF SOC ELECTROCHEMICAL REACTOR

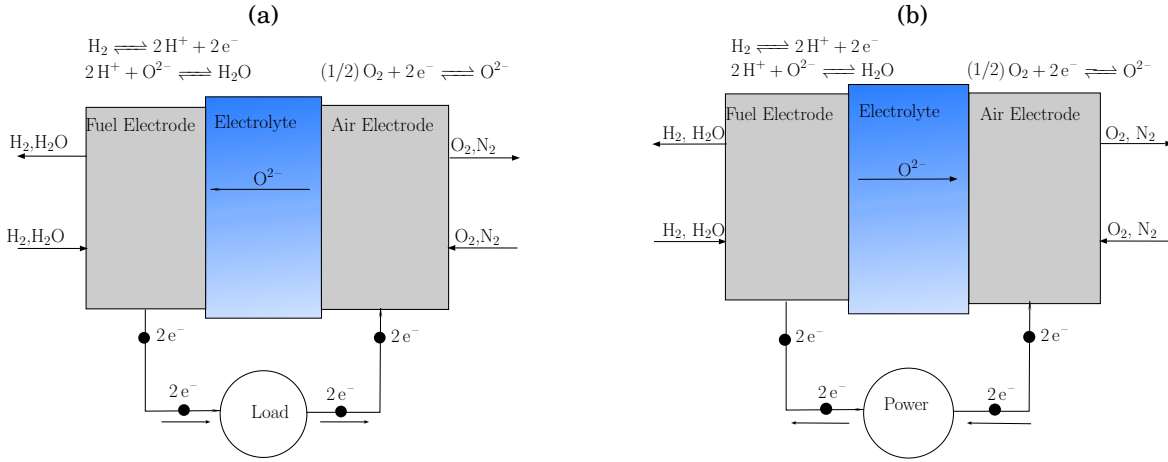


FIGURE 3.1. (a) Schematic of a SOC reactor process in SOFC mode, forward direction of reaction (R 3.1). (b) Schematic of SOC process in SOEC in mode, reverse direction of reaction (R 3.1).

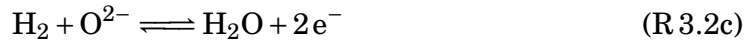
in the membrane. The working of a SOC reactor can be explained using the hydrogen combustion reaction as shown in reaction (R 3.1). A schematic of SOC working principle is shown in Figure 3.1. The reaction (R 3.1) represents the overall chemical reaction of a reversible hydrogen combustion reaction. Let us consider the forward direction of the combustion reaction. The combustion reaction is exothermic and spontaneous. Hydrogen is sent to the fuel electrode and oxygen/air to the oxygen electrode chamber. No work is extracted when the external circuit is open. When the reactants are introduced, the chemical potential difference exists. Hence, the gases quickly equilibrate, resulting in an electrochemical potential difference such that the chemical potential difference is zero. This electrochemical potential difference between the two electrodes is referred to as Open Circuit Voltage (OCV). When the external circuit is closed, electrons can flow from fuel electrode to oxygen electrode hence producing an electric current. Work extraction affects the equilibrium which is shifted, driving the reaction forward. The hydrogen supplied to the fuel electrode disassociates to produce proton and two electrons. Two protons then react with the oxygen ion which is supplied to the fuel electrode from the oxygen electrode via the electrolyte. Thereby water and electrons are produced. At the fuel electrode, the fuel is oxidised and electrons are produced hence, the fuel electrode is the **anode**. The anode half cell reaction is shown in equations (R 3.2c).



Reactions at the fuel electrode



Net reaction at the fuel electrode



Reaction at the oxygen electrode



The electrons produced on the anode side travel to the air electrode via the external circuit. At oxygen electrode, the oxygen consumes the two electrons and is reduced to form the oxygen ion. Hence, the air electrode acts as a *cathode*. The cathode reactions are presented in equation (R 3.2d). Due to the electrochemical potential established across the electrolyte membrane, the oxygen ion diffuses to the anode from the cathode through the electrolyte. The sum of reaction (R 3.2c) and (R 3.2d) results in overall reaction (R 3.1). The rate of all the individual reactions and hence the overall reaction is linked to the electrical work produced. This process is referred to as **Fuel Cell** reaction producing work from an exothermic combustion reaction [86, 89, 90].¹ For SOC reactors, it is known as the SOFC process. The process scheme is visualised in Figure 3.1(a).

The reaction (R 3.1) is spontaneous in moving from left to right towards water formation. To shift the reaction towards the left in a conventional reactor requires thermal energy at high temperatures around 1200 °C. But the same can be achieved in an SOC reactor by supplying a part or all the energy required to split the water in form of electric work [91]. This process is known as electrolysis or as SOEC process when performed using a SOC reactor. The SOEC process is the reverse process of SOFC process. Reactants, either steam/water or gas mixture of steam-H₂ is supplied to the fuel electrode. Under open circuit conditions, the gas equilibrates and an OCV is attained. When electric work is supplied to the SOC reactor, the polarities reverse resulting in a potential difference

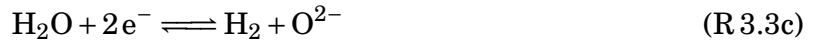
¹It should be noted that fuel cell operation are also possible with endothermic reactions. For example, direct oxidation of carbon to carbon monoxide is an endothermic reaction and can produce electric work when carried out in an electrochemical reactor. Such fuel cells are called Direct Carbon Fuel Cells.

across the electrolyte, higher than the OCV. The equilibrium is now disturbed and hence the reaction (R 3.1) moves towards to left to attain a new equilibrium. The reactions (R 3.3c) and (R 3.3d) occur at the fuel electrode and oxygen electrode. Unlike the SOFC process, in SOEC the fuel electrode is the cathode and air electrode is the anode.

At the fuel electrode



Net reaction at fuel electrode



At air electrode



At the fuel electrode, when work is supplied to the SOC reactor, water is reduced producing H_2 and O^{2-} . The electrochemical potential difference over the electrolyte drives the oxygen ion towards to the air electrode. At the air electrode, the oxygen ion is oxidised to produce oxygen and two electrons. The electrons produced travel via the external circuit and enter the fuel electrode. The scheme of the SOEC process is represented in Figure 3.1(b).

3.1.2 Ideal work and Ideal voltage of SOC reactor

An open, steady state SOC electrochemical reactor process as described in Figure 3.2 is assumed. The reactants enter the reactor with a certain temperature (T'), pressure (p') and composition (x'). The electrochemical reactions take place at reactor temperature and pressure for a given extent of electrochemical reaction (ξ) and the products of the reaction leave the reactor at a temperature (T''), pressure (p'') and composition (x''). Subscript a and f stands for air electrode chamber reactants and fuel electrode chamber respectively. \dot{W} and \dot{Q} are the electric work rate and thermal power produced or consumed by the reactor during the process. By convention, the work produced by the system is considered positive and work consumed by the system as a negative quantity. The work produced by

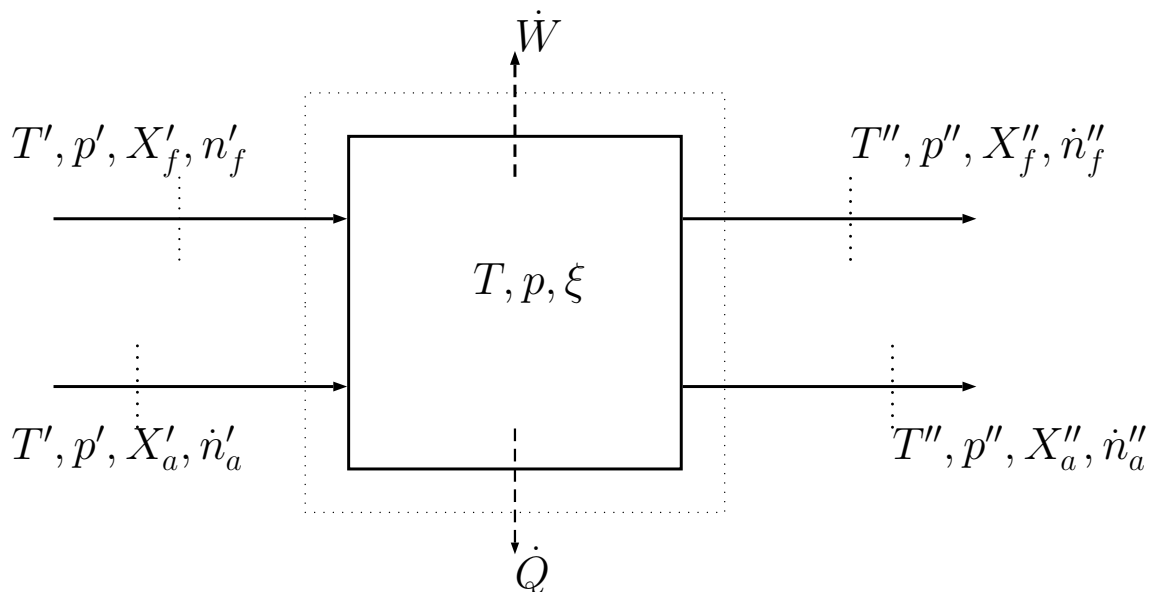


FIGURE 3.2. Thermodynamic scheme of SOC reactor

the system or work consumed by the system depends on thermodynamic state conditions before and after the reaction. In order to define ideal voltage and ideal work, the extent of electrochemical reaction and its relation to the current must be established.

Actual current and maximum current for SOC reactor

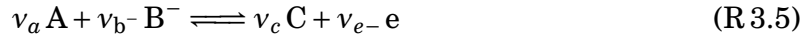
As discussed earlier, the rate of progress of an electrochemical reaction is proportional to the work extracted or supplied to the reactor. This corresponds to the current and hence to the rate of flow of electrons in the external circuit. Since the flux of ion transport across the electrolyte is also coupled to the current, the progression of electrode reactions and therefore the net reaction can be described by the parameter *extent of reaction* (ξ). In chemical reactions, the extent of reaction can be defined as an 'internal state parameter' that describes how far a certain reaction has progressed. The unit for extent of reaction is mole. Consider a generalised chemical reaction as given in (R 3.4). The same reaction can be written as in equation (3.1a). The extent of reaction can then be defined as in equation (3.1b).



$$\sum_i \nu_i m_i = 0 \quad (3.1a)$$

$$\frac{\Delta n_A}{\nu_a} = \frac{\Delta n_b}{\nu_b} = \frac{\Delta n_c}{\nu_c} = \xi \quad (3.1b)$$

If the same reaction is carried out in a SOC reactor, with the electrode reactions as shown in equations (R 3.5) and (R 3.6), the extent of electrochemical reaction can be represented by any of the half cell reactions since it is same as the extent of reaction of the net reaction.



Global net reaction



For an electrochemical reactor, writing the extent of electrochemical reaction in relation to the charge carrier ion is convenient. The transfer of the charge carrier is proportional to the current by Faraday's law. Hence, for a SOC reactor, the extent of electrochemical reaction can be described with respect to oxygen ion transfer through the electrolyte or the change in oxygen atoms in the reactant stream of either electrode. Therefore, the extent of electrochemical reaction can be written in terms of the reaction at the oxygen electrode (equation (R 3.8)) as given by (3.2). The total charge transferred during the reaction is equal to the extent of reaction. The reactor current is then the rate of change of the extent of electrochemical reaction given by (3.3). Similarly, the maximum charge transferred corresponds to the maximum extent of reaction for the given composition of reactants and maximum current possible is equal to rate of change of maximum extent of electrochemical reaction.



$$\xi = \frac{2\Delta n_{\text{O}_2}}{1} = \frac{\Delta n_{\text{O}^{2-}}}{1} = \frac{\Delta n_{\text{e}^-}}{2} \quad (3.2)$$

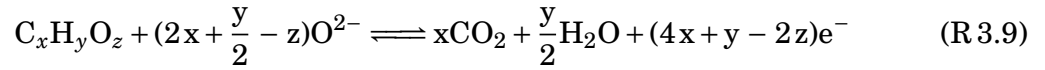
$$\frac{d\xi}{dt} = \Delta \dot{n}_{\text{O}_2} = \frac{I}{4F} \quad (3.3)$$

Another performance parameter essential in electrochemical reaction is the conversion ratio. For an electrochemical reaction, the conversion ratio is the ratio of current through the SOC reactor to the maximum current through the SOC reactor. Since the rate of change extent of electrochemical reaction is proportional to the current, the conversion ratio of an electrochemical reaction can also be given as the ratio rate of change of extent of electrochemical reaction to rate of change of maximum extent of electrochemical reaction as shown in equation (3.4a) and (3.4b). The conversion ratio (χ) is commonly referred to as the Utilisation of the reactant. ²

$$\chi = \frac{I}{I_{max}} \quad (3.4a)$$

$$\chi = \frac{d\xi}{d\xi_{max}} \quad (3.4b)$$

The definition of maximum current can vary depending on the operation mode and the reactant components. In the fuel cell mode, the maximum current is the current obtained for complete oxidation of the fuel or oxidisable components in the reactant mixture. The general description of electrochemical oxidation of the fuel as described in equation (R 3.9) [92],



The maximum current in fuel cell mode is given by (3.5) [92] and is normally called as Faradaic current.

$$I_{max,fc} = \dot{n}_e F \quad (3.5)$$

Likewise, for a SOC reactor operating in electrolysis mode, the maximum current is defined as the current supplied to the reactor to completely reduce all the oxidised components such as H_2O to H_2 and CO_2 to CO or C . In most practical cases, in order to avoid carbon deposition, CO_2 is not completely reduced to C but to CO . Therefore, maximum current in electrolysis mode is given by (3.6)

$$I_{max,ec} = 2F(\dot{n}_{CO_2} + \dot{n}_{H_2O}) \quad (3.6)$$

²For SOFC process it is normally referred to fuel utilisation and for SOEC process it is commonly referred to as steam utilisation.

Ideal work and voltage of SOC reactor

The ideal work produced or consumed by the reactor can be determined by applying the fundamental laws of thermodynamics for the control volume shown in Figure 3.2. In the present analysis, the electrochemical reactor is seen as a black box and its mechanical design and construction are not known. It is assumed that the concentration in the reactor is uniform and the reactor operates at constant temperature (T), pressure (p) similar to a well-stirred tank assumption. A steady state process is assumed. Applying the law of conservation of mass to the control volume we obtain the equation (3.7). Since a steady state process is assumed, the differential term is zero.

$$\dot{m}'_f + \dot{m}'_a - \dot{m}''_f - \dot{m}''_a = 0 \quad (3.7)$$

The reactor voltage can be discussed under two particular cases of (i) open circuit voltage or no work condition or (ii) ideal voltage during work extraction.

Case 1: Reactor voltage at OCV or no work condition: The reactor is assumed to be in a zero current state, that is, the external circuit is open and therefore no electrochemical reaction occurs in the reactor. Chemical reactions may occur if conditions are suitable. Due to the difference in the chemical potentials of the reactants on the fuel electrode side and air electrode side, the system tries to drive towards equilibrium [93]. This is achieved by the establishing an electrochemical potential across the electrolyte to establish an electrochemical equilibrium. Considering the H₂-H₂O electrochemical reaction as given in reactions (R 3.1) - (R 3.3d), the condition for equilibrium is given by the equation (3.8a)

$$v_i \mu_i = 0 \quad (3.8a)$$

The equilibrium for the reaction is given by the equation (3.8c).

$$\mu''_{\text{H}_2\text{O}} + \mu_{e^1} - \mu'_{\text{H}_2} - 0.5\mu'_{\text{O}_2} - \mu_{e^2} = 0 \quad (3.8b)$$

$$\mu''_{\text{H}_2\text{O}} - \mu'_{\text{H}_2} - 0.5\mu'_{\text{O}_2} = \mu_{e^I} - \mu_{e^II} \quad (3.8c)$$

The two terms on the right-hand side of equation (3.8c) represent the chemical potential of electrons in two electrode terminals. The difference in chemical potential of electrons on two electrodes is synonymous to the electrical potential difference [94]. This results in an expression for OCV as given in equation (3.9a). The chemical potential can be written as in equation (3.9b) assuming ideal gas equation of state. Hence, a final

form for voltage is derived as given in (3.9d). U° is the electric potential at standard conditions where the reactants and products are at atmospheric pressure. The equation (3.9d) is valid only under the assumption of chemical equilibrium.

$$-zFU = \mu''_{\text{H}_2\text{O}} - \mu'_{\text{H}_2} - 0.5\mu'_{\text{O}_2} \quad (3.9a)$$

$$\mu = \mu^\circ + RT \ln p_i \quad (3.9b)$$

$$-zFU = \Delta\mu^\circ + RT \ln \prod p_i^{v_i} \quad (3.9c)$$

$$U = U^\circ - \frac{1}{2F} RT \ln \prod p_i^{v_i} \quad (3.9d)$$

Case 2: Reactor voltage during work extraction or consumption: Once the external circuit is closed, work is extracted from or supplied to the reactor. During this process, the electrochemical reaction progresses by a certain extent. An expression for work can be derived from the first and second law of thermodynamics to the control volume described in Figure 3.2. The term $\dot{\Pi}$ in equation (3.10b) represents the entropy generation due to irreversibility or losses during the process. A detailed discussion on entropy generation and causes for entropy generation can be found in Appendix A.1.1.

First law

$$\dot{m}'_f h'_f(T', p', x'_f) + \dot{m}'_a h'_a(T', p', x'_a) - \dot{m}''_f h''_f(T'', p'', x''_f) - \dot{m}''_a h''_a(T'', p'', x''_a) - \dot{W} - \dot{Q} = 0 \quad (3.10a)$$

Second law

$$\dot{m}'_f s'_f(T', p', x'_f) + \dot{m}'_a s'_a(T', p', x'_a) - \dot{m}''_f s''_f(T'', p'', x''_f) - \dot{m}''_a s''_a(T'', p'', x''_a) - \frac{\dot{Q}}{T} + \dot{\Pi} = 0 \quad (3.10b)$$

Assuming the process to be reversible, the entropy generation term in (3.10b) is set to zero. Eliminating the \dot{Q} term from the first law and solving for work results in equation (3.11).

$$\dot{W}_{rev} = -(G'' - G') = -\left(\sum_i \dot{m}''_i g''_i - \sum_i \dot{m}'_i g'_i\right) \quad (3.11)$$

The term " G " and " g " in equation (3.11) represents the Gibbs function and specific Gibbs function respectively. The Gibbs function is a thermodynamic state parameter. Gibbs function and specific Gibbs function are evaluated by formula $G = H - TS$ and

$g = h - Ts$ respectively. A detailed discussion on Gibbs function is provided in the Appendix A.1.2. Therefore, the ideal work of the electrochemical reactor is the difference in Gibbs function before and after the reaction. The formulation given in equation (3.11) is a direct result of the application of the first and second law of thermodynamics. The equation can be seen as a more general form for evaluating the ideal work. In conventional methods as described in literature, the ideal work is briefly described as the change in Gibbs function due to the particular chemical reaction at reference conditions (ΔG°). Use of (ΔG°) to calculate the ideal work is only valid in the case where the reactants entering the reactor are in the pure state (i.e. at a partial pressure equal to atmospheric pressure) and products leaving the reactor as pure components. The relation in equation (3.11) will result in the same if the fuel and oxygen entering the reactor and products leaving the reactor are pure substances. The effect of product and reactant dilution is taken into account when the exact form of Gibbs function is used to evaluate the work. This results in a traditional form and commonly used Nernst equation as shown in (3.12) [95].

$$\dot{w}_{rev} = -\Delta g^\circ - RT \ln \left(\frac{\prod p_{i,products}}{\prod p_{i,reactants}} \right) \quad (3.12)$$

The Nernst equation is a valid approximation for evaluating the ideal work of an electrochemical reactor. Though the equation may not be entirely sufficient to evaluate the mixing effects and entropy due to mixing occurring in the reactor due to inert gas components and other gas in the reactants and products. Hence, under these circumstances, a generalised formulation for estimating the ideal work (equation (3.11)) of an electrochemical reactor is utilised in this thesis. Moreover, the Gibbs function being a state function, it does not depend on the path and hence encompasses all changes in moving from one state to another. A similar method is employed by Ratkje et al. [96] and Gaggioli et al. [95].

From an exergy perspective, the ideal work of an electrochemical reactor described in Figure 3.2 can be obtained from solving an exergy balance over the control volume. This results in an equation for ideal work as expressed in equation (3.13b). The work term, \dot{W}_{rev} , in equation (3.13b) and (3.11) are indeed the same. Hence, by comparing the two equations, it can be established that the difference in Gibbs function between the inlet and outlet of the reactor is equal to the difference in exergy between the inlet and outlet

plus the exergy of heat at the reactor temperature [97].

$$0 = \sum_i \dot{E}x' - \sum_i \dot{E}x'' - \dot{W} - \dot{Q} \left(1 - \frac{T_0}{T}\right) \quad (3.13a)$$

$$\dot{W}_{rev} = -\left(\sum_i \Delta \dot{E}x\right) - \dot{Q} \left(1 - \frac{T_0}{T}\right) \quad (3.13b)$$

3.1.3 Lost work in electrochemical reactor

Like in any thermodynamic system, lost work due to entropy generation occurs in an electrochemical reactor. The lost work can be due to material related properties such as ohmic resistance, reactor design, heat transfer, fluid dynamics or possibly due to other chemical reactions occurring in the electrochemical reactor or entropy generation due to mixing. Some entropy generation is avoidable and some is not in an engineering process. The entropy generation due to mixing, chemical reactions and heat transfer over finite temperature difference are some examples of unavoidable entropy generation. In a SOC electrochemical reactor, the major sources of entropy generation are due to the electrochemical losses such as ohmic losses, activation overpotential, diffusion and concentration losses. They will be addressed in detail in section 4.1. These losses can be minimised by better engineering of the materials and reactor design. The other source of entropy generation in an SOC reactor is due to the unavoidable thermodynamic losses. This is due to chemical reactions, mixing and heat transfer. In most SOC reaction systems using hydrocarbons (H-C-O) in the fuel electrode other chemical reactions apart from electrochemical reactions can occur within the SOC reactor. Methane, reformate, syngas and biogas are commonly used fuels in an SOC reactor in SOFC operation. During such operations, internal steam reforming reaction, water gas shift reactions and other plausible chemical reactions will occur. The work potential of these chemical reactions is not utilised hence resulting in lost work. It is important to account for the lost work due to these chemical reactions (which do not occur electrochemically) to be considered when either equation (3.11) or (3.13b) is used to calculate the ideal work of an SOC reactor. The lost work due to chemical reactions is nothing but the change in Gibbs energy due to the chemical reaction which is not converted to useful form of work. This can be evaluated using equation (A.35) [96].

3.2 Thermodynamics of rSOC systems

Theoretically, a rSOC electrochemical reactor can be switched from SOFC to SOEC mode by the applying an electric potential greater than the equilibrium potential for a given reactant mixture. This can be achieved by supplying electrical work to the electrochemical reactor and also thermal work (if the net electrolysis reaction is endothermic). Therefore, this enables to convert electrical energy (and also thermal energy) into chemical energy. This process is referred to as PtX, offering an attractive option of storing electrical energy in form of chemical energy. When electrical energy is required, the SOC reactor can be operated in SOFC mode to convert the chemical energy back to electrical energy, commonly referred to as XtP. In this section, a theoretical system concept for the rSOC system will be described. Theoretical limits for roundtrip efficiency based on reaction thermodynamics and processes will be discussed.

3.2.1 rSOC system concepts

A simple rSOC system concept is shown in Figure 3.3. The simple system is used to evaluate the theoretical limit for roundtrip efficiency of an rSOC system. In order to do so, an ideal SOC reactor is assumed. An ideal SOC reactor is assumed to have no entropy generation due to electrochemical losses. Though it can have inherent (unavoidable) entropy generation due to the chemical reaction itself, incomplete reaction, gas mixing etc. as mentioned in section 3.1.3. The Figures 3.3(a) and 3.3(b) represent the rSOC system operating in fuel cell mode and electrolysis mode respectively. The following assumptions are made to simplify the analysis.

1. The SOC reactor is assumed to be isothermal and isobaric.
2. Reactions occur at the isothermal reactor temperature.
3. The time period of reactor operation in fuel cell mode is equal to that of electrolysis mode.

$$t_{fc} = t_{ec} \quad (3.14)$$

4. The charge transferred during the discharge mode (fuel cell) is equal to the charge transferred during the charging mode (electrolysis).

$$\Delta n_{o,fc} = \Delta n_{o,ec} \quad (3.15)$$

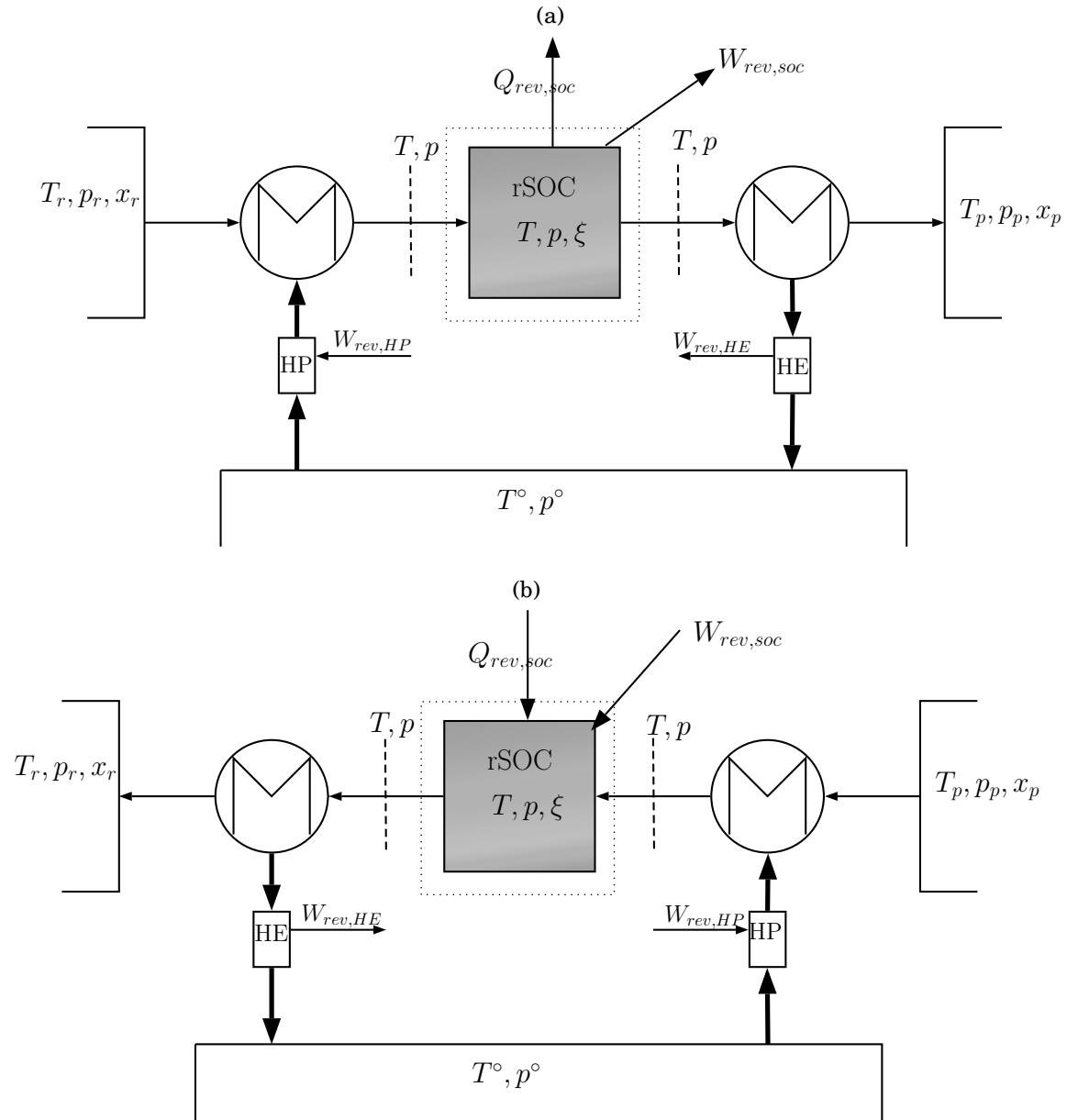


FIGURE 3.3. (a) Schematic representation of a process system in fuel cell mode, indicating directions of mass and energy flows. (b) Schematic representation of a process system in electrolysis mode, indicating directions of mass and energy flows. The subscript 'r' and 'p' represents the fuel tank and the product tank respectively. HP and HE represents heat pump and heat engine respectively

- Assumptions 3 and 4 imply that the current obtained from the SOC reactor in SOFC mode is equal in magnitude (but opposite in sign) to the current supplied to

SOC reactor in SOEC mode.

$$\Delta I_{fc} = \Delta I_{ec} \quad \text{and} \quad \xi_{fc} = \xi_{ec} \quad (3.16)$$

6. Assumptions 3 – 5 ensure that the fuel tank (subscript r) and exhaust tank (subscript p) in the system are brought to the same thermodynamic state before discharge.
7. Ideal heat transfer is assumed for heat recovery units. Due to this assumption, the effect on system performance is purely due to the reactor in the system.
8. All the gases are modelled using ideal gas equation of state.

The fuel used during the SOFC operation is stored in the fuel tank. In fuel cell mode, the fuel is supplied to the SOC reactor where it undergoes oxidation. Chemical energy is converted to electric energy and heat by the reactor. The oxidised fuel is stored in the exhaust tanks. In electrolysis mode, the oxidised fuel stored in exhaust tanks, mostly consisting of H₂O (and CO₂), is supplied to the SOC reactor. Electrical energy and heat (if required) are supplied to the SOC reactor. The SOC reactor converts the electrical and thermal energy to chemical energy. The oxidised reactants are converted to corresponding reduced states as fuel. Thermodynamic conditions of the tank are chosen such that there is no condensation of water or any phase changes. The gas preheating to reactor temperature from storage tank condition and cooling from reactor temperature to storage tank conditions are performed using a combination of reversible heat pump and heat engine. The heat engine (HE) operates between the gas medium as a heat source and environment as a heat sink. Whereas, the heat pump (HP) operates with the environment as a heat source and gas mediums as a heat sink. The performance of the rSOC system can be evaluated under different circumstances based on atomic elements involved in the reaction systems.

Roundtrip efficiency

The roundtrip efficiency is defined as the ratio of energy produced in the fuel cell mode to the total energy supplied in the electrolysis mode. For the system described in Figure 3.3, the total energy produced in SOFC mode consists of electric work and heat. If the heat energy ($Q_{rev,SOC}$) is not utilised, then the useful output energy is only the electric work ($W_{rev,SOC}$). From thermodynamics, that total reversible work is given by ΔG . In SOEC mode, the total energy consumed by the reactor is equal to the sum of electrical

energy and thermal energy (if the process is endothermic). The energy required for the reduction of oxidised reactants is equal to the enthalpy change of the reaction. This energy is supplied by a combination of electrical work (ΔG) and thermal energy ($T\Delta S$). Hence, the roundtrip efficiency is given by equation (3.17b).

$$\eta_{RT} = \frac{W_{rev,fc}}{W_{rev,ec} + Q_{rev,ec}} \quad (3.17a)$$

$$\eta_{RT} = \frac{-\Delta G_{fc}}{\Delta H_{ec}} = \frac{-\Delta G_{fc}}{\Delta G_{ec} + T_{ec}\Delta S_{ec}} \quad (3.17b)$$

In most of the considered reaction schemes, if the $\Delta G \leq \Delta H$, hence the $\eta_{RT} \leq 1$. Though for some reaction schemes, it is possible that $\Delta G \geq \Delta H$ and hence leading to $\eta_{RT} \geq 1$. This is purely due to the definition of efficiency based on first law [97]. Hence, a second law efficiency based on exergy analysis is well suited where the efficiencies will never be above 100 %.

On further analysis of equation (3.17b), it can be shown that the roundtrip efficiency for reaction systems which are exothermic in fuel cell mode and endothermic in electrolysis mode is always less than 1. This can be improved if the reversible heat $Q_{rev,fc}$ produced due to entropy change of the reaction is utilised. Additionally, the roundtrip efficiency can increase if $Q_{rev,ec}$ in the denominator of equation (3.17b) is reduced. Finally, a combination of both methods can be utilised. This can be achieved by thermal management.

Thermal management

Thermal management between exothermic fuel cell reaction and endothermic electrolysis reaction can aid to improve round trip efficiency. One possible strategy of thermal management involves storing the heat produced during in SOFC mode in a heat storage medium at a certain temperature and later using it during the SOEC operation. By this approach, the heat produced during SOFC is utilised within the system. The second strategy involves coupling the endothermic electrochemical reaction with an exothermic chemical reaction in the SOC reactor. In this method, the heat required by the reactor is reduced. When the rate of internal exothermic chemical reaction is high enough, the heat produced by the internal chemical reaction can balance the endothermic electrochemical reaction. The advantage and challenges of both strategies will be further assessed. In a real SOC reactor, the heat produced due to the electrochemical losses can overcome

the thermal demands of endothermic electrochemical reaction. But heat due to the irreversible entropy generation represents a loss of electrical energy and therefore leads to lower roundtrip efficiencies.

Thermal management by heat storage requires a heat storage medium at a temperature T_{hs} which stores the heat released by SOC the reactor in SOFC mode. The stored heat is supplied to the SOC reactor in SOEC mode. A temperature difference is required for heat transfer to occur. This enforces a condition that the reactor temperature in SOFC mode should be greater than the heat storage temperature. Also, the heat storage temperature should be greater than the reactor temperature in SOEC operation mode. The scheme of a proposed system with heat storage integration is shown in Figure 3.4.

$$T_{fc} > T_{hs} > T_{ec} \quad (3.18)$$

Assumptions described earlier are valid for the system described in Figure 3.4. The energy output of the system in SOFC mode equals $W_{rev,fc}$. The reversible heat produced during the SOFC mode, $Q_{rev,fc}$, is stored in the heat storage medium at a temperature T_m . In the SOEC mode (Figure 3.4(b)), the net energy supplied to the system equals the electric work $W_{rev,ec}$. The reversible heat required for the endothermic reaction is extracted from the heat storage medium. Hence, by this method the reversible heat produced during SOFC operation is stored and utilised during SOEC mode. Hence, it is retained within the system. The roundtrip efficiency for the system is then given by equation (3.19).

$$\eta_{RT} = \frac{W_{rev,fc}}{W_{rev,ec}} = \frac{\Delta G(T_{fc}, p, \xi)}{\Delta G(T_{ec}, p, \xi)} \quad (3.19)$$

Thermal management with an internally coupled exothermic reaction requires the reactor and system to be operated in SOEC mode at conditions favourable for the exothermic reaction. Secondly, a sufficient reaction rate of exothermic reaction is necessary to meet the thermal requirements of endothermic electrochemical reaction. Such a method for thermal management requires complex reaction networks. Bierschenk et al. proposed an rSOC system with internal thermal management using H-C-O chemistry [81]. Finally, such a system might require further optimisation to the reactor design to promote the exothermic chemical reaction. The roundtrip efficiency is described by equation (3.17b) with $Q_{rev,ec}$ tending to zero.

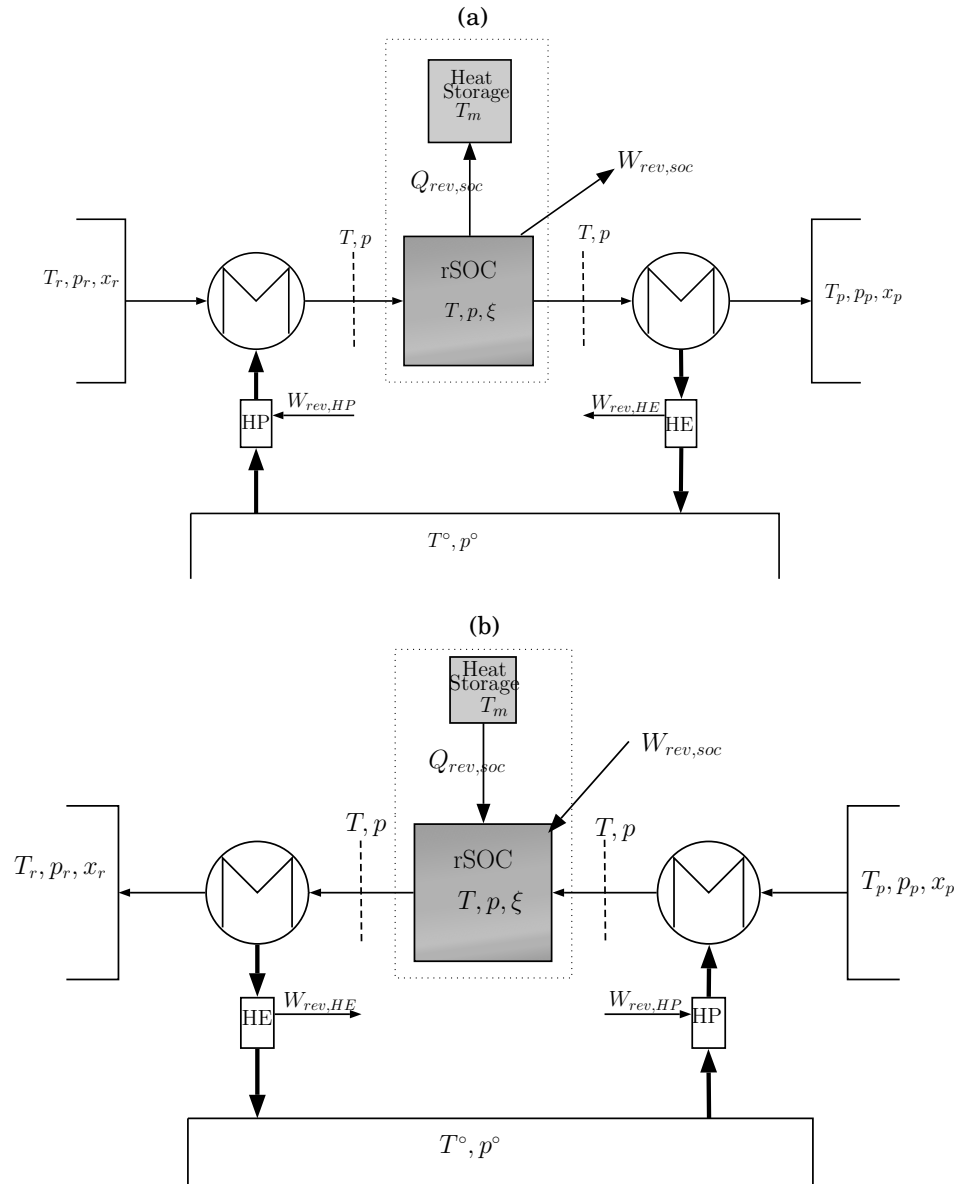


FIGURE 3.4. (a) Schematic representation of an rSOC process system with heat storage integration in fuel cell mode, indicating directions of mass and energy flows. (b) Schematic representation of an rSOC process system with heat storage integration in electrolysis mode, indicating directions of mass and energy flows. The subscript 'r' represents the fuel tank and 'p' represents the product tank. HP and HE represent heat pump and heat engine respectively

3.2.2 rSOC systems based on H-O chemistry

The H₂-H₂O reaction is the common electrochemical reaction system for fuel cell and electrolysis. Most of the SOC electrochemical reactors are developed and optimised for electrochemical reaction of H₂ to H₂O. In this analysis, an rSOC reactor system based on H₂-H₂O is considered with and without thermal management. The theoretical limit for roundtrip efficiencies is quantified. The impact of key system parameters on the roundtrip efficiencies is identified.

A H₂-H₂O fuel mixture in the fuel tank is assumed to have a composition of 90 mol% H₂ and 10 mol% of H₂O. This corresponds to a fuel with a Lower Heating Value (LHV) of 60 MJ/kg. In the SOFC mode, the reactants are preheated to the reactor temperature. A certain extent of electrochemical oxidation of H₂ occurs at the fuel electrode. The product gases, mainly consisting of H₂O and unreacted fuel (H₂) are cooled at the heat recovery unit. Power and reversible heat produced by the SOC reactor in SOFC mode is calculated at reactor temperature, pressure and for a given extent of electrochemical reaction. The reversible heat is produced due to the exothermic electrochemical reaction which can either be stored for thermal management or not stored and therefore lost. In the SOEC operation mode, the product gases stored in the product tank are preheated to the reactor temperature supplied to the SOC reactor. Due to assumptions 3 and 4, the extent of electrochemical electrolysis reaction is the same as in the fuel cell reaction. The electric power and heat required for the endothermic reaction are calculated at reactor temperature and pressure for the given extent of electrochemical reaction. The heat required is either supplied from an external source or from heat storage if the heat storage thermal management method is employed.

The maximum reactor current in SOEC and SOFC mode is calculated using equations (3.6) and (3.5) respectively. The SOC reactor current is then calculated from the maximum current from the relation between conversion ratio (χ) and maximum current (I_{max}). The value of χ_{fc} is provided as input, the corresponding value for χ_{ec} in SOEC mode is calculated to satisfy the conditions of equal current in fuel cell and electrolysis operation.

Roundtrip efficiency without thermal management

The roundtrip efficiency of an rSOC system without thermal management is given by equation (3.17b). Reaction thermodynamics of H₂-H₂O reaction system are shown in Fig-

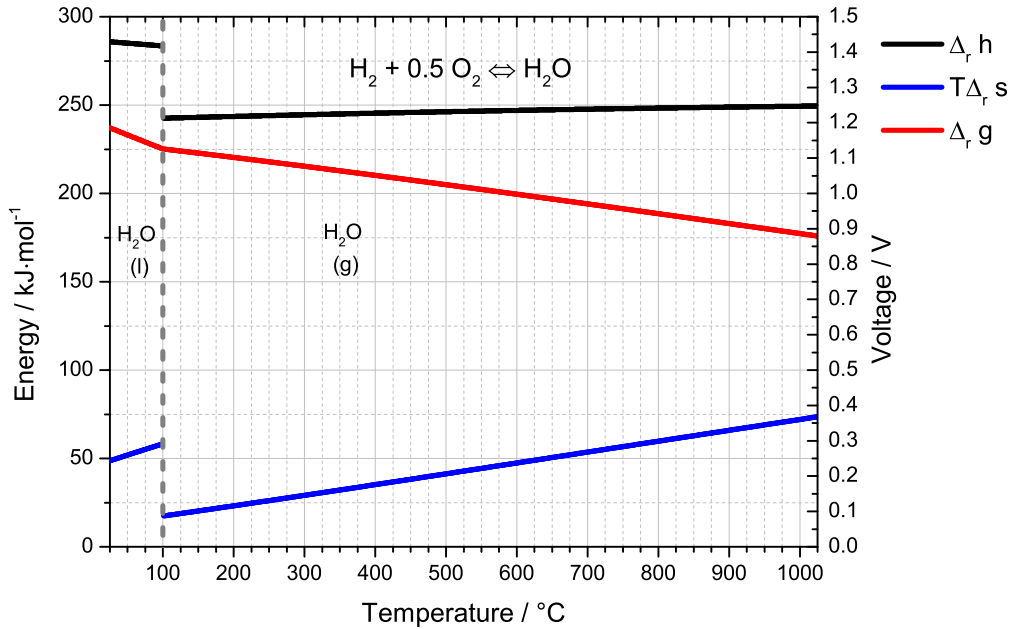


FIGURE 3.5. Thermodynamics of H_2 - H_2O system showing the variations of $T\Delta_{rxn}S$, $\Delta_{rxn}G$ and $\Delta_{rxn}h$ at atmospheric pressure

Figure 3.5. As the reaction temperature increases, the value of $T\Delta_{rxn}S$ increases and $\Delta_{rxn}G$ decreases. Hence, the maximum roundtrip efficiency for the H-O system without thermal management system varies with temperature as shown in Figure 3.6. The theoretical limit of roundtrip efficiency for the system with no heat storage or thermal management varies strongly with pressure. For an ideal gas, the variation of the $\Delta_{rxn}h$ with pressure is negligible and is more or less constant whereas, $\Delta_{rxn}g$ varies strongly with pressure. The increase in pressure leads to an increase in roundtrip efficiency. A steep increase in efficiency is observed until 10 bar. Above 10 bar, the efficiency increase is marginal. Gibbs function is a logarithmic function of pressure within the term $RT \ln p_i$. The logarithmic behaviour leads to the observed effect.

The impact of the extent of electrochemical reaction on the theoretical limit of roundtrip efficiency can be observed in 3.6. The roundtrip efficiency of the system increases when the extent of electrochemical reaction is reduced. The extent of electrochemical reaction is directly proportional to the work extracted or supplied to the reactor.

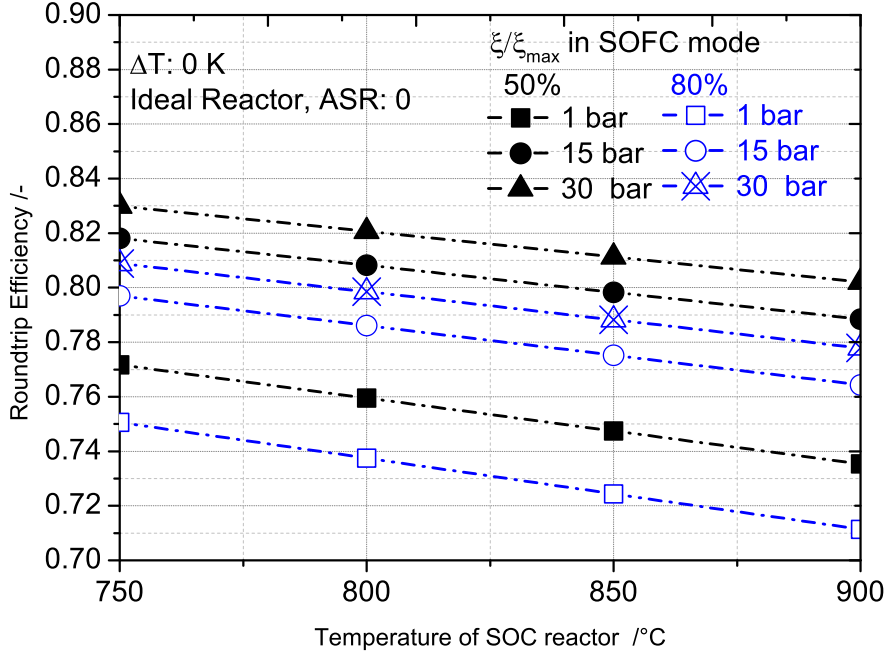


FIGURE 3.6. Variation of theoretical limit of round trip efficiency of H-O chemistry system with temperature at different reactor pressures.

When the extent of electrochemical reaction is higher, then the work is extracted from the reactor is high. This results in a higher driving force for the electrochemical reaction as explained in section 3.1.1. This leads to unavoidable entropy generation within the reactor [93]. Therefore, $W_{rev,fc}$ reduces with increases in extent of electrochemical reaction. Hence, the roundtrip efficiency decreases with increasing extent of electrochemical reaction.

Roundtrip efficiency with heat storage thermal management

By integrating heat storage in the rSOC system facilitates the use of heat produced in SOFC mode to be utilised in SOEC mode. The heat generated in SOFC mode is retained within the system and is used in SOEC mode when needed. Thereby, an external heat source is not required to supply the reversible heat required for the electrolysis reaction. Heat transfer between the SOC reactor and heat storage requires a temperature difference. Therefore, the SOC reactor temperature in SOFC mode (T_{fc}) must be greater than the heat storage temperature (T_m) and reactor temperature in SOEC mode (T_{ec})

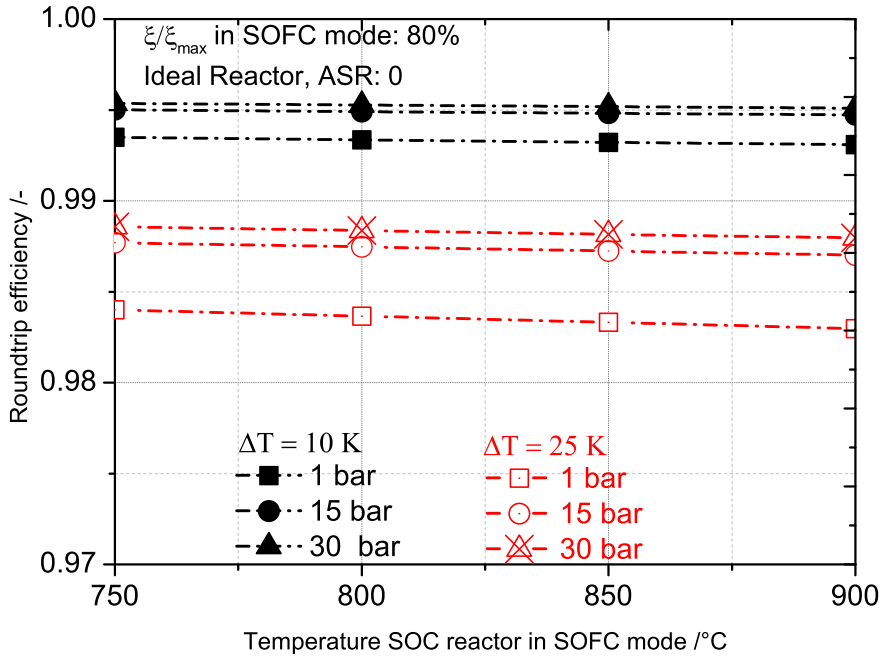


FIGURE 3.7. Variation of theoretical limit of round trip efficiency of an H-O chemistry system with temperature at different reactor pressures and ΔT values between SOC reactor and heat storage medium.

must be lower than heat storage temperature. Hence, the SOC reactor operates at two different temperature levels between SOFC and SOEC operation modes. The difference between the SOC reactor temperature and heat storage is defined as ΔT as in equation (3.20a). The roundtrip efficiency for the system is given by equation (3.19).

$$T_{fc} - T_{hs} = \Delta T = T_{hs} - T_{ec} \quad (3.20a)$$

$$T_{fc} - T_{ec} = 2 \times \Delta T \quad (3.20b)$$

By using the heat storage method to manage the thermal demands of SOEC operation, the upper limit for ideal round trip efficiency was increased close to 100 %. The roundtrip efficiency decreases with increasing ΔT between the reactor and the heat storage. The operation temperature of SOC reactor in SOEC mode is lower than in SOFC mode. For an H-O system, the change in Gibbs function increases with lowering temperatures for a given pressure and extent of reaction as shown in Figure 3.5. Since, the reactor temperature during the SOFC operation is higher than the reactor temperature during the SOEC operation, the change in Gibbs function during the SOFC mode is lower than

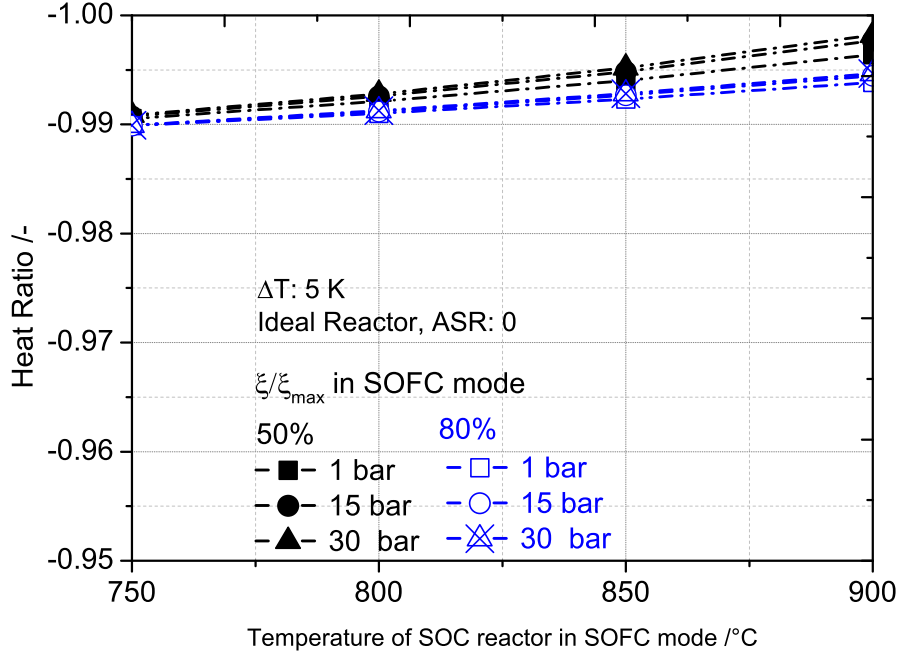


FIGURE 3.8. Variation of theoretical heat ratio for H-O system with temperature at different reactor pressures and ΔT values between SOC reactor and Heat storage medium

the change in Gibbs function during the SOEC operation mode.

$$T_{fc} > T_{ec}$$

$$\Delta_{rxn}G(T_{fc}) < \Delta_{rxn}G(T_{ec}) \quad (3.21)$$

Hence, it can be observed that the roundtrip efficiency decreasing with increasing ΔT . The efficiency decrease is a marginal value of 1 – 2 %. Based on the analysis, heat storage temperature should be selected based on an optimisation between engineering material demands, roundtrip efficiency and area of heat transfer. The reactor pressure had the same effect on the roundtrip efficiency as observed for a system without heat storage. For a given value of ΔT , the round trip efficiency increased with pressure. The parameter heat ratio (θ) is defined to study the thermal management benefits. The heat ratio, θ is defined in equation (3.22) as the ratio of thermal energy stored in heat storage during SOFC mode to thermal energy extracted from heat storage by the SOC reactor in SOEC mode.

$$\theta = \frac{Q_{SOC,ec}}{Q_{SOC,fc}} \quad (3.22)$$

In equation (3.22) by convention exothermic heat production (Q_{fc}) is negative and endothermic heat consumption by the reactor is positive. The variation of θ with reactor temperature in SOFC mode for different values of ΔT and p is shown in Figure 3.8.

3.2.3 rSOC systems based on H-C-O chemistry

The H-C-O reaction chemistry is of certain interest in SOC systems. Due oxygen ion being the charge carrier, theoretically any fuel including hydrocarbons can be oxidised by operating an SOC reactor in SOFC mode. Direct oxidation of hydrocarbon fuel in SOC reactors is written in a generalised form as shown in equation (R 3.9). A common fuel usually considered for SOC reactors is methane. Hence, the H-C-O chemistry for methane is considered in this analysis. The system operation and design are similar to the system described in section 3.2.2. The fuel tank consists of H-C-O chemistry. For the current analysis, a methane-based system is considered. The ratio of H/C/O is chosen such that sufficient methane formation is possible during SOEC mode and to avoid carbon deposition in both SOFC and SOEC operations. For the present analysis, a H/C ratio of 7 and O/C ratio of 1.5 for the fuel tank is used. By thermodynamic equilibrium study, it was earlier shown that a value of H/C of 6 to 7 is required for methane formation in electrolysis mode [81, 85].

Direct oxidation of methane as given in equation (R 3.10) is theoretically possible in SOC reactors. Direct oxidation of methane is reported in the literature [98–103]. But the possibility of it occurring is dictated by electrode kinetics and the feasibility of such a system is disputed [104, 105]. The most common reaction mechanism involves a reverse steam reforming reaction, reverse water gas shift reaction followed by electrochemical oxidation of hydrogen and carbon monoxide as given by equations (R 3.11) – (R 3.14).

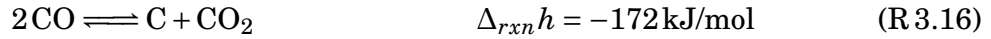
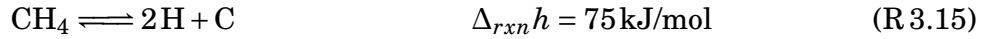
Direct methane oxidation



Reaction pathway



The CO oxidation (reaction (R 3.14)) is slower than the water gas shift reaction as the water gas shift reaction quickly reaches equilibrium. Carbon depositions are possible to occur within the reactor via reaction (R 3.15) – (R 3.18). This can be prevented by maintaining a sufficient O/C ratio of at least 1.5. In literature O/C values of 2 are used for safe operation of real systems [106–109].



Likewise, it is possible to perform co-electrolysis of both water and carbon dioxide to hydrogen and carbon monoxide respectively. It is theoretically possible to reduce CO₂ to C but it is seldom performed to avoid carbon deposition. The syngas produced during co-electrolysis can be further processed to other useful hydrocarbons in the downstream process. According to thermodynamics it is possible to directly synthesise hydrocarbons within the SOC reactor under relevant conditions [81, 87, 88]. Ultimately, the feasibility is dictated by the reaction and electrode kinetics [83, 110].

Roundtrip efficiency without heat storage thermal management

The process is similar the process scheme described for an rSOC system based on H-O chemistry. A fuel with a composition of 40 mol% CH₄ and 60 mol% H₂O is fed to the rSOC system in SOFC mode. The reactants are preheated to the reactor temperature. The reaction pathway is as discussed between reaction (R 3.11)–(R 3.14). The exhaust or product gas consists mainly of the H₂O, CO₂ and remaining non utilised fuel. In the SOEC mode, the gases from the product tank are supplied to the rSOC reactor after being preheated to the reactor temperature. The electric work and heat (if required) are

supplied to the reactor. The produced fuel is then cooled and sent to the fuel tank.

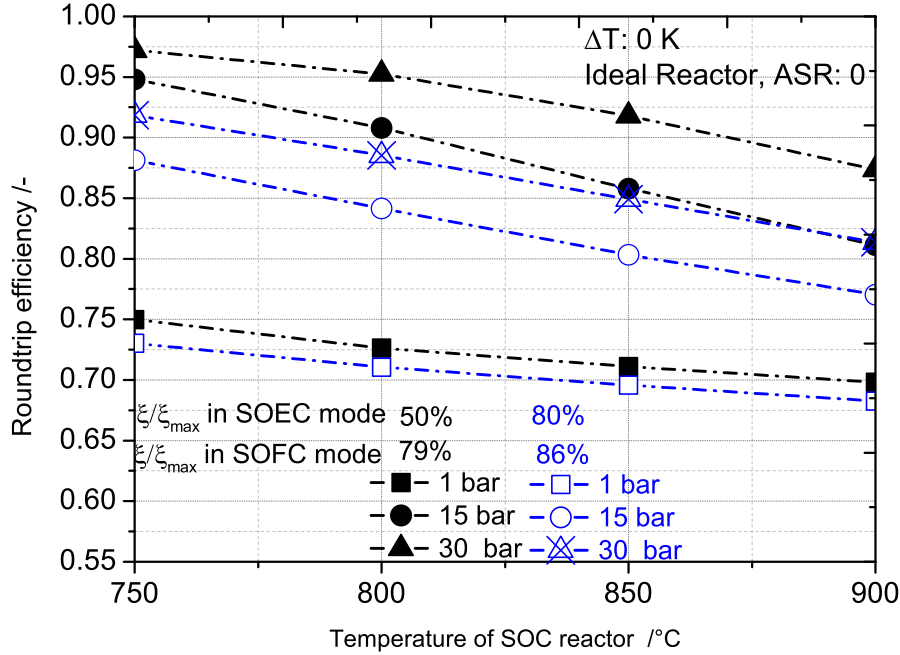


FIGURE 3.9. Variation of the roundtrip efficiency for rSOC system with no heat storage, based on H-C-O chemistry at different conversion ratios and pressures.

For the system with no heat storage for thermal management, the roundtrip efficiency is given by equation (3.17b). For the rSOC system described, the variation of roundtrip efficiency with temperature at different pressures and extent of reaction is shown in Figure 3.9. The proposed reaction pathway for the CH_4 fuelled rSOC system is based on reactions (R 3.11)–(R 3.14). The CH_4 is more likely to undergo endothermic steam reforming chemical reaction rather than the direct electrochemical oxidation of methane because the reaction (R 3.11) is thermodynamically favourable. Therefore, the work production $W_{rev,fc}$, in the SOFC mode is only due to electrochemical oxidation of H_2 and CO based on reactions (R 3.13) and (R 3.14) respectively. Therefore, the work potential of reaction (R 3.11) is lost [93, 96]. The lost work due to chemical reaction can be evaluated using equation (A.35). Therefore, the numerator of equation (3.17b) is given by equation (3.23).

$$W_{rev,fc} = -(G'' - G') - (-\Delta_{R3.11}G) \quad (3.23)$$

In the SOEC mode, the total energy to be supplied to the reactor corresponds to the total enthalpy change of the reactions. For the rSOC system under consideration the total energy input to the system is equal to the sum of enthalpy change of individual reactions (equation (3.24)).

$$\Delta H_{ec} = \sum_i \Delta_{rxn,i} H, \quad i \in (\text{R 3.11}) - (\text{R 3.14}) \quad (3.24)$$

Similar to the SOFC mode, in SOEC mode, only the reverse reactions of (R 3.13) and (R 3.14) occur electrochemically. Hence, the electrical energy input corresponds to those reactions only. The heat input to the reactor is then the sum of heat required for endothermic electrochemical reduction reactions of (R 3.13) and (R 3.14) and the exothermic chemical reaction of the reverse steam reforming reaction (R 3.11) which is also commonly known as methanation reaction.

$$Q_{rev,ec} = \xi_{(\text{R 3.13})} T \Delta_{(\text{R 3.13})} S + \xi_{(\text{R 3.14})} T \Delta_{(\text{R 3.14})} S + \xi_{(\text{R 3.11})} \Delta_{(\text{R 3.11})} h \quad (3.25)$$

$$W_{rev,ec} = -(G'' - G') + \Delta_{(\text{R 3.11})} G \quad (3.26)$$

The behaviour of roundtrip efficiency of the system with reactor temperature and pressure as observed in Figure 3.9 shows that the roundtrip efficiency of the system increases with increasing pressure and decreasing temperature for a given extent of electrochemical reaction. This behaviour can be explained based on (3.24), (3.23) and (3.25). Similar to the case of an rSOC system with H-O chemistry, the reversible work in SOFC mode $W_{rev,fc}$ decreases with increasing temperature. Yet, at higher temperatures, the total energy required by the rSOC system in SOEC mode also increases. This leads to decreasing roundtrip efficiency with increasing reactor temperature. The reverse steam methanation reaction (R 3.11) is exothermic and hence becomes thermodynamically unfavourable at higher temperatures. The enthalpy change is then dictated predominantly by the endothermic electrochemical reduction of H_2O and CO_2 (equation (3.24)).

As the system operation pressure is increased, it can be observed that the roundtrip efficiency increases significantly. This effect is due to multiple reasons. In the SOFC mode, as the pressure is increased, the reversible work performed by the reactor ($W_{rev,fc}$) increases. In the SOEC mode, as the pressure increases the total energy input to the reactor decreases. This is because higher pressure is favourable for the reverse reaction of (R 3.11) which is an exothermic reaction. Therefore, as pressure increases, the extent of reverse reaction of (R 3.11) increases due to Le' Chateliers rule, thereby producing heat internally. The effect of pressure on CH_4 production by the reverse reaction of (R 3.11)

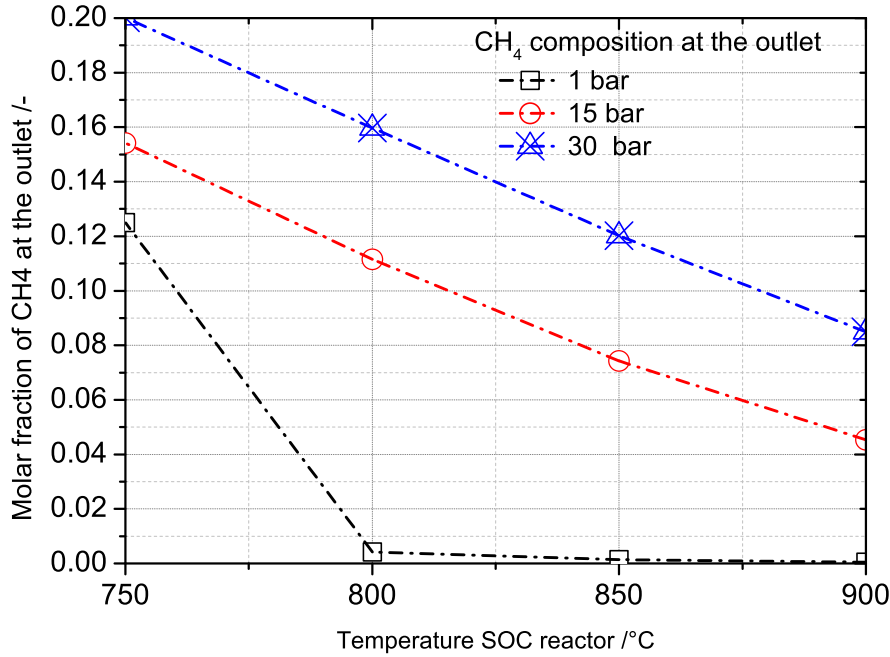


FIGURE 3.10. The variation of the methane composition at the outlet of rSOC reactor in SOEC mode with temperature and pressure. The methane mole fraction at the outlet indicates the extent of reaction (R 3.11) in backward direction.

can be observed in Figure 3.10. The extent of electrochemical reaction is set as constant due to assumptions 3 and 4. Hence, by equation (3.25), the heat required by rSOC reactor in SOEC mode decreases. Therefore, as a result of increasing $W_{rev,fc}$ in SOFC mode and decreasing $Q_{rev,ec}$ in SOEC mode, the roundtrip efficiency of the rSOC system increases with increasing pressure for all temperatures. This effect is predominant at lower reactor temperatures and higher pressures. On comparing Figure 3.9 and Figure 3.6, it can be seen that at 1 bar system pressure, rSOC system based on H-O chemistry and rSOC system based on H-C-O chemistry have similar theoretical roundtrip efficiencies.

The impact of the extent of electrochemical reaction on the theoretical limit to roundtrip efficiency can be observed in Figure 3.9. The roundtrip efficiency increases with decreasing extent of electrochemical reaction. As explained in section 3.2.2 for the H-O system, the reversible work in SOFC mode decreases with an increase in

extent of electrochemical reaction. The same explanation holds true for the H-C-O system. Additionally, in the H-C-O system, due to the internal exothermic methanation reaction (reverse of reaction (R 3.11)), the $Q_{rev,ec}$ decreases with decreasing extent of electrochemical reaction. This effect is prominent when the rSOC system operates at higher pressures and lower temperatures. From equation (3.25), the endothermic heat demand reduces as $\xi_{(R3.13)}$ and $\xi_{(R3.14)}$ reduce. This heat demand is easily met by the internal exothermic reaction. Hence, due to this compounded effect the roundtrip efficiency increases substantially with decreasing extent of electrochemical reaction for an rSOC system based on H-C-O chemistry. For the rSOC system operating at 750 °C and 30 bar pressure, the theoretical limit for roundtrip efficiency reaches as high as 95 % when the extent of electrochemical reaction is lowered.

3.3 Results and discussion

A theoretical analysis of rSOC systems based on thermodynamics was presented. Two concepts for rSOC systems were presented based on the thermal management strategy. In the first concept, a heat storage mechanism is employed to store the heat produced during the SOFC mode. The stored heat can then later be used in SOEC mode. The second strategy involves coupling an exothermic chemical reaction within the rSOC reactor to supplement the endothermic electrolysis reaction during the SOEC process. Feasibility and merits of both strategy were analysed. It was shown that the heat storage thermal management technique is essential for an rSOC system based on H-O chemistry. By employing a heat storage, the theoretical limit for roundtrip efficiency is close to 100 %.

The strategy of coupling an exothermic internal chemical reaction within the rSOC reactor in SOEC mode is viable for rSOC systems based on H-C-O chemistry. The analysis presented here focussed on the reversible CH₄ oxidation via the reaction mechanism described in reactions (R 3.11)–(R 3.14). From the analysis, it can be seen that the exothermic methanation reaction occurring within the reactor more or less balances the thermal requirement of the endothermic electrochemical reaction. At a certain pressure and temperature of the rSOC reactor, it is possible for the reverse of (R 3.11) to completely balance the heat required for endothermic electrochemical reaction.

A summary of ideal roundtrip efficiency of the rSOC system concepts at different

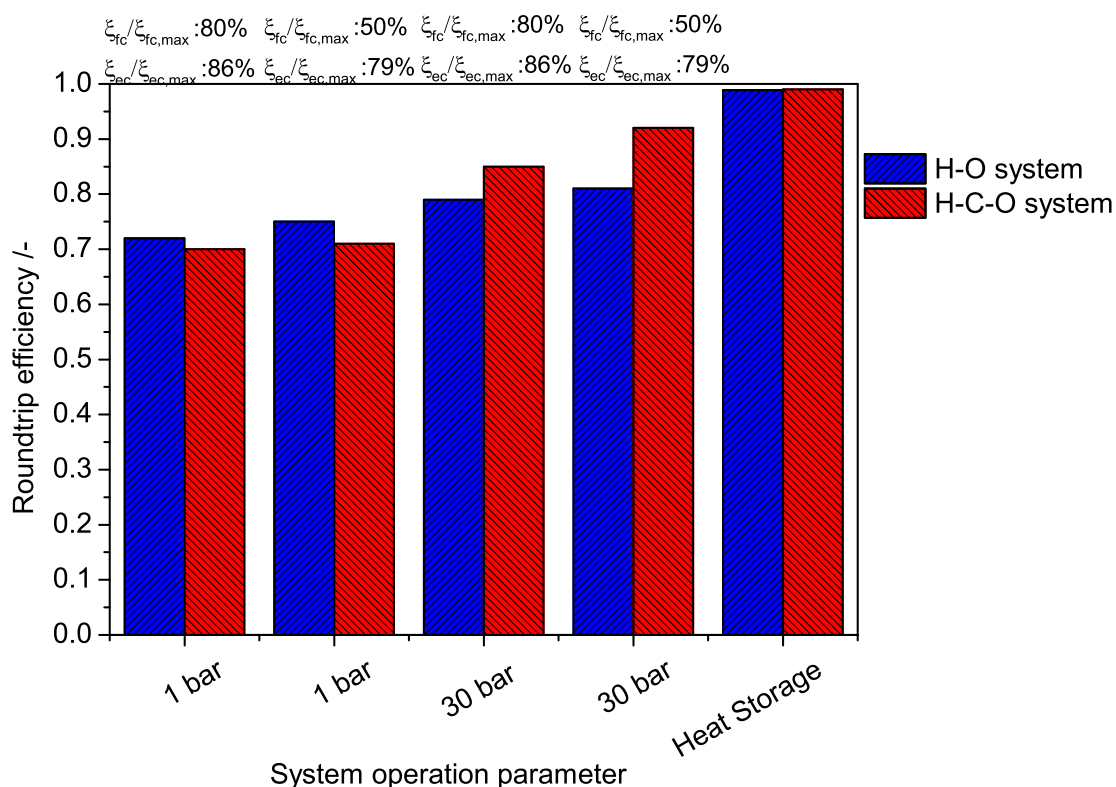


FIGURE 3.11. Ideal roundtrip efficiency of different rSOC system concepts

conditions is presented in Figure 3.11. The impact of key thermodynamic operational parameters for both system concepts were analysed. Operating the rSOC system at lower extent of electrochemical reaction can result in higher roundtrip efficiency. But the practical feasibility should be taken into consideration. For a given power output/input, a lower extent of electrochemical reaction will require large reactant flow rate. This will likely increase the operational and running costs. Hence, a higher extent of electrochemical reaction is chosen. To summarise, in the following chapters, rSOC systems based on both H-O chemistry and H-C-O chemistry will be considered for further analysis. Heat storage is chosen as the main method of thermal management for both H-O and H-C-O chemistry based systems. Integrating heat storage with rSOC systems will store heat produced during the exothermic operation of rSOC. This heat then can be used during the endothermic operation during the SOEC process or to supply heat to other interlinked processes. In the future one can envisage a heat storage integrated rSOC energy system in industrial processes and chemical processes where high temperature

heat is used or produced.



4 Analysis of commercial rSOC reactors and roundtrip efficiency

An analysis of rSOC systems using available rSOC reactors is presented based on the fundamentals established in chapter 3. A brief introduction to SOC reactors is provided in section 4.1 where the state of the art of SOC reactor is provided. The state of the art for electrodes, electrolytes and interconnects is provided in section 4.1. An experimental analysis of a commercial rSOC system is discussed in section 4.2. An extension of the theoretical analysis of rSOC system presented in section 3.2 in chapter 3 is presented by incorporating the experimental results. The roundtrip efficiency for an rSOC system based on a commercially available rSOC reactor is discussed in section 4.3. System operation parameters and their impact on roundtrip efficiency will be discussed. The summary of results and its implication for process engineering is discussed in section 4.4.

4.1 rSOC electrochemical reactors

Solid oxide cell electrochemical reactor is capable of directly converting chemical energy into electrical energy and heat in fuel cell mode. These SOC reactor are also capable of operating in reverse direction by converting electrical energy into chemical form in the electrolysis mode. The operation principle of SOC reactors was explained in detail in section 3.1.1. They consist of a oxygen ion conducting ceramic membrane as an electrolyte. The operation temperature of SOC reactors is determined by ion conductivity properties

of the electrolyte membrane and the nominal operation temperature of SOC reactor is in the range of 600 to 900 °C. The electrolyte is sandwiched by the air and fuel electrodes. The air and fuel electrodes have different functionalities and requirements. The electrode–electrolyte–electrode configuration together is commonly referred to as Membrane Electrode Assembly (MEA) or single cell. Different types of SOC reactor designs and MEA assemblies are available. Based on the reactor design, they can be broadly classified as a) planar SOC reactors and b) tubular SOC reactors. The planar or the tubular design can be further classified based on the MEA structure. The MEA design is optimised based on maximising mechanical and thermal stability and minimising the electrochemical losses. Three standard MEA are a) electrolyte supported cell (ESC), b) fuel electrode supported cells, commonly referred to as ASC and c) the metal substrate supported cells design. To increase power and voltage, a number of cells are stacked together connected either in series or parallel to form a SOC reactor commonly referred to as a SOC stack. The SOC reactors or stacks are generally designed to be modular. The SOC reactors can be further arranged together to form a SOC reactor module for higher power requirements [111, 112].

4.1.1 Functional Layers and Materials

The SOC reactor has 4 major functional layers. They are the fuel electrode, electrolyte, air electrode and interconnect. Apart from these main functional layers other protective layers between two functional layers may or may not be present. This depends on the materials used for the functional layers.

Electrolyte

The electrolyte is the key component in a rSOC reactor and is comprised of oxygen ion conducting ceramic materials. The material used for the electrolyte is expected to meet certain requirements. It should be chemically stable at high temperatures and also have good oxygen ion conductivity at these temperatures. The thermal stability of these materials is also important at high temperatures. Thermal expansion coefficients should match with other materials in all temperatures, from room temperature to fabrication temperature, in order to avoid cracking and delamination of the electrolyte. Lastly it should be dense to prevent gas leakage between fuel electrode to oxygen electrode through the electrolyte. The commonly used ceramic material for the electrolyte is Yttria Stabilised Zirconia (YSZ). The YSZ electrolytes exhibit good oxide ion conductivity in the

temperature range of 750-1000 °C. They are the state of the art in SOC electrolytes and its behaviour is altered by varying the composition of Yttria. Two commonly used forms of YSZ electrolytes are the 3 mol% YSZ and 8 mol% YSZ. Each has its own advantages and disadvantages [113, 114].

Lowering of operation temperature is of prime importance in SOC reactors in order to

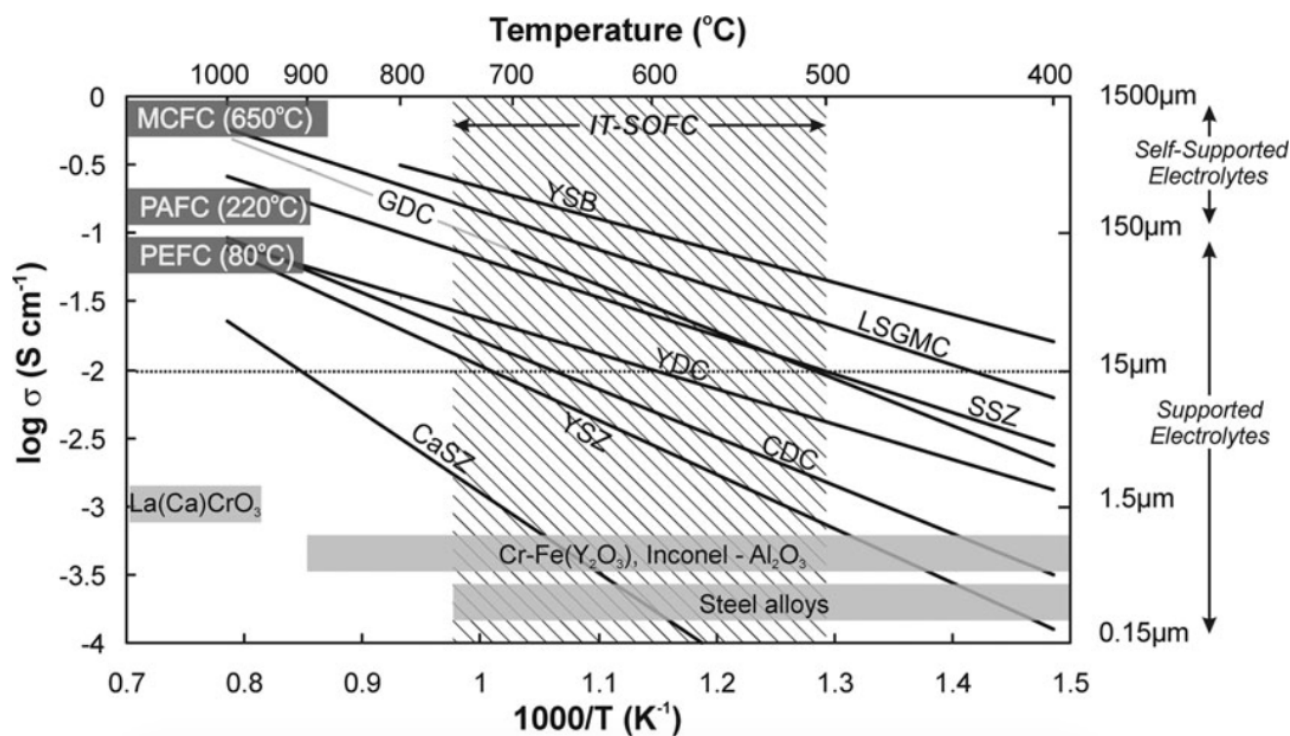


FIGURE 4.1. Variation of ionic conductivity with temperature for different electrolyte material [115]

increase the lifetime of the reactor. Hence, electrolytes with better conductivity at lower temperatures are being developed. Gadolinium doped ceria (GDC) exhibits mixed ionic and electronic conductivity (MIEC). GDC offers high conductivity at lower temperatures than YSZ in the range of 600-750 °C. But the MIEC behaviour can potentially lead to lower efficiency because some of electrons produced will conduct through the electrolyte and not pass through the external circuit. This will reduce the work produced by the SOC reactor. Apart from GDC other electrolytes with nano particles are also being developed [115–118]. Electrolyte material choices suitable for intermediate operation temperature of SOC reactors are shown in Figure 4.1.

Fuel Electrode

The fuel electrode in a SOC reaction should be able to facilitate redox reactions. In SOFC mode, the fuel electrode performs the role of anode by oxidising the fuel reactants, mostly hydrogen. In the SOEC mode, the electrode material should exhibit good kinetic behaviour for the reduction of oxidised gases such as H_2O and CO_2 . They should have high electronic conductivity. Apart from being thermally and chemically stable at high temperature, they should also be compatible with the electrolyte and its thermal expansion properties. Finally, they should be porous enough so that the gas diffusion to the reactant sites/triple phase boundary (TPB) is possible. The most common and widely used material for the fuel electrode is nickel cermet with corresponding electrolyte. Nickel is also a good catalyst for steam reforming, water gas shift and methanation reactions. The drawback of nickel is its propensity for carbon formation reactions which damage the electrodes [119]. Though for rSOC other possible materials such as perovskites for the fuel electrode are being investigated [116, 120].

Oxygen Electrode

The air electrode in SOC reactors should have a good kinetic profile for both oxygen reduction reaction and oxygen evolution reactions. It operates as the cathode in SOFC mode and anode in SOEC mode. The other requirements for the oxygen electrode mirrors that of fuel electrode. Perovskites are often used for the oxygen electrode. The most standard cathode materials are made of lanthanum manganite materials. More recently, Lanthanum strontium cobalt ferrate (LSCF) is widely used and proposed as standard for oxygen electrode owing to its better performance. The air electrode reactions are generally the slower reactions and rate limiting. Additionally, in rSOC operation and especially in SOEC operation, the air electrode exhibits higher degradation and delamination effects. Hence, intense research is being undertaken to improve the kinetics, stability and long term performance [115, 121–126].

4.1.2 Electrochemical loss mechanisms

As explained briefly in section 3.1.3, entropy is generated within SOC reactors due to internal irreversibility. The irreversibility can be either due to the process itself (such as chemical reactions, heat transfer over finite temperature difference etc.) which is unavoidable and can be explained using thermodynamics or due to electrochemical losses of the functional layers. The latter can be reduced by better engineering of the reactor and

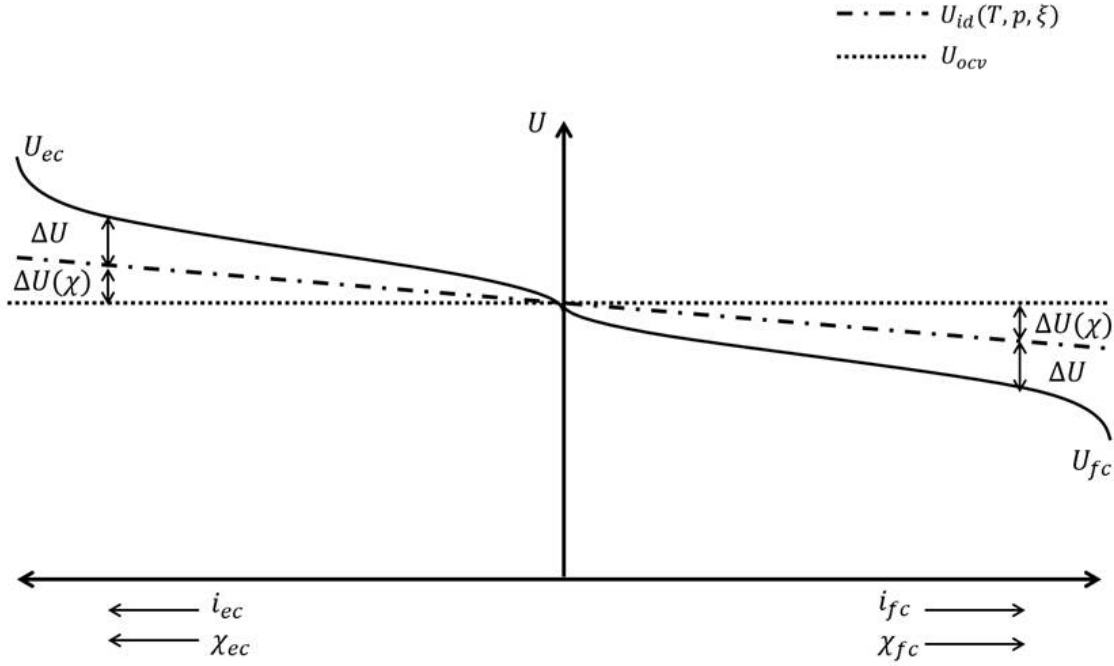


FIGURE 4.2. Variation of voltage losses in an SOC reactor in both SOFC and SOEC mode due to internal irreversibility.

optimising the materials used for the functional layers. In SOFC mode, the irreversibility leads to work loss in form of heat and hence producing less work than ideally possible value. In SOEC mode, the irreversibility indicates the additional work that should be supplied to the reactor to overcome the losses. The variation of reactor voltage and losses with current density is shown in Figure 4.2. In the figure, U_{OCV} represents the open circuit voltage at given composition, temperature and pressure when current is zero. The OCV is calculated using equation (3.9d). The voltage loss, $\Delta U(\chi)$ is due to extent of reaction and conversion ratio. This voltage loss or work loss is of thermodynamic nature as explained in section 3.1 and is unavoidable. The ideal voltage U_{id} can be evaluated by using either equation (3.11) or equation (3.12). The voltage loss ΔU is the loss due to electrochemical loss mechanisms and the reactor voltage is then given by equation (4.1). The major loss mechanisms are the ohmic, activation and diffusion losses.

$$U_{SOC} = U_{id} \pm \Delta U \quad (4.1)$$

$$\Delta U = \Delta U_{ohmic} + \Delta U_{activation} + \Delta U_{diffusion} \quad (4.2)$$

The performance of SOC reactors are generally described in equivalent resistance or Area Specific Resistance (ASR). The general definition of ASR is given by equation (4.3).

$$ASR = \frac{\Delta U}{j} \quad (4.3)$$

Ohmic

The ohmic voltage losses are a result of resistance to the movement of charge carriers. The biggest contribution of the ohmic losses arises from the electrolyte. The oxygen ion conductivity of the electrolyte is the measure of its performance. The lower the conductivity, the higher the resistance and hence the higher the ohmic contribution to the voltage loss. The ohmic loss obeys Ohm's law and is given by equation 4.4.

$$\Delta U_{ohm} = jASR_{ohm} \quad (4.4)$$

The ohmic resistance (ASR_{ohm}) is the sum of electrolyte resistance to oxygen ion transport, resistance of electrodes to electron transport. Additionally, in the reactor and reactor module, the resistance of the other functional layers such as contacting layer, interconnects and protective barrier layers are also included. The ohmic resistance of the electrolyte has a significant contribution to the total ohmic resistance. Therefore the thicker the electrolyte layer, then higher the ohmic loss. Hence, the ohmic resistance and total voltage losses are higher for ESC SOC reactor due to their thick electrolyte layer [86, 127, 128].

Activation

The activation losses are due to the charge transfer reactions that occur at the electrode–electrolyte interfaces. The activation losses are dictated by the electrode reaction kinetics and reaction mechanisms. This represents the energy or work required to overcome the energy barrier of the electrode reactions. The activation losses can be empirically described as the resistance to charge transfer and reaction, though the behaviour is not linear [129]. The activation losses are significant at lower current densities and reduce with higher temperatures. They are commonly described with the Butler-Volmer equation [86, 130].

Diffusion and conversion

The diffusion and conversion losses occur predominantly at higher current densities. At higher current densities the reactant conversion is high leading to lower concentration of reactants at the reaction surface. Additionally, the reactants in the flow channel must diffuse through the electrode to reach the reaction site and likewise the products should be able to diffuse out. This process also leads to work loss if the process is slow. Typically, in the electrode supported or metal supported cell design, the diffusion process can be significant [128].

4.1.3 Current State of the Art

Progress in SOC reactors has been achieved in both SOFC and SOEC operation. The current state of the SOC reactor development is primarily focussed on reducing the cost and degradation of the reactor. One aspect of cost reduction is to lower the operation temperature of the reactor. Lowering the operation temperature can potentially improve the lifetime and help in using relatively cheap materials for the different functional layers [118, 131]. Long operation hours with stable performances have been achieved for SOC reactors in both SOEC and SOFC operation mode [132, 133].

Development of rSOC reactors optimised for reversible operation is relatively new. There are certain material and durability challenges in developing rSOC reactors capable of running in both SOEC and SOFC mode. A key challenge in the reversible operation of SOC reactors arises from the oxygen electrode. Operation of current SOFC based reactors in SOEC mode can lead to delamination at the oxygen electrodes and degradation issues [134–136]. Though it has been reported in the literature that periodic and cyclical reversible operation of SOC reactors can help in reducing the overall degradation effects [137]. Further research and development work are being performed to improve electrode performance and rSOC reactors [30, 121, 122, 135, 138, 139]. Intermediate temperature rSOC reactors are also being developed to increase the lifetime and reduce degradation [140]. rSOC reactors with symmetrical electrode material were also proposed. Symmetrical rSOC reactors have the more or less similar electrodes for fuel and air side [141, 142]. Currently only few SOC reactors are commercially available. A planar ESC reactor is readily available in market [22].

4.2 Experimental study of commercial rSOC reactor

In this section a brief experimental analysis on a commercially available rSOC reactor is presented. The rSOC reactor was experimentally characterised with DLR's pressurised test rig facility. Series of experimental studies were performed in both SOFC and SOEC operation under different conditions. A brief overview of the experimental methodology is presented in section 4.2.1. The losses and ASR of the stack were evaluated. A simple empirical model was developed. The empirical model is further used for extending the theoretical rSOC system investigation presented in the previous chapter.

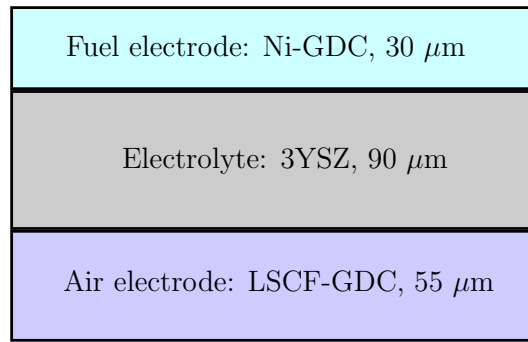


FIGURE 4.3. Schematic diagram of the planar ESC design commercial rSOC reactor used for experimental analysis.

The commercial rSOC reactor is a planar ESC design. The schematic diagram of the commercial rSOC reactor is provided in the Figure 4.3. It is a 10 cell planar stack with a maximum power output of 300 W in SOFC operation mode and a maximum electrical power intake of 1200 W in SOEC operation mode. The reactor has a closed fuel electrode and open air electrode design for gas manifolds. A single cell or Single Repeating Unit (SRU) of the stack is made of a 90 μm electrolyte made of 3 mol% of Yttria stabilized zirconia (3YSZ). For the fuel electrode a Ni-GDC cermet with a thickness of 30 μm is used. The LSCF perovskite is used for the air electrode. A GDC protective coating layer is used between the air electrode and electrolyte to prevent reactions between them. Together with the coating layer, the air electrode has a total thickness of 55 μm .

4.2.1 Experimental methods

The electrochemical losses in the rSOC reactor are evaluated by performing a series of experiments on the reactor. The series of experiments is designed to identify the different

loss mechanisms and quantify their losses. By this way the major losses in the reactor and effects of operation parameters on the reactor performance can be identified. Two major types of experiments performed to electrochemically characterise an rSOC reactor are i) $U(i)$ characterisation curves and ii) electrochemical impedance spectroscopy. The two methods will be briefly explained.

$U(i)$ characterisation plots

The $U(i)$ plot provides insight to the variation of voltage with current density. It also provides information on the resistances occurring in the cell. The $U(i)$ curves are generated by incrementally loading the cell with a constant current density in specified time intervals. At every loading, both current density and voltage are measured and plotted against each other. The loading is performed until a defined operational voltage is achieved [143]. The $U(i)$ characterisation curves can be performed under steady state and dynamic conditions. In steady state mode, the reactant flow to the rSOC reactor is set accordingly to maintain a constant reactant conversion at each current density. Whereas in dynamic measurements the reactant flow is constant and the current density is changed leading to varying reactant conversion values.

Electrochemical impedance spectroscopy (EIS)

Electrochemical Impedance Spectroscopy (EIS) is an experimental method to identify the different loss mechanisms occurring in rSOC reactor. It is based on the theory of electrical impedances. The resistance or polarisation losses in the rSOC reactor, especially the process such as the gas diffusion process and charge transfer reactions at the electrode–electrolyte interfaces are time dependant. Hence, unlike the ohmic resistance, the activation and diffusion polarisations losses have an impedance similar to a capacitive and inductive elements in electrical circuits. Hence, the losses can be broken down into different components by measuring the impedance of the rSOC reactor. The complex impedance is measured as a function of frequency over a wide range from 10 mHz to 800 kHz. An AC current or voltage perturbation is supplied to the reactor. The AC current signal at the output is phase shifted from the input signal and through this the impedance is measured. The impedance is resolved by plotting the imaginary part of the impedance with the real part in a Nyquist plot [144, 145]. Further reading on EIS can be found in literature [146–148].

Evaluation of ASR

The ASR of the rSOC reactor can be evaluated from either of the two experimental methods described above. For the present analysis, the rSOC reactor can be treated as a black box. The ASR can be evaluated from the $U(i)$ characterisation curves and is given by the equation (4.3). The evaluation of $\Delta U(j)$ in equation (4.3) is not straightforward. It can be evaluated from the OCV via equation (4.5).

$$ASR = \frac{\Delta U}{j} = \frac{U_{OCV} - U(j)}{j} \quad (4.5)$$

ASR evaluated by equation (4.5) is valid for experiments with low conversion (χ) values because the conversion effect is neglected when using U_{OCV} . In a process system higher reactant conversions (fuel utilisation) values are used. Hence, higher reactant conversion values are used for rSOC reactor experiments to simulate system relevant conversion rates. Therefore, the ASR values evaluated using (4.5) will be overestimated. A reactant conversion correction should be incorporated in the ASR evaluation to overcome the error induced by (4.5). This can be achieved by evaluating the ΔU assuming the reactor to be either a Continuously Stirred Tank Reactor (CSTR) or a Plug Flow Reactor (PFR). Assuming CSTR behaviour, the ASR is given by equation (4.6). The average ideal voltage is evaluated by using the outlet composition due to CSTR assumption [143]. The CSTR assumption is valid though it is not strictly correct. This assumption can lead to slight underestimation of the ASR of rSOC reactor.

$$ASR = \frac{U_{id,avg} - U(j)}{j} = \frac{U_{id}(x'', T, p) - U(j)}{j} \quad (4.6)$$

In reality the rSOC reactor is closer to PFR behaviour. For a PFR model, the ideal voltage must be integrated over the length of the reactor taking into account the composition variation along the length. Apart from the composition, temperature and local current density may vary as well. This leads to more complex forms of equation of ASR [143, 149]. In this work, the ASR is evaluated based on reactant conversion dependent ideal voltage. The voltage difference is calculated by rearranging equation (4.1). The ASR is then given by equation (4.7)

$$ASR = \frac{U_{id}(T, p, \xi) - U(j)}{j} \quad (4.7)$$

where:

$$U_{id} = \frac{W_{rev}}{I} = \frac{-(G_2 - G_1)}{I}$$

The ideal voltage $U_{id}(T, p, \xi)$ is calculated from ideal work (W_{rev}) as described in (3.11) in section 3.1.

4.2.2 rSOC reactor experimental analysis

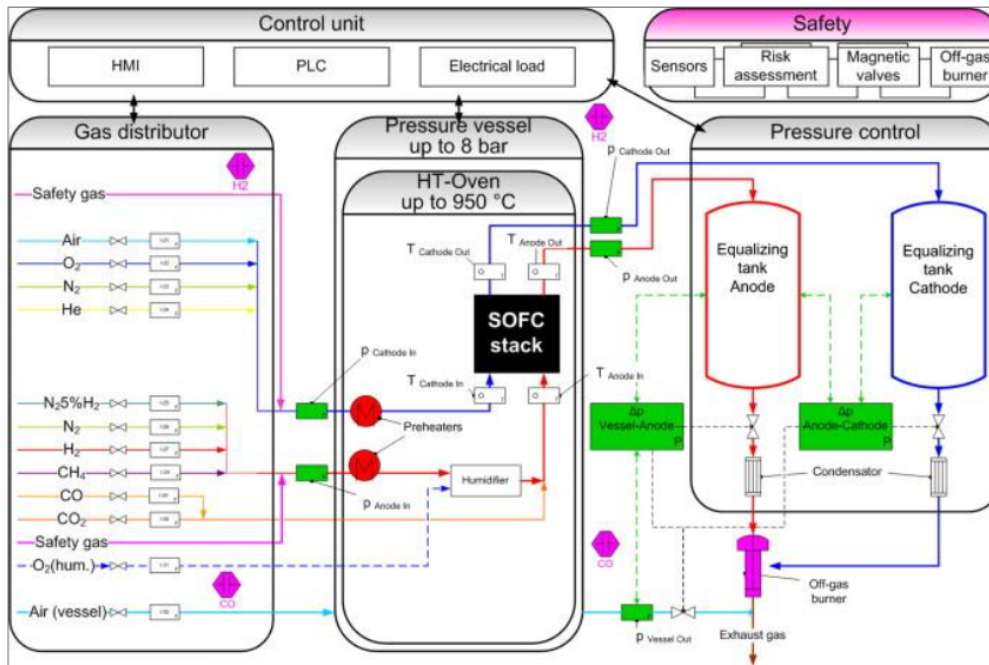


FIGURE 4.4. Scheme of pressurised test rig facility at DLR [150].

The commercial rSOC reactor was experimentally characterised at the DLR's pressurised test facility. The scheme of DLR's pressurised test facility is shown in Figure 4.4. It can reach a maximum pressure of 8 bar. A differential pressure of 10 mbar to 500 mbar between the fuel chamber and air chamber can be maintained. The furnace can reach a maximum temperature of 950 °C. For more details on the test facility please refer to Seidler et al. [150].

The U(i) characterisation curves and electrochemical impedance spectroscopy analysis was performed in both SOEC and SOFC operation modes. The experimental conditions were selected such that they closely resemble the system operation conditions. Experiments were performed at steady conditions with constant reactant conversion and under dynamic mode with varying reactant conversion. The reactor pressure and furnace temperature were from varied from 1.4 bar to 8 bar and 750 °C to 850 °C respectively in both SOFC and SOEC mode. The reactant conversion was varied from 55 - 85 % in SOFC mode and 60 - 75 % in SOEC mode. EIS measurements were performed at OCV conditions at different temperatures from 700 °C to 850 °C. They were primarily performed to accurately quantify the ohmic resistance in the rSOC reactor. EIS measurements under

loaded steady state conditions were also performed at selected current densities. During all the measurements, the core reactor temperature was measured by measuring the temperatures of the centre SRU (fifth cell in a 10 cell SOC reactor) of the SOC reactor. Temperatures were measured at the inlet, outlet and at the centre of the fifth SRU. It is expected that the temperature measured at the centre of the SRU located at the middle of the SOC reactor represents the "*core reactor temperature*" which would henceforth be referred to as the "*characteristic reactor temperature*".

Error estimation

The test rig was calibrated before the commencement of each experimental campaign. The gas flow rates were measured and controlled using industrial standard mass flow controllers. The mass flow controllers had an inherent error of 0.05 % for the flow rates. The voltage was measured using an Siemens SPS unit with an error percentage of 0.2 %. The temperature measurements within the stack was measured using standard K-type thermocouples with an error of 0.5 %. The thermocouples were approximately placed at the inlet, outlet and middle of the SOC. The uncertainty in placement of thermocouple was not easily quantifiable and was estimated to be about 5 %, hence the temperature measured may not be exactly at the centre of the SRU. The OCV measured by the test rig was ± 5 mV from the OCV values theoretically predicted for the experimental conditions.

4.2.3 Analysis of experimental results

The U(i) characterisation curves for the rSOC reactor in SOFC mode measured under steady state conditions is shown in Figure 4.5. The measurements were performed with a gas composition of 40 % H₂ and 60 % N₂. Air flow rate was varied such that the air utilisation is constant at 25 % at all current densities. The behaviour of the rSOC stack with pressure is shown at top right in Figure 4.5. The U(i) curves are plotted for a reactant conversion of 70 % in SOFC mode. The corresponding variation of the characteristic reactor temperature at different pressures is shown in the top right graph in Figure 4.5. The characteristic reactor temperature is the temperature measured at the centre of an SRU which is located at the middle of a SOC reactor. It can be seen that the pressure has a positive effect on the rSOC performance in SOFC mode and it is significant at lower pressures but diminishes at higher pressure [151]. The effect of reactant conversion on the rSOC performance in SOFC mode can be observed from

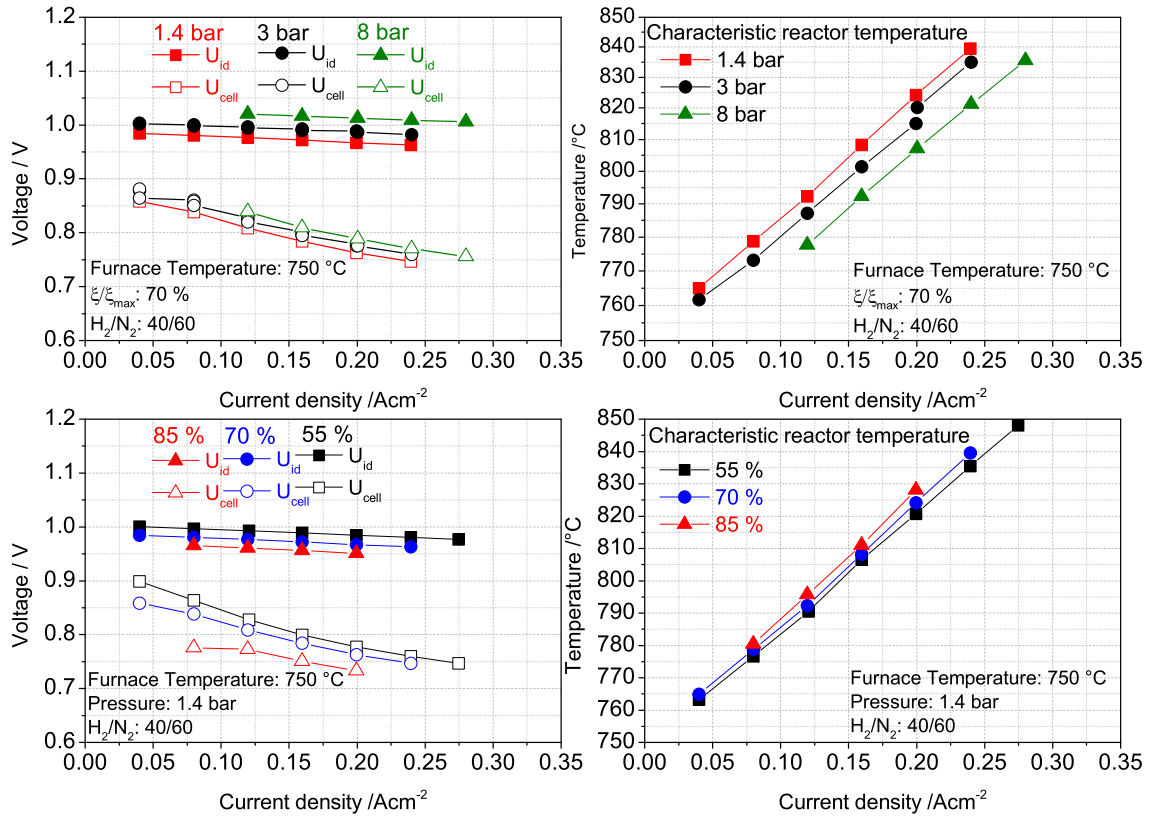


FIGURE 4.5. Top left: $U(i)$ characterisation curve in SOFC mode at different pressures at reactant conversion of 70 % and furnace temperature of 750 °C. Top right: Variation of the measured characteristic reactor temperature at different different pressure for reactant conversion of 70 % and furnace temperature of 750 °C. Bottom left: the $U(i)$ performance at different conversion rates in SOFC mode at 1.4 bar pressure and 750 °C furnace temperature. Bottom right: variation of characteristic reactor temperature at different conversion rates is shown for pressure of 1.4 bar and furnace temperature at 750 °C. An error of 0.2 % is estimated for voltage measurements and 0.5 % is estimated for temperature measurements.

bottom left graph of Figure 4.5 and variation of characteristic reactor temperature with reactant conversion can be seen from bottom right graph in Figure 4.5 Higher reactant conversion has a negative on the SOFC voltage. As discussed in section 3.2 from thermodynamics, higher reactant conversion results in faster work extraction thereby resulting in higher entropy generation. This is shown in the ideal voltage plot at 85 % and 55 %. The performance of the reactor is analysed to understand the behaviour and effect of operation parameters on the different loss phenomena.

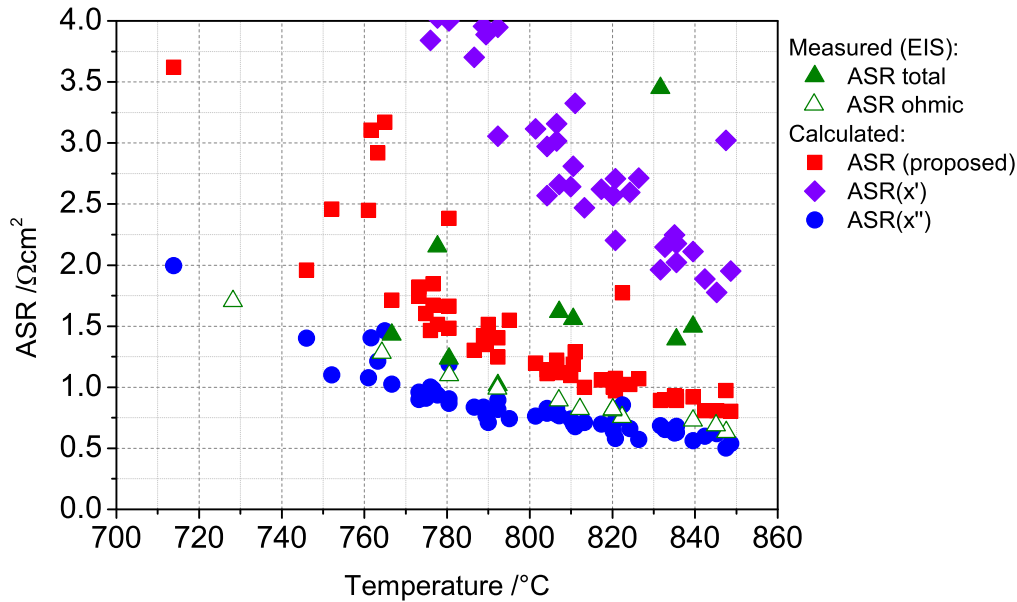


FIGURE 4.6. The ASR is calculated using the equations (4.5) and (4.6) using equation (4.7). Red squares show the ASR computed by using equation (4.7). Blue cross indicates ASR calculated using Nernst equation with outlet composition for computing ideal voltage. Green triangles indicate ASR measure with EIS at selected current densities. Purple stars indicate ASR computed using Nernst equation with inlet composition for calculating the ideal voltage

The ASR calculated from the $U(i)$ measurements is shown in Figure 4.6. In this work, the ASR (indicated by red squares in the figure) is calculated from the $U(i)$ measurements using equation (4.7). The ASR calculated using EIS measurements were

taken as reference to compare the ASR calculated using the proposed method. The ASR calculated by the proposed method is closer (or within range) to the ASR measured using EIS. Hence, this further validates the use of equation (4.7) for calculating the ideal voltage. A comparison of ASR calculated using other methods is also shown in Figure 4.6. The blue cross in Figure 4.6 indicates ASR calculated by using Nernst equation with outlet composition as shown in equation (4.6) to calculate the ideal voltage. This yields an ASR considerably lower than the value measured using EIS and also lower than the ohmic component of ASR measured using EIS. Likewise, the purple stars in Figure 4.6 indicate the ASR calculated with ideal voltage calculated using Nernst equation with inlet compositions as shown in equation (4.5). This results in ASR values considerably higher than the values measured using EIS. Hence, this analysis further reaffirms the use of equation (4.7) to calculate the ideal voltage and ASR of an rSOC reactor from $U(i)$ measurements.

Impact of pressure

The impact of pressure on the rSOC reactor is studied by discretising the ASR calculated using (4.7). The ohmic losses were characterised from EIS measurements performed at OCV conditions at different temperatures. These measurements act as a baseline for ohmic losses as a function of temperature. The ohmic loss for the same reactor from EIS measurements is reported in [152]. A temperature dependant polynomial function for the ohmic losses was obtained. In Figure 4.7 the variation of the characteristic reactor temperature measured at different current densities with pressure under steady state conditions is shown. An interesting trend of lower reactor temperature at higher pressure is observed. This can be either due to test rig preheater limitation or due to the air utilisation rate used during experiments. Air utilisation value determines amount excess air supplied to the SOC reactor than the stoichiometric requirement. This is done in order to remove the heat produced due to the losses. Lower air utilisation implies large flow rates of air supply than required. For the experiments, a constant air flow rate corresponding to an air utilisation of 25 % was used at all pressures. At higher pressures, the voltage losses are lower and therefore less heat is generated. Due to which, the high air flow rate used during the experiments is further cooling the reactor and reducing the core reactor temperature at higher pressures. This temperature decrease leads to higher ohmic voltage losses with pressure seen from bottom figure in Figure 4.7. Secondly, a linear increase of the ohmic voltage loss is expected with increasing current density. But as it can be seen in Figure 4.7, for a given pressure, the temperature also

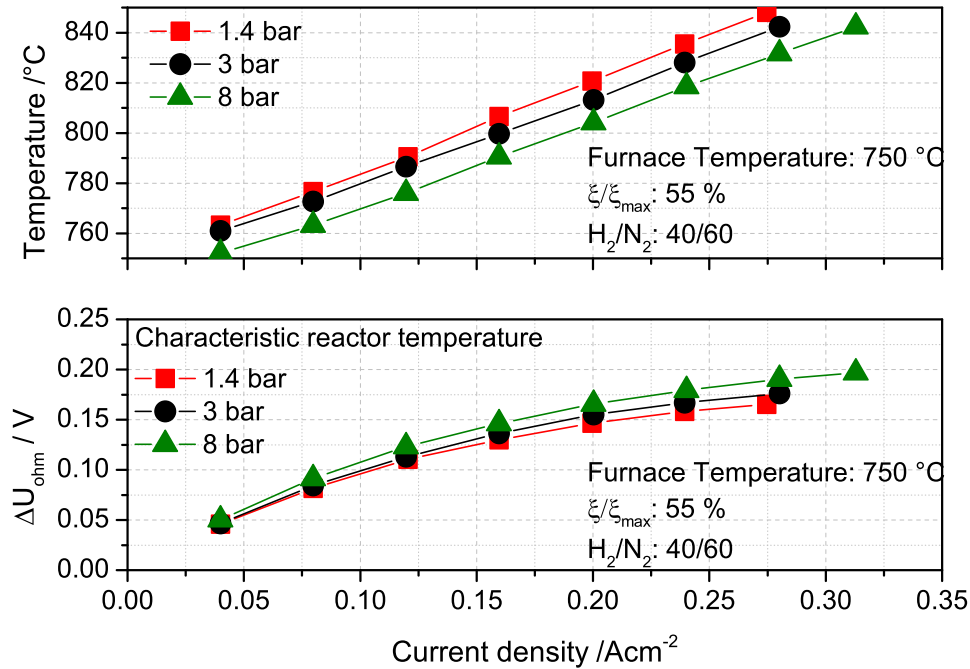


FIGURE 4.7. Impact of pressure on the SOC reactor performance is shown. The top figure shows the variation of characteristic reactor temperature with current density at different pressures at a conversion ratio of 55 %. Corresponding ohmic voltage loss vs. current density at different pressures is depicted in bottom figure

increases with current density. The ohmic resistance of the reactor is non linear function of temperature. Therefore, we observe a non-linear behaviour of ohmic voltage losses with increasing current density due the temperature effect.

The impact of pressure on polarisation losses ($\Delta U_{activation} + \Delta U_{diffusion}$) can be observed in Figures 4.8 and 4.9. The effects of pressure and temperature on activation losses due to the electrode reactions are not straightforward. Higher pressures can lead to higher partial pressure of reactants. This in turn promotes adsorption of reactants on the reaction sites leading to improved kinetics thereby decreasing activation losses. On the other hand, lower temperatures lead to sluggish reaction kinetics at the electrodes leading to higher activation losses [153–155]. From the Figure 4.8 and Figure 4.9 a clear trend is observed, the polarisation losses decrease from 1.4 bar to 3 bar but increase for 8 bar. Also, it can be observed from both the figures, as the pressure is increased, the

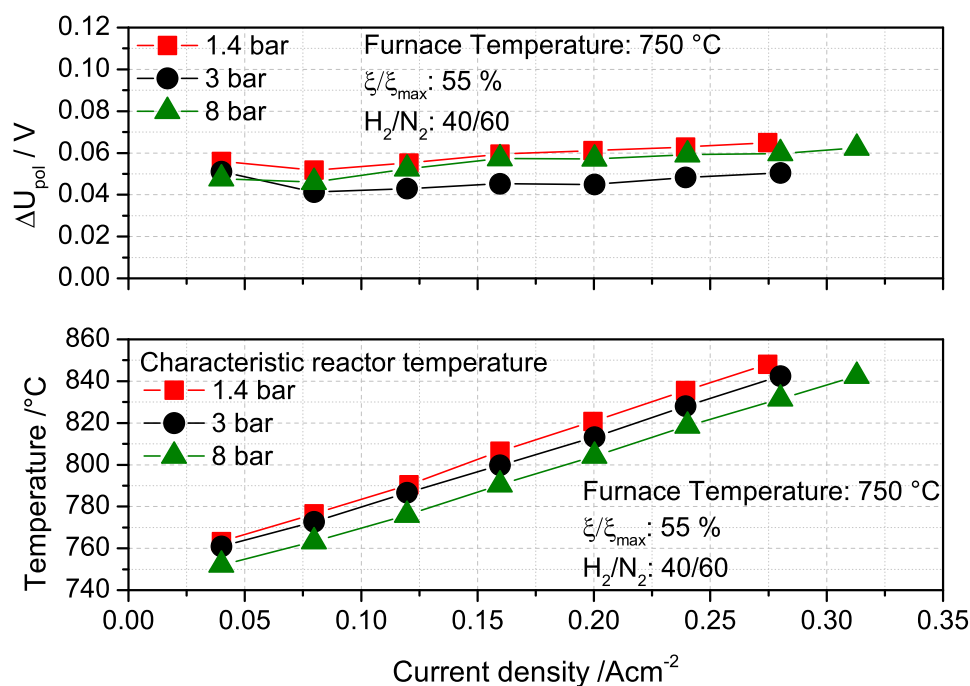


FIGURE 4.8. Variation of polarisation losses with pressure for rSOC reactor at different pressures for a conversion ratio of 55 % is shown in the top figure. The bottom figure depicts the variation of characteristic reactor temperature with current density at different pressures for a conversion ratio of 55 %.

measured characteristic temperature of the rSOC reactor is decreasing. The reason for the decrease in measured core temperature was discussed earlier. Hence, based on this observation an explanation for the behaviour of the polarisation losses with pressure can be formulated. One hypothesis for the observed effect is as follows. From 1.4 bar to 3 bar, the increase in pressure has a positive effect on the electrode process overcoming the negative temperature effect leading to lower polarisation losses. At 8 bar, the positive effect of pressure is no longer able to overcompensate the negative temperature effect leading to higher polarisation losses. Though a further experimentation and analysis is required to substantiate the hypothesis. Pressure increase has positive effect on diffusion of gases thereby reducing diffusion losses [155]. The diffusion effect is generally negligible for ESC type SOC reactors [156]. With increasing current density, an increase in polarisation losses is normally expected due to the losses caused by diffusion of reactants through the electrodes to the reaction sites. In Figure 4.8, it can be seen that

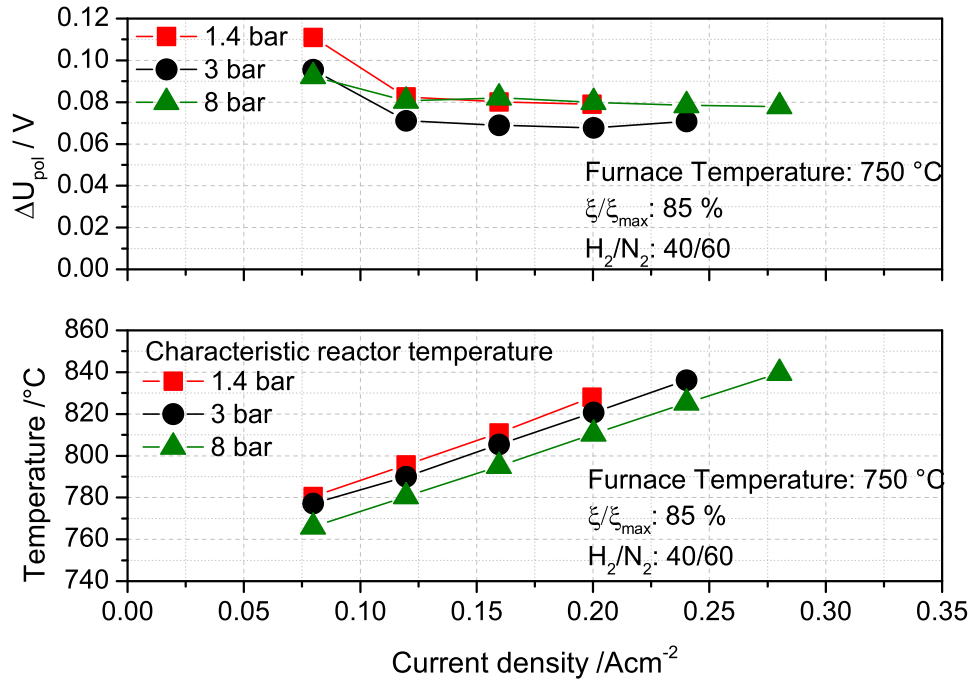


FIGURE 4.9. Variation of polarisation losses with pressure for rSOC reactor at different pressures for a conversion ratio of 85 % is shown in the top figure. The bottom figure depicts the variation of characteristic reactor temperature with current density at different pressures for a conversion ratio of 85 %.

that the polarisation voltage losses is almost constant as current density in increased. This further validates the negligible effect of diffusion on the polarisation losses of ESC type SOC reactors since ESC type SOC reactors have very thin electrodes.

Impact of reactant conversion

The impact of reactant conversion on the reactor behaviour can be described based on the polarisation losses. The variation of polarisation losses on the reactant conversion is shown in Figure 4.10. It can be seen that the polarisation losses increase with increasing reaction conversion. At higher conversion rates, a higher concentration of reactants is utilised possibly leading to lower concentrations towards the end of the reactor. Therefore, leading to an increase in both activation and conversion losses. The losses increase by 10 mV when increasing the conversion rate from 55 % to 85 %. Higher polarisation losses were observed at lower current densities at 70 % and 85 % reaction conversion rates.

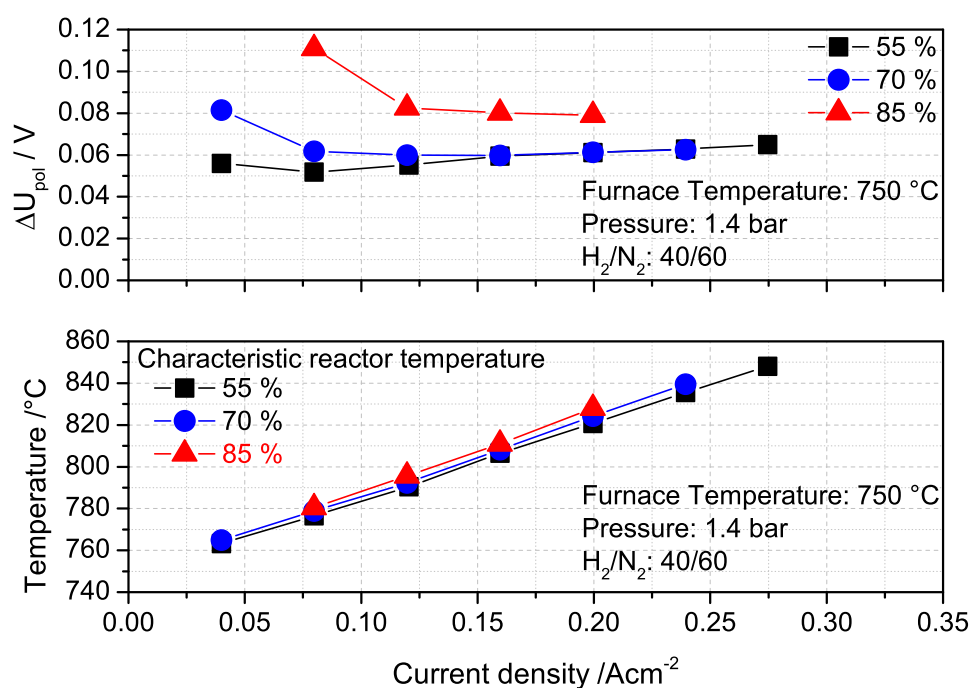


FIGURE 4.10. Variation of polarisation losses for different reactant conversion ratios at 1.4 bar pressure is shown in the top figure. The bottom figure depicts the variation of characteristic reactor temperature with current density at different conversion ratio at a pressure of 1.4 bar.

To maintain high reaction conversion rates at low current densities (below 0.1 A/cm²), low flow rates of reactants were used. This could have led to an uneven distribution of reactants within the reactor and reactant depletion effects towards the end of the reactor. Hence, we observe higher polarisations at lower current densities for 70 % and 85 % conversion ratios. This hypothesis should be tested with further experiments.

To summarise, both pressure and reactant conversion has impact on the rSOC reactor performance. In SOFC mode, it was shown that at the higher pressure experiments, lower reactor temperatures were observed. This can be either due to two possible reasons.

1. Gas preheater limitations in the test rig such that the gas was not sufficiently preheated to furnace temperature therefore, the gas cooled the rSOC reactor at higher pressures.
2. At higher pressures, the rSOC reactor has a higher voltage leading to less heat

generation. Hence, the high air flow rate is cooling the reactor, thereby reducing the core reactor temperature at higher pressures.

Both hypotheses has to be verified. In effect, it is difficult to maintain constant temperature at all experimental points in steady state rSOC stack measurements. In comparing the contribution of different loss components to ASR, it can be seen from the above analysis that the ohmic losses are most dominating at all conditions. The ohmic losses account to almost 75 % of ASR at all measured conditions. Though the analysis was presented for SOFC operation, the effects of pressure and reactant conversion on polarisation losses is expected to be similar in SOEC mode. The loss phenomena are highly dominated by the ohmic loss from electrolyte. The ohmic loss will be dominant also in SOEC mode. In SOEC mode, the pressure will have a negative effect on the theoretical ideal voltage as discussed in section 3.2. But with increase in pressure, the reaction kinetics can increase performance and reduce the polarisation losses. For SOEC mode, the operation pressure should be found as an optimum between the negative thermodynamic effect of pressure and the positive effect of pressure on reaction kinetics [157].

4.2.4 Phenomenological ASR model

Based on the analysis presented above a simple phenomenological ASR model was developed. The model purpose is to quickly compute the rSOC reactor performance at desired system operation conditions. This is useful for quick computation of system performance. A more detailed rSOC reactor model with proper resolution of the loss mechanism is discussed in chapter 5.

From the experimental analysis it was observed that the ASR of the commercial ESC design rSOC reactor varies strongly with temperature. Effect of pressure on the ASR of rSOC reactors is observed to be minimal in comparison to the effect of temperature. Due to the thick electrolyte layer of the rSOC reactor, the ohmic loss is the major loss mechanism. The ohmic resistance of the electrolyte is a function of temperature and not of pressure. The observed effect is true for an ESC type SOC reactor as reported in literature [128, 156, 158]. Hence, a simple temperature dependant phenomenological model of ASR as described by (4.8) is justified.

$$ASR = a_1 + a_2 \cdot \exp(a_3 \cdot T) \quad (4.8)$$

The parameters a_1, a_2 and a_3 are fitted to the ASR values using the Levenburg Marquardt algorithm of nonlinear curve fit. Fitted phenomenological model and ASR

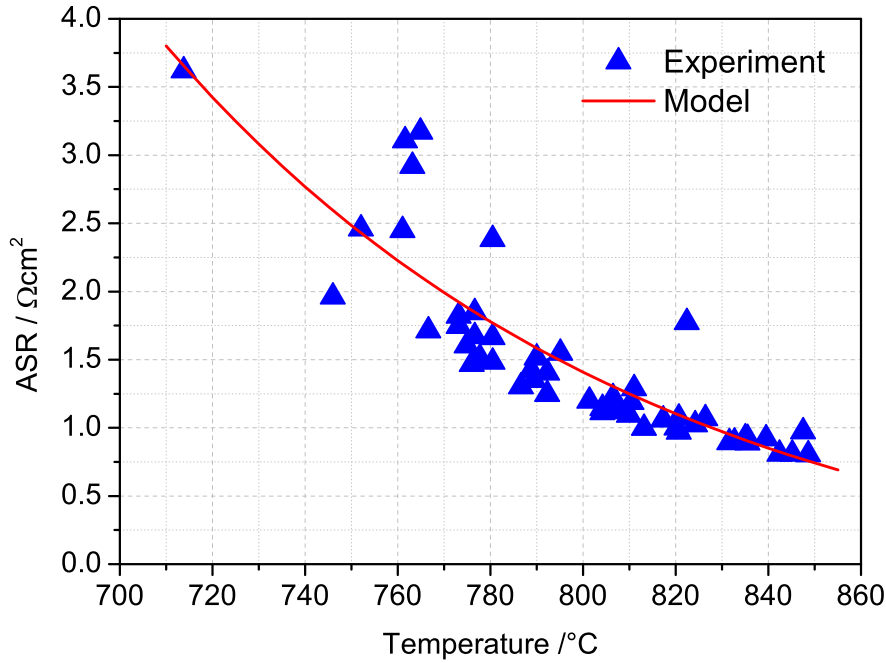


FIGURE 4.11. Comparison of the phenomenological ASR model fitted to experimental results.

values calculated from measurements using equation (4.7) is shown in Figure 4.11. The Figure 4.12 depicts the $U(i)$ characteristic in SOEC mode measured and calculated using the phenomenological model. Though the phenomenological model was developed from ASR values obtained using SOFC measurements, it gives reasonable accuracy when applied to $U(i)$ characteristic curves in SOEC mode.

4.3 rSOC system round trip efficiency using commercial rSOC reactor

In this section an rSOC system based on the commercial rSOC reactor is presented. The achievable roundtrip efficiency using the commercial rSOC reactor is compared against the theoretical ideal limit presented in section 3.2. The system performance for H-O and H-CO chemistry based rSOC systems are analysed.

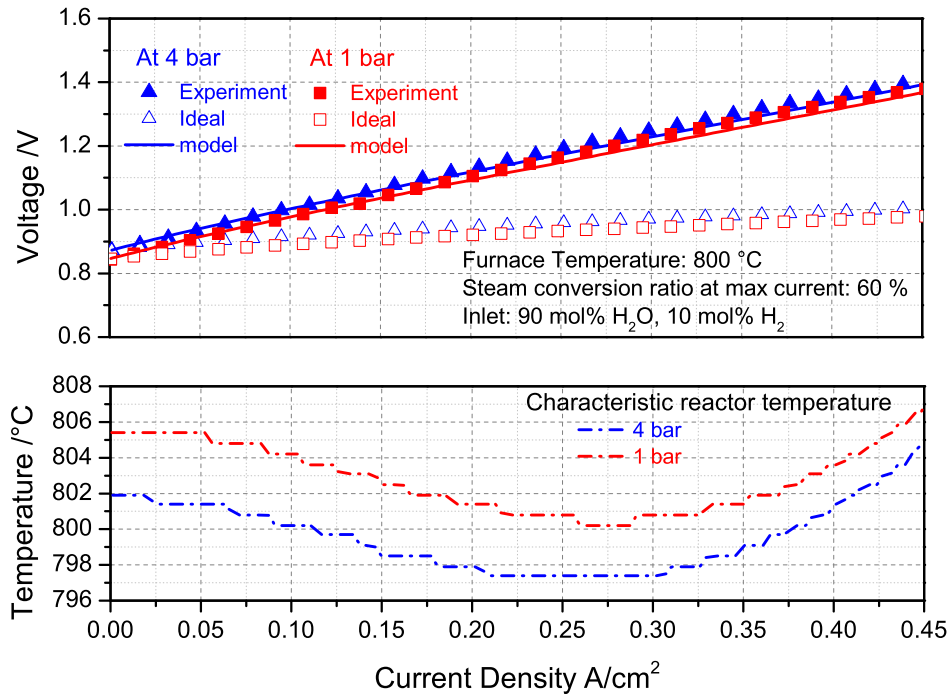


FIGURE 4.12. (Top) Experimental values presented for r-SOC furnace temperature 800 °C, pressure 1 bar (red) and 4 bar (blue). Inlet conditions of 90 mol% H₂O and 10 mol% H₂. Steam conversion ratio of 60 % at maximum current density. (Bottom) Variation of the characteristic reactor temperature with current density during the U(i) measurements.

4.3.1 System description

Two concepts were presented based on the thermal management strategy between the SOFC and SOEC operation. The benefits and the advantages of employing heat storage as a thermal management system between the SOEC and SOFC mode were highlighted. In this section, the theoretical rSOC system concept with heat storage thermal management is used as a basis. The phenomenological electrochemical model of the rSOC reactor presented in section 4.2.4 is used. The assumptions made for the theoretical model presented in section 3.2 are used here. They are repeated here for completeness.

Assumptions:

1. The SOC reactor is assumed to be isothermal and isobaric.

4.3. RSOC SYSTEM ROUND TRIP EFFICIENCY USING COMMERCIAL RSOC REACTOR

2. Reactions occur at the isothermal reactor temperature.
3. Time period of reactor operation in fuel cell mode is equal to that of electrolysis mode.

$$t_{fc} = t_{ec} \quad (4.9)$$

4. Charge transferred during the discharge mode (fuel cell) is equal to the charge transferred during the charging mode (electrolysis).

$$\Delta n_{o,fc} = \Delta n_{o,ec} \quad (4.10)$$

5. Assumptions 3 and 4 imply that the current obtained from the SOC reactor in SOFC mode is equal in magnitude to the current supplied to SOC reactor in SOEC mode.

$$I_{fc} = I_{ec} \quad \text{and} \quad \xi_{fc} = \xi_{ec} \quad (4.11)$$

6. Assumptions 3 – 5 ensure that the fuel tank (subscript r) and exhaust tank (subscript p) in the system are brought to the same thermodynamic state before discharge.
7. Ideal heat transfer is assumed for heat recovery units. Therefore, the system performance is a measure of the reactor performance.
8. All the gases are modelled using ideal gas equations of state.

The roundtrip efficiency for an rSOC system with heat storage using the commercial reactor is given by 4.12.

$$\eta_{rt} = \frac{W_{fc}}{W_{ec}} \quad (4.12)$$

where

$$W_{fc} = (U_{id,fc} - \Delta U_{fc}) I_{fc}$$

$$W_{ec} = (U_{id,ec} + \Delta U_{ec}) I_{ec}$$

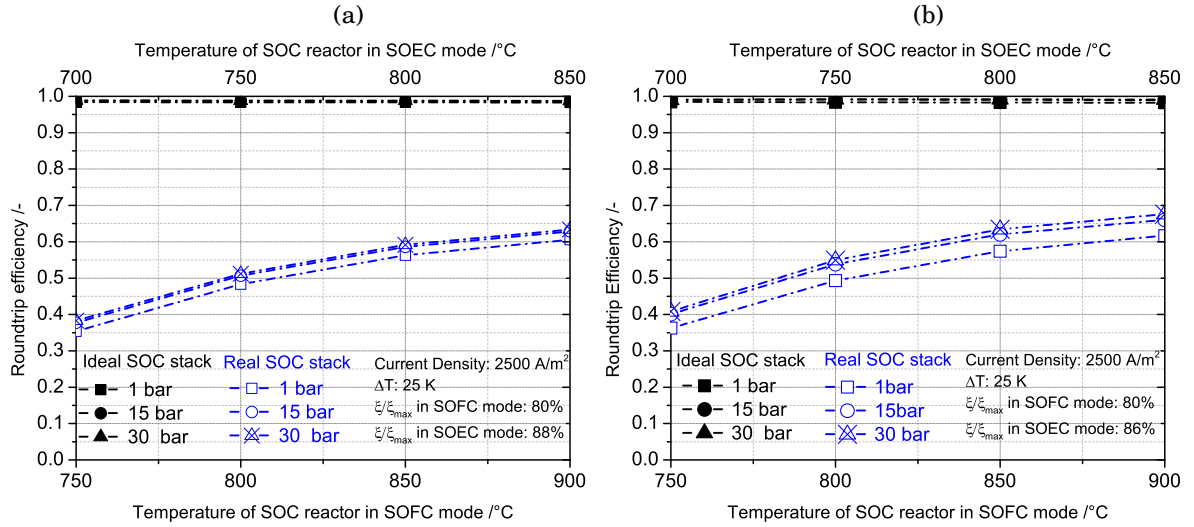


FIGURE 4.13. (a) Comparison of roundtrip efficiency of an rSOC system with ideal reactor and commercial reactor for H-O system $\frac{\xi}{\xi_{max}} = 88\%$ in SOEC mode and $\Delta T = 25K$. (b) Comparison of roundtrip efficiency of an rSOC system with ideal reactor and commercial reactor for H-C-O system $\frac{\xi}{\xi_{max}} = 88\%$ in SOEC mode and $\Delta T = 25K$. $T_{fc} - T_{ec} = 2\Delta T$.

4.3.2 Results and Discussion

The roundtrip efficiency of an rSOC system with a commercial reactor is shown in Figure 4.13. At a reactor temperature of 850 °C in SOFC mode and $T_{fc} - T_{ec}$ of 50 K, a roundtrip efficiency of 55 % is achievable for an H-O chemistry system at 1 bar pressure and 80 % conversion in SOFC mode. Under the same conditions a similar roundtrip efficiency is achievable for an H-C-O system. The roundtrip efficiency of an rSOC system with an ideal reactor under the same conditions was shown to be around 98 %. The difference is due to the high ASR of the commercial rSOC reactor. With a better rSOC reactor with lower ASR, the roundtrip efficiency can move towards ideal roundtrip efficiency. For the rSOC system with commercial reactor, the roundtrip efficiency varies strongly with reactor temperature due to the inverse relation of ASR with temperature. Roundtrip efficiency of the commercial rSOC reactor falls to 35 % at 750°C for both H-O and H-C-O system.

The heat ratio (θ) is defined as the ratio of heat required in SOEC operation to heat produced in SOFC operation. Negative values indicate endothermic operation in SOEC mode and heat is supplied to the rSOC reactor from heat storage. Positive values indicate the rSOC reactor has entered exothermic region during SOEC mode. This occurs when

4.3. RSOC SYSTEM ROUND TRIP EFFICIENCY USING COMMERCIAL RSOC REACTOR

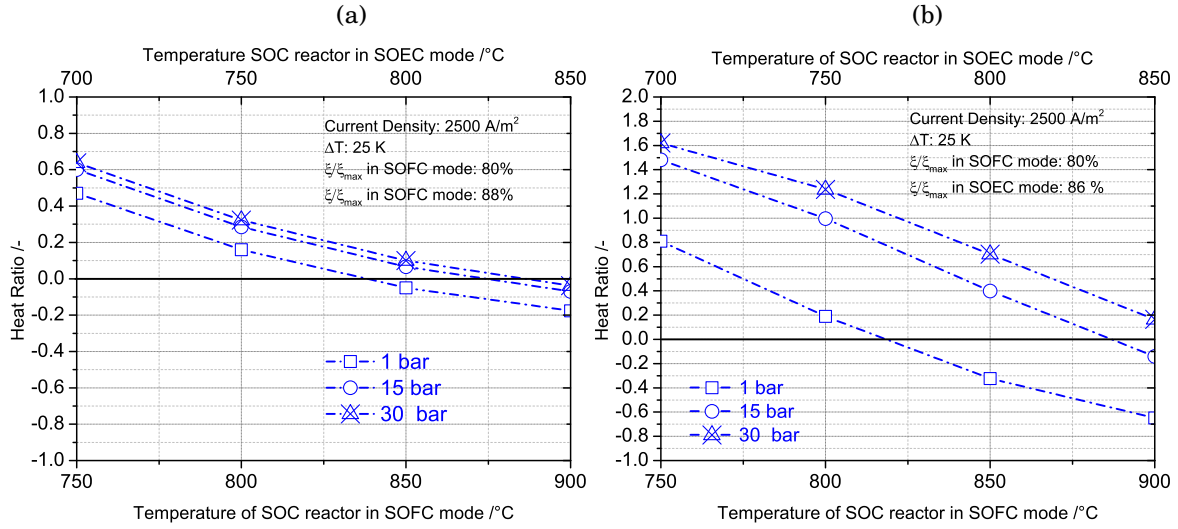


FIGURE 4.14. (a) Heat ratio for H-O system with commercial reactor, $\frac{\xi}{\xi_{max}} = 88$ % in SOEC mode. (b) Heat ratio for H-C-O system with commercial reactor, $\frac{\xi}{\xi_{max}} = 86$ % in SOEC mode.

the total heat generated due to internal losses and other internal chemical reactions is greater than the endothermic heat required for electrolysis H_2O and CO_2 . The impact of system operation parameters on heat ratio is shown in Figure 4.14. For the same conditions of 850 °C in SOFC mode, 1 bar pressure, conversion ratio of 80 % in SOFC mode and $T_{fc} - T_{ec} = 50K$, the heat ratio (θ) for the real system is just around -5 % for H-O system. Meaning, only 5% of heat produced in SOFC mode is consumed in SOEC mode. Meanwhile, for the same conditions, the heat ratio (θ) was found to be around -30 % for an H-C-O system. A higher value of θ for a H-C-O system is due to lower heat production in SOFC mode. In the SOFC mode, along with the electrochemical reaction, the endothermic internal reforming reaction (R 3.11) takes place within the reactor. This reduces the heat produced during the SOFC operation and hence reducing the heat stored in the heat storage. In the SOEC mode at 1 bar and 800 °C, the reverse of reaction (R 3.11), the methanation reaction, is not thermodynamically feasible and does not occur within the reactor. Additionally, the heat generated due to the losses is not sufficient to meet the thermal requirements of the endothermic electrochemical reactions and SOEC process is highly endothermic. Hence, a higher value of heat ratio for the H-C-O system is obtained.

At lower reactor temperatures, the ASR increase and therefore the heat generated

due to the losses increase. Hence, rSOC reactor can become exothermic in both SOEC and SOFC modes. This can be observed from the heat ratio of the H-O system. At 750 °C in SOFC mode and 30 bar pressure, the heat ratio is 60 %. This imply that the SOEC operation is exothermic and heat produced during SOEC operation is 60 % of the heat produced during the SOFC process. In the H-C-O system this is further pronounced due to internal methanation reaction (reverse of reaction (R 3.11)) which occurs at lower temperatures at higher pressures. The value of heat ratio at 750 °C in SOFC mode and 30 bar pressure is 1.6. This indicates, that SOEC operation is 1.6 times more exothermic than SOFC operation.

Impact of Temperature difference

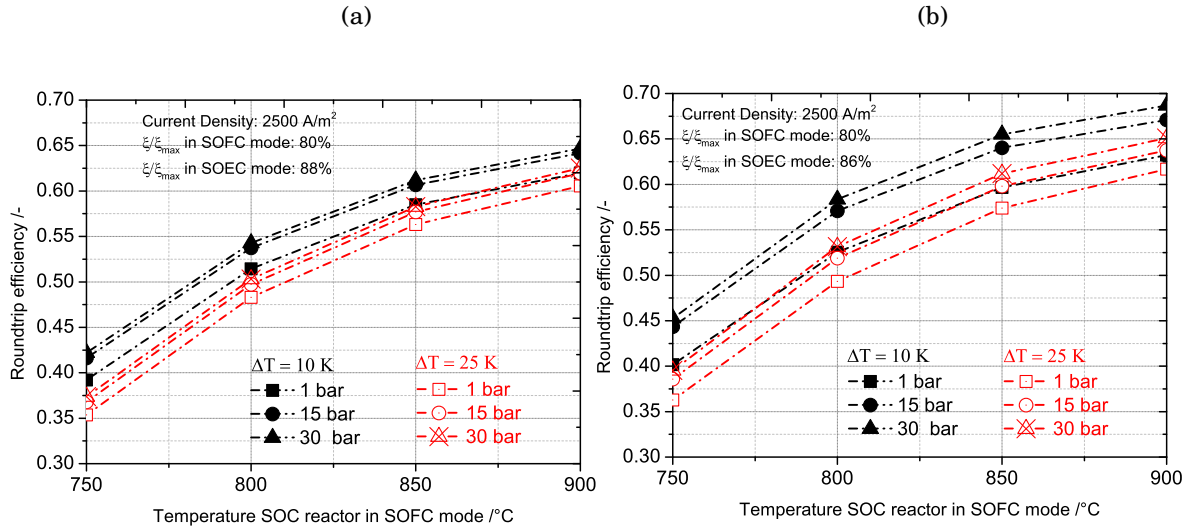


FIGURE 4.15. (a) Impact of ΔT on roundtrip efficiency for H-O system with commercial reactor, $\frac{\xi}{\xi_{max}} = 88\%$ in SOEC mode. (b) Impact of ΔT on roundtrip efficiency for H-C-O system with commercial reactor, $\frac{\xi}{\xi_{max}} = 86\%$ in SOEC mode. $T_{fc} - T_{ec} = 2\Delta T$

The impact of the temperature difference between the rSOC reactor and heat storage is shown in Figure 4.15. Temperature difference between rSOC reactor and heat storage implies a temperature difference between two operation modes. A temperature difference of 25 K between the rSOC reactor and heat storage would result in a temperature difference of 50 K between SOFC operation temperature and SOEC operation temperature. At a reactor temperature of 850 °C in SOFC mode and 1 bar pressure, the roundtrip efficiency increased from 56 % to 58 % when ΔT was reduced from 25 K to 10 K for H-O

4.3. RSOC SYSTEM ROUND TRIP EFFICIENCY USING COMMERCIAL RSOC REACTOR

system. Same magnitude of change can be observed for the H-C-O system as well. In general, the effect can be observed at other rSOC reactor temperatures.

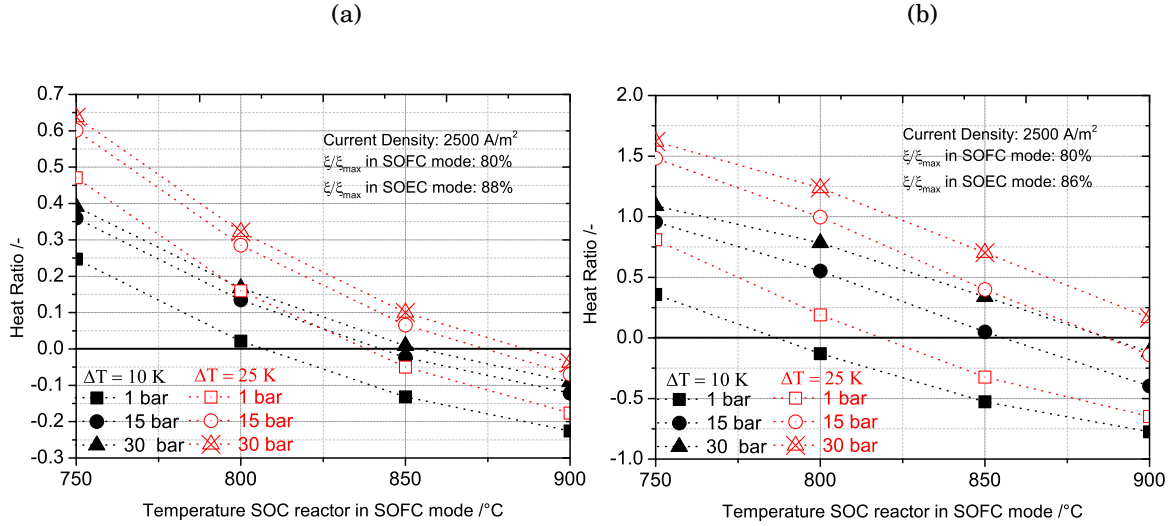


FIGURE 4.16. (a) Impact of ΔT on heat ratio for H-O system with commercial reactor, $\frac{\xi}{\xi_{max}} = 88\%$ in SOEC mode. (b) Impact of ΔT on heat ratio for H-C-O system with commercial reactor, $\frac{\xi}{\xi_{max}} = 86\%$ in SOEC mode. $T_{fc} - T_{ec} = 2\Delta T$.

The effect of temperature difference between the two operation modes on heat ratio is shown in Figure 4.16. In the H-O system, as the temperature difference is reduced, the heat ratio moves towards endothermic regions. At the reference conditions of 850 °C in SOFC mode and 1 bar pressure, the heat ratio moved from -15 % to 5 % as ΔT was increased from 10 K to 25 K. There are two reasons for the observed behaviour. The first reason is purely due to thermodynamics, with a ΔT of 10 K, the rSOC reactor operates at 830 °C in SOEC mode in contrast to 800°C when the ΔT is 25 K. Therefore, the endothermic heat requirement is higher in the former than in latter scenario. The second reason is due to the behaviour of ASR with temperature, the ASR and the heat generated due to losses are lower at 830°C than at 800°C. Hence, the heat ratio moves towards endothermic region as the temperature difference between the operation modes is reduced. Out of the two reasons discussed, the effect of ASR is more significant when compared to the thermodynamic effect. The effect is similar for the H-C-O system. For the H-C-O system, the effect of pressure on the heat ratio is far more significant than the temperature difference between the operation modes.

Impact of current density

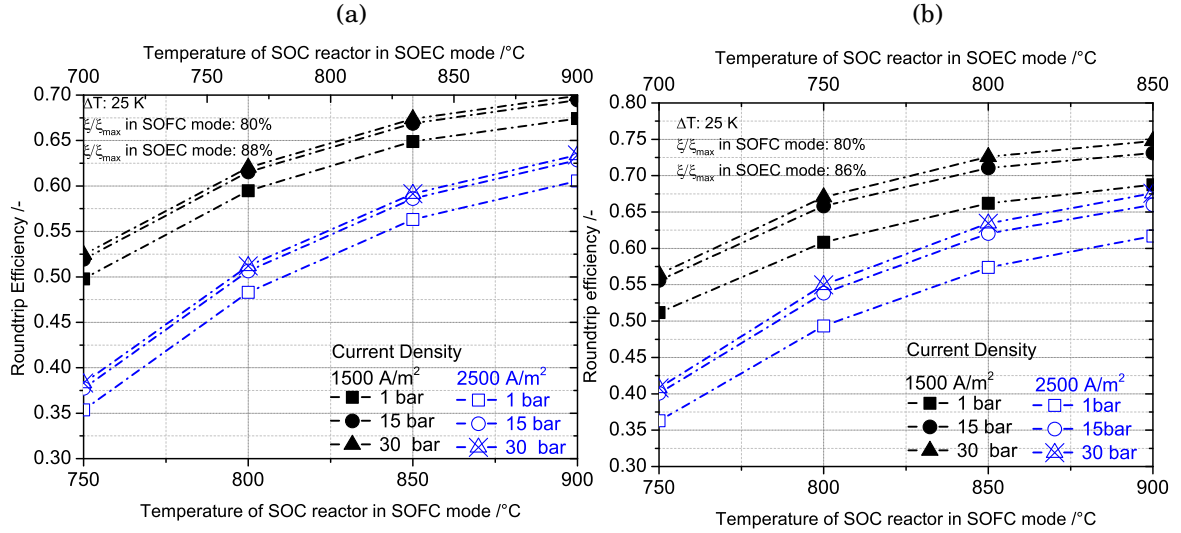


FIGURE 4.17. (a) Impact of current density on roundtrip efficiency for H-O system with commercial reactor, $\frac{\xi}{\xi_{max}} = 88\%$ in SOEC mode. (b) Impact of current density on roundtrip efficiency for H-C-O system with commercial reactor, $\frac{\xi}{\xi_{max}} = 86\%$ in SOEC mode. $T_{fc} - T_{ec} = 2\Delta T$

The effect of current density is shown in Figure 4.17. The Impact of current density on the rSOC system performance is straightforward. The voltage losses are a product of current density and ASR. Hence, at lower current densities, the losses are reduced. Therefore, the work output from the rSOC reactor in SOFC mode is higher and work input to the rSOC reactor in SOEC mode is reduced. This leads to higher roundtrip efficiencies at lower current densities.

4.4 Summary

In this section, a brief introduction to rSOC electrochemical reactors was presented. A literature review of the materials and current state of the art of rSOC reactors was presented. The different electrochemical loss mechanisms experienced in an electrochemical reactor were described. The achievable roundtrip efficiency of an rSOC system based on a commercial reactor was quantified.

4.4.1 Commercial rSOC reactor performance

The rSOC reactor performance was experimentally characterised and the different loss mechanisms were identified and quantified. The ASR was calculated from the $U(i)$ measurements using equation (4.7). EIS was used to quantify the ohmic contributions. From the analysis of the experimental results it was shown that for the ESC based rSOC reactor, the ohmic losses were the most dominant. The ohmic contribution to the ASR amounts to at least 75 % of the total ASR. The impact of pressure and reactant conversion on the rSOC reactor performance was discussed. It was shown that temperature is the most dominating parameter on the ASR due to high contribution of ohmic losses. Based on the analysis of experimental results a temperature dependent phenomenological model for ASR was developed. The phenomenological model was used for analysis of rSOC system performance based on the commercial reactor.

4.4.2 rSOC system performance using commercial reactor

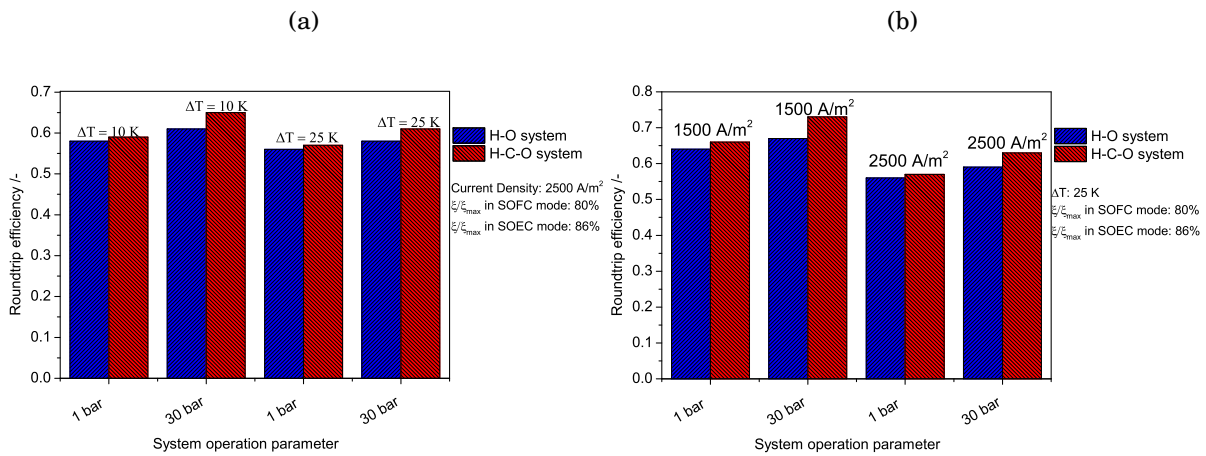


FIGURE 4.18. (a) Summary of roundtrip efficiencies at different ΔT . $T_{fc} - T_{ec} = 2\Delta T$. (b) Summary of roundtrip efficiencies at different of current density.

The rSOC system concept with heat storage thermal management presented in section 3.2 was used. The phenomenological electrochemical model of an rSOC reactor developed in section 4.2.4 is used to model the reactor behaviour and the performance was analysed for different operating conditions. The difference between the ideal limit for roundtrip efficiency and roundtrip efficiency for a system with a commercial rSOC reactor indicates the development state of the rSOC reactor. As shown in Figure 4.18

that roundtrip efficiencies as high as 60 % is achievable for both H-O and H-C-O based systems at 30 bar and current density of 2500 A/m². The temperature difference between the rSOC reactor and heat storage and therefore between the two operation modes should be optimised for heat transfer area and roundtrip efficiency. Also lower current densities can lead to higher efficiency, but also leads to higher reactor areas and hence higher capital costs. Based on this analysis, current density of 2500 A/m² and $\Delta T = 25 K$ are chosen for the detailed process system modelling. Operation at 30 bar pressure seems favourable but needs to be weighed against the requirements of balance plant components.



5

SOC reactor modeling

To meet the necessities of process engineering of rSOC systems, proper rSOC reactor models are required to simulate its behaviour at different operation conditions. The rSOC reactor models developed in this chapter are used for detail process system modelling of rSOC systems. A brief literature review of SOC reactor models for both SOFC and SOEC operation is provided in section 5.1. The need for a different resolution of rSOC models is discussed briefly. A one dimensional (1-D) model of a SRU of an rSOC reactor is detailed in section 5.2. The 1-D model is utilised to study the impact of system operation conditions within the reactor. For process system modelling, a zero dimensional model (0-D) model was developed. The 0-D model was developed to be used in ASPEN, a commercial chemical process engineering software. The model is presented in section 5.3.

5.1 Literature Review

A rich collection of literature can be found on the modelling of SOC reactors operating in SOEC or SOFC mode. The literature can be classified based on the resolution and purpose of these models. On a macroscopic level, the models can be distinguished as 0-D, 1-D, 2-D models and 3-D models.

0-D models otherwise known as black-box are developed to be used within bigger process system models. These models are computationally quick and generally capture

the physics of the components. Fundamental equations for thermodynamic systems and electrochemical models are employed to obtain the necessary output parameters. No further details on reactor behaviour can be obtained using a 0-D model. Advantages of a 0-D model are that they are fast and provide sufficient information for process system modelling. The potential pitfalls include overestimating/underestimating the performance, inaccurate calculation of some key parameters such as air flow rate, characteristic reactor temperature etc [159]. Miscalculation of the air flow rate can result in hotspots or cold spots within the reactor which can be detrimental for the reactor and system. 0-D models in both SOFC and SOEC operation mode within system contexts are available in the literature [56, 57, 65, 160–162].

1-D models are developed by considering only one geometrical axis. It is assumed that the fluid, thermodynamic and electrical properties along the other two axes are distributed uniformly. 1-D models are employed along the axis parallel to the direction of gas flow for co-flow and counter flow geometries. 1-D models can give insight into distribution of temperature, gas concentrations, current density, local ASR along the length of the reactor. These provide valuable information on the possible hot spots or cold spots within the reactor that can lead to failure of the reactor. 1-D models have been developed for both SOFC and SOEC operation [163–167].

2-D models considers a combination of 2 geometrical axes. General geometric considerations in 2-D model are the axis along the flow direction (length of the reactor) and along the height of the reactor. 2-D models are required for cross flow SOC geometry. These models are generally employed to increase understanding of the gas diffusion process, reaction kinetics and electrochemical potentials along the electrode height etc. [168–171].

3-D models considers property distribution in all the three geometric axes. Complete resolution of the parameters within the reactor can be obtained. 3-D models require intensive computational power. They are generally used for studying the reactor design [172–174].

The macroscopic models can be developed on a cell level or for the complete reactor. The level of discretisation employed depends on the problem statement and purpose of these models. The reactor level models are normally used by industry designing the SOC reactor gas manifolds, to understand the fluid flow behaviour, thermal distribution and

insulation etc. They employ tools such as the computation fluid dynamics to optimise fluid flow, thermal insulation etc. Microscopic scale models of SOC reactors are also developed. These models employ fundamental electrochemistry and reaction kinetics from the microscopic scale. They are usually employed to identify reaction mechanisms and optimisation of electrode structures etc [175–178].

5.2 1-D rSOC model

In this section a 1-D model of an rSOC reactor capable of operating in both SOFC and SOEC mode is detailed. The model is capable of operating under steady state conditions or as a transient model to study the dynamic behaviour. The purpose of the 1-D model is twofold:

1. The 1-D model is used to investigate if any undesirable conditions are developed within the reactor at different system operation points. In most system analyses, 0-D models are used which do not provide information on the internal constraints. For example, a large temperature gradient between the minimum temperature point to maximum temperature point can lead to reactor failure. In SOC reactors, when air acts as a heat transfer medium to maintain the thermal gradient limit within the reactor. Since the internal temperature resolution is not determined in a 0-D model, this can lead to an error calculating the air flow requirement. M. Li et al. reported that by replacing a 0-D model with a multi-dimensional model in a process system, the required air flow rate to cool the SOFC had to be increased. Thereby reducing the system efficiency [159]. Therefore, 1-D model is utilised to ensure the internal constraints are within the boundary conditions for safe operation of the rSOC reactor.
2. The 1-D model is used to determine the "characteristic" reactor temperature and "effective" ASR required to model a 0-D reactor. This takes into account the internal constraints addressed in the previous point.

5.2.1 Modelling paradigm, assumptions and subsystems

The development of the 1-D model is based on the procedure detailed in the literature [165, 179]. The model is implemented in an open source equation based object oriented (EEO) software called Modelica. Modelica is an acausal programming language. In an acausal programming, the inputs and outputs can be interchanged based on the physics

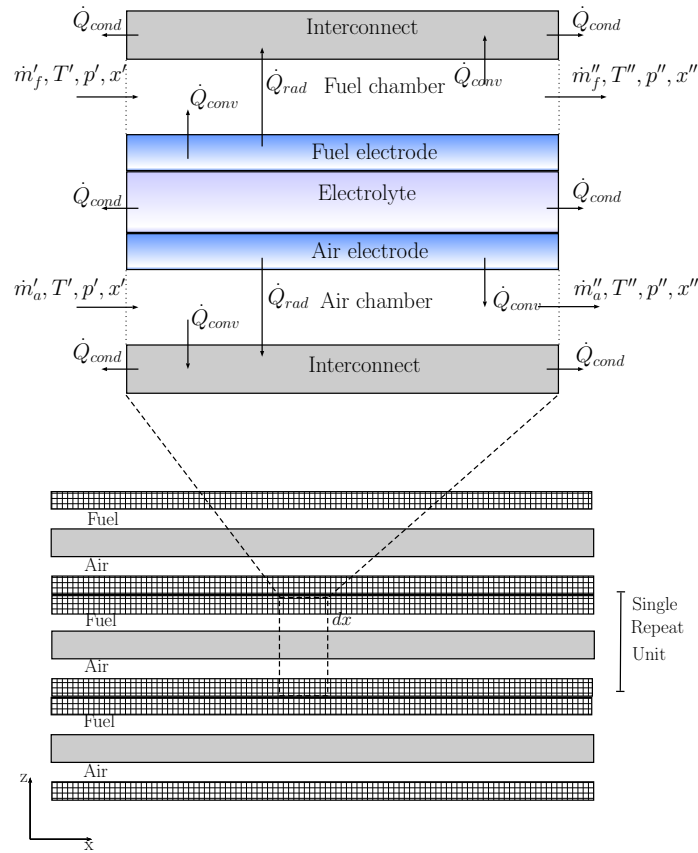


FIGURE 5.1. A schematic of a single repeat unit in a planar SOC stack. An exploded view of infinitesimal length control volume considered for the model is shown on top.

of the problem. This provides greater flexibility and reusability of the model [38, 180–182].

The 1-D model is developed for a SRU in a SOC stack. It is a representative unit cell of the rSOC reactor module and is located in the middle of an rSOC reactor. It is a valid assumption as long as the boundary conditions of the SRU are independent. A schematic representation of the SRU is shown in Figure 5.1. It consists of the fuel chamber, air chamber, membrane-electrode assembly (MEA) and interconnects. A small control volume of length dx along the length of the reactor is considered. The exploded view of the control volume is shown at top of Figure 5.1.

Assumptions

To simplify the model routine, certain assumptions are made. The physical processes considered and assumptions made are listed below:

1. Fuel and air chambers are modelled as well stirred reactors.
2. Pressure drop along the flow channels are considered and mass storage is modelled in the flow channels.
3. Energy accumulation occurs in both solid parts and gas volume.
4. Convective heat transfer between the solid and gas are considered.
5. Radiative heat transfer between solid parts (interconnect – MEA) is modelled.
6. Conductive heat transfer between the solid parts of neighbouring control volume is modelled.
7. H_2/H_2O electrochemical reaction is assumed to occur at the electrode electrolyte interface and other reactions such as reverse steam methane reforming (R 3.11) and reverse water gas shift reaction (R 3.12) are assumed to occur at the electrode surface towards the flow channels.
8. It is assumed that the CO/CO_2 reactions proceed faster via reverse water gas shift reaction. Only the H_2/H_2O electrochemical reaction is considered. This assumption is partly valid since the reverse water gas shift reaction proceeds faster than CO/CO_2 electrochemical reaction. Moreover, H_2/H_2O is a dominant electrochemical reaction accounting for 98 % of current. In most cases the reverse water gas shift reaction reaches equilibrium quickly, hence the OCV calculated by CO/CO_2 and H_2/H_2O is the same [183].
9. Temperature gradient of solid parts along the z-axis (height axis) is neglected.
10. The ideal gas law is used.

5.2.2 Fuel and air chamber

The gas flows in the flow channel are modelled in the fuel and air chamber object. The fluid flow in the flow channels are assumed to be laminar. Conservation and constitutive equations are provided in general form that are valid for both fuel flow and air flow chamber.

Conservation equations

The conservation equations are provided for both fuel and air flow channels. Conservation of mass, species, momentum are written in relation to the extensive variables. In the present model, they are converted to intensive variables. The intensive variables used for modelling are enthalpy (h), pressure (p) and mole fractions (x). The mass conservation equation has to be written for the entire flow and also for individual species. Mass conservation and species conservation equation are given by (5.1) and (5.2) respectively.

$$\frac{dm}{dt} = \dot{m}' - \dot{m}'' + \Delta \dot{m}_{O,trans} \quad (5.1)$$

$$\frac{dm_i}{dt} = \dot{m}'_i - \dot{m}''_i + b l M_i \sum_{k=1}^3 \nu_{i,k} r_k \quad i \in \text{H}_2, \text{CO}, \text{CO}_2, \text{H}_2\text{O}, \text{N}_2, \text{O}_2, \text{CH}_4$$

$$k \in (\text{smr}, \text{wgs}, \text{hor}) \quad (5.2)$$

In equation (5.1), the term $\Delta \dot{m}_{O,trans}$ indicates the mass rate of the oxygen atoms added to the fuel reactant flow in the SOFC mode. In SOEC mode, the value becomes negative and indicates the mass rate of oxygen atoms removed from the fuel reactant (H_2O and CO_2) flow. The index ' i ' in equation (5.2) indicates the chemical components and ' k ' stands for the reaction number. At fuel chamber, reverse steam methane reforming reaction (R 3.11) and reverse water gas shift reaction (R 3.12) are considered. Only the $\text{H}_2/\text{H}_2\text{O}$ electrochemical reaction is modelled. The term $\nu_{i,k}$ stands for the stoichiometric value for species ' i ' in reaction ' k ' and term ' r ' stands for the reaction rate of reaction ' k '.

The momentum conservation equations for the flow channels are given by equation (5.3).

$$\dot{m}' = \rho' \frac{bZ^3}{12\nu} \frac{p' - p''}{l} \quad (5.3)$$

The equation for the momentum balance is obtained from the Navier Stokes equation by assuming a laminar ideal gas flow between infinitely long channels [165]. The energy balance for the fuel flow channels and air flow channels are provided in equation (5.4a) and (5.4b) respectively.

Fuel flow channel

$$\frac{dE}{dt} = \dot{m}'_f h'_f - \dot{m}''_f h''_f + \dot{Q}_{conv}^{mea,f} + \dot{Q}_{conv}^{ic,f} - (-\Delta_{hor} h r_{hor}) \quad (5.4a)$$

Air flow channel

$$\frac{dE}{dt} = \dot{m}'_a h'_a - \dot{m}''_a h''_a + \dot{Q}_{conv}^{mea,a} + \dot{Q}_{conv}^{ic,a} \quad (5.4b)$$

In the energy balance equation of fuel flow channel (5.4a), the last term on the right-hand side is the energy released/consumed during the electrochemical reaction. The energy released/consumed from the electrochemical reaction is subtracted from the energy balance in the fuel channel because it is considered to be released at the electrode-electrolyte interface. The enthalpy of formation of each component is already considered within the gas models. Hence, the reaction enthalpy change of other chemical reactions is already taken into consideration.

Constitutive equations

The constitutive equations are necessary to complete the system of equations. Three reactions are considered to occur in the fuel side and one on the air side. The reaction rate for the electrochemical reaction ((R 3.13)) is given by the Faraday's law (equation (5.5))

$$r_{hor} = \frac{j}{2F} \quad (5.5)$$

The rate of the reverse steam reforming reaction (R 3.11) is shown in equation (5.6a). Many authors have investigated the kinetics of steam reforming of methane. A brief overview of internal steam reforming and its kinetics is presented by Mogensen et al. [105]. The initial kinetic models of the steam methane reforming reaction over nickel (Ni) catalysts are provided by Xu and Forment el al. [184]. Their model is a Langmuir-Hinshelwood kinetic model based on experiments performed on Ni catalyst with Zirconia supports. Achenbach and Reinsche et al. developed a first order kinetic model with respect to methane [185]. A model considering carbon deposition and auxiliary reaction schemes is presented by Wang et al. [186]. A detailed reaction mechanism for methane reforming on Ni/YSZ catalysts is experimentally studied by Hecht et al., but no kinetic model is presented [187]. A most common kinetic model for steam reforming is based on Achenbach model [185]. Lehnert et al. [188] developed a first order reaction model based on the work of Xu and Forment et al., and is also commonly used for internal reforming in SOC . Timmerman et al. [189] extended the work of Lehnert et al. and applied the model to predict both internal reforming and methanation. The model parameters was

obtained experimentally. Hence, in this work the model proposed in [189] is utilised.

$$r_{smr} = k_{smr}^+ p_{CH_4} p_{H_2O} - k_{smr}^- p_{H_2}^3 p_{CO} \quad (5.6a)$$

The equilibrium constant is given by:

$$\begin{aligned} \kappa_{smr} &= \frac{k_{smr}^+}{k_{smr}^-} \\ \kappa_{smr} &= 1.0267 \cdot 10^{10} \exp(-0.2513[K^4]Z^4 + 0.3665[K^3]Z^3 \\ &\quad + 0.581[K^2]Z^2 - 27.134[K]Z + 3.277) \\ k_{smr}^+ &= 2395[\text{mol}/(\text{m}^2 \text{ s})] \exp\left(\frac{-231266[\text{J}/\text{mol}]}{RT}\right) \\ Z &= \frac{1000}{T} \end{aligned} \quad (5.6b)$$

The reverse water gas shift reaction is generally fast and assumed to achieve equilibrium fairly quickly in both directions. For the SOC model, a first order rate equation is utilised as given in (5.7a) [169].

$$r_{wgs} = k_{wgs}^+ p_{CO} p_{H_2O} - k_{smr}^- p_{H_2} p_{CO_2} \quad (5.7a)$$

The equilibrium constant is given by:

$$\begin{aligned} \kappa_{wgs} &= \frac{k_{smr}^+}{k_{smr}^-} \\ \kappa_{wgs} &= \exp(-0.2935[K^3]Z^3 + 0.6351[K^2]Z^2 + 4.1788[K]Z + 0.3169) \\ k_{wgs}^+ &= 0.0171[\text{mol}/(\text{m}^2 \text{ s})] \exp\left(\frac{-103191[\text{J}/\text{mol}]}{RT}\right) \\ Z &= \frac{1000}{T} \end{aligned} \quad (5.7b)$$

The convective heat transfer between the gas and solid parts are given by equations (5.8a)–(5.8d). The convective heat transfer coefficient can be obtained by assuming constant Nusselt number for laminar flow. Values for the heat transfer coefficient reported in literature can be found in Table 5.1. In planar SOC reactors, a constant convective heat transfer coefficient is assumed in literature. Convective heat transfer between the solid part and fuel flow are given by equations (5.8a) and (5.8b). Similarly, the convective heat transfer between the solid parts and air flow is provided by equations (5.8c) and (5.8d).

Convective heat transfer between solid parts and fuel flow

$$\dot{Q}_{conv}^{mea,f} = \alpha_f b l (T_{mea} - T_f) \quad (5.8a)$$

$$\dot{Q}_{conv}^{ic,f} = \alpha_f b l (T_{ic,f} - T_f) \quad (5.8b)$$

Convective heat transfer between solid part and air side flow

$$\dot{Q}_{conv}^{MEA-a} = \alpha_a b l (T_{mea} - T_a) \quad (5.8c)$$

$$\dot{Q}_{conv}^{ICf-f} = \alpha_a b l (T_{ic,a} - T_a) \quad (5.8d)$$

TABLE 5.1. Heat transfer coefficients for air and fuel flow in SOC reactor flow channels reported in literature

Literature	Heat Transfer Coefficient	Reference	Comment
Aguiar et al.	$\alpha_f = \alpha_a = 100 \text{ W}/(\text{m}^2\text{K})$	[190]	Planar SOC
Xue et al.	$\alpha_f = 2987 \text{ W}/(\text{m}^2\text{K})$ $\alpha_a = 1322 \text{ W}/(\text{m}^2\text{K})$	[37]	Tubular SOC

5.2.3 Membrane-Electrode-Assembly

The solid electrolyte, fuel electrode and air electrode are modelled as one solid unit. The temperature variation along the height is not considered. Energy accumulation is accounted for and temperature of the MEA is lumped together. No mass accumulation occurs within the MEA.

Conservation equations

Only energy conservation is considered and mass accumulation does not occur in the MEA. The MEA is stationary and hence momentum conservation is not required. As mentioned in the assumptions, the energy released or consumed during the electrochemical reaction is assumed to be released at the electrode-electrolyte interface. The energy conservation equation is given by equation (5.9).

$$\rho_{mea} c_{mea} \delta_{mea} b l \frac{dT_{mea}}{dt} = r_{hor} b l \Delta_{hor} h + \dot{Q}_{conv}^{mea,f} + \dot{Q}_{conv}^{mea,a} + \dot{Q}_{rad}^{mea,ic,f} + \dot{Q}_{rad}^{mea,ic,a} + \dot{Q}_{cond}^{mea} - U_{cell} I_{cell} \quad (5.9)$$

Constitutive equations

The first term on right side of the energy balance equation (5.9) provides the heat released or consumed by the electrochemical reaction. Convective, radiative and conductive heat transfer are considered and are addressed earlier in the section. Radiative heat transfer occurs between the two solid parts, MEA and interconnects, and is given by equation (5.10) and equation (5.11).

Radiative heat transfer between MEA and fuel side interconnect:

$$\dot{Q}_{rad}^{mea,ic,f} = \frac{5.67 \times 10^{-8} [\text{W}/(\text{m}^2 \text{K}^4)] b l \epsilon_{mea} \epsilon_{ic,f} (T_{mea}^4 - T_{ic,f}^4)}{\epsilon_{mea} + \epsilon_{ic,f} - \epsilon_{mea} \epsilon_{ic,f}} \quad (5.10)$$

Radiative heat transfer between MEA and aid side interconnect:

$$\dot{Q}_{rad}^{mea,ic,a} = \frac{5.67 \times 10^{-8} [\text{W}/(\text{m}^2 \text{K}^4)] b l \epsilon_{mea} \epsilon_{ic,a} (T_{mea}^4 - T_{ic,a}^4)}{\epsilon_{mea} + \epsilon_{ic,a} - \epsilon_{mea} \epsilon_{ic,a}} \quad (5.11)$$

The conductive heat transfer with the neighbouring volume elements is lumped to the geometric centre. The conductive heat transfer is given by the following equation.

$$\dot{Q}_{cond} = \lambda_{mea} l \nabla T_{mea} \quad (5.12)$$

Electrochemical model

The last term in the energy balance corresponds to the work consumed or produced by the reactor. The voltage of the SRU is calculated by the electrochemical model. Electrochemical losses are calculated by resolving each loss mechanism. The rSOC reactor current in SOFC mode is taken as positive value and in SOEC mode as negative value. The cell voltage is calculated using the equation (5.13).

$$U_{cell} = U_{ocv} - j A S R_{\Omega} - \Delta U_{activation} - \Delta U_{diffusion} \quad (5.13)$$

Ohmic losses account for the voltage drop due to resistance to the charge transport process. The total resistance to the charge transport is equal to the sum of the electrolyte resistance to oxygen ion transport, electron transport in the electrodes and interconnects. Apart from the functional layers, there are other layers in an rSOC reactor. Additional

protection layers are added between the air electrode and electrolyte to prevent chemical reactions between them. Likewise, protective layers are added between electrodes and interconnects. Moreover, with continuing SOC research new cells/reactors tend to have not just different materials but also different number of functional layers. Finding conductivity data for all the materials is difficult. Secondly, the exact description of the materials in the functional layers is not provided and these are mostly a mixture/cermet of varying composition. Hence, the exact data is not available. In light of these realities, the ohmic loss is divided in to two parts. The first term (in equation (5.14)) takes into account the resistance due to fuel electrode, air electrode and electrolyte with available material data and the second term includes the resistance of the rest of the components such as interconnects, current collectors, protective layers etc. The ohmic component of the ASR is calculated from equation (4.4)

$$ASR_{\Omega} = \left(\frac{\delta_{fe}}{\sigma_{fe}} + \frac{\delta_{se}}{\sigma_{se}} + \frac{\delta_{ae}}{\sigma_{ae}} \right) + ASR_{reactor} \quad (5.14)$$

$$ASR_{reactor} = A_1 + A_2 T + A_3 T^2 + A_4 T^3 \quad (5.15)$$

The temperature dependent relation for conductivity is calculated using (5.16).

$$\sigma_i = \frac{\sigma_o}{T} \exp\left(\frac{-E_{act}}{RT}\right) \quad (5.16)$$

The term $ASR_{reactor}$ is a 3rd degree polynomial function of temperature. The coefficients are obtained by fitting the function to the difference between the total ohmic resistance calculated from EIS measurements and ASR_{Ω} .

Activation losses are typically evaluated using a semi empirical Butler-Volmer equation (BV). The BV is an electrochemical rate kinetic equation similar to a first order rate kinetic equation of chemical reaction. The classical form of BV is shown in equation (5.17).

$$j = j_o \left(\exp\left(\frac{(1-\beta)F U_{activation}}{RT}\right) - \exp\left(\frac{-\beta F U_{activation}}{RT}\right) \right) \quad (5.17)$$

The term j_o is the exchange current density. It is the current density at equilibrium state when no reaction takes. Value of the symmetry factor ' β ' varies between 0.25-0.5 [191, 192]. The symmetry factor indicates how the activation energies of forward and backward reaction are affected by voltage. Using $\beta = 0.5$ in equation (5.17), the equation is simplified to an inverse hyperbolic function. The inverse hyperbolic simplification of

BV provides higher accuracy for a wide range of current densities for $\beta \leq 0.7$ [193]. For the model, the activation loss is calculated using the simplified BV as shown in equation (5.18). The exchange current density for the fuel electrode and oxygen electrode are given by equation (5.19) and (5.20) respectively. The partial pressure of the species used in equation (5.19) and (5.20) are the values at the triple phase boundary

$$U_{activation} = \frac{RT}{0.5F} \sinh^{-1} \left(\frac{j}{2j_o} \right) \quad (5.18)$$

Fuel electrode:

$$j_{o,fe} = \gamma_{fe} \left(\frac{p_{H_2}^{TPB}}{p} \right)^m \left(\frac{p_{H_2O}^{TPB}}{p} \right)^n \exp \left(\frac{-E_{act,fe}}{RT} \right) \quad (5.19)$$

Oxygen electrode

$$j_{o,ae} = \gamma_{ae} \left(\frac{p_{O_2}^{TPB}}{p} \right)^k \exp \left(\frac{-E_{act,ae}}{RT} \right) \quad (5.20)$$

Diffusion losses are due to the mass transport effect. The electrochemical reactions occur at the electrolyte-electrode interfaces. The reactants must therefore diffuse to the reaction sites through the porous electrodes. The rate of electrochemical reaction at the reaction sites leads to the concentration gradient across the electrodes for both reactants and products which drives the diffusion transport phenomenon. Fick's Model, Stefan-Maxwell Model and Dusty Gas Model (DGM) are commonly used for modelling the mass transport in SOC reactors [183, 194, 195]. An overview of performance of the three different models is presented by [194]. The DGM has a higher accuracy but is difficult to obtain an analytical solution and requires numerical methods adding to computational costs. Stefan-Maxwell model omits Knudsen diffusion which is significant for pressurised systems [155]. Hence, in this work an extended Fick's law model with Knudsen diffusion is employed, assuming $\frac{dp}{dz} = 0$, is used for calculating the concentrations at the reaction sites. The diffusion losses are calculated using equations (5.21) - (5.22).

$$U_{diffusion,fe} = -\frac{RT}{2F} \ln \left(\frac{x_{H_2}^{TPB} x_{H_2O}}{x_{H_2O}^{TPB} x_{H_2}} \right) \quad (5.21)$$

$$U_{diffusion,fe} = -\frac{RT}{4F} \ln \left(\frac{x_{O_2}^{TPB}}{x_{O_2}} \right) \quad (5.22)$$

A detailed derivation for the calculation of the gas concentrations ($x_{H_2}^{TPB}$, $x_{H_2O}^{TPB}$, $x_{O_2}^{TPB}$) at the reaction sites (TPB) is provided in the Appendix B.

5.2.4 Interconnects

Interconnects are modelled as a lumped solid component. Only thermal energy accumulation is accounted considered in the interconnects. The resistance due to charge transport is considered in the electrochemical model in the previous section. Hence, it is not considered here.

Conservation equation

The energy conservation equation for the interconnect is given by (5.23). Radiative, conductive and convective heat transfers are considered.

$$\rho_{ic} c_{ic} \delta_{ic} b l \frac{dT_{ic}}{dt} = \dot{Q}_{conv}^{mea,f} + \dot{Q}_{conv}^{mea,a} + \dot{Q}_{rad}^{mea,ic,f} + \dot{Q}_{rad}^{mea,ic,a} + \dot{Q}_{cond}^{ic} \quad (5.23)$$

Constitutive equation

Similar to the MEA model, the conductive heat transfer is lumped to the geometric centre of the interconnect. The conductive heat transfer with neighbouring elements is calculated using equation (5.24).

$$\dot{Q}_{cond} = \lambda_{ic} l \nabla T_{ic} \quad (5.24)$$

5.2.5 Modelica implementation

The model equations are implemented in modelica language which is an Equation based object oriented (EEO) language. A commercial editor Dymola from Dassault systems, is used. Different components of the model that are reused can be modelled as separate objects. These objects can be called upon when required. Each subsystem described above forms an object on its own. There are four main objects based on the subsystems; (i) Fuel flow chamber, (ii) Air flow chamber, (iii) MEA, (iv) Interconnect. Additionally, three objects are defined based on the three heat transfer mechanism; (i) Conductive heat transfer, (ii) Radiative heat transfer, (iii) Convective heat transfer.

The heat transfer objects and subsystem objects are connected accordingly to obtain the necessary model structure. The layout of the control volume defined in Figure 5.1 is shown in Figure 5.2(a). It can model an SRU but under the assumption of an SRU behaving like a CSTR reactor. To get a more realistic model, the control volume is

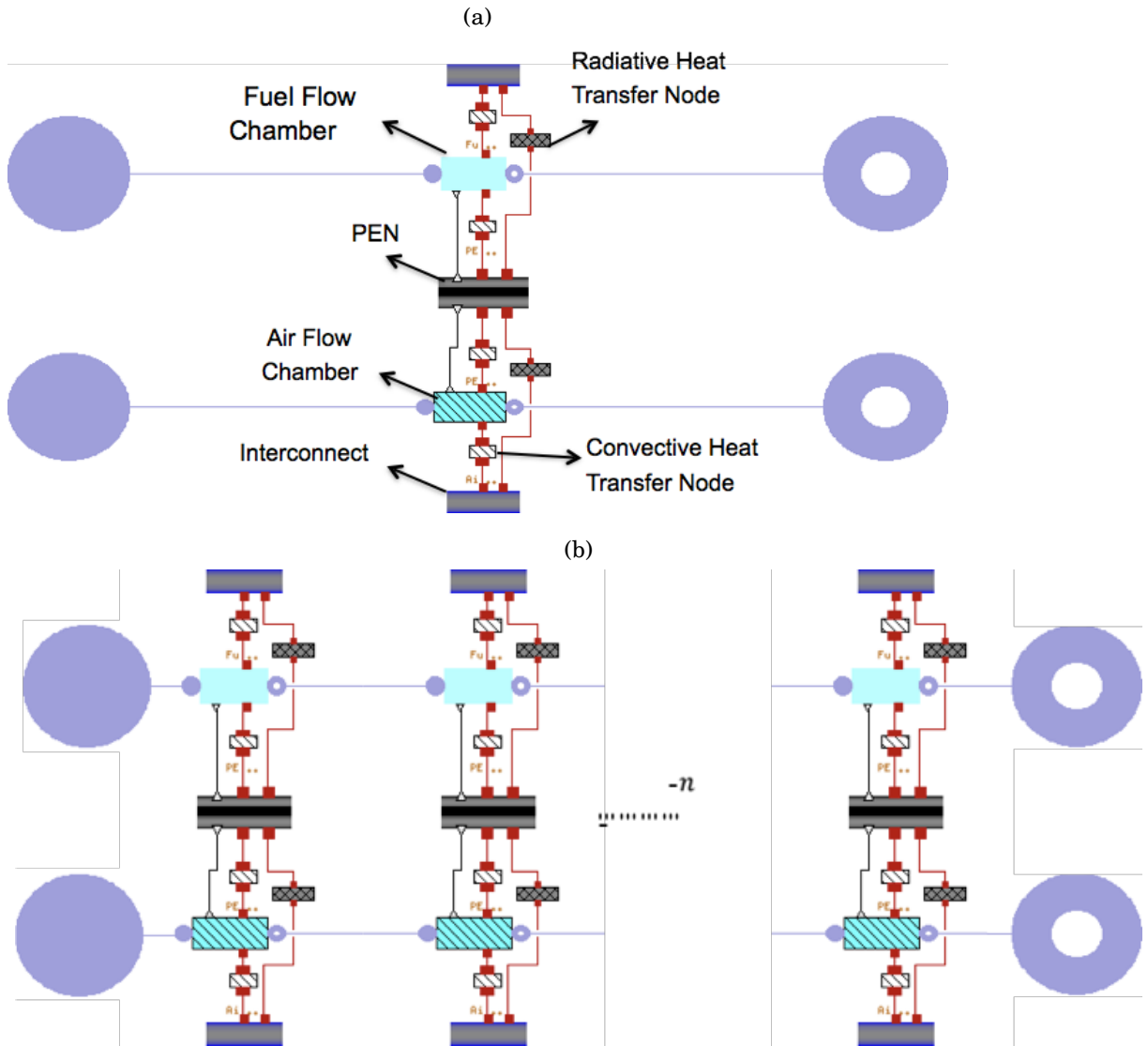


FIGURE 5.2. (a) Modelica implementation of the control volume as described in Figure 5.1. (b) 1-D implementation of SRU of rSOC reactor in modelica with repeating control volumes.

repeated n times based on the required discretisation to model a plug flow type SRU. The model shown in Figure 5.2(b) is a complete representation of the SRU. The gas flows are connected in series according to the flow direction. The MEA's are connected as parallel electrical circuits. This is valid assumption because the electrode surfaces are almost equipotential surfaces. The system of equations is solved for the boundary conditions (5.25a) and (5.25b). Local current density, local ideal voltage, local compositions, local ASR etc. are resolved accordingly.

$$U_{i=1\dots n} = U_{cell} \quad (5.25a)$$

$$I_{cell} = \sum_{i=1}^{i=n} I_i \quad (5.25b)$$

5.2.6 Results and experimental validation

The 1-D rSOC model was implemented for the commercial rSOC reactor experimentally characterised at DLR. The physical characteristics of the rSOC reactor are provided in Table 5.2.

TABLE 5.2. Functional materials and dimensions of the commercial rSOC reactor

Functional layer	Material	Thickness/ μm	Porosity
Fuel electrode contact	Ni	15	0.4
Fuel electrode	Ni-GDC	15	0.4
Electrolyte	3YSZ	90	0
Air electrode contact	GDC	25	0.4
Air electrode	LSCF	30	0.4

Input parameters

The input parameters for the 1-D model are shown in the Table 5.3. The material properties for ionic/electrical conductivity, activation energies, specific heat capacity, thermal conductivity and emissivity were adopted from literature. The SRU of the commercial rSOC reactor is 9 cm in length. It has an effective cell area of 127.8 cm². Accordingly, the effective width of the SRU was determined to be 14.2 cm.

TABLE 5.3. Material and physical parameters used for 1-D model

Parameters	Value	Unit	Reference
Fuel Electrode			
σ_o	$95 \cdot 10^6$	S K/m	[183]
E_{act}/R	-1150	K	[183]
Air Electrode			
σ_o	$42 \cdot 10^6$	S K/m	[183]
E_{act}/R	-1200	K	[183]
Electrolyte			
$\sigma_{o,se}$	$5.15 \cdot 10^7$	S K/m	[183] ^a
E_a/R	-10300	K	[183]
Physical Dimension			
Length	$90 \cdot 10^{-3}$	m	
Width	0.142	m	
Height	$1 \cdot 10^{-3}$	m	
MEA			
Heat Capacity	500	J/(kg K)	[196]
Emissivity	0.8		[192, 196]
Thermal conductivity	2	W/(m K)	[196]
Density	6000	kg/m ³	[196]
Interconnect			
Heat Capacity	500	J/(kg K)	[196]
Emissivity	0.1		[192, 196]
Thermal conductivity	25	W/(m K)	[196]
Density	8000	kg/m ³	[196]

^aConverted from $3.34 \cdot 10^4$ S/m reported for YSZ

Fit Parameters

The model parameters such as the activation energy for electrode reactions, pre-exponential factor and tortuosity factor were fitted to the polarisation resistance calculated from experiments described in section 4.2.2. The fitting parameters and the coefficients for the polynomial expression of $ASR_{reactor}$ as defined in equation (5.15) is provided in Table 5.4.

TABLE 5.4. Fitting parameters and starting values used for 1-D model of commercial rSOC reactor

Parameter	Literature	Fitted value	Unit	Equation
γ_{fe}	$5.50 \cdot 10^8$	$1.33 \cdot 10^6$	A/m ²	(5.19)
γ_{ae}	$7 \cdot 10^8$	$1.14 \cdot 10^7$	A/m ²	(5.20)
$E_{act,fe}$	110	52.198	kJ/mol	(5.19)
$E_{act,ae}$	117	66.239	kJ/mol	(5.20)
m	-0.1	-		(5.19)
n	0.33	-		(5.19)
k	0.22	-		(5.20)
ψ_{fe}	2.5	6.8166	1	
ψ_{ae}	2	5.1847	1	
A1		0.02348	1	(5.15)
A2		$-6.18903 \cdot 10^{-5}$	$\Omega \text{ m}^2/\text{K}$	(5.15)
A3		$5.47259 \cdot 10^{-8}$	$\Omega \text{ m}^2/\text{K}^2$	(5.15)
A4		$-1.6207 \cdot 10^{-11}$	$\Omega \text{ m}^2/\text{K}^3$	(5.15)

SOFC mode

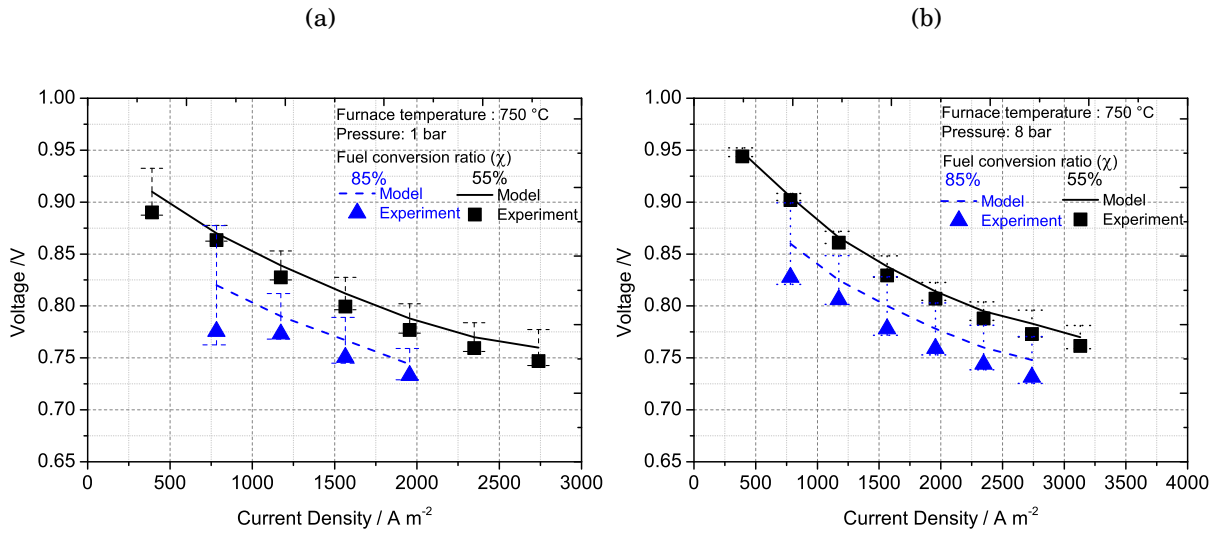


FIGURE 5.3. (a) Comparison of 1-D model prediction versus steady state measurements at 1 bar in SOFC mode. (b) Comparison of 1-D model prediction versus steady state measurements at 8 bar in SOFC mode

The 1-D model with the input parameters described in the Table 5.3 and Table 5.4 is compiled in SOFC mode. The model was run for experimental measurements

reported in section 4.2.2. The 1-D rSOC model was validated against the experimental measurements for both steady state and dynamic $U(j)$ characteristic curves. The model prediction versus the experimental measurements for SOFC mode is shown in 5.3. The model prediction is in reasonable tolerance with the measurements at both low and high pressures. The model was able to predict experimental results with a maximum error of two percentage points (2 %) of total value for fuel conversion of 55 % and a maximum error of four percentage points (4 %) of total value for experiments with fuel conversion of 85 %. The higher deviation for the 85 % fuel conversion is largely at the lower current density. This could partly be due to the inaccuracy of measurement at low current densities at 85 % fuel conversion since volume flow rates of the reactants at these experimental points were very low. At these conditions, the inaccuracy of the mass flow controllers in the test rig increases.

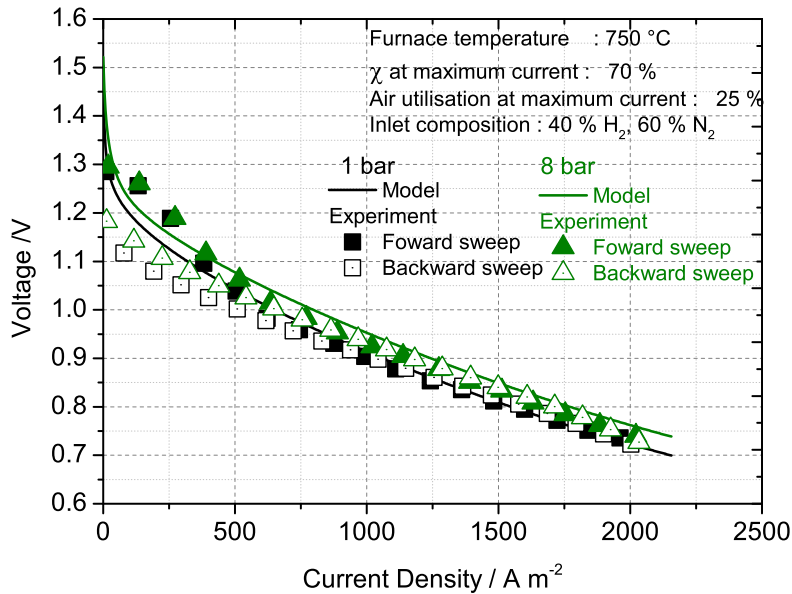


FIGURE 5.4. Validation of 1-D model with dynamic measurements in SOFC mode.

The validation of the 1-D model with SOFC dynamic $U(i)$ measurements at all pressures is shown in Figure 5.4. Good accuracy of the model with measurements at current densities above 500 A/m^2 is observed. The maximum error is two percentage points (2 %) of the total value. At current densities lower than 500 A/m^2 , the discrepancy between the measured values and one generated by the model is high. Two possible

reasons for this are discussed below:

1. At these current densities, the activation overpotential loss is expected to be the dominating loss mechanism which is computed using the BV equation. Hence, the error in the model could be either due to the approximation of the BV equation to an inverse hyperbolic function. On the other hand, the effect of the approximation is not seen in the other $U(i)$ measurements simulated using the model. For example, in the simulation of steady state $U(i)$ measurements as shown in Figure 5.3, the model can predict the voltage at current density lower than 500 A/m^2 with reasonable accuracy to the experimentally measured value. Also, a good fit at lower current densities can be observed for the simulated dynamic $U(i)$ measurements in the SOEC operation mode shown in Figure 5.3.
2. The deviation could be due to an anomaly in the experiments. Though dry fuel was used, a small percent (less than 0.01 %) of water vapour is expected to present in the feed gas as impurity. This can be calculated from the OCV of 1.3 V measured during the forward sweep. During the forward sweep (current density is increased from 0 A/m^2 to 2000 A/m^2), the voltage produces an arching behaviour at low current density (till 500 A/m^2). This could be due to low concentrations of water evolution at low current densities which is then quickly flushed out by the incoming gas flow, therefore, resulting in a "dry" condition on the fuel electrode side. As the current density is increased, due to the prevalent "dry" condition on the fuel side, a higher voltage is measured. Once a current density of 500 A/m^2 is reached, sufficient water is generated on the fuel side which is still present in the flow channel and hence a drop in voltage is observed as expected behaviour for fuel cell operation. During the back sweep (current density is decreased from 2000 A/m^2 to 0 A/m^2), it can be observed that a voltage of 1.2 V is observed at 0 A/m^2 compared to 1.3 V during forward sweep. Moreover, the arching behaviour of the voltage is not seen at lower current densities during back sweep. Sufficient water is produced by the time the forward sweep ends, which is then retained in the electrode pores and is not completely flushed out. This entrapped water in the pores is present during the back sweep, resulting in the observed behaviour. In the model, the complex phenomenon behind the observed effect is not captured.

Further analysis of the experimental results and the model is necessary to verify the two hypotheses.

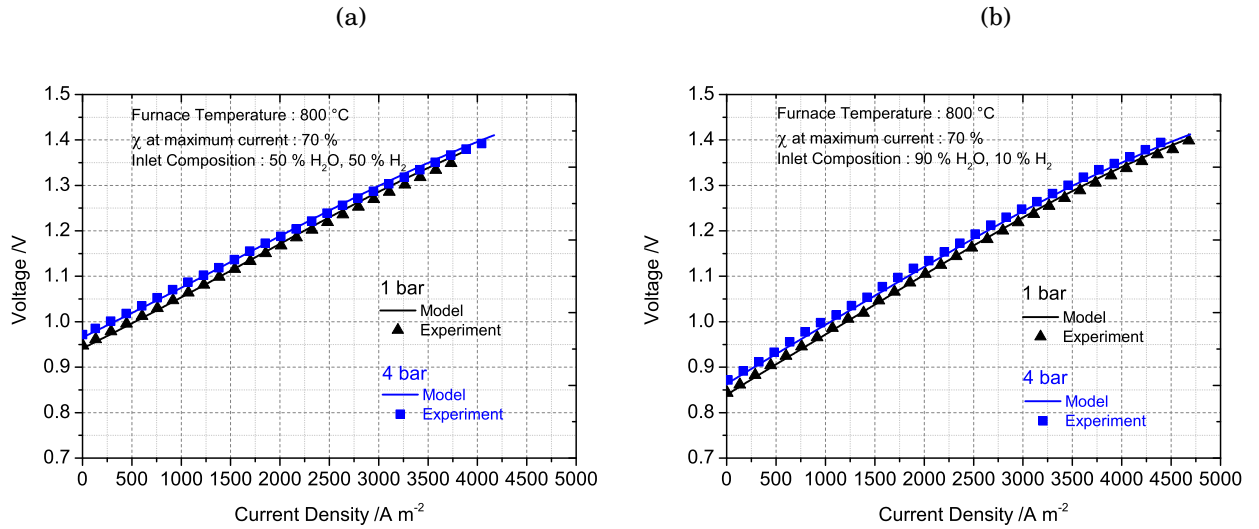


FIGURE 5.5. (a) Comparison of 1-D model prediction versus dynamic measurements at different pressures in SOEC with 50 % H₂O and 50 % H₂. (b) Comparison of 1-D model prediction versus dynamic measurements at different pressures in SOEC with 90 % H₂O and 10 % H₂

SOEC mode

The model was validated with SOEC mode with both steady state and dynamic measurements. In Figure 5.5, the validation of model in SOEC mode under two different pressure conditions and gas compositions can be observed. The model has good accuracy with the measurements. It should be noted, that the fitting parameters used for the model validation in SOEC is same as reported in Table 5.4. The fitting parameters were obtained from a wide range of SOFC measurements but still give good accuracy in SOEC mode. Overall, the deviation between the model and experimental results was less than 1 % in the SOEC operation mode.

5.2.7 Error discussion and uncertainties

In the SOFC operation mode, the model results deviated from the experimental results by an average of two percentage points (2 %) of the total value. The deviation was larger at low current density and higher fuel conversion (85 %) in the steady state SOFC measurements. One possible reason for the higher deviation could be due to the use of inverse hyperbolic simplification of Butler-Volmer equation to calculate the activation voltage losses. Secondly, at 85 % fuel conversion and low current density, the experiments

results has higher inaccuracy due to the very low volume flow rates used for these measurements. This can also be seen from the experimental result. In the SOEC operation mode, the model deviation was less than one percentage points (1 %) of total value.

The uncertainties in the certain input values may have also resulted in the observed deviations. The values such as the density, heat capacity, thermal conductivity etc. were obtained from literature for given material combination and might vary from the actual values. Furthermore, the complex flow field geometry in the SRU of the reactor was approximated to a simpler geometry for the modelling purposes. Finally, heat losses from the reactor and to surrounding volume in the furnace was estimated by lumped model which could have led to the deviation from experimental results.

5.3 0-D model for process system analysis

The 0-D reactor model is developed for implementation in a process system model. Although the 1-D model provides greater details, it has a higher computational demand. When combined with a detailed process system model, the total computation requirements are higher. For these reasons a 0-D reactor model is employed. Within a process system analysis, the internal conditions within the SOC reactor are not necessary for evaluation of system performance. The model should evaluate the outlet conditions, reactor efficiency and current/voltage for given input parameters [197]. The 0-D model is a black box model and hence the following assumptions are made to simplify the model.

Assumptions

1. The 0-D model assumes an adiabatic reactor, the outlet temperatures of both the fuel side and air side stream are assumed to be equal.
2. Reactions are assumed to attain thermodynamic equilibrium at the outlet. Gas compositions at the outlet are calculated assuming thermodynamic equilibrium.
3. Chemical and electrochemical reactions are assumed to occur at a lumped representative reactor temperature. The representative reactor temperature is calculated from the 1-D model.
4. The electrochemical performance (ASR) is evaluated at the representative reactor temperature.

The 0-D model is developed to obtain system and reactor performance at different current densities, conversion ratios, system operation pressure etc.

5.3.1 Thermodynamic model

The thermodynamic model calculates the outlet composition and temperature by assuming thermodynamic equilibrium is achieved at the outlet. The thermodynamic equilibrium is calculated at the representative reactor temperature. At outlet the gas components, CH₄, H₂, CO, CO₂, H₂O are considered. The equilibrium calculation is obtained using a Gibbs energy minimisation routine. The outlet temperature is obtained from solving the global energy and mass balance in accordance with equation (3.10a) and equation (3.7) respectively for adiabatic conditions. The moles of oxygen molecules supplied to or removed from the fuel reactant stream is obtained for the reactor current. Inlet conditions are provided as input or obtained from the previous system component. Current density and reactant conversion ratio are provided as input.

5.3.2 Electrochemical model

The electrochemical model employed for the 0-D model is based on the general theory presented in section 3.1. Based on the SOFC or SOEC operation, the reactor current is calculated from equations (5.26b) and (5.26e) respectively.

SOFC mode:

$$I_{max,fc} = 2F(4\dot{n}'_{CH_4} + \dot{n}'_{H_2} + \dot{n}'_{CO}) \quad (5.26a)$$

$$I_{fc} = \xi_{fc} I_{max,fc} \quad (5.26b)$$

$$\Delta\dot{n}_{O_2} = \frac{I_{fc}}{4F} \quad (5.26c)$$

SOEC mode:

$$I_{max,ec} = 2F(\dot{n}'_{H_2O} + \dot{n}'_{CO_2}) \quad (5.26d)$$

$$I_{ec} = \xi_{ec} I_{max,ec} \quad (5.26e)$$

$$\Delta\dot{n}_{O_2} = \frac{I_{ec}}{4F} \quad (5.26f)$$

The cell voltage is calculated is from equation (5.27). An average reactor current density (j) is provided as an input which is positive for SOFC mode and negative for

SOEC mode. The ASR is calculated based on the phenomenological model presented in section 4.2.4 given by equation (4.8). The ASR and the ideal voltage (U_{id}) are evaluated at the characteristic reactor temperature.

$$U = U_{id} - jASR \quad (5.27)$$

In equation (5.27), the calculation of the ideal voltage is not straightforward. In literature, the ideal voltage is typically calculated based on inlet composition or outlet composition or an average between inlet and outlet composition. The calculation based on inlet composition does not account for variation of ideal voltage with extent of electrochemical reaction. Whereas, using the outlet composition accounts for the extent of electrochemical reaction but the corresponding current density at the end of the reactor is unknown. Bove et al. [197] proposed an integration of the ideal voltage over the extent of electrochemical reaction. A similar method is proposed by De Groot [127]. In this work, the ideal voltage is calculated based on the ideal work proposed in section 3.1.2. The ideal work of a reactor is purely a thermodynamic function. The work from the reactor or supplied to the reactor depends on the final and initial thermodynamic state parameter. This takes into account the reactant conversion on fuel and air side, excess air ratio etc. A similar method is proposed by Gaggioli et al. [95]. The ideal voltage is calculated using equation (5.28).

$$U_{id} = \frac{d\dot{W}_{id}}{dI} = \frac{-(G'' - G')_{hor}}{I} \quad (5.28)$$

Equation (5.28) should be used carefully when other chemical reactions are present. Only the electrochemical reaction contributes to the work term. The $\Delta_{rxn}G$ due to chemical reaction such as steam methane reforming and water gas shift reaction should be regarded as losses and hence subtracted from equation (5.28).

Representative reactor temperature

In order to evaluate the ASR and electrochemical performance of 0-D model, a new definition of the reactor temperature is required. As mentioned in the assumptions, the ASR , ideal voltage and reaction equilibrium are calculated at a lumped temperature of the rSOC reactor. The lumped temperature is the representative reactor temperature. It is defined as the reactor temperature at which the 0-D model yields the same power output, outlet temperature and electrochemical performance as that of a detailed 1-D rSOC reactor model. The representative reactor temperature is evaluated from the 1-D model. In the 1-D model, axial variations of temperature, current density, ASR and

ideal voltage are calculated. Accordingly, an average or effective ASR for the reactor can be obtained by integrating the local variation of ASR along the axial direction of the reactor and divided by length. Therefore, the representative reactor temperature is a uniform or lumped reactor temperature which yields an ASR equal to the effective ASR obtained from the 1-D model. The mathematical definition is provided in equations (5.29a)–(5.29d).

The effective ASR from the 1-D model is obtained by integrating the local ASR over the length and dividing by length.

$$ASR^{eff} = \frac{1}{l} \int_0^l ASR(x) dx \quad (5.29a)$$

$$ASR^{eff} = \frac{1}{l} \int_0^l \frac{dU(x)}{j(x)} dx = \frac{1}{l} \int_0^l \frac{U_{id}(x) - U}{j(x)} dx \quad (5.29b)$$

The ASR is a function of temperature

$$ASR^{eff} = f(T^{eff}) \quad (5.29c)$$

Therefore the characteristic reactor temperature is given by

$$T^{eff} = f^{-1}(ASR^{eff}) \quad (5.29d)$$

5.3.3 Aspen implementation

The 0-D model is implemented in Aspen Plus. Aspen Plus is commercial chemical process engineering software. The inbuilt reactor models within the Aspen suite were used for developing the thermodynamic model. Appropriate inbuilt reactor models were combined to obtain the thermodynamic behaviour of rSOC reactor. The following algorithm is implemented in Aspen Plus for modelling the 0-D reactor model. A schematic representation is provided in Figure 5.6.

1. The reactant streams are first brought to the characteristic reactor temperature by heating/cooling the reactant stream.
2. The streams are then brought to thermodynamic equilibrium
3. The electrochemical reaction for a given conversion ratio is carried out.

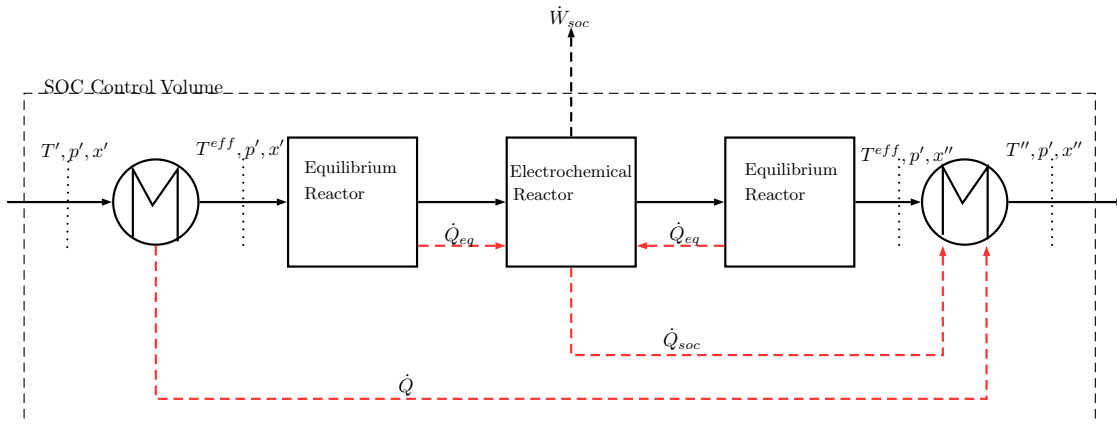


FIGURE 5.6. Algorithm of 0-D rSOC model implemented in Aspen Plus. The reactants are brought to effective reactor temperature by cooling or heating the reactants. Equilibrium, electrochemical reaction, equilibrium is calculated. The total energy balance is performed in the end to obtain outlet temperature

4. The product gases are brought into thermodynamic equilibrium at the outlet.
5. The electrochemical model to calculate reactor power, voltage, heat generated and current is implemented in a user's model block using Fortran programming.
6. A global energy balance is solved to obtain the outlet temperature of the product streams.

The thermodynamic equilibrium is calculated using the "RGibbs reactor" model in Aspen Plus. An "RGibbs" reactor model is also used to model the fuel electrode reactions in SOFC mode. The global energy balance to calculate the outlet temperature is implemented using the "Heater" model available within Aspen library. The Aspen Plus implementation and flowsheet of model can be found in the Appendix C.

5.4 Summary

A 1-D model for the rSOC reactor was implemented. The model was validated against experimental results in both SOFC and SOEC mode. The 1-D model is developed for two purposes.

1. To identify system operation conditions that lead to hazardous conditions within the rSOC reactor that can lead to failure of the reactor and therefore the system.

2. Evaluate the characteristic reactor temperature as a function of ASR and reactor performance. The characteristic reactor temperature is used within the 0-D reactor model in the system context

Accordingly, a 0-D rSOC reactor model was developed and implemented in Aspen Plus and is used for the detailed process system model of rSOC systems. Both the 0-D and 1-D rSOC model lay the foundation of the detailed process system analysis of rSOC systems. The 0-D model is used for system modelling. The 1-D model will be used to verify the operability of the system and rSOC reactor for the desired system operation points.



6 Process system analysis

A theoretical limit for an ideal roundtrip efficiency of an rSOC system was established in chapter 3. Accordingly, the achievable roundtrip efficiency using a commercial rSOC reactor was presented in chapter 4. In both the chapters, the advantages and potential of integrating a thermal energy storage system was highlighted. In this chapter a detailed process system analysis of an rSOC system is discussed. A detailed process system analysis is performed to answer the following questions:

1. What are the achievable roundtrip efficiencies of an rSOC process system with a commercially available ESC reactor taking into account the balance of plant requirements and losses related to balance of plant, heat exchangers etc.? Can the rSOC process system achieve the roundtrip efficiencies predicted in chapter 4?
2. How can thermal management be integrated with the process system and is it feasible to obtain a thermal self sustaining rSOC system?

The analysis is performed for both H-O and H-C-O chemistries based rSOC systems. A brief description of an rSOC process system is provided in section 6.1. Process system analysis of a closed system and a gas grid connected rSOC system are presented in sections 6.2 and section 6.3 respectively.

6.1 rSOC process system description

Depending on the functionality, an rSOC process system can be described as a closed or an open system.

Closed system concepts consist of closed gas storage tanks in which the reactants and products are stored separately. There is no interaction between the rSOC system and other industries or systems. In SOEC mode, the electricity is converted to fuel and is stored in a fuel tank which can be used during SOFC mode. In SOFC mode, the fuel from the storage tank is used to produce electricity. The oxidised fuel or product gas is stored in the product gas tank which is then used as reactants in SOEC mode. A closed rSOC system primarily acts a Power to Power (PtP) electricity storage system. The closed system operation is easier in comparison to an open system.

Open system concepts allows for the rSOC system to interact with chemical industries, gas networks etc. Both energy and matter can flow in and out of the rSOC system boundary. The fuel/chemicals produced during the charging mode (SOEC operation) is fed to the existing natural gas grid or supplied to chemical industries. Likewise, in the SOFC mode, the fuel required is fed from the natural gas grid or other sources. An open system offers flexibility and greater use for rSOC systems apart from electricity storage. On the other hand, the system complexity increases and additional balance of plant components are required.

An rSOC system is comprised of four major functional blocks. These are the rSOC reactor, thermal energy storage, downstream process and the heat recovery unit. The commercial rSOC reactor was analysed and a detailed discussion is provided in the preceding chapters. A brief description of the other functional blocks are provided below. An overview of key assumptions made for the analysis of the rSOC process system is discussed. Finally, the key performance parameters used to quantify the system performance are laid down at end of this section.

6.1.1 Process system assumptions

The following assumptions are made for the analysis of the rSOC process system. The assumptions are valid for all the system architectures considered within this study.

1. Charge transferred in the rSOC system during the charging (SOEC operation mode) and discharging (SOFC operation mode) are assumed to be equal. This implies the moles of oxygen transferred through the electrolyte of the rSOC reactor are the same in both the operation modes.
2. A symmetric operation of the rSOC system is considered. The duration of the charging process (SOEC operation) is equal to the duration of discharging process (SOFC operation).
3. Due to assumptions 1 and 2, the rSOC reactor current during the charging process (SOEC operation) is equal to the reactor current during the discharging process (SOFC operation).

6.1.2 Thermal energy storage

Thermal energy storage is used as the preferred means of a thermal management system for the rSOC system in this study. It is a technique of storing heat at the required temperature and utilising the stored heat when required. Thermal energy storage is also proposed as a means of energy management technique for renewable energy systems specifically in solar thermal systems [198, 199]. Three types of thermal energy storage are possible. They are (i) sensible heat storage, (ii) latent heat storage, (iii) thermochemical heat storage. In this study a latent heat storage method is utilised for thermal management in the rSOC process system due to its higher thermal energy storage density.

Sensible heat storage utilises the specific heat capacity, temperature change and mass of the material to store the heat. The basic principle of sensible heat storage is represented by equation (6.1) [200].

$$\dot{Q} = \int_{T'}^{T''} \dot{m} c_p dT = \int_{T'_{hs}}^{T''_{hs}} \dot{m}_{hs} c_p dT \quad (6.1)$$

Latent heat storage exploits the enthalpy of phase transition to store heat. The heat storage material undergoes a phase transition during the heat storage and extraction processes. Solid-liquid phase transition is preferred due to low volume expansion and high enthalpy of phase change leading to high energy storage density. The heat storage capacity and storage temperature depends on the melting point temperature and heat

of fusion of the phase change material [201, 202]. The heat stored in the medium is provided by equation (6.2). Materials used for latent heat storage are referred to as Phase Change Materials (PCM) [203–207].

$$\dot{Q} = \dot{m}_{hs} c_{p,l}^{hs} (T_{hs,l} - T_{hs}) + \dot{m}_{hs} c_{p,s}^{hs} (T_{hs} - T_{hs,s}) + \dot{m}_{hs} \Delta h \quad (6.2)$$

Phase change materials

The PCM are the heat storage media used for the latent heat storage technique. In principle any material that undergoes phase change is a candidate to be latent heat storage media. For engineering purposes additional constraints should be satisfied in order for the material to be used as a PCM. The PCMs are selected based on thermophysical characteristics such as latent heat of fusion, thermal conductivity, density, and melting point. A candidate PCM for heat storage should satisfy the following requirements; high enthalpy of fusion, thermal conductivity, density, and chemical stability. An overview of PCMs based on their melting point temperatures is presented in the literature [208–212]. The rSOC reactors operate in the temperature range of 700-900 °C, therefore PCMs with phase change temperatures in the range of 700-900 °C are required for the heat storage system. Salts such as lithium fluoride, sodium fluoride, potassium fluoride and non eutectic mixtures of magnesium are prospective PCM candidates for the latent heat storage system [202, 210, 213–215]. Based on the results from theoretical analysis presented in chapter 4, a latent heat storage system with a melting point of PCM in the temperature range of 700-900 °C is required. A brief summary of PCM materials suitable for the heat storage system is presented in the Table 6.1.

Aspen Plus implementation

A latent heat storage system model is implemented in Aspen Plus for process system modelling. The implementation is based on the following assumptions

1. The heat storage and extraction is assumed to occur at the melting temperature of the PCM. This assumption is not an exact representation, but it is justified when the main aim of the work is to study the energy and exergy efficiency when system properties are altered. With this in mind, the assumption should not drastically affect the results [207].

TABLE 6.1. A brief summary of the possible PCM materials suitable for rSOC latent heat storage. The database is a consolidated summary of materials reported in literature [202, 210]

Composite	Melting point / °C	Heat of fusion / kJ/kg
70 % LiF + 30 % MgF ₂	728	520
65 % NaF + 23 % CaF ₂ + 12 % MgF ₂	743	568
67 % LiF + 33 % MgF ₂	746	947
74 % LiF + 13 % KF + 13 % MgF ₂	749	860
80 % LiF + 20 % CeF ₃	756	500
81.5 % LiF + 19.5 % CaF ₂	769	820
85 % KF + 15 % CaF ₂	780	440
85 % KF + 15 % MgF ₂	790	520
64 % NaF + 20 % MgF ₂ + 16 % KF	804	650
62.5 % NaF + 22.5 % MgF ₂ + 15 % KF	809	543
68 % NaF + 32 % CaF ₂	810	600
75 % NaF + 25 % MgF ₂	832	627
LiF	848	1080
KF	856	486
40 % NaF + 40 % MgF ₂ + 20 % CaF ₂	914	590
49 % CaF ₂ + 41.4 % CaSO ₄ + 9.6 % CaMoO ₄	943	237

2. The material database and model of the PCM material used is not available within the Aspen Plus library. Hence, steam is used to generically model the behaviour. The use of an alternate material database in the modelling routine does not greatly affect the system performance as long as the state parameters are maintained. This is achieved by maintaining the temperature difference of the process stream, temperature of heat storage medium and quantity of heat transfer are maintained the same. A similar method to model sodium heat pipes was used in the literature [56].
3. The phase transition is assumed to occur over a small temperature difference of 1 K. Though the phase change theoretically occurs at isothermal temperature, it has been shown experimentally that the phase change occurs over a small temperature range of 0.1 K. An assumption of 1 K for temperature range facilitates ease of modelling the latent heat storage [216].

Based on the assumptions made above, the latent heat storage system is modelled using the counter flow heat exchanger model available within the Aspen Plus component library.

6.1.3 Downstream processes

A downstream chemical process provides added value in SOEC mode of the rSOC system. In the SOEC process, different chemicals, liquids and gaseous fuels can be produced by selecting the appropriate downstream process. This is essentially attractive for H-C-O chemistry based rSOC system where hydrocarbons of industrial value can be produced. Downstream processes such as the Fischer-Tropsch process, Methanation process, Dimethyl ether process etc. have been proposed to be coupled with co-electrolysis of H₂O and CO₂ [13, 66, 72, 217, 218]. They are especially attractive for an open grid rSOC system, since during the SOEC process, the electrical energy can be converted to useful chemicals of industrial value and sold to the corresponding industries. By this method, apart from being an electricity storage system, the rSOC system also produces useful chemicals through which revenue can be generated.

In this work, a downstream methanation process is considered. The H₂ and CO produced by the rSOC reactor in SOEC is converted to methane (CH₄). Methane can then be stored or supplied to the gas grid which can act as infinite reservoir for the energy storage in form of methane. The downstream methanation process is modelled as equilibrium reactors process based on minimisation of Gibbs energy.

6.1.4 Balance of plant components and heat recovery unit

Apart from the main components, auxiliary components are required to complete the process system. These components are referred to as the BoP components which consists of pumps, compressors, turbines or expanders, blowers, valves, and heat exchangers. The BoP components generally consume work/energy and hence lead to parasitic losses.

The heat recovery unit is critical in a process system. It is a network of heat exchangers used to preheat the inlet streams by extracting the heat from the outlet streams and thereby cooling the outlet streams. A well-designed heat exchanger network is necessary for an efficient system. Lower thermal losses and heat transfer losses are achieved by proper matching of the heat loads, temperature and heat sources. Optimisation of heat recovery is an active research topic in field of process system engineering [219–222]. A pinch point analysis is the commonly utilised method for optimising the heat recovery unit. The performance parameters for the BoP components and pinch point temperature for the heat exchangers used in this study is provided in the Table 6.2.

TABLE 6.2. Performance parameters for BoP components and heat exchangers

Parameters	Value	Unit
Compressors		
Isentropic efficiency	85	%
Mechanical efficiency	90	%
Expanders/turbine		
Isentropic efficiency	85	%
Mechanical efficiency	90	%
Pumps		
Isentropic efficiency	85	%
Mechanical efficiency	90	%
Blower		
Isentropic efficiency	88	%
Mechanical efficiency	90	%
Heat exchangers		
Pinch point temperature difference	10	K
Pressure drop	10	mbar

The inbuilt models available in Aspen Plus are used for modelling the pumps, blowers, compressors and expanders. The heat exchangers are modelled as counter flow heat exchangers and the models are available in the Aspen Plus library. Pinch point temperature is specified for all the heat exchangers.

6.1.5 Performance indicators

To quantify the system performance, the following key performance indicators are defined. These parameters help to understand the system performance and effect of thermal management in the process system.

System Roundtrip efficiency ($\eta_{RT,sys}$): The system roundtrip efficiency is the key parameter to quantify the performance of the rSOC system. It is defined as the ratio of the net work produced during the discharging process (SOFC) to the net energy

consumed during the charging process (SOEC).

$$\eta_{RT,sys} = \frac{\sum \dot{W}_{fc} t_{fc}}{\sum \dot{W}_{ec} t_{ec}} \quad (6.3)$$

Due to assumption 2, we get

$$\eta_{RT,sys} = \frac{\sum \dot{W}_{fc}}{\sum \dot{W}_{ec}} \quad (6.4)$$

Net work is equal to sum of reactor work and work corresponding to BoP

$$\eta_{RT,sys} = \frac{\dot{W}_{fc} - \dot{W}_{BoP,fc}}{\dot{W}_{ec} + \dot{W}_{BoP,ec}} \quad (6.5)$$

Reactor Roundtrip efficiency ($\eta_{RT,soc}$): The reactor roundtrip efficiency indicates the performance of the rSOC reactor within the system. It is defined as the ratio of energy produced by reactor in SOFC mode to the energy consumed by the reactor in SOEC mode.

$$\eta_{RT,soc} = \frac{W_{fc}}{W_{ec}} \quad (6.6)$$

Φ : In the SOFC mode, Φ represents the value of electrical work, heat produced by the reactor or heat stored in the heat storage medium normalised by dividing by the chemical power supplied as input the rSOC system. In SOEC mode, Φ represents the electrical work, heat consumed from the heat storage systems and heat produced/consumed by the reactor, normalised by dividing by the chemical power produced in the SOEC mode.

$$\Phi = \frac{\text{electric power or heat}}{\dot{m}_{fuel} LHV_{fuel}} \quad (6.7)$$

θ : Indicates the performance of the heat storage system. It is the ratio of the heat consumed from heat storage during the SOEC operation to the heat stored in the heat storage system during the SOFC operation.

ζ : Represents the ratio of the heat required for endothermic electrolysis reaction in the SOEC operation mode to the total heat consumed from the heat storage during the SOEC operation.

6.2 Closed system architecture for electricity storage

The first of the rSOC system architectures considered within this chapter is the closed system architecture. In the closed system architecture, there are no mass flows of reactants entering or leaving the system boundary. The fuel/chemicals produced during the charging mode (SOEC operation) is stored in the fuel storage tank. If the SOEC process is carried out in endothermic mode, the heat required for the process is obtained from the heat storage. The fuel stored in the fuel tanks is used during the discharge mode (SOFC operation). The heat produced during the SOFC operation is stored within the heat storage system and the electricity is supplied to the grid. Products of SOFC operation are stored in the "exhaust tanks" which are later used as reactants for the SOEC operation.

The closed system architecture of the rSOC system can be based on either H-O chemistry or the H-C-O chemistry. Analysis of a closed system architecture based on the hydrogen electrochemical oxidation reaction is discussed. The hydrogen based closed system architecture of the rSOC process system would be henceforth be referred to as the closed grid system.

6.2.1 Model description

The simplified process flow diagram of the hydrogen based rSOC process system is presented in the Figure 6.1. The Figure 6.1(a) describes the process during the SOFC operation mode of the rSOC system. The SOEC operation mode of the rSOC system is described by the Figure 6.1(b).

SOFC operation mode

In the SOFC operation mode, the fuel from the fuel tank is supplied to the rSOC reactor. The fuel is preheated in the heat recovery unit using the heat from the exhaust streams. The fuel is brought to the rSOC reactor inlet temperature of 750 °C. Meanwhile, the air required for the SOFC operation is supplied from the ambient. The air is compressed to the system pressure using a four stage compression process. For the atmospheric pressure system, the air compressor is replaced by a blower to overcome the pressure drops. The air stream is then preheated to the required inlet temperature. After the

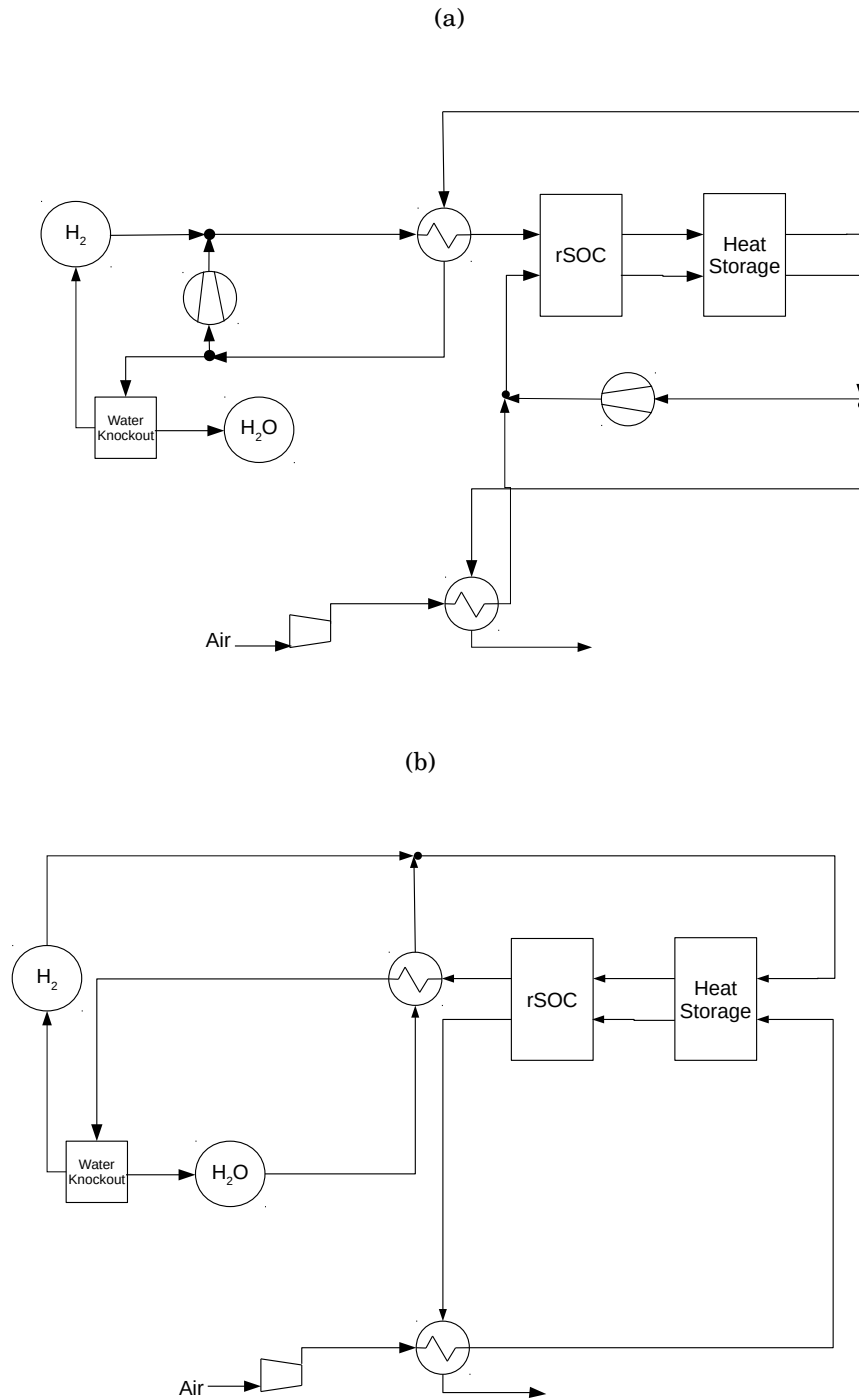


FIGURE 6.1. (a) Simplified process flow diagram of the hydrogen based rSOC system during the SOFC operation mode. (b) Simplified process flow diagram of the hydrogen based rSOC system during the SOEC operation mode.

SOFC operation, the oxidised fuel and depleted air exit the rSOC reactor. The air acts a cooling medium to maintain the rSOC reactor within safe operation limits. The heat carried by the fuel and the air exhaust streams is stored in two heat storage tanks. The first one stores heat at 850 °C and the later at 750 °C. The exhaust gases enter the first heat recovery unit, where the reactant streams are preheated. A portion of the fuel exhaust stream is recycled and mixed with the inlet fuel supplied to the rSOC reactor. By employing a fuel recycle loop, a higher total fuel conversion can be attained while maintaining a lower single pass conversion ratio. An air recycle loop is present and it is controlled in order to attain the required air inlet temperature of the rSOC reactor. The exhaust streams is fed to the water knockout unit where they are further cooled and the unconverted hydrogen in the fuel exhaust is separated from the water. The remaining hydrogen is sent to the fuel tank. Water is further cooled and stored in the water tank.

SOEC operation mode

During the SOEC operation mode, the water is supplied to the steam generation unit. The water is first preheated and undergoes evaporation in the heat recovery units. The steam is then fed to the heat storage units, where it is preheated to the required steam inlet temperature of the rSOC reactor at 820 °C. Air is supplied to the system as a sweep gas to flush the oxygen produced during the SOEC process. Moreover, it acts as a heat transfer medium to supply the heat required for endothermic SOEC operation. Finally, it helps to maintain a lower partial pressure of oxygen on the air side within the rSOC reactor and thereby lowering the voltage of the rSOC reactor. The hydrogen fuel produced is then cooled in the heat recover units. It is then fed to the water knockout unit to separate the fuel from the unconverted water. The hydrogen fuel is then compressed and sent to the fuel tank. The oxygen enriched air exhaust is cooled in the heat recovery unit and released to the ambient.

Gas storage tanks

The hydrogen and water are stored in the storage tanks. The hydrogen is stored in a pressurised fuel tank at 25 bar and temperature of 25 °C. Water is stored as liquid in the water tank maintained at 25 °C.

Heat storage

A two stage cascaded heat storage system is utilised. A cascaded latent heat storage has the advantage of better heat transfer behaviour, lower losses and hence more thermal energy can be stored. The first stage heat storage system stores heat at temperature of 850 °C, henceforth referred to as HT-PCM. The second stage heat storage system stores heat at a temperature of 750 °C and is referred to as LT-PCM. For the HT-PCM, LiF is chosen as the suitable PCM heat storage based on the Table 6.1. From the Table 6.1, the composite, 74 % LiF + 13 % KF + 13 % MgF₂, is chosen as the heat storage medium for the LT-PCM

rSOC reactor

A commercially available rSOC reactor is used for the process system. The rSOC reactor is modelled as an adiabatic reactor and its performance is modelled based on the experimental results presented in chapter 4. The 0-D model presented in section 5.3 is used. For the SOFC mode, the fuel and air inlet temperature are set at 750 °C and 700 °C respectively. The maximum temperature difference between the maximum and the minimum temperature within the SRU of the rSOC reactor is equal to 250 °C. In most cases, this corresponds to the temperature difference between the inlet and outlet streams. In the SOEC operation mode, the inlet temperatures are at 820 °C for both air and steam inlet streams. The characteristic rSOC reactor temperature is calculated from the 1-D model through an iterative method. Initially a first estimate for the effective rSOC reactor temperature is provided. The system model is executed and boundary conditions of the rSOC reactor are obtained. The rSOC inlet parameters for the system operation point are translated to the 1-D model and simulated. The air flow rate is varied until the safe operation point of the reactor is reached. The safe operation point is a locus of air flow rates for which the maximum temperature difference within the SRU is less than 250 °C and the effective reactor temperature is not greater than 850 °C. It should also be noted that the temperature profile within the SRU should not vary drastically between SOFC and SOEC operation mode. This will induce a greater thermal stress in the reactor and might hence lead to failure. Based on the analysis presented in section 4.3, the difference between the effective reactor temperature between SOFC and SOEC mode is limited to 50 K.

Operation parameters

The system behaviour is analysed for two operational pressures. The system is studied at atmospheric pressure and at a pressure of 25 bar. Based on the analysis presented in chapter 4, the average current density for the rSOC reactor is equal to 2500 A/m² for both operation modes. A lower current density will require a bigger reactor area and hence lead to higher costs. An overview of system operational parameters and boundary conditions is presented in the Table 6.3.

TABLE 6.3. Operation parameters and boundary conditions of the closed loop hydrogen based rSOC system

Parameters	Value	Unit
Current density	2500	A/m ²
SOFC operation mode		
Fuel inlet temperature of rSOC	750	°C
Air inlet temperature of rSOC	700	°C
Maximum ΔT in rSOC reactor	250	°C
Total fuel conversion	90	%
Single pass fuel conversion	85	%
SOEC operation mode		
Steam inlet temperature of rSOC	820	°C
Air inlet temperature of rSOC	820	°C
Maximum ΔT in rSOC reactor	250	°C
Heat Storage		
HT-PCM heat storage temperature	850	°C
LT-PCM heat storage temperature	750	°C
Gas Storage tanks		
Fuel tank temperature	25	°C
Fuel tank pressure	25	bar
Water tank temperature	25	°C
Water tank pressure	1	bar

6.2.2 Results and discussion

The process system performance and behaviour of an hydrogen based closed architecture rSOC process system with a commercial ESC design rSOC reactor was studied at two

different operation pressure. The analysis was performed at 1 bar and at 25 bar. For the system operating at atmospheric pressure, the hydrogen fuel produced during the SOEC process has to be compressed to gas storage tank pressure. Whereas for the pressurised system, the air flow required must be compressed to the system pressure. The results of the two operational conditions are discussed below.

System performance at atmospheric pressure

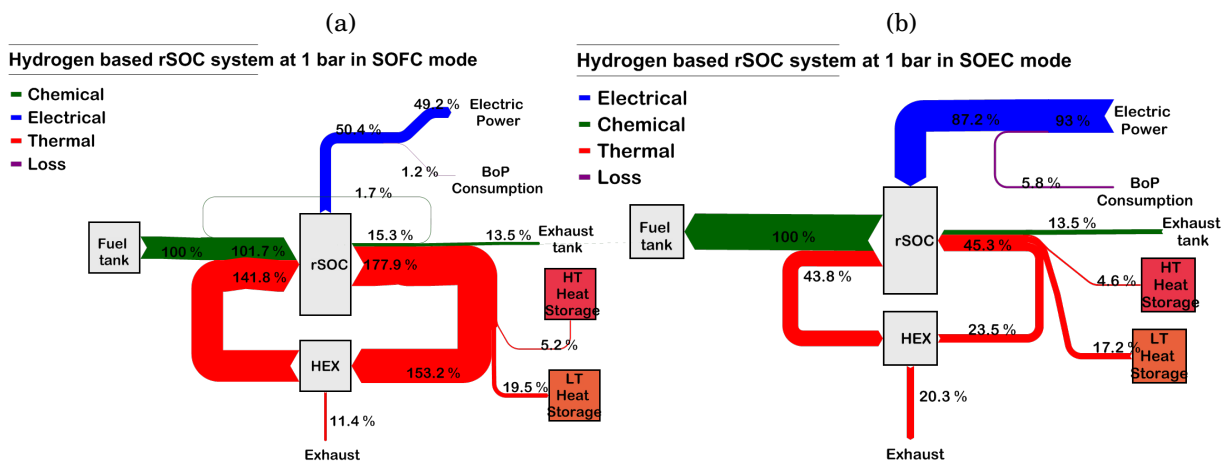


FIGURE 6.2. Chemical, electrical and thermal energy flows represented in Sankey diagram for the hydrogen based closed architecture rSOC system at 1 bar. (a) Represents the energy flows in SOFC operation mode. All flows are normalised by dividing by the chemical energy input to the system. (b) Represents the energy flows in SOEC operation mode. All flows are normalised by dividing by the chemical energy output of the system

A sankey diagram depicting the chemical, thermal and electrical energy flows in the system during both the modes of operation is presented in Figure 6.2. The energy flows are normalised by dividing the energy flows by the chemical energy in the fuel tank. The overall system performance at 1 bar is summarised in the Table 6.4. The gross roundtrip efficiency of 57 % was achieved. Taking into account the balance of plant energy consumption, a net roundtrip efficiency of 52 % was achieved.

The chemical, thermal and electrical energy flow in the system during the SOFC operation mode is presented as Sankey diagram in the Figure 6.2(a). The chemical, electrical energy and thermal energy flow within the rSOC system are normalised by dividing by the chemical energy supplied from the fuel tank to the system during

TABLE 6.4. rSOC system performance at 1 bar for the hydrogen based closed architecture rSOC system

Parameter	Value	Unit
SOFC		
Characteristic reactor temperature	845	°C
Cell voltage	0.731	V
Net efficiency in SOFC mode	49.4	%
SOEC		
Characteristic reactor temperature	809	°C
Cell voltage	1.262	V
Net efficiency in SOEC mode	107.1	%
Roundtrip efficiency		
Reactor (Gross)	57.8	%
System (Net)	52.9	%

SOFC operation. In the SOFC operation mode, pure hydrogen from the fuel tank which corresponds to the 100 % of the chemical energy is supplied to the system. The fuel from the storage tank is at a pressure of 25 bar and hence is expanded to the system operation pressure of 1 bar and exits the heat recovery stage with a temperature of 300 °C. A recycle ratio (defined as ratio of mass flow rate of exhaust gas recirculated as reactant to the mass flow rate of exhaust gas at the outlet of the rSOC reactor) of 11 % is maintained resulting in fuel composition of 90 mol% of H₂ and 10 mol% of H₂O and thereby increasing the chemical energy entering the rSOC reactor to 101.7 %. The H₂-H₂O fuel mixture is the finally preheated to the reactor inlet temperature of 750 °C. Air is preheated in the heat recovery unit to the required inlet temperature of 700 °C. The air and fuel stream entering the rSOC reactor carry thermal energy equivalent to 142 % of the chemical energy supplied to the system. For the given inlet conditions for the rSOC reactor in SOFC operation mode, the variation of temperature, ideal voltage, voltage losses, current density and concentration within the SRU of the rSOC reactor is shown in the Figure 6.3(a). The temperature of the MEA increases along the gas flow direction due to the exothermic hydrogen oxidation reaction. A maximum solid temperature is reached near the end of the reactor. The ideal voltage (U_{id}) decreases along the flow direction due to the increase in temperature and reducing concentration of the reactants along the flow direction. The voltage loss along the length of the flow channel mirrored the

behaviour of ideal voltage. The higher temperatures along the reactor length resulted in a lower ohmic losses along reactor length and hence we observe a decreasing voltage loss along the reactor length. The voltage losses and ideal voltage distribution resulted in SRU voltage of 0.731 V. Using the results of the detailed model, the characteristic rSOC reactor temperature for the 0-D model was determined to be 845 °C. The characteristic reactor temperature is calculated based on the procedure described in section 5.3.2. Fuel and air streams exit the rSOC reactor at 876 °C and carry the heat generated in the rSOC reactor during the SOFC operation. The gross electrical energy produced by the rSOC reactor constitutes close to 50 % of the chemical energy supplied to the system. This represents the gross electrical efficiency of the system during SOFC operation. The BoP electrical energy consumption equals 1.2 % of the chemical energy supplied to the system. Therefore a net electrical efficiency of 49.4 % is achieved. Heat produced due to exothermic reaction and internal losses accounts for 36 % of the chemical energy supplied to the system. The heat produced in the reactor is carried by the product streams (both fuel and air) and hence, the thermal energy at reactor outlet increases to 177 %. The remaining 15 % of the supplied chemical energy exits the rSOC reactor as unconverted chemical energy in the fuel stream. The heat produced in the reactor is first stored in the HT-PCM unit at 850 °C and in the LT-PCM unit at 750 °C. The total thermal energy stored in the heat storage unit accounts for 25 % of the chemical energy supplied, close to 20 % is stored in LT-PCM and 5 % is stored in HT-PCM. The remaining heat produced in the reactor is retained in the process streams which are used for preheating the inlet process streams.

The different components of energy flow in the rSOC system during the SOEC operation is shown in Figure 6.2(b). The energy flows are normalised by dividing by the chemical energy produced the SOEC operation. The chemical energy produced by the system during the SOEC operation is equivalent to the chemical energy supplied to the system during the SOFC operation. In the SOEC operation mode, the product gas produced from the SOFC operation is used as the reactant. The water stored in the water tank is supplied to the rSOC reactor. The water is first preheated in the economiser and later passes through the evaporator unit. A saturated steam exits the evaporator with a temperature of 100 °C. The steam is then mixed with the hydrogen stream, which was preheated to 100 °C. Hydrogen is required to be mixed with the steam to prevent the oxidation of Ni in the fuel electrode. Oxidation of Ni leads to volume increase, delamination and also inactivity of the electrode and hence higher losses. Secondly, the mass flow rate

6.2. CLOSED SYSTEM ARCHITECTURE FOR ELECTRICITY STORAGE

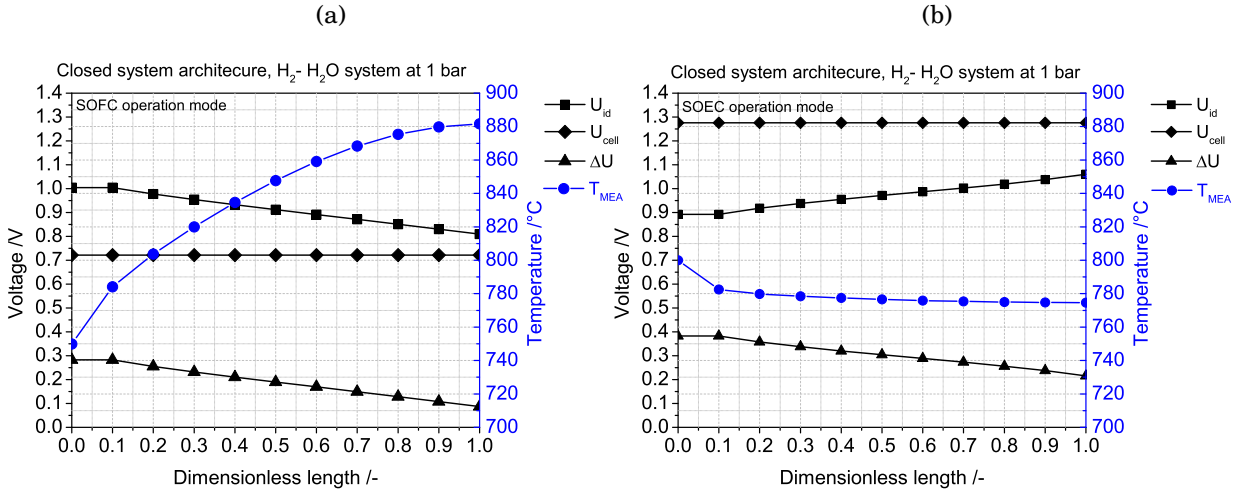


FIGURE 6.3. Variation of temperature, ideal voltage and losses in SRU at system operation conditions with current density at 2500 A/m² and 1 bar pressure in (a) SOFC operation mode and (b) SOEC operation mode

of hydrogen feed is determined such that the outlet gas composition of the fuel stream in the SOFC operation is same as the reactant composition supplied to the rSOC reactor in SOEC operation mode. After mixing, the reactant has a composition of 90 mol% of H₂O and 10 mol% of H₂. The inlet reactant stream contain chemical energy equivalent to 13.5 % of the chemical energy produced by the system. The SOEC reactants then enter the LT-PCM heat storage unit and HT-PCM heat storage unit, where the reactant stream is preheated to the rSOC inlet boundary condition for SOEC operation. The steam mixture then enters the rSOC reactor. Air is supplied to the rSOC reactor as a sweep gas in order to flush the oxygen (O₂) produced during SOEC mode. The sweep gas is preheated to the rSOC reactor inlet temperature in the heat recovery unit and the HT-PCM heat storage unit. The total thermal energy consumption from the heat storage tanks is equivalent to 22 % of the chemical energy produced. Of which, the thermal energy consumption from HT-PCM tank amounts to 5 % and from the LT-PCM tank it amounts to 17 % of the chemical energy produced. The reactants enter the rSOC reactor with an inlet temperature of 820 °C. The total thermal energy carried by the reactant streams is equal to 45.8 % of the chemical energy produced by the system. Variation of ideal voltage, ASR and temperature is shown in the Figure 6.3(b). For the given inlet conditions, the rSOC reactor operates in the endothermic SOEC mode. The temperature decreases along the reactor length from 820 °C at inlet to 778 °C at the outlet. The ideal voltage increases

along the length of the reactor. This is partly due to the reducing temperature and an increasing hydrogen concentration along the reactor length. The voltage loss decreases along the reactor length even though the temperature decreases along the reactor length. The temperature gradient is not steep along the reactor length therefore, the local ASR variation along the reactor length is not steep. But the voltage loss behaviour can be explained by the distribution of local current density. The H_2O concentration is higher near inlet of the reactor resulting in a higher reaction rate and hence higher local current density near the inlet. The high local current density at the inlet results in higher voltage losses at the inlet. The reaction rate is much lower near the reactor exit resulting in low local current density and hence a lower voltage loss close to the reactor exit. Based on the predictions of the 1-D model, the characteristic reactor temperature was determined to be $809\text{ }^\circ\text{C}$. The reactant utilisation was calculated as 88% satisfying the assumption 1-3 provided in section 6.1.1. The reactor operates at a SRU voltage of 1.26 V which is 0.02 V lower than the thermoneutral voltage for $\text{H}_2\text{-H}_2\text{O}$ reaction. The gross electrical energy consumption of the rSOC reactor contributed 87% of the total chemical energy produced. The BoP required to compress produced hydrogen from 1 bar to 25 bar consumed 5.8% of the chemical produced as electrical energy. Hence, resulting in a net electrical energy consumption of 93% of the chemical energy produced. The thermal energy required for endothermic SOEC operation accounted for 1.5% of the total chemical energy produced. The thermal energy was consumed from the reactant streams, hence, the thermal energy of the product streams decreased to 43% of the chemical energy produced. The product gases exited the rSOC reactor at $781\text{ }^\circ\text{C}$ which was used to preheat the reactant streams. The net efficiency of the rSOC system in SOEC operation mode is equal to 107% which is equal to the inverse of the net electrical energy consumption.

Thermal management and the role of heat storage is shown to be crucial for the system performance. From the Figure 6.2, it was shown that the thermal energy contribution to chemical energy in SOEC operation is only 1.5% . The rSOC reactor is only slightly endothermic during SOEC operation, but still a higher percentage of thermal energy is consumed from the heat storage tanks. Most of the thermal energy consumption from the heat storage tanks is used for process heating requirements. The heat is used for preheating the inlet reactants to the required boundary conditions and also for the steam generation. The vapour fraction of the $\text{H}_2\text{-H}_2$ reactant mixture after the final heat recovery unit is only 0.46 . Hence, a significant proportion of the thermal energy

consumption from the LT-PCM tank in SOEC operation is used for the steam generation and super heating the steam. Therefore, apart from providing the heat for endothermic behaviour for the rSOC reactor in SOEC operation, the heat storage also meets the demands of the process heating requirements, hence achieving a self sustaining system. If the heat storage is not available, the entire heat requirement has to be met by an external heat source such as electrical heat or fuel combustion leading to even lower roundtrip efficiencies. In total, 88 % of the thermal energy stored in the heat storage during the SOFC operation is consumed during the SOEC operation of the system.

System performance at 25 bar

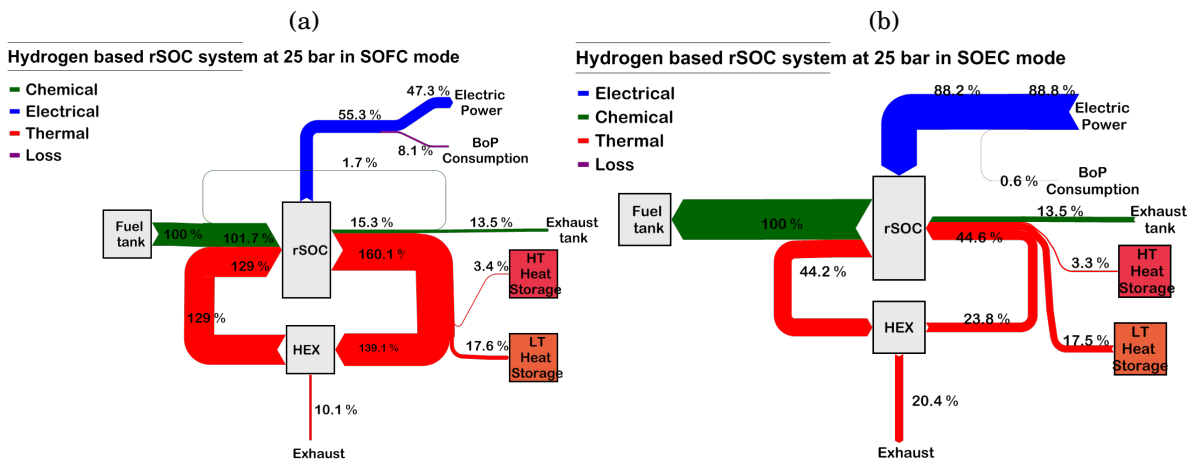


FIGURE 6.4. Chemical, electrical and thermal energy flows represented in Sankey diagram for the hydrogen based closed architecture rSOC system at 25 bar. (a) Represents the energy flows in SOFC operation mode. All flows are normalised by dividing by the chemical energy input to the system. (b) Represents the energy flows in SOEC operation mode. All flows are normalised by dividing by the chemical energy output of the system

The performance of the hydrogen based closed rSOC system architecture under pressurised operation is discussed. In chapter 4, it was shown that the pressurised operation leads to higher roundtrip efficiency from a reactor perspective. In this section, it is shown that the effect does not hold true from a system perspective. For the pressurised system operation, an rSOC reactor roundtrip efficiency of 62.7 % was achieved. In contrast, the system roundtrip efficiency of only 53.2 % was achievable. The pressurised operation yielded only a marginal increase in system performance. This drastic drop between the reactor and system roundtrip efficiency is due to the BoP work consumption. The

summary of system performance is provided in the Table 6.5. On comparing the Tables 6.4 and 6.5, the difference in BoP consumption can be observed. For the atmospheric system operation, the hydrogen produced in the SOEC operation has to be pressurised to 25 bar before storing it in the gas tanks. Hence, the BoP consumption in SOEC mode is more than in SOFC mode. Whereas for the pressurised operation, the BoP power consumption in SOFC mode is higher. This is because in the SOFC operation mode, the air supplied to the reactor has to be pressurised to 25 bar from ambient state. This leads to higher parasitic losses and hence lower system roundtrip efficiency.

TABLE 6.5. System performance of hydrogen based rSOC system under pressurised operation at 25 bar

Parameter	Value	Unit
SOFC		
Characteristic reactor temperature	845	°C
Cell voltage	0.803	V
Net efficiency in SOFC mode	47.5	%
SOEC		
Characteristic reactor temperature	809	°C
Cell voltage	1.279	V
Net efficiency in SOEC mode	112.1	%
Roundtrip efficiency		
Reactor (Gross)	62.7	%
System (Net)	53.2	%

The mass flow rate of the fuel supply and the process scheme of the pressurised system is similar to that of an atmospheric system. The energy flows in the rSOC system during SOFC operation is depicted in Figure 6.4(a). In the SOFC operation mode, the fuel from the tank at 25 bar is supplied to the system. No expansion process is required. The chemical power supplied to the rSOC system is maintained the same as in the non-pressurised system. The fuel is preheated and mixed with the recycle stream before it is supplied to the rSOC reactor at 750 °C. The fuel recycle ratio is retained at 11 %. Therefore, chemical energy entering the rSOC reactor is equal to 101.7 % of the chemical energy supplied from the fuel tank. Air is supplied to the system from the ambient. It is compressed to 25 bar in the four stage compression process and exits the compressor

with a temperature of 80 °C. The pressurised air is then passed through the initial heat recovery units, where it is heated to 500 °C and is then mixed with the air recycle stream. The air recycle loop is activated for the pressurised system. A portion of the air exhaust from the rSOC reactor after the SOFC operation is recycled within the system. The recycle ratio is controlled such that the mixed air stream reaches the required inlet temperature of 700 °C for the rSOC reactor in SOFC operation mode. An air recycle ratio of 78 % is attained for optimum performance. The high air recycle ratio has certain advantages and disadvantages. Firstly, a high recycle ratio, leads to less volume flow rate of fresh air from the atmosphere. This in turn reduces the work consumed by the air compressor. Secondly, less heat in heat recovery units is needed to preheat the air to the required boundary condition. Hence, work can be extracted in an expansion turbine before the product air from the rSOC reactor is released to the atmosphere. Together, this reduces the BoP power consumption. But, high air recirculation reduces the partial pressure of oxygen in the air entering the rSOC reactor. This reduces the ideal voltage and also possibly increases the activation losses on the air electrode in the rSOC reactor though it is expected that the advantages of air recirculation outweigh the disadvantages. The reactants fed to the rSOC reactor carry thermal energy equivalent to 129 % of the chemical energy supplied to the system. The temperature, ideal voltage and voltage loss distribution along the reactor length is provided in Figure 6.5(a). The behaviour of the key parameters along the reactor length at 25 bar is similar to its behaviour for system operation at 1 bar. For the inlet conditions, the characteristic reactor temperature was determined to be 845 °C and a SRU voltage of 0.803 V was obtained. The gross electrical energy produced by the rSOC reactor amounts to 55 % of the chemical energy fed to the system. This is 5 % more than the power produced at non-pressurised operation. The higher electric power is due to the positive effect of pressure on the SOFC operation. The BoP components consume 8 % of the chemical energy supplied to the system as electrical energy. The high electrical energy consumption of the BoP components is attributed to the energy required to compress air. Therefore, reducing the net electrical energy produced by the system to 47.3 % of the chemical energy supplied to the system. This corresponds to the net electrical efficiency for the system in SOFC operation. Around 31 % of the chemical energy supplied to the system is converted to thermal energy in the rSOC reactor during SOFC operation. The heat produced is carried by the product streams exiting the rSOC reactor. The thermal energy of the product streams leaving the rSOC reactor is increased to 160 % of the chemical energy supplied to the system. The remaining 15 % of the chemical energy supplied to the system is retained in the product

streams as unconverted fuel of which 1.7 % is recirculated to the reactants. The thermal energy stored in the heat storage is equivalent to 21 % of the chemical energy supplied. The heat stored in HT-PCM and LT-PCM amounts to 3.4 % and 17.6 % respectively. Due to positive effect of pressure on rSOC reactor in SOFC operation, less heat is produced and hence less heat is available for storage than in the non-pressurised scenario.

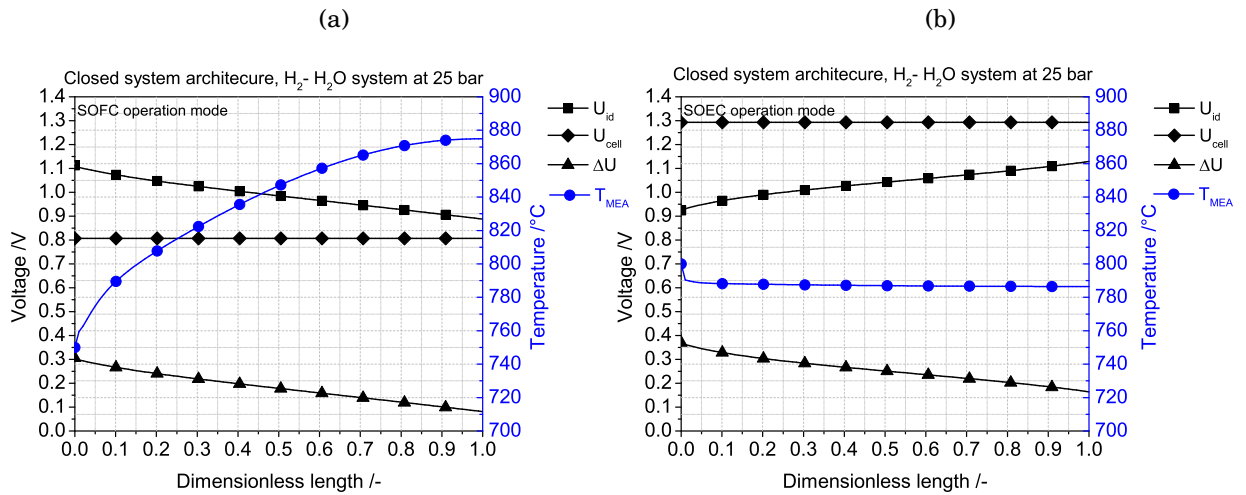


FIGURE 6.5. Variation of temperature, ideal voltage and losses in SRU at system operation conditions with current density at 2500 A/m^2 and 25 bar pressure in (a) SOFC operation mode and (b) SOEC operation mode

The different components of energy flow in the rSOC system during the SOEC operation is shown in Figure 6.4(b). The energy flows are normalised by dividing by the chemical energy produced the SOEC operation. In the SOEC operation mode, the steam and 10 mol% of H_2 is supplied to the rSOC reactor similar to the non-pressurised operation. The H_2 - H_2O carry 13.5 % of the chemical energy produced by the system. Air from the atmosphere is compressed to 25 bar in a 4 stage compression process and is supplied to the system. Unlike in SOFC operation mode, air recirculation loop is not activated, since the mass flow rate of air is not as high as in SOFC mode. The reactants are preheated in the heat recovery units and fed to the heat storage units where they are brought to the required boundary conditions. The reactants are fed to the rSOC reactor at an inlet temperature of $820 \text{ }^\circ\text{C}$. The reactant streams contain thermal energy equal to 44.6 % of the chemical energy produced by the system. Out of the total thermal energy available in the reactant streams entering the rSOC reactor, the heat storage unit

contributed 20.8 % of the chemical energy produced as process heat. The distribution of temperature, voltage loss and ideal voltage along the reactor length during electrolysis operation is shown in Figure 6.5(b). The rSOC reactor is almost thermoneutral at 25 bar, the temperature along the length of SRU is constant. The behaviour of ideal voltage and voltage loss is similar to the case of non pressurised operation. For the given inlet conditions, the rSOC reactor operates at a SRU voltage of 1.279 V which is almost equal to the thermoneutral voltage for H_2 - H_2O reaction. The electrical energy consumed by the rSOC reactor accounts for 88 % of the chemical energy produced whereas the contribution of thermal energy is only 0.4 % of the chemical energy produced by the system. This implies the rSOC reactor is almost thermoneutral during the SOEC operation. The electrical energy consumption of the BoP components is marginal at 0.6 % of the chemical energy produced by the system. The product streams exit the rSOC reactor at 800 °C. The fuel stream is cooled in the heat recovery unit. The hydrogen is separated from the remaining water and is stored in the fuel tank. Hot product air is used for preheating the compressed air. It is then expanded in an expansion turbine to recover the work required for the compressor. It is expanded to atmospheric pressure and released to the ambient. The rSOC system achieves a net efficiency of 112 % in SOEC operation.

Thermal management is again shown to be essential for optimal system performance. Though the rSOC reactor is almost thermoneutral, 99 % of the thermal energy stored in the heat storage tanks during the SOFC operation is consumed in the SOEC operation mode. Similar to the case of the non-pressurised system, thermal energy from the heat storage tanks was utilised for process heating and steam generation. This further highlights the importance of heat storage and thermal management even for thermoneutral operation of rSOC reactors in the SOEC operation mode. Most of the heat consumed from the LT-PCM tank is used for the steam generation process.

Summary of closed system architecture

The performance of the hydrogen based closed rSOC system architecture was studied under pressurised and non-pressurised conditions. It was shown that even though the pressure has a positive effect on reactor roundtrip efficiency, the effect on system roundtrip efficiency is only marginal. This is due to the high BoP consumption during the pressurised operation. The compression of air during the SOFC operation of the pressurised rSOC system was more energy intensive than downstream hydrogen compression

during the SOEC operation of the non-pressurised rSOC system. High air recirculation and complex system designs are required for achieving the reported system performance for the pressurised rSOC system. The system performance is summarised in the Figure 6.6.

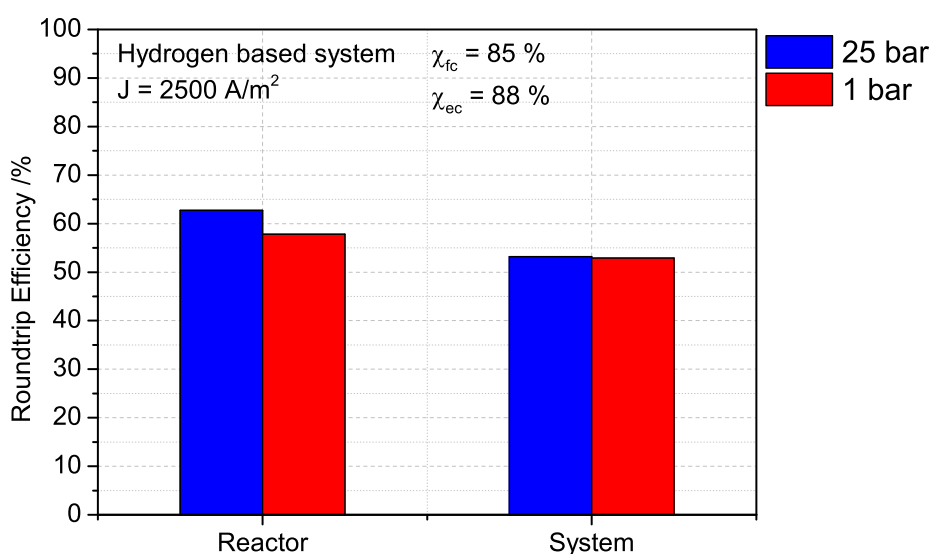


FIGURE 6.6. Summary of hydrogen based closed rSOC system performance at 1 bar and 25 bar.

Further, the importance of thermal management and heat storage was highlighted for both operation conditions. The rSOC reactor was operating in the endothermic region and close to the thermoneutral point during the SOEC operation of the system in non-pressurised and pressurised condition respectively. In both cases, a significant portion of the heat stored in the heat storage system was consumed for process heating. This proves that the thermal management is essential for an efficient rSOC system. The heat ratio of the non-pressurised and the pressurised system are 88 % and 99 % respectively. The heat ratio is summarised in the Figure 6.7.

A closed rSOC system architecture based on hydrocarbons and with the methanation downstream process during the SOEC operation was also studied. A similar qualitative result was obtained for the same. For a hydrocarbon based closed rSOC system architec-

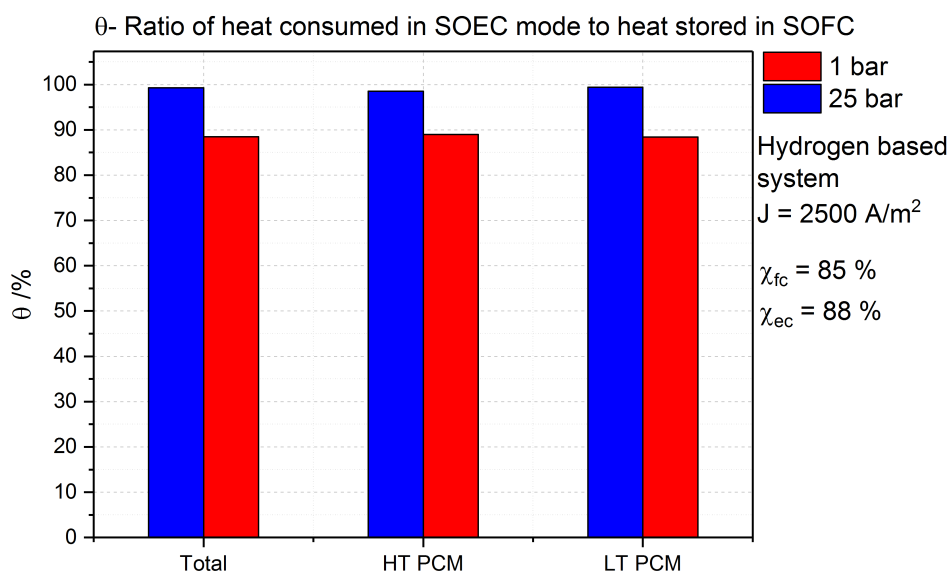


FIGURE 6.7. Heat ratio of hydrogen based closed rSOC system at 1 bar and 25 bar.

ture, the pressurised operation had a positive effect on the energy storage density. The fuel produced during the SOEC operation for a pressurised system resulted in higher LHV and hence higher storage density. Moreover, pressurised operation can promote exothermic methanation within the rSOC reactor leading to better thermal management of the system. The detailed analysis of hydrocarbon based closed rSOC system is discussed in [223].

6.3 Hydrocarbon based rSOC system for sector coupling

The functionality of rSOC reactors can be extended using an open system configuration. Apart from energy storage, the rSOC reactor systems are ideal for sector coupling. In the open system configuration, during the SOEC operation, the fuel/chemical produced is supplied to gas grids or other energy, chemical or process industries. Likewise, in SOFC operation, the fuel required is obtained from gas grids, chemical industries or other sources. This allows for greater flexibility and use of the rSOC reactors and systems. Useful chemicals or fuels used by other process industries are largely based on hydrocarbons.

Hence, in this analysis, a hydrocarbon based open rSOC system architecture is analysed. Many synthesis routes are possible producing various hydrocarbons depending upon the final use. Methane (CH_4) is one of the most common and abundantly used hydrocarbons in the energy and chemical process industries. Additionally, storing electrical energy as methane can exploit the existing vast network of natural gas grids. The gas grids provides a huge storage capacity and allows for easy transportation of the energy. Hence, a methane based gas grid connected rSOC system (henceforth referred to as the methane based rSOC system) is considered in this analysis.

The methane based gas grid connected system is an extension of the hydrogen based closed architecture rSOC system with additional downstream process in SOEC operation mode and BoP components. In the charging or SOEC operation, the electrical energy is utilised to electrolyse water and carbon dioxide to produce syngas. The syngas is then converted to methane in the downstream process and fed to the gas grid. During the discharge or fuel cell operation, methane as fuel from the natural gas grid is supplied to the rSOC system.

6.3.1 Model descripton

The simplified process flow diagram of the methane based gas grid connected rSOC system is depicted in the Figure 6.8. The SOFC and SOEC process are described in the Figure 6.8(a) and Figure 6.8(b) respectively.

SOFC operation mode

Methane from the natural gas grid is supplied as fuel to the rSOC system during the SOFC operation. It is assumed that the fuel is supplied to the system at the operational pressure of 25 bar. Natural gas at these pressures can be obtained from the intermediate pressure natural gas pipelines. The pressures at these pipelines are in the range of 25-50 bar. Hence, no additional compressor work is required to compress the natural gas to the system operational pressure. It is initially preheated in the first heat recover units by the exhaust streams from the rSOC reactor. The fuel is then mixed with the fuel exhaust recycle stream. The fuel exhaust recycle stream is at a temperature of 670 °C. The fuel exhaust stream of the rSOC reactor consists mainly of steam and carbon dioxide. Steam is required to be added to the fuel for the reforming reaction to take place in the pre-reformer. Also, steam is added to the fuel stream to maintain a high

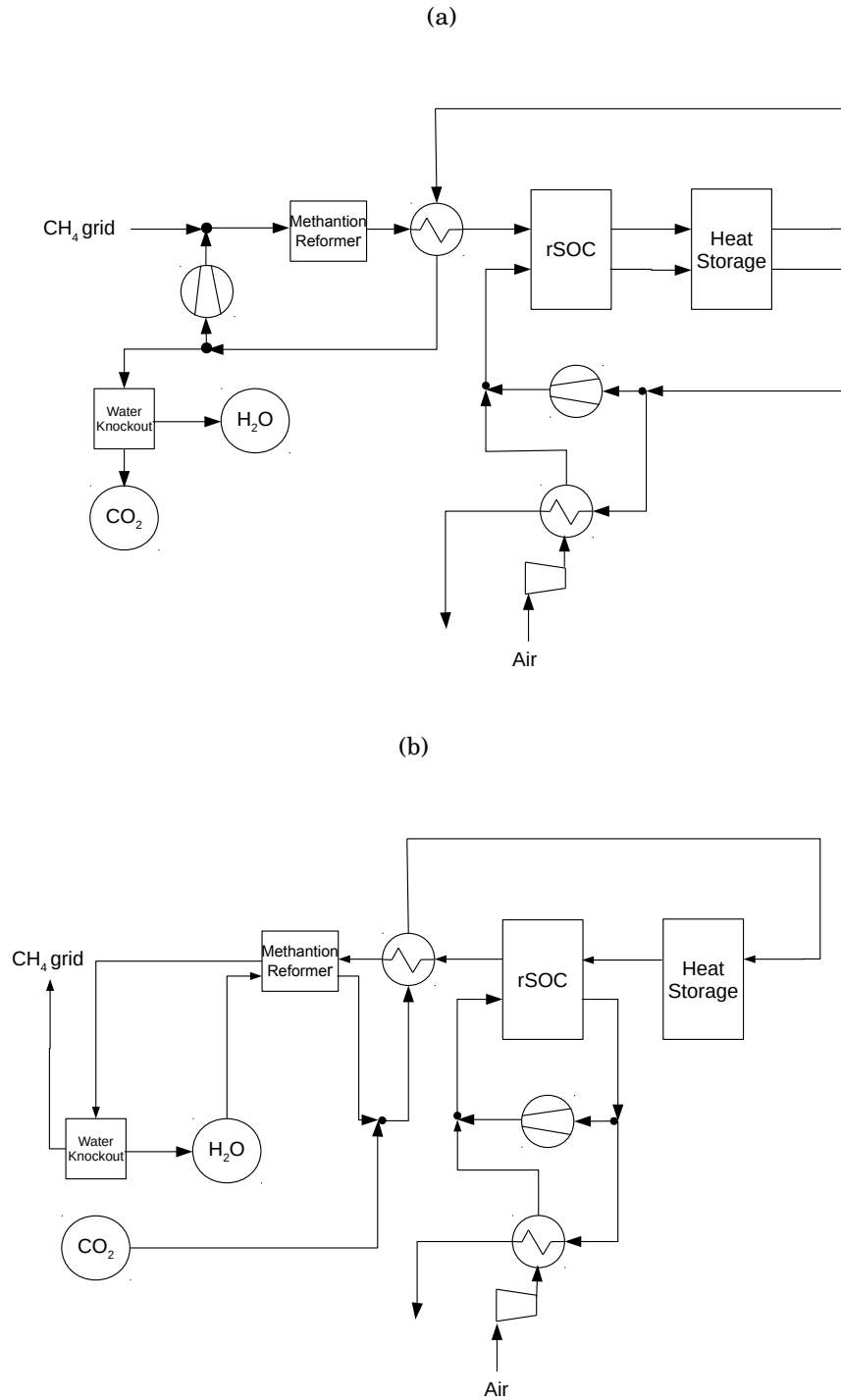


FIGURE 6.8. (a) Process flow diagram of the methane based gas grid connected rSOC system during the SOFC operation mode (b) Process flow diagram of the methane based gas grid connected rSOC system during the SOEC operation mode.

Steam to Carbon Ratio (STCR) of 2 and above to prevent carbon deposition in the system. Hence, the fuel exhaust recycle loop eliminates the need for a steam generation unit in the SOFC operation. The fuel exhaust recycle ratio is varied accordingly to achieve a STCR of 2 after mixing. After mixing, the resultant fuel mixture reaches a temperature of 459 °C. The resulting fuel mixture is then preheated in the heat recovery units to a temperature of 670 °C and fed to the pre-reformer where the methane undergoes steam reforming. The reformat product gas has a lower temperature at the outlet due to the endothermic reforming reaction. It is then fed to the final heat recovery unit where it is heated to the required fuel inlet temperature of 750 °C for the rSOC reactor during the SOFC operation. Air is supplied to the system from the ambient and is compressed to the system pressure of 25 bar. It is then preheated in the heat recovery units and mixed with the air exhaust recycle stream. Similar to the closed system architecture, the recycle ratio is determined such that the air mixture temperature achieves the inlet temperature of 700 °C required for the rSOC reactor during SOFC operation. The product gas from the SOFC exhaust mostly consists of H₂O, CO₂ and unconverted H₂ and CO. The air and fuel exhaust streams from the rSOC reactor are sent to heat storage unit, where the heat produced in the rSOC reactor is stored. Remaining heat in the exhaust streams are used for preheating the inlet streams in the heat recovery unit and part of the fuel exhaust stream is recycled to the inlet. The fuel exhaust stream is further cooled to condense and remove the water. The remaining CO₂ and the unreacted CO and H₂ is fed to the exhaust tank. Likewise, the air stream is partly recycled and excess is cooled in the heat recovery unit. It is then expanded to atmospheric pressure and released to the environment.

SOEC operation mode

During the SOEC process, H₂O and CO₂ is fed to the rSOC reactor for co-electrolysis. The CO₂ required for co-electrolysis is obtained from the gas stored in the exhaust tank during the SOFC operation. The mass flow rates of H₂O and the exhaust gas mixture are chosen such that H/C ratio is equal to 7 which is required for high methane production [85]. The gas composition is controlled such that the reactant composition fed to the rSOC reactor during SOEC operation is similar to the product composition from the rSOC reactor during the SOFC operation. Water is first pumped to the system operational pressure of 25 bar. It is then fed to the steam generation unit which is coupled to the methanation reactor unit. Heat produced during the exothermic methanation downstream process is used for steam generation. The produced steam is then fed to

the final heat recovery unit and mixed with the CO₂ dominated exhaust gas mixture which is preheated in the heat recovery unit. The CO₂ dominated exhaust gas mixture contains some amount of H₂ required to prevent oxidation of Ni in the fuel electrode. The mixture of steam, carbon dioxide and hydrogen is then fed to the heat storage units where it absorbs the heat stored during the SOFC operation and enter the rSOC reactor at an inlet temperature of 785 °C. A lower inlet temperature is chosen for the SOEC operation for the methane based system as compared to the hydrogen based system. This is because for the methane based system, the rSOC reactor is expected to operate in the exothermic region during the SOEC process. Air is fed to the system from the atmosphere. Due to the exothermic nature of this SOEC process, air is used as sweep gas and also as cooling medium for the rSOC reactor. Air is first compressed to the system pressure and preheated in the heat recovery unit. An air exhaust recycle unit is employed also for the SOEC process. The preheated air is then mixed with the air exhaust recycle stream. The recycle ratio is determined such that the air mixture temperature achieves the inlet temperature of 785 °C. After the co-electrolysis, the fuel gas (syngas) produced by the rSOC reactor is cooled to a temperature of 300 °C and fed to the downstream process. A four stage methanation process is employed for the downstream process and is addressed below. The final fuel with high methane content is separated from the water and fed to the natural gas grid. The air exhaust from the rSOC reactor is partly recycled and cooled in the heat recovery unit. It is then expanded to the atmospheric pressure before released to the environment.

Gas storage

Unlike the closed system architecture, in the methane based system the fuel is stored in the gas grid. Gas storage tanks in the methane based system are used for storing the CO₂ and water produced during the SOFC process. The CO₂ exhaust tank is at 25 bar and temperature of 25 °C. Water is stored as liquid at 25 °C. The number of storage tanks remains the same as in the closed system architecture.

Heat Storage

The heat storage system employed in the open system architecture is similar to the one described for the hydrogen based closed system architecture.

rSOC reactor

The model and boundary conditions of the rSOC reactor essentially remains the same as for the closed system architecture. The inlet temperature of the fuel and air inlet to the rSOC reactor during the SOFC operation is retained at 750 °C and 700 °C respectively. The allowable temperature difference between the maximum temperature and minimum temperature in the SRU is set at 250 K. Internal steam reforming and methanation reactions are expected to occur within the rSOC reactor during the SOFC and SOEC operations respectively. This can induce cold spots (low temperature point) and hot spots (high temperature point) within the reactor which can lead to failure. This further attenuates the need to verify if the system operation conditions lead to hazardous behaviour within the rSOC reactor. The inlet boundary conditions for the rSOC reactor during the SOEC operation are different than in the hydrogen based system. It is expected that the rSOC reactor will operate in exothermal mode during the SOEC process. Hence, the inlet temperatures of the fuel and air reactants are lowered to 785 °C. The characteristic rSOC reactor temperature for the 0-D model is determined by the method described earlier in section 6.2.1.

Methanation process and pre-reformer

In the SOFC operation of the rSOC system, a pre-reformer is employed to partially reform the methane fuel. The reformer is modelled as an adiabatic equilibrium reactor. The minimum temperature (either at inlet or outlet) is set at 300 °C. Below this temperature, the commonly used nickel based catalysts are not activated. A four stage downstream methanation process is employed during the SOEC process. The methanation process is modelled based on the commercial TREMP methanation process developed by Haldor Topsoe. The TREMP process employs multistage adiabatic methanation reactors. Due to exothermic nature, the products from the reactors are cooled before fed to the next methanation reactor. Intermediate cooling is employed to move the gas temperatures towards higher equilibrium conversions [224]. The TREMP methanation process is characterised by a low and high temperature region. The low temperature region (third and fourth stage methanation reactors) can operate in the temperature range between 250 °C to 350 °C [225] and the high temperature region (first and second stage methanation reactors) can reach temperatures up to 700 °C [226, 227]. State of the art catalyst (e.g. MCR-2X) can handle high temperatures till 700 °C [225, 228]. Integrating heat recovery for steam generation with the methanation process improves the exergy efficiency of the process.

High pressure steam can be generated by extracting the heat from the methanation reactors for steam generation [225]. The high temperature operation region of the methanation process has a similar operational range for the steam methane reforming reaction. The same catalyst can indeed act as catalyst for reformer. Hence, in the methane based rSOC process system, the 1st methanation reactor is used as a pre-reformer during the SOFC operation process. For the system modelling activity, the methanation reactors are modelled as equilibrium reactor. The equilibrium compositions represent the limit for conversion. Additionally, with proper dimensioning of the reactor and optimised value for the space velocity, the reactant conversions close to equilibrium values can be attained. Hence, the equilibrium assumption for the modelling is justifiable. Though for a proper sizing of the reactor, a kinetic model should be employed based on the selected catalyst.

Operation parameters

The methane based gas grid connected rSOC system is analysed for two current densities. Though it was shown earlier that the pressurised operation is challenging from the system perspective, pressurised operation of the methane based rSOC system is considered. The reasons for the pressurised operation are presented here. In chapter 4, it was shown that for an H-C-O system using a commercial rSOC reactor, an exothermic operation is achieved at 25 bar at a current density of 2500 A/m². Since, during the co-electrolysis process hydrogen and carbon monoxide are produced which, under the relevant conditions (high pressure) can undergo the exothermic methanation reaction within the rSOC reactor. This leads to an exothermic behaviour of the rSOC reactor during the SOEC operation. Yet it was shown for the H-O based system that the SOEC process is still endothermic or close to thermoneutral at 25 bar and 2500 A/m². Therefore, the possibility of internal methanation at 25 bar for co-electrolysis in the SOEC operation can help in thermal management of the SOEC process. Moreover, the downstream methanation process requires a pressurised process for high methane production. Due to the above reasons, a pressurised operation of the methane based rSOC system is considered. The exothermic SOEC process is achievable at a current density of 2500 A/m² and possibly even at lower current densities resulting in higher roundtrip efficiency. Hence, the system is analysed for two current densities. An overview of the system operational parameters and boundary conditions is provided in the Table 6.6.

TABLE 6.6. Operation parameters and boundary conditions of the gas grid connected methane based gas grid rSOC system

Parameters	Value	Unit
System pressure	25	bar
SOFC operation mode		
Fuel inlet temperature of rSOC	750	°C
Air inlet temperature of rSOC	700	°C
Maximum ΔT in rSOC reactor	250	°C
Total fuel conversion	90	%
Single pass fuel conversion	85	%
SOEC operation mode		
Steam inlet temperature of rSOC	785	°C
Air inlet temperature of rSOC	785	°C
Maximum ΔT in rSOC reactor	250	°C
Heat storage		
HT-PCM heat storage temperature	850	°C
LT-PCM heat storage temperature	750	°C
Gas storage tanks		
Exhaust tank temperature	25	°C
Exhaust tank pressure	25	bar
Water tank temperature	25	°C
Water tank pressure	1	bar
Methanation and reforming		
Minimum temperature in reactor	300	°C
Maximum temperature in reactor	700	°C
No. of stages in downstream process	4	

6.3.2 Results and discussion

The methane based rSOC system was analysed for the nominal operating current density of 2500 A/m² and for a lower current density of 1500 A/m². For both the operational current densities, the system pressure was maintained at 25 bar. The system performance at both the current densities is discussed below. A sankey diagram showing the energy flows in the system is presented Figure 6.9. The energy flows are normalised by dividing them by the chemical energy supplied to the system in SOFC operation or produced by the system in SOEC operation. The chemical energy produced by the system in the SOEC operation mode is equal to the chemical energy supplied to the system in the SOFC operation mode due the assumptions one to three.

TABLE 6.7. Performance of the methane based gas grid connected rSOC system at a current density of 2500 A/m²

Parameter	Value	Unit
SOFC		
Characteristic reactor temperature	845	°C
Cell Voltage	0.772	V
Net efficiency in SOFC mode	57	%
SOEC		
Characterisitic reactor temperature	800	°C
Cell voltage	1.235	V
Net efficiency in SOEC mode	92.9	%
Roundtrip efficiency		
Reactor (gross)	62.2	%
System (net)	52.9	%

The performance of the methane based rSOC system is summarised in the Table 6.7. The reactor roundtrip efficiency of 62.2 % and the net system roundtrip efficiency of 52.9 % was achievable for the methane based grid connected rSOC system. Similar to the case of pressurised hydrogen based system, the lower system roundtrip efficiency as compared to the reactor roundtrip efficiency is due to the high BoP work consumption during the SOFC process. The sankey diagram depicting the energy flows in the system is depicted in Figure 6.9(a). During the SOFC operation mode, methane is supplied to the system after sulphur removal. Methane supplied to the system from the gas grid corresponds

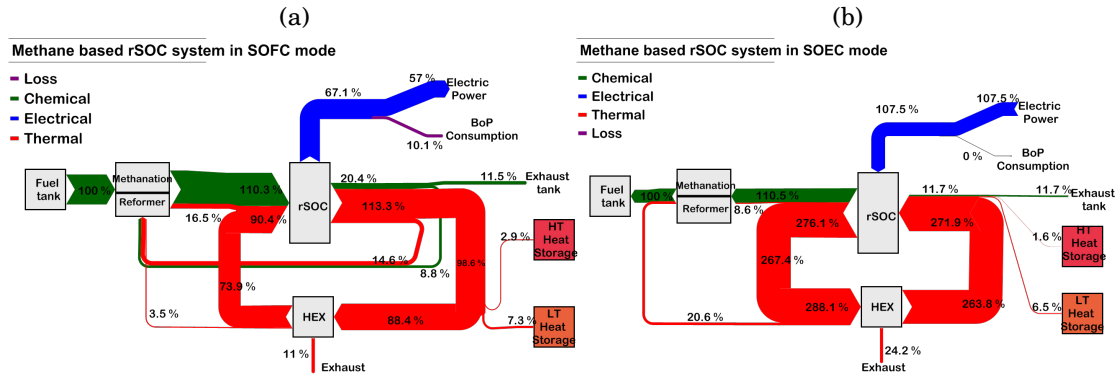


FIGURE 6.9. Chemical, electrical and thermal energy flows represented in Sankey diagram for the methane based rSOC system at 2500 A/m^2 . (a) Represents the energy flows in SOFC operation mode. All flows are normalised by dividing by the chemical energy input to the system. (b) Represents the energy flows in SOEC operation mode. All flows are normalised by dividing by the chemical energy output of the system

to the 100 % of the chemical energy supplied. It is mixed with the fuel exhaust recycle stream obtained from the rSOC exhaust stream. The temperature of the fuel exhaust recycle stream is $678 \text{ }^\circ\text{C}$. A recycle ratio of 48 % is required to achieve the required STCR to avoid carbon deposition in the pipe, reformer and the rSOC reactor. The exhaust recycle stream contains 8.8 % of the chemical energy supplied to the system. It also transmits thermal energy equivalent to 14.6 % of the chemical energy supplied to the system due to its high temperature. The resulting fuel mixture is at a temperature of $459 \text{ }^\circ\text{C}$ and further is preheated to $670 \text{ }^\circ\text{C}$ in the heat recovery unit where it absorbs thermal energy equal to 3.5 % of the chemical energy supplied to the system. It is then fed to the pre-reformer unit where it is pre-reformed. The reformat gas exits the pre-reformer at a temperature of $594 \text{ }^\circ\text{C}$. The lower outlet temperature is due to the endothermic reforming reaction. The chemical energy of the reformat is increased to 110 % of the chemical energy supplied to the system. It is then preheated to the required fuel inlet temperature of $750 \text{ }^\circ\text{C}$. The air required for the SOFC operation, is compressed to 25 bar from the ambient. The compressed air is then preheated in the heat recovery unit and mixed with the air exhaust recycle stream. An air exhaust recycle ratio of 48 % was required to raise the temperature of the air mixture to the required inlet temperature of $700 \text{ }^\circ\text{C}$. The reactants entering the rSOC reactor carry 90.4 % of the chemical energy supplied to the system as thermal energy. For the given inlet conditions, the variation of MEA temperature, ideal voltage and voltage loss along the length of the rSOC reactor

during the SOFC operation is shown in the Figure 6.10(a).

TABLE 6.8. Gas composition at the outlet of rSOC and exhaust tank for methane based system in SOFC mode

Gas species	rSOC outlet	Exhaust storage tank
H ₂	8 %	20 %
H ₂ O	58 %	0.00 %
CO	4 %	9 %
CO ₂	30 %	71 %
CH ₄	0.00 %	0.00 %
O ₂	0.00 %	0.00 %
N ₂	0.00 %	0.00 %
C	0.00 %	0.00 %

A drop in the MEA temperature is observed near the inlet of the rSOC reactor. This temperature reduction is due to the endothermic steam reforming reaction which occurs close to the reactor inlet. The temperature then further increases along the reactor length due to exothermic oxidation reaction and losses. The local ideal voltage of the reactor decreases along the reactor length due to decreasing concentration of fuel components (H₂ and O₂) and increasing temperature along reactor length. The voltage loss also decreases along the reactor length. This is due to decreasing ASR with higher temperature towards reactor outlet. From detailed model results for the system operating conditions, the characteristic temperature of the rSOC reactor in SOFC operation was determined to be 843 °C. The rSOC reactor operates at a cell voltage of 0.773 V. The gross electrical energy produced by the rSOC reactor in SOFC operation amounts to 67 % of the chemical energy supplied to the system. This corresponds to the gross electrical efficiency of the system in SOFC operation. Electrical energy equal to 10 % of the chemical energy supplied to the system is consumed by the BoP components. Hence, a net electrical efficiency of 57 % is achieved in SOFC operation of the rSOC system. The thermal energy generated in the rSOC reactor accounts for 23 % of the chemical energy input to the system. The heat generated in the rSOC reactor is carried by the product streams leaving the rSOC reactor. Hence, the thermal energy of the product stream is increased to 113 % of the chemical energy supplied to the system. The fuel and air stream exits the reactor at a temperature of 876 °C. The concentration of the fuel exhaust at the outlet of the rSOC

reactor is provided in the Table 6.8. The fuel exhaust stream contains 20.4 % of the chemical energy supplied to the system as unreacted fuel of which 8.8 % is recycled to the reformer. A part of the thermal energy in the exhaust streams is stored in the heat storage units. The heat stored in the thermal energy storage system accounts for only 10 % of the input chemical energy and is significantly lower than in the hydrogen based system presented in section 6.2.2. Heat produced during the SOFC operation is significantly lower for the methane based system. This is due to the endothermic internal reforming occurring within the rSOC reactor which absorbs a part of the heat produced due to exothermic oxidation and losses. The remaining thermal energy in the exhaust streams is used to the preheat in the inlet reactants and support the reforming reaction in the pre-reformer. The fuel exhaust stream is cooled in water knock out unit, where CO_2 , unreacted H_2 and CO are separated from water and sent to the exhaust tank. The fuel exhaust stream fed to the exhaust tanks contains chemical energy equal to 11.5 % of the chemical energy supplied to the system.

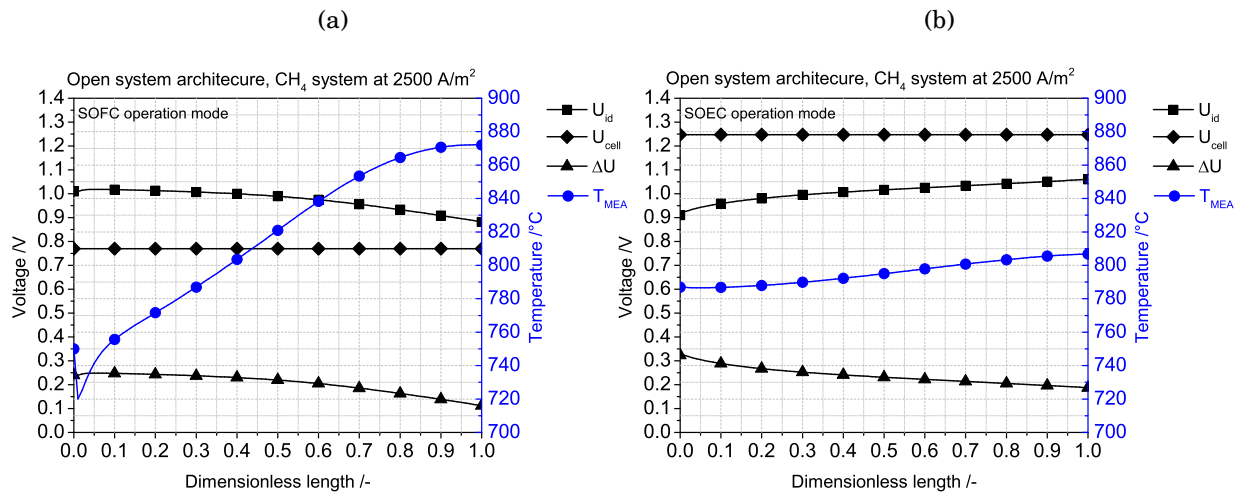


FIGURE 6.10. Variation of temperature, ideal voltage and losses in SRU at system operation conditions with current density at 2500 A/m^2 in (a) SOFC operation mode and (b) SOEC operation mode

The energy flows for the rSOC system in SOEC operation mode is shown in Figure 6.9(b). The energy flows are normalised by dividing by the chemical energy produced by the system. In the SOEC operation mode, the mixture of H_2O and CO_2 is fed to the rSOC reactor as reactant. The reactant mixture also contains some amount of H_2 and CO .

Therefore, it possesses chemical energy equal to 11.7 % of the chemical energy produced by the system. The water is supplied to the system from the water tank at 25 °C and is first pumped to the system pressure of 25 bar before it is fed to the steam generation unit. The steam generation unit is interlinked with the downstream methanation process. As the methanation process is exothermic, the heat produced during the methanation process is utilised for the steam generation. The methanation process generates 20.6 % of the chemical energy produced by the system as thermal energy. This thermal energy is used for steam generation. A superheated steam at a temperature 480 °C is obtained at the outlet of the steam generator. The CO₂ exhaust mixture from the exhaust tank is preheated to around 325 °C and mixed with the steam. The mixture of H₂O-CO₂ is then passed through the heat storage units where it is brought to the inlet temperature of 785 °C required for the rSOC reactor in SOEC operation mode. Air as sweep gas and also as heat transfer media is compressed to the system pressure of 25 bar from ambient conditions. The compressed air is preheated in the heat recovery unit and mixed with the air from the exhaust recycle unit. The air mixture is then supplied to the rSOC reactor at a temperature of 785 °C. The air and reactant mixture entering the rSOC reactor possesses thermal energy equal to 272 % of the chemical energy produced by the system. The total heat absorbed by the reactant mixture and air from the heat storage unit accounted for 8 % of the chemical energy produced by the system. The HT-PCM contributed 1.6 % and LT-PCM contributed 6.5 % of the chemical energy produced by the system as heat. The variation of temperature, ideal voltage and voltage losses along the length of the SRU for the given inlet conditions during the SOEC operation is shown in the Figure 6.10. The temperature of the MEA initially decreases due to the endothermic electrochemical reaction. Towards the end of the SRU, the temperature increases due to the exothermic internal methanation reaction. The fuel and air product streams exit the rSOC reactor with a temperature 806 °C. This results in an exothermic behaviour of the electrolysis operation. The local ideal voltage gradually increases along the reactor length due to increasing concentration of fuel components (H₂, CO and O₂) towards the reactor outlet. The local voltage loss decreases along the reactor length. This is due to the increase in temperature along reactor length which lowers the local ASR. From the 1-D model results, the characteristic temperature of the rSOC reactor during the SOEC operation was determined to be 800 °C. The rSOC reactor consumes 107.5 % of the chemical produced by the system as electrical energy. The BoP electrical energy consumption is insignificant and hence electrical energy consumption of the reactor represents the net electrical energy consumption of the system. The rSOC reactor operates at a cell voltage

of 1.235 V and producing a syngas mixture with a small mol% of methane at the outlet. The composition of the fuel produced by the rSOC reactor during the SOEC process is provided in the Table 6.9. The chemical energy of the syngas mixture is 110 % of the chemical energy produced by the system. The thermal energy of the product stream from the rSOC reactor increased to 5 % to 276 % of the chemical energy produced by the system. This is due to the exothermic SOEC operation of the rSOC reactor. The syngas mixture is then processed in the downstream methanation process. The syngas mixture is first cooled to 300 °C corresponding to the inlet temperature of the 1st methanation reactor and the heat is used for process heating. The cooled syngas mixture undergoes the methanation reaction in the 1st methanation reactor and exits the reactor with a temperature of 666 °C. The product gas is then again cooled to 300 °C and supplied to the subsequent reactor. The process is repeated until the final stage of the methanation process. The temperature of the product gas after the second and third methanation reactors was 532 °C and 409 °C. The final product gas exits the methanation unit with a temperature of 335 °C and is then cooled to remove the water from the fuel stream. The final fuel gas contains 92 mol% of CH₄, 7 mol% of H₂ and traces of CO₂ and CO. At the end of the methanation process, the produced fuel lost 10.5 % of chemical energy in the raw syngas from the rSOC reactor and the chemical energy of the final product fuel is 100 %. The lost chemical energy from the syngas is converted to heat during the exothermic methanation reactions. Composition of the produced fuel is provided in the Table 6.9. The methane fuel is then compressed to the pipeline pressure and fed to the natural gas grid network. Part of the air at the outlet of the rSOC reactor is recycled back to the inlet. The remaining air is then cooled in the heat recovery unit and then finally expanded to the ambient pressure to extract work. A net efficiency of 93 % was achieved for the rSOC system in SOEC operation.

Thermal management is shown to be essential for the methane based system as well. In spite of the exothermic behaviour of the rSOC reactor and exothermic downstream methanation process, a significant proportion of thermal energy is consumed from the heat storage tanks. The thermal energy consumption from the storage tanks is equal to 8 % of the chemical energy produced. Though the size and dimension of the thermal management system is smaller when compared to the hydrogen based system. The rSOC reactor operates in exothermic mode at 2500 A/m² and at 25 bar due to internal methanation occurring within the rSOC reactor during the SOEC operation. Additionally,

TABLE 6.9. Gas composition at the outlet of rSOC and after downstream methanation process for methane based system in SOEC mode

Gas species	rSOC outlet	Fuel composition
H ₂	45 %	7 %
H ₂ O	25 %	0.00 %
CO	8 %	0.00 %
CO ₂	5 %	2 %
CH ₄	16 %	91 %
O ₂	0.00 %	0.00 %
N ₂	0.00 %	0.00 %
C	0.00 %	0.00 %

the exothermic downstream methanation process produces enough heat required for the steam generation. Still, 80 % of the heat stored during the SOFC operation mode is consumed during the SOEC operation mode. Hence, the thermal management system still plays a significant role in providing the necessary heat for process heating. Also, it should be noted that less heat is stored in the heat storage during the SOFC operation, since less heat was generated within the rSOC reactor during the SOFC operation due to endothermic internal steam reforming reaction.

6.3.2.1 Summary of methane based rSOC system

A process system analysis of a methane based gas grid connected rSOC system was presented. It was shown that a system roundtrip efficiency of 53 % is achievable for an operating current density of 2500 A/m² and at 25 bar. In this system, the fuel or chemical produced during the SOEC process is not stored within the system boundary but instead is distributed to an existing gas grid network. During the SOFC operation, the required fuel was obtained from the natural gas grid. This enhances the usability of the rSOC system. Additional BoP and downstream processes are required for such systems as compared to a simple hydrogen based rSOC system. A system roundtrip efficiency of 53 % was still achievable for the system. The performance of the system is equal to the hydrogen based systems in spite of the additional components and process. A similar analysis of the system was performed for an operation current density of 1500 A/m². A lower current density operation was feasible as compared to the hydrogen based system.

The qualitative performance of the rSOC at 1500 A/m^2 is similar to the system operating at 2500 A/m^2 . The system roundtrip efficiency of the system at 1500 A/m^2 was found to be equal to 62 %. This was expected due to lower voltage losses at lower current density. The rSOC reactor operated in the exothermic mode during the SOEC process even for the lower current density of 1500 A/m^2 . Lower current density, implies that the reactor area for the same current would need to be higher. Hence, increasing the capital expenditures. The comparison of reactor and system roundtrip efficiency for the methane based rSOC system is provided in the Figure 6.11.

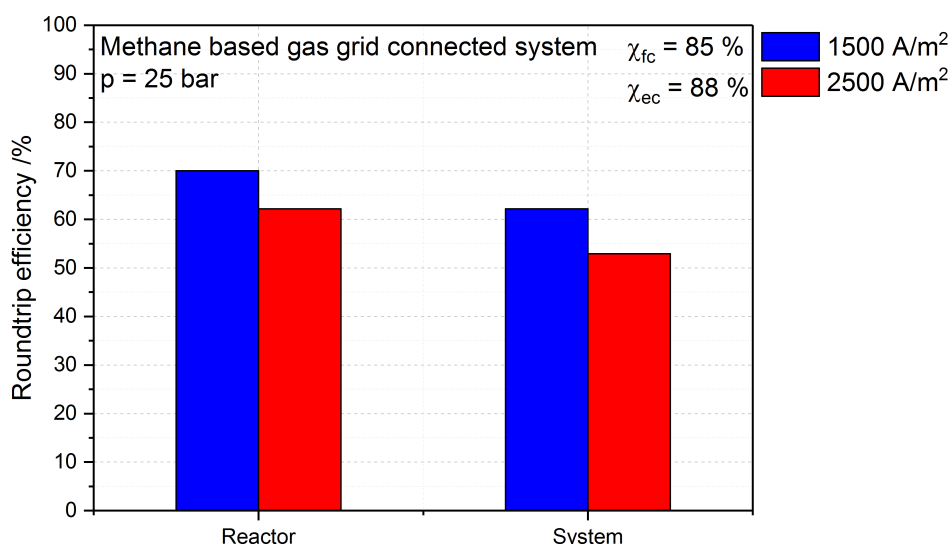


FIGURE 6.11. Summary of methane based gas grid connected rSOC system performance at 1500 A/m^2 and 2500 A/m^2

Thermal management was shown to be essential even for the exothermic SOEC process. During the SOFC operation mode, less heat is generated within the rSOC reactor due to internal reforming. Hence, less heat is stored in the heat storage system. During the SOEC operation mode, though the rSOC reactor was exothermic and the downstream methanation process generated enough heat for steam generation, significant proportions of thermal energy were absorbed from the heat storage tank. The heat absorbed from the heat storage tanks was largely used process heating. An analysis of the system at 1500 A/m^2 yielded the same qualitative results concerning the heat storage. The heat

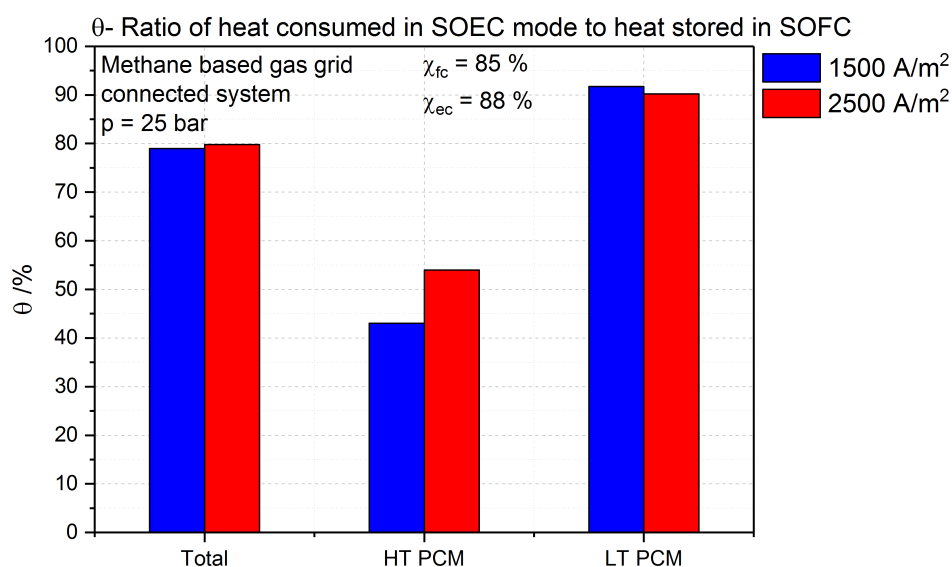


FIGURE 6.12. Heat ratio of methane based gas grid connected rSOC system at 1500 A/m² and 2500 A/m²

ratio of the methane based rSOC system for both the operational current densities is shown in the Figure 6.12.

6.4 Summary

A detailed process system study of a PtP system using a commercially available rSOC reactor was performed. Based on the functionality, two system architectures were defined; an open system architecture and a closed system architecture. In the closed system architecture, the chemical energy is retained within the system boundary by storing it in the fuel and the gas storage tanks. The fuel produced during the SOEC operation of the rSOC system is stored in fuel tanks which is then later utilised during the SOFC operation. The closed system architecture of the rSOC system was studied for the H₂-H₂O and CH₄ oxidation reaction chemistry. A hydrogen oxidation based closed rSOC system is the simplest form of all the rSOC system architectures. In the open system architecture, the chemical energy is not stored within the system boundary. The fuel required during the SOFC operation can be obtained from external sources such as the natural gas grid, biogas plants etc. Likewise, the fuel produced during the SOEC

operation is not stored within the system but is supplied to other interacting process industries, natural gas grids, downstream processes etc. The prime function of the closed system rSOC architecture is electricity storage. The open system architecture functions as energy storage system and also sector coupling.

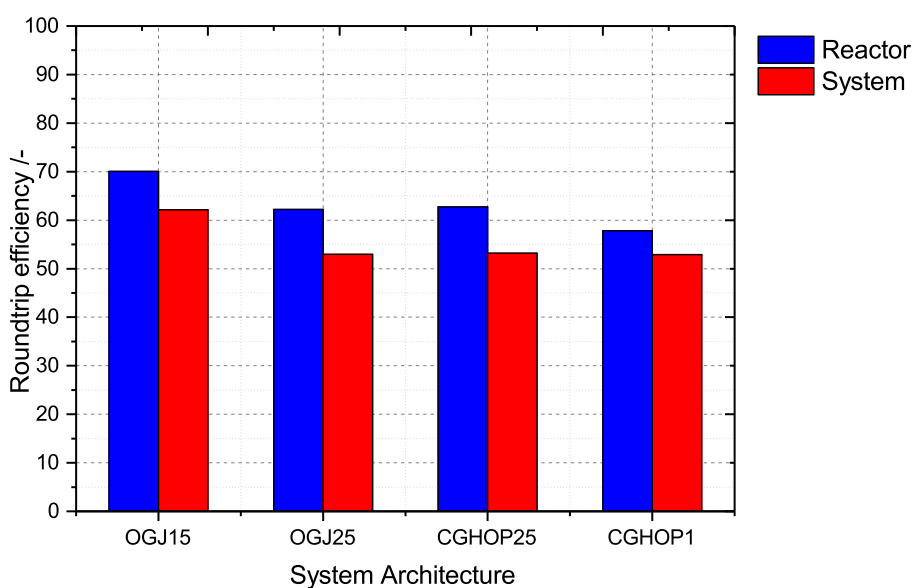


FIGURE 6.13. Summary of achievable roundtrip efficiency of the different rSOC system architecture. OGJ15 - Methane based gas grid system at 1500 A/m², OGJ25 - Methane based gas grid system at 2500 A/m², CGHOP25 - Hydrogen based closed architecture rSOC system at 25 bar, CGHOP1 - Hydrogen based closed architecture rSOC system at 1 bar

A summary of roundtrip efficiencies achievable for the different system architectures is presented in the Figure 6.13. Pressurisation is beneficial for the reactor performance but not for the system performance. In order to achieve a roundtrip efficiency of 53 % at 25 bar, air exhaust recycle loop was employed to limit the BoP work of air compression for the hydrogen based closed rSOC system. Hence, complex system configuration are required to achieve higher system efficiencies. For the hydrocarbon based closed rSOC system configuration, a similar qualitative result was attained [223]. An alternate solution was employed to improve the system performance under pressurised operation. Instead of the air recycle loop, a compressed air storage tank was used for the hydrocarbon based closed rSOC system to improve the system efficiency to 60 % at 25 bar. Adding a compressed

air storage tank increased system efficiency but also increases the complexity, capital and operational cost of the system. For the methane based gas grid connected system, a pressurised operation was considered. During the SOEC process of the methane based system, co-electrolysis (reduction of CO_2 and H_2O to CO and H_2 respectively) occurs within the rSOC reactor. Therefore, by operating the system under pressure an exothermic internal methanation occurs within the rSOC reactor. The heat produced due to exothermic internal methanation reaction offsets the thermal demand for endothermic electrochemical reduction of CO_2 and H_2O . Moreover, pressurised operation is required for the downstream methanation process to attain a high methane yield. The roundtrip efficiency of 53 % and 62 % was achieved for system operation at current densities of 2500 A/m^2 and 1500 A/m^2 respectively. The rSOC reactor is exothermic in both SOFC and SOEC operation modes. Therefore, the demands on the thermal management system are eased. Due to this, the system can also operate at lower current density of 1500 A/m^2 which was not possible for the hydrogen based closed rSOC system. At 1500 A/m^2 , the rSOC reactor was highly endothermic during the SOEC operation of the hydrogen based system. Hence, the hydrogen based closed architecture rSOC system was not thermally self sustaining at a current density of 1500 A/m^2 . An air recycle loop was utilised during both the SOFC and the SOEC operation of the methane based gas grid connected rSOC system. This was required to achieve the reported roundtrip efficiency. Hence, the complexity level of the methane based gas grid connected rSOC is high. Operation of the system at lower current density leads to higher efficiency but is not preferred since it rSOC reactor area and hence increasing the capital cost of the system.

Thermal management plays a key role for all the system configurations. The importance of thermal management can be understood from the Figure 6.14. The Figure 6.14 represents the ratio of heat required by the rSOC reactor during SOEC operation to the total heat consumed from the heat storage tank during the SOEC operation of the system. During the SOEC operation mode, the rSOC reactor operates in the endothermic region for the hydrogen based closed rSOC system and for the hydrocarbon based closed rSOC system at 1 bar. Therefore, resulting in higher roundtrip efficiency. The heat required for the endothermic operation of the rSOC reactor accounts for 5 – 8 % of the total heat consumed from the heat storage system during the SOEC operation. This implies that the 90 – 95 % of the heat consumed from the heat storage tanks was used for process heating requirements especially for steam generation. Therefore, further emphasising the importance of the thermal management system. For the hydrocarbon based closed

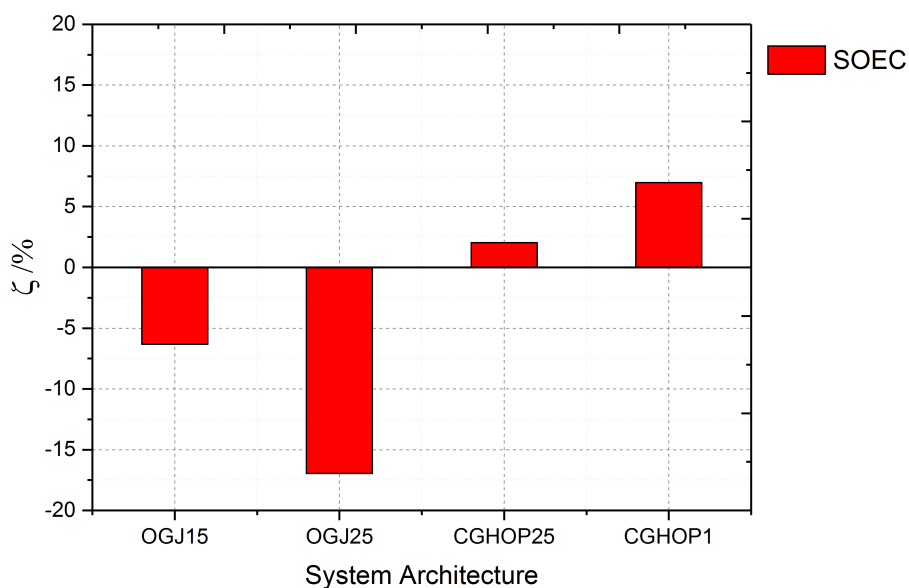


FIGURE 6.14. Summary of ζ of different rSOC system architecture. OGJ15 - Methane based gas grid system at 1500 A/m², OGJ25 - Methane based gas grid system at 2500 A/m², CGHOP25 - Hydrogen based closed rSOC system at 25 bar, CGHOP1 - Hydrogen based closed architecture rSOC system at 1 bar.

rSOC system at 25 bar and the methane based gas grid connected rSOC system, the value of ζ is negative. The negative value of ζ implies that the rSOC reactor becomes exothermic and produces heat during the SOEC operation. The heat generated by the rSOC reactor during the SOEC operation is in the range of 5 – 30 % of heat consumed from the heat storage tanks during the SOEC process. This implies, the heat generated in the rSOC reactor is not enough to meet the demands of heating the reactants to the boundary conditions. Hence, the remaining heat required for the process heating purposes should be supplied from the heat storage tanks. This further highlights the importance of the thermal management system. In absence of an effective thermal management system, all the process heat demands have to be met through an external source or operating the rSOC reactor in highly exothermic mode during the SOEC operation. This would negatively impact the roundtrip efficiency. Hence, a thermal management system enables a close to endothermic or slightly exothermic SOEC process thereby resulting in higher roundtrip efficiency.



7

Conclusion and future work

The increasing penetration of renewable energy in the energy matrix is desired but also poses additional challenges. Energy storage and management systems are required to tide over the time varying nature of the renewable energy supply and electrical energy demand. With greater renewable energy penetration, electrical energy becomes the prime mover. The gradual shift from chemical energy to electrical energy as a prime mover implies that alternate synthesis routes have to be established to produce important industrial chemicals that are currently derived from fossil fuels. Electrochemical reactors and more specifically Solid Oxide Cell (SOC) reactor can address the above challenges. An SOC reactor converts chemical energy to electrical energy when operated as a fuel cell and electrical energy to chemical form when operated as electrolyser. The bidirectional operability of the SOC reactor makes it ideal for energy storage and management. With production of chemical energy when operated as electrolyser, an SOC reactor offers an alternate route to produce necessary chemicals from renewable electrical energy.

A three step approach was adopted to obtain realisable reversible Solid Oxide Cell (rSOC) systems for energy storage and sector coupling in the near future. In the first step, the roundtrip target efficiencies that are achievable were established taking into consideration the thermodynamic constraints and current state of the art of the rSOC reactor. A simplified conceptual model of an rSOC system was developed to evaluate the theoretical roundtrip efficiency and achievable roundtrip efficiency. A commercial rSOC reactor was experimentally analysed to quantify its performance. The achievable

roundtrip efficiency of the rSOC system was determined by feeding the reactor performance into a thermodynamic model. The achievable roundtrip efficiency is limited by the reactor performance and is the target roundtrip efficiency to be achieved by the rSOC process system. In the second step, different system architectures are analysed to achieve the roundtrip efficiency close to the target efficiencies predicted in the first step. A detailed process system analysis is performed accounting for the BoP requirements and heat exchange losses. During this step, steps to improve the system performance towards to the target performance were investigated and the causes limiting the system performance were identified. In the final step, the feasibility of the system architecture and system operating parameters was determined. A 1-D reactor model was utilised to identify hazardous operating conditions which can lead to a breakdown of the rSOC reactor. Accordingly, the system architectures and operation conditions were amended to achieve a feasible system operation point. A convergence of system architecture and safe operation point was obtained by an iterative method. The system performance was analysed and quantified for final feasible system architecture.

A hydrogen based rSOC system and hydrocarbon based rSOC system was developed and analysed. The hydrogen based rSOC system was developed mainly for the purpose of electricity storage. The hydrocarbon system was considered for both electricity storage and sector coupling. A methane based system was considered for the same. The rSOC systems were developed based on a commercially available rSOC reactor. The rSOC reactor was an ESC stack with an open air manifold design. It was experimentally characterised and its performance quantified. The electrolysis reaction (reduction of water and or carbon dioxide) is endothermic in nature. Hence, along with electrical energy heat has to be supplied to the reactor for the electrolysis reaction to occur. The heat required to support the electrolysis reaction can be supplied either from an external source or by operating the reactor in exothermic or thermoneutral region during the SOEC operation. At exothermic and thermoneutral region, the heat generated within the reactor due to the internal resistance supports the electrolysis reaction. This results in lower roundtrip efficiency, as more electrical energy is used than required. Hence, endothermic operation of the rSOC during the SOEC mode results in higher roundtrip efficiency. Therefore, a thermal management strategy was proposed to operate the SOEC process in the endothermic region. In this method, the heat produced by the reactor due to exothermic oxidation reaction and internal losses during the SOFC operation is stored in a heat storage system. The stored heat is later used to supply the heat

required for the endothermic operation of the rSOC reaction during the SOEC mode. An rSOC system with heat storage thermal management utilising a commercially available reactor was analysed. From the first step, a target roundtrip efficiency in the range of 55...60 % was achieved for the hydrogen rSOC when operated in the endothermic region during the SOEC mode. The target efficiency reduced to 35 45 % when the SOEC process was operated in the exothermic region. A similar target efficiency was achieved for the hydrocarbon based system. The highest target roundtrip efficiency was attained for higher reactor pressures of 25 bar. The importance of thermal management is reduced at higher pressures for the hydrocarbon based systems. At higher pressures, the exothermic internal methanation reaction can occur within the rSOC reactor during the SOEC operation. The total heat generated due to exothermic internal methanation reaction and internal losses meets the heat required for electrolysis of H₂O and CO₂. Therefore, considering the performance of the commercial rSOC reactor and thermodynamic constraints, a target efficiency of 55 % at 1 bar and 60 % at 25 bar was prescribed at an operating current density of 2500 A/m².

In the second step, detailed process systems of the rSOC systems were developed. The process systems were classified as closed system and open grid connected system based on the system boundary. In a closed grid system, fuel consumed during the SOFC operation and produced during the SOEC operation is stored within the fuel storage tank. The closed boundary rSOC system functions purely as a electricity storage system. For both the hydrogen and hydrocarbon based closed boundary rSOC system, a roundtrip efficiency of 54 % was achieved for a non-pressurised system. The system efficiency achieved for the non pressurised system is close to the target efficiency of 55 % prescribed for the non-pressurised system in the first step. The 1 % difference comes from the BoP losses and heat exchange losses. Hence, a well defined system was developed for the closed boundary rSOC system for both cases. On the contrary for the pressurised system a roundtrip efficiency of 55 % was achieved for both hydrogen and hydrocarbon based closed boundary system. The achieved system efficiency under pressurised operation is way lower than 60 % target efficiency prescribed for the system at 25 bar in the first step. The significant difference between the achieved system performance and target value is due to the increased BoP work consumption for the pressurised operation. Higher BoP work entailed compression of process air to the system operation pressure. A complex system architecture was required to achieve system efficiency of 55 % for the pressurised hydrogen based closed boundary rSOC system. The pressurised operation of hydrocarbon

based closed boundary rSOC system resulted in higher energy storage density. At pressurised operation, a higher yield of methane was obtained in the fuel produced during the SOEC operation of the system. This resulted in lower volume of the storage tanks and hence lower capital cost of the fuel storage tank. Therefore, to improve the system performance to the target value, an additional complexity was introduced to the system architecture. A compressed air storage tank was introduced to eliminate the parasitic BoP work consumption. By introducing the compressed air storage tank, a roundtrip efficiency of 60 % was achieved for the pressurised operation of hydrocarbon based closed boundary rSOC system. The negative effect includes increased system complexity, capital costs and system control requirements.

In *open boundary* rSOC system, the chemical energy is not stored within the system boundary. The fuel required during the SOFC operation is obtained from external sources and the fuel/chemical produced during the SOEC operation is fed to external process industry or natural gas grid etc. The open boundary rSOC system serves the purpose of electricity storage and as well as sector coupling. This configuration represents the future direction for integrating energy storage with chemical and other process industries. In this thesis, a natural gas grid connected open boundary rSOC system was developed. The natural gas from the gas grid was used as fuel during the SOFC operation. Methane was produced during the SOEC operation which was fed to the gas grid. The methane fed to the gas grid can be used by other process industries, energy generation etc. A pressurised operation was considered. A system roundtrip efficiency of 53 % was achieved. The achieved system efficiency is 7 % lower than target value due to the BoP effect. Further complexity was not introduced to improve the system performance.

The final conclusion comment centres on the role of the thermal management in all the system architectures and configurations. The thermal management system played a key role in achieving the reported system performance. For SOEC operation of the hydrogen based system and the non-pressurised hydrocarbon system, the rSOC reactor was in the endothermic region. For these systems, apart from providing the heat required for the rSOC reactor in the SOEC mode, a significant portion of the heat from the heat storage system was utilised for process heating during the SOEC operation. In the absence of a thermal management system, all the process heating requirements would have to be supplied from an external source or by running the rSOC in highly exothermic mode during the SOEC process. This would result in a significantly lower system performance.

For the pressurised hydrocarbon based rSOC system, the rSOC reactor was operated in the slightly exothermic region during the SOEC process. Therefore, no heat from the thermal management system was required by the rSOC reactor but heat from the heat storage tanks were utilised for the process heating requirements. In the absence of the thermal management, the heat required for process heating would have to be supplied externally. Hence, even for an exothermic operation of the rSOC reactor during the SOEC process, the thermal management system plays a significant role in achieving the reported system performance. A summarised conclusion of all the system architectures is provided in the Table 7.1. In the Table 7.1, the plus (+) sign rates the level of the evaluation criteria. For example, the atmospheric hydrogen based rSOC system has one '+' sign for reactor performance compared to three '+' signs for pressure system, this means that reactor performance is better for the pressurised system compared to reactor performance at atmospheric condition. Likewise, pressurised system has two '+' signs for complexity compared to one for atmospheric system, implying, that the pressurised system is more complex than the atmospheric system.

7.1 Future work

The thesis presents one of the initial works in the field of rSOC systems. The thesis was aimed to open new avenues and research directions. Along with answering certain pertinent questions, it was also meant to raise further research questions. A brief list of future research direction as a continuation of this work is provided below.

1. A commercially available rSOC reactor was used as the basis for the entire analysis. The achievable roundtrip efficiency is limited by the reactor performance. With better rSOC reactors with lower losses, a higher system performance can be achieved. Further research is required to develop better rSOC reactor with lower electrochemical losses. Additionally, further research is needed to improve the degradation stability of the rSOC reactor in both SOFC and SOEC operation mode to increase the system lifetime.
2. The analysis presented here was based on a symmetric system operation, an equal charging and discharging duration was assumed. In real scenarios, the wind and solar energy supply profile is not symmetric and also the electrical energy demand is not symmetric. The analysis should be extended for different asymmetric system operation. It can be performed either as a off design system operation points or

TABLE 7.1. A summarised conclusion of system architectures of the rSOC systems for energy storage and sector coupling

Architecture	Complexity	Reactor performance	System performance	Cost	Energy storage	Sector coupling
Hydrogen based closed boundary system						
Atmospheric pressure		+	+	+	+	No
Presurised system 25 bar	++	+++	+	++	+	No
25 bar with compressed air storage	++	+++	+++	+++	++	No
Hydrocarbon based closed boundary system						
Atmospheric pressure		+	+	++	+	No
Presurised system 25 bar	++	+++	+	+++	++	No
25 bar with compressed air storage	++	+++	+++	+++	++	No
Methane based gas grid connected system						
Low current density		++	++	+++	+	Yes
High current density		+	++	+	+	Yes

design operation point for either wind or solar energy supply for varying electricity demand profile.

- Dynamic analysis is necessary to understand system operability and to engineer the control units for the rSOC systems. Dynamic system analysis is essential to ensure safe transition from SOFC operation to SOEC operation and vice versa. Additionally, an energy storage system should be capable of managing a fluctuating energy load and supply.
- The high temperature heat storage systems proposed in this study are in early stages of development (TRL 2). Further research is required to address the fea-

sibility and solve the engineering challenges for high temperature heat storage. Alternate solutions for thermal management and heat storage systems should be investigated. Accordingly, the process system should be altered.

5. Finally, only one out of the various sector coupling possibilities was presented here. Alternatives such as ammonia, Fischer Tropsch liquids, methanol and other synthesis routes should be explored.

It is indeed an early stage in the development of rSOC reactors and systems but it is encouraging to note that some points raised above will be addressed in upcoming EU projects and other national level projects as this thesis is being written. This indicates there is a positive outlook for this topic in the near future and pertinent questions will be answered.



Bibliography

- [1] P. J. Hall and E. J. Bain, “Energy-storage technologies and electricity generation,” *Energy Policy*, vol. 36, pp. 4352–4355, dec 2008.
- [2] H. Ibrahim, A. Ilinca, and J. Perron, “Energy storage systems – Characteristics and comparisons,” *Renewable and Sustainable Energy Reviews*, vol. 12, no. 5, pp. 1221–1250, 2008.
- [3] A. Evans, V. Strezov, and T. J. Evans, “Assessment of sustainability indicators for renewable energy technologies,” *Renewable and Sustainable Energy Reviews*, vol. 13, pp. 1082–1088, jun 2009.
- [4] R. M. Dell and D. A. J. Rand, “Energy storage - A key technology for global energy sustainability,” *Journal of Power Sources*, vol. 100, pp. 2–17, 2001.
- [5] J. Kondoh, I. Ishii, H. Yamaguchi, A. Murata, K. Otani, K. Sakuta, N. Higuchi, S. Sekine, and M. Kamimoto, “Electrical energy storage systems for energy networks,” *Energy Conversion and Management*, vol. 41, no. 17, pp. 1863–1874, 2000.
- [6] T. U. Daim, X. Li, J. Kim, and S. Simms, “Evaluation of energy storage technologies for integration with renewable electricity: Quantifying expert opinions,” *Environmental Innovation and Societal Transitions*, vol. 3, pp. 29–49, 2012.
- [7] Z. Yang, J. Zhang, M. C. W. Kintner-Meyer, X. Lu, D. Choi, J. P. Lemmon, and J. Liu, “Electrochemical energy storage for green grid,” 2011.

BIBLIOGRAPHY

- [8] A. Sternberg and A. Bardow, "Power-to-What? - Environmental assessment of energy storage systems," *Energy & Environmental Science*, vol. 8, no. 2, pp. 389–400, 2015.
- [9] H. Chen, T. N. Cong, W. Yang, C. Tan, Y. Li, and Y. Ding, "Progress in electrical energy storage system: A critical review," *Progress in Natural Science*, vol. 19, no. 3, pp. 291–312, 2009.
- [10] K. Hemmes, J. M. Guerrero, and T. Zhelev, "Highly efficient distributed generation and high-capacity energy storage," *Chemical Engineering and Processing: Process Intensification*, vol. 51, pp. 18–31, 2012.
- [11] K. Hemmes, G. Barbieri, Y. M. Lee, E. Drioli, and H. J. H. W. De Wit, "Process intensification and fuel cells using a multi-source multi-product approach," *Chemical Engineering and Processing: Process Intensification*, vol. 51, pp. 88–108, 2012.
- [12] E. Harkins, M. Pando, and D. Sobel, "Electrical Energy Storage Using Fuel Cell Technology," 2011.
- [13] G. Gahleitner, "Hydrogen from renewable electricity: An international review of power-to-gas pilot plants for stationary applications," *International Journal of Hydrogen Energy*, vol. 38, no. 5, pp. 2039–2061, 2013.
- [14] F. Mitlitsky, B. Myers, and A. Weisberg, "Regenerative fuel cell systems," *Energy & Fuels*, vol. 400, no. 5, pp. 56–71, 1998.
- [15] S. H. S. Jensen, X. Sun, S. S. D. Ebbesen, R. Knibbe, and M. Mogensen, "Hydrogen and synthetic fuel production using pressurized solid oxide electrolysis cells," *International Journal of Hydrogen energy*, vol. 35, no. 18, pp. 9544–9549, 2010.
- [16] A. Hauch, S. D. Ebbesen, S. H. Jensen, and M. Mogensen, "Highly efficient high temperature electrolysis," *Journal of Materials Chemistry*, vol. 18, no. 20, p. 2331, 2008.
- [17] A. B. Stambouli and E. Traversa, "Solid oxide fuel cells (SOFCs): A review of an environmentally clean and efficient source of energy," *Renewable and Sustainable Energy Reviews*, vol. 6, no. 5, pp. 433–455, 2002.

- [18] T. a. Adams, J. Nease, D. Tucker, and P. I. Barton, "Energy Conversion with Solid Oxide Fuel Cell Systems: A Review of Concepts and Outlooks for the Short- and Long-Term," *Ind. Eng. Chem. Res.*, vol. 52, no. 9, pp. 3089–3111, 2012.
- [19] BloomEnergy, "Bloomenergy - sofc system and stack developed-what is an energy server?." Available at <http://www.bloomenergy.com/fuel-cell/energy-server/> (2017/07/22).
- [20] B. Borglum and H. Ghezel-Ayagh, "Development of solid oxide fuel cells at Versa Power Systems and FuelCell Energy," *ECS Transactions*, vol. 57, no. 1, pp. 61–66, 2013.
- [21] SolidPower, "Solidpower - sofc system and stack developer." Available at <http://www.solidpower.com/en/> (2017/07/22).
- [22] N. Aldag, "sunfire supplies world's largest commercial reversible electrolysis (RSOC) system." <http://www.sunfire.de/en/company/press/detail/sunfire-supplies-boeing-with-worlds-largest-commercial-reversible-electrolysis-2016>.
- [23] Convion, "Convion, fuel cell systems for distributed power generation markets." Available at <http://convion.fi> (2017/07/22).
- [24] Elcogen, "Elcogen, fuel cell technology." Available at <http://www.elcogen.com/products/> (2017/07/22).
- [25] Kyocera, "Kyocera develops industry's first 3-kilowatt solid-oxide fuel cell for institutional cogeneration." Available at http://global.kyocera.com/news/2017/0702_bnfo.html (2017/07/22).
- [26] Aisin, "Aisin sofc in japanese market and entry into european market." Available at http://www.fuelcellnetwork.eu/wp-content/uploads/20140626_FCEN_Webinar_AISIN.pdf (2017/07/22).
- [27] Mitsubishi-Hitachi, "Implementation initiatives for fuel cell power generation systems." Available at https://www.mhps.com/en/technology/business/power/sofc/approach_practical.html (2017/07/22).
- [28] D. Kusunoki, "Development of Mitsubishi-planar reversible cell?Fundamental test on hydrogen-utilized electric power storage system*1," *International Journal of Hydrogen Energy*, vol. 20, no. 10, pp. 831–834, 1995.

BIBLIOGRAPHY

- [29] G.-B. Jung, L.-H. Fang, C.-Y. Lin, X.-V. Nguyen, C.-C. Yeh, C.-Y. Lee, J.-W. Yu, S.-H. Chan, W.-T. Lee, S.-W. Chang, *et al.*, “Electrochemical performance and long-term durability of a reversible solid oxide fuel cell,” *Int. J. Electrochem. Sci*, vol. 10, pp. 9089–9104, 2015.
- [30] Y. Rao, S. Zhong, F. He, Z. Wang, R. Peng, and Y. Lu, “Cobalt-doped BaZrO₃: A single phase air electrode material for reversible solid oxide cells,” *International Journal of Hydrogen Energy*, vol. 37, pp. 12522–12527, sep 2012.
- [31] J. Mermelstein and O. Posdziech, “Development and Demonstration of a Novel Reversible SOFC System for Utility and Micro Grid Energy Storage,” vol. 0306, pp. 59–70, 2016.
- [32] D. Bhattacharyya and R. Rengaswamy, “System Identification and Nonlinear Model Predictive Control of a Solid Oxide Fuel Cell,” *Industrial & Engineering Chemistry Research*, vol. 49, no. 10, pp. 4800–4808, 2010.
- [33] T. Ota, M. Koyama, C. J. Wen, K. Yamada, and H. Takahashi, “Object-based modeling of SOFC system: Dynamic behavior of micro-tube SOFC,” *Journal of Power Sources*, vol. 118, no. 1-2, pp. 430–439, 2003.
- [34] R. Kandepu, L. Imsland, B. A. Foss, C. Stiller, B. Thorud, and O. Bolland, “Modeling and control of a SOFC-GT-based autonomous power system,” *Energy*, vol. 32, no. 4, pp. 406–417, 2007.
- [35] R. A. Roberts and J. Brouwer, “Dynamic Simulation of a Pressurized 220 kW Solid Oxide Fuel-Cell, Gas-Turbine Hybrid System: Modeled Performance Compared to Measured Results,” *Journal of Fuel Cell Science and Technology*, vol. 3, no. 1, p. 18, 2006.
- [36] Y. Qi, B. Huang, and K. T. Chuang, “Dynamic modeling of solid oxide fuel cell: The effect of diffusion and inherent impedance,” *Journal of Power Sources*, vol. 150, no. 1-2, pp. 32–47, 2005.
- [37] X. Xue, J. Tang, N. Sammes, and Y. Du, “Dynamic modeling of single tubular SOFC combining heat/mass transfer and electrochemical reaction effects,” *Journal of Power Sources*, vol. 142, no. 1-2, pp. 211–222, 2005.

-
- [38] D. Andersson, E. Åberg, J. Yuan, B. Sundén, and J. Eborn, "Dynamic modeling of a solid oxide fuel cell system in modelica," in *ASME 2010 8th International Conference on Fuel Cell Science, Engineering and Technology*, pp. 65–72, American Society of Mechanical Engineers, 2010.
- [39] A. Salogni, P. Iora, and S. Campanari, "Dynamic Analysis and Control of a Planar IT-SOFC System," in *ASME 2009 7th International Conference on Fuel Cell Science, Engineering and Technology*, pp. 879–887, ASME, 2009.
- [40] A. M. Murshed, B. Huang, and K. Nandakumar, "Control relevant modeling of planer solid oxide fuel cell system," *Journal of Power Sources*, vol. 163, no. 2, pp. 830–845, 2007.
- [41] R. Roberts, J. Brouwer, F. Jabbari, T. Junker, and H. Ghezel-Ayagh, "Control design of an atmospheric solid oxide fuel cell/gas turbine hybrid system: Variable versus fixed speed gas turbine operation," *Journal of Power Sources*, vol. 161, no. 1, pp. 484–491, 2006.
- [42] J. Padullés, G. Ault, and J. McDonald, "An integrated SOFC plant dynamic model for power systems simulation," *Journal of Power Sources*, vol. 86, no. 1-2, pp. 495–500, 2000.
- [43] H. Xi, J. Sun, and V. Tsourapas, "A control oriented low order dynamic model for planar SOFC using minimum Gibbs free energy method," *Journal of Power Sources*, vol. 165, no. 1, pp. 253–266, 2007.
- [44] N. Autissier, F. Palazzi, F. Marechal, J. van Herle, and D. Favrat, "Thermo-Economic Optimization of a Solid Oxide Fuel Cell, Gas Turbine Hybrid System," *Journal of Fuel Cell Science and Technology*, vol. 4, no. 2, p. 123, 2007.
- [45] A. Sciacovelli, "Thermodynamic optimization of a monolithic-type solid oxide fuel cell," *International Journal of Thermodynamics*, vol. 13, no. 3, pp. 95–103, 2010.
- [46] M. C. Romano, S. Campanari, V. Spallina, and G. Lozza, "Thermodynamic Analysis and Optimization of IT-SOFC-Based Integrated Coal Gasification Fuel Cell Power Plants," *Journal of Fuel Cell Science and Technology*, vol. 8, no. 4, p. 041002, 2011.
- [47] E. Facchinetti, M. Gassner, M. D'Amelio, F. Marechal, and D. Favrat, "Process integration and optimization of a solid oxide fuel cell ,À Gas turbine hybrid

- cycle fueled with hydrothermally gasified waste biomass,” *Energy*, vol. 41, no. 1, pp. 408–419, 2012.
- [48] L. Chen, S. Gao, and H. Zhang, “Performance Analysis and Multi-Objective Optimization of an Irreversible Solid Oxide Fuel Cell-Stirling Heat Engine Hybrid System,” *Int. J. Electrochem. Sci.*, vol. 8, pp. 10772–10787, 2013.
- [49] J. Godat and F. Marechal, “Optimization of a fuel cell system using process integration techniques,” *Journal of Power Sources*, vol. 118, no. 1-2, pp. 411–423, 2003.
- [50] F. Calise, M. Dentice d’Accadia, L. Vanoli, and M. R. von Spakovsky, “Full load synthesis/design optimization of a hybrid SOFC-GT power plant,” *Energy*, vol. 32, no. 4, pp. 446–458, 2007.
- [51] C. Athanasiou, F. Coutelieris, E. Vakouftsi, V. Skoulou, E. Antonakou, G. Marnellos, and a. Zabaniotou, “From biomass to electricity through integrated gasification/SOFC system-optimization and energy balance,” *International Journal of Hydrogen Energy*, vol. 32, no. 3, pp. 337–342, 2007.
- [52] T. S. Lee, J. N. Chung, and Y. C. Chen, “Design and optimization of a combined fuel reforming and solid oxide fuel cell system with anode off-gas recycling,” *Energy Conversion and Management*, vol. 52, no. 10, pp. 3214–3226, 2011.
- [53] A. Franzoni, L. Magistri, A. Traverso, and A. F. Massardo, “Thermoeconomic analysis of pressurized hybrid SOFC systems with CO₂ separation,” *Energy*, vol. 33, no. 2, pp. 311–320, 2008.
- [54] M. Gandiglio, A. Lanzini, P. Leone, M. Santarelli, and R. Borchiellini, “Thermoeconomic analysis of large solid oxide fuel cell plants: Atmospheric vs. pressurized performance,” *Energy*, vol. 55, pp. 142–155, 2013.
- [55] C. Bang-Møller and M. Rokni, “Thermodynamic performance study of biomass gasification, solid oxide fuel cell and micro gas turbine hybrid systems,” *Energy Conversion and Management*, vol. 51, no. 11, pp. 2330–2339, 2010.
- [56] S. Santhanam, C. Schilt, B. Turker, T. Woudstra, and P. Aravind, “Thermodynamic modeling and evaluation of high efficiency heat pipe integrated biomass Gasifier,Solid Oxide Fuel Cells,Gas Turbine systems,” *Energy*, vol. 109, pp. 751–764, 2016.

- [57] P. V. Aravind, T. Woudstra, N. Woudstra, and H. Spliethoff, "Thermodynamic evaluation of small-scale systems with biomass gasifiers, solid oxide fuel cells with Ni/GDC anodes and gas turbines," *Journal of power sources*, vol. 190, no. 2, pp. 461–475, 2009.
- [58] M. Rokni, "Thermodynamic and thermoeconomic analysis of a system with biomass gasification, solid oxide fuel cell (SOFC) and Stirling engine," *Energy*, vol. 76, pp. 19–31, 2014.
- [59] J. Palsson, "Thermodynamic Analysis of Combined Solid Oxide Fuel Cell and Gas Turbine Systems .pdf," 2000.
- [60] V. Verda and M. C. Quaglia, "Solid oxide fuel cell systems for distributed power generation and cogeneration," *International Journal of Hydrogen Energy*, vol. 33, no. 8, pp. 2087–2096, 2008.
- [61] F. Calise, M. Dentice d'Accadia, a. Palombo, and L. Vanoli, "Simulation and exergy analysis of a hybrid Solid Oxide Fuel Cell (SOFC), Gas Turbine System," *Energy*, vol. 31, no. 15, pp. 3278–3299, 2006.
- [62] K. Bedringås and I. Ertesvåg, "Exergy analysis of solid-oxide fuel-cell (SOFC) systems," *Energy*, vol. 22, no. 4, pp. 403–412, 1997.
- [63] L. Fryda, K. D. Panopoulos, J. Karl, and E. Kakaras, "Exergetic analysis of solid oxide fuel cell and biomass gasification integration with heat pipes," *Energy*, vol. 33, no. 2, pp. 292–299, 2008.
- [64] R. Toonssen, S. Sollai, P. V. Aravind, N. Woudstra, and A. H. M. Verkooijen, "Alternative system designs of biomass gasification SOFC/GT hybrid systems," *International Journal of Hydrogen Energy*, vol. 36, no. 16, pp. 10414–10425, 2011.
- [65] Z. Wang, M. Mori, and T. Araki, "Steam electrolysis performance of intermediate-temperature solid oxide electrolysis cell and efficiency of hydrogen production system at 300 Nm³ h⁻¹," *International Journal of Hydrogen Energy*, vol. 35, no. 10, pp. 4451–4458, 2010.
- [66] S. H. Jensen, X. Sun, S. D. Ebbesen, R. Knibbe, and M. Mogensen, "Hydrogen and synthetic fuel production using pressurized solid oxide electrolysis cells," *International Journal of Hydrogen Energy*, vol. 35, no. 18, pp. 9544–9549, 2010.

- [67] J. P. Stempien, O. L. Ding, Q. Sun, and S. H. Chan, "Energy and exergy analysis of Solid Oxide Electrolyser Cell (SOEC) working as a CO₂ mitigation device," *International Journal of Hydrogen Energy*, vol. 37, pp. 14518–14527, oct 2012.
- [68] G. Cinti, A. Baldinelli, A. Di Michele, and U. Desideri, "Integration of Solid Oxide Electrolyzer and Fischer-Tropsch: A sustainable pathway for synthetic fuel," *Applied Energy*, vol. 162, pp. 308–320, 2016.
- [69] L. Mingyi, Y. Bo, X. Jingming, and C. Jing, "Thermodynamic analysis of the efficiency of high-temperature steam electrolysis system for hydrogen production," *Journal of Power Sources*, vol. 177, no. 2, pp. 493–499, 2008.
- [70] Q. Cai, E. Luna-Ortiz, C. S. Adjiman, and N. P. Brandon, "The Effects of Operating Conditions on the Performance of a Solid Oxide Steam Electrolyser: A Model-Based Study," *Fuel Cells*, vol. 10, no. 6, pp. 1114–1128, 2010.
- [71] S. D. Ebbesen, C. Graves, and M. Mogensen, "Production of Synthetic Fuels by Co-Electrolysis of Steam and Carbon Dioxide," *International Journal of Green Energy*, vol. 6, no. 6, pp. 646–660, 2009.
- [72] W. Becker, R. Braun, M. Penev, and M. Melaina, "Production of Fischer-Tropsch liquid fuels from high temperature solid oxide co-electrolysis units," *Energy*, vol. 47, no. 1, pp. 99–115, 2012.
- [73] J. O'Brien and M. McKellar, "High-temperature electrolysis for large-scale hydrogen and syngas production from nuclear energy - summary of system simulation and economic analyses," *International of hydrogen energy*, vol. 35, no. 10, pp. 4808–4819, 2010.
- [74] A. Houaijia, M. Roeb, N. Monnerie, and C. Sattler, "Concentrating Solar Systems as Heat and Electricity Source for a Solid Oxide Electrolyzer,"
- [75] Y. Bo, Z. Wenqiang, X. Jingming, and C. Jing, "Status and research of highly efficient hydrogen production through high temperature steam electrolysis at INET," *International Journal of Hydrogen Energy*, vol. 35, no. 7, pp. 2829–2835, 2010.
- [76] M. F. Orhan and B. S. Babu, "Investigation of an integrated hydrogen production system based on nuclear and renewable energy sources: Comparative eval-

- uation of hydrogen production options with a regenerative fuel cell system,” *Energy*, vol. 88, pp. 801–820, 2015.
- [77] J. Ren, S. R. Gamble, a. J. Roscoe, J. T. S. Irvine, and G. Burt, “Modeling a Reversible Solid Oxide Fuel Cell as a Storage Device Within AC Power Networks,” *Fuel Cells*, vol. 12, no. 5, pp. 773–786, 2012.
- [78] S. Kasai, “Hydrogen electrical energy storage by high-temperature steam electrolysis for next-millennium energy security,” *International Journal of Hydrogen Energy*, vol. 39, no. 36, pp. 21358–21370, 2014.
- [79] C. Wendel, P. Kazempoor, and R. Braun, “Novel electrical energy storage system based on reversible solid oxide cells: System design and operating conditions,” *Journal of Power Sources*, vol. 276, pp. 133–144, 2015.
- [80] A. Monti, C. Wendel, M. Santarelli, and R. J. Braun, “Energy dense storage using intermediate temperature reversible solid oxide cells,” *ECS Transactions*, vol. 68, no. 1, pp. 3289–3300, 2015.
- [81] D. M. Bierschenk, J. R. Wilson, and S. A. Barnett, “High efficiency electrical energy storage using a methane,oxygen solid oxide cell,” *Energy & Environmental Science*, vol. 4, no. 3, p. 944, 2011.
- [82] C. H. Wendel, P. Kazempoor, and R. J. Braun, “A thermodynamic approach for selecting operating conditions in the design of reversible solid oxide cell energy systems,” *Journal of Power Sources*, vol. 301, pp. 93–104, 2016.
- [83] C. H. Wendel, Z. Gao, S. A. Barnett, and R. J. Braun, “Modeling and experimental performance of an intermediate temperature reversible solid oxide cell for high-efficiency, distributed-scale electrical energy storage,” *Journal of Power Sources*, vol. 283, pp. 329–342, 2015.
- [84] S. H. Jensen, C. Graves, M. Mogensen, C. Wendel, R. Braun, G. Hughes, Z. Gao, and S. A. Barnett, “Large-scale electricity storage utilizing reversible solid oxide cells combined with underground storage of CO₂ and CH₄ ,” *Energy Environ. Sci.*, vol. 8, pp. 2471–2479, 2015.
- [85] J. Gao, Y. Wang, Y. Ping, D. Hu, G. Xu, F. Gu, and F. Su, “A thermodynamic analysis of methanation reactions of carbon oxides for the production of synthetic natural gas,” *RSC Advances*, vol. 2, no. 6, p. 2358, 2012.

BIBLIOGRAPHY

- [86] R. O'hayre, S.-W. Cha, F. B. Prinz, and W. Colella, *Fuel cell fundamentals*, John Wiley & Sons, 2016.
- [87] M. Stoukides, "Solid-Electrolyte Membrane Reactors: Current Experience and Future Outlook," *Catalysis Reviews*, vol. 42, pp. 1–70, 2000.
- [88] G. Marnellos and M. Stoukides, "Catalytic studies in electrochemical membrane reactors," *Solid State Ionics*, vol. 175, no. 1-4, pp. 597–603, 2004.
- [89] W. Winkler, "Chapter 3 - Thermodynamics," in *High Temperature and Solid Oxide Fuel Cells* (S. C. Singhal and K. Kendal, eds.), pp. 53–82, Amsterdam: Elsevier Science, 2003.
- [90] R. Ormerod, "Solid oxide fuel cells," *Chemical Society Reviews*, 2003.
- [91] J. E. O'Brien, "Thermodynamic Considerations for Thermal Water Splitting Processes and High Temperature Electrolysis," in *Volume 8: Energy Systems: Analysis, Thermodynamics and Sustainability; Sustainable Products and Processes*, pp. 639–651, ASME, 2008.
- [92] M. P. Heddrich, M. Jahn, a. Michaelis, R. Näge, and a. Weder, "SOFC system design using ideal efficiency modeling - Model and experimental implementation," *Fuel Cells*, vol. 13, no. 4, pp. 612–622, 2013.
- [93] S. L. Miller, M. N. Svrcek, K. Y. Teh, and C. F. Edwards, "Requirements for designing chemical engines with reversible reactions," *Energy*, vol. 36, no. 1, pp. 99–110, 2011.
- [94] K.G. Denbigh, *The Principles of Chemical Equilibrium with applications in chemistry and chemical engineering*. Cambridge Univ Press, fourth edi ed., 1981.
- [95] R. A. Gaggioli and W. R. Dunbar, "Emf, maximum power and efficiency of fuel cells," *Journal of energy resources technology*, vol. 115, no. 2, pp. 100–104, 1993.
- [96] S. K. Ratkje and S. Møller-Holst, "Exergy efficiency and local heat production in solid oxide fuel cells," *Electrochimica Acta*, vol. 38, no. 2-3, pp. 447–453, 1993.
- [97] S. E. Wright, "Comparison of the theoretical performance potential of fuel cells and heat engines," *Renewable Energy*, vol. 29, pp. 179–195, 2004.

- [98] F. J. Gardner, "Thermodynamic processes in solid oxide and other fuel cells," *Proceedings of the Institution of Mechanical Engineers, Part A: Journal of Power and Energy*, vol. 211, no. 5, pp. 367–380, 1997.
- [99] J. B. Wang, J.-C. Jang, and T.-J. Huang, "Study of Ni-samaria-doped ceria anode for direct oxidation of methane in solid oxide fuel cells," *Journal of Power Sources*, vol. 122, no. 2, pp. 122–131, 2003.
- [100] Z. Zhan, Y. Lin, M. Pillai, I. Kim, and S. A. Barnett, "High-rate electrochemical partial oxidation of methane in solid oxide fuel cells," *Journal of Power Sources*, vol. 161, no. 1, pp. 460–465, 2006.
- [101] E. S. Putna, J. Stubenrauch, J. M. Vohs, and R. J. Gorte, "Ceria-Based Anodes for the Direct Oxidation of Methane in Solid Oxide Fuel Cells," *Langmuir*, vol. 11, no. 12, pp. 4832–4837, 1995.
- [102] E. P. Murray, T. Tsai, and S. A. Barnett, "A direct-methane fuel cell with a ceria-based anode," vol. 400, pp. 649–651, aug 1999.
- [103] R. Gorte, H. Kim, and J. Vohs, "Novel SOFC anodes for the direct electrochemical oxidation of hydrocarbon," *Journal of Power Sources*, vol. 106, pp. 10–15, apr 2002.
- [104] M. Mogensen and K. Kammer, "Conversion of Hydrocarbons in Solid Oxide Fuel Cells," *Annual Review of Materials Research*, vol. 33, no. 1, pp. 321–331, 2003.
- [105] D. Mogensen, J. D. Grunwaldt, P. V. Hendriksen, K. Dam-Johansen, and J. U. Nielsen, "Internal steam reforming in solid oxide fuel cells: Status and opportunities of kinetic studies and their impact on modelling," *Journal of Power Sources*, vol. 196, no. 1, pp. 25–38, 2011.
- [106] J. Mermelstein, M. Millan, and N. Brandon, "The impact of steam and current density on carbon formation from biomass gasification tar on Ni/YSZ, and Ni/CGO solid oxide fuel cell anodes," *Journal of Power Sources*, vol. 195, no. 6, pp. 1657–1666, 2010.
- [107] M. Liu, M. G. Millan, P. V. Aravind, and N. Brandon, "Influence of Operating Conditions on Carbon Deposition in SOFCs Fuelled by Tar-Containing Biosyngas," *Journal of The Electrochemical Society*, vol. 158, no. 11, pp. B1310–B1318, 2011.

- [108] K. Girona, J. Laurencin, J. Fouletier, and F. Lefebvre-Joud, "Carbon deposition in CH₄/CO₂ operated SOFC: Simulation and experimentation studies," *Journal of Power Sources*, vol. 210, pp. 381–391, 2012.
- [109] M. Liu, P. V. Aravind, T. Woudstra, V. R. M. Cobas, and A. H. M. Verkooijen, "Development of an integrated gasifier–solid oxide fuel cell test system: A detailed system study," *Journal of Power Sources*, vol. 196, no. 17, pp. 7277–7289, 2011.
- [110] T. Yamaguchi, H. Shimada, U. Honda, H. Kishimoto, T. Ishiyama, and Y. Fujishiro, "Development of electrochemical methanation reactor with co-electrolysis of humidified CO₂," *ECS Transactions*, vol. 68, no. 1, pp. 3459–3463, 2015.
- [111] L. Carrette, K. A. Friedrich, and U. Stimming, "Fuel cells: principles, types, fuels, and applications," *ChemPhysChem*, vol. 1, no. 4, pp. 162–193, 2000.
- [112] N. Q. Minh, "Solid oxide fuel cell technology - Features and applications," *Solid State Ionics*, vol. 174, no. 1-4, pp. 271–277, 2004.
- [113] N. M. Sammes and Z. Cai, "Ionic conductivity of ceria/yttria stabilized zirconia electrolyte materials," *Solid State Ionics*, vol. 100, no. 1-2, pp. 39–44, 1997.
- [114] M. Ghatee, M. H. Shariat, and J. T. S. Irvine, "Investigation of electrical and mechanical properties of 3YSZ/8YSZ composite electrolytes," *Solid State Ionics*, vol. 180, no. 1, pp. 57–62, 2009.
- [115] D. J. L. Brett, A. Atkinson, N. P. Brandon, and S. J. Skinner, "Intermediate temperature solid oxide fuel cells," *Chem. Soc. Rev.*, vol. 37, no. 8, pp. 1568–1578, 2008.
- [116] E. Ivers-Tiffée, A. Weber, and D. Herbstritt, "Materials and technologies for SOFC-components," *Journal of the European Ceramic Society*, vol. 21, no. 10, pp. 1805–1811, 2001.
- [117] M. L. Faro, D. L. Rosa, V. Antonucci, and A. S. Arico, "Intermediate temperature solid oxide fuel cell electrolytes," *Journal of the Indian Institute of Science*, vol. 89, no. 4, pp. 363–380, 2012.
- [118] B. Steele, "Materials for IT-SOFC stacks - 35 years R&D: The inevitability of gradualness?," *Solid State Ionics*, vol. 134, pp. 3–20, 2000.

- [119] M. Mogensen, K. V. Jensen, M. J. Jorgensen, and S. Primdahl, "Progress in understanding SOFC electrodes," *Solid State Ionics*, vol. 150, no. 1-2, pp. 123–129, 2002.
- [120] W. Z. Zhu and S. C. Deevi, "A review on the status of anode materials for solid oxide fuel cells," *Materials Science and Engineering A*, vol. 362, no. 1-2, pp. 228–239, 2003.
- [121] O. A. Marina, L. R. Pederson, M. C. Williams, G. W. Coffey, K. D. Meinhardt, C. D. Nguyen, and E. C. Thomsen, "Electrode Performance in Reversible Solid Oxide Fuel Cells," *Journal of The Electrochemical Society*, vol. 154, no. 5, p. B452, 2007.
- [122] H.-N. Im, S.-Y. Jeon, D.-K. Lim, B. Singh, M. Choi, Y.-S. Yoo, and S.-J. Song, "Steam/CO₂ Co-Electrolysis Performance of Reversible Solid Oxide Cell with La_{0.6}Sr_{0.4}Co_{0.2}Fe_{0.8}O₃-Gd_{0.1}Ce_{0.9}O₂- Oxygen Electrode," *Journal of the Electrochemical Society*, vol. 162, no. 1, pp. F54–F59, 2014.
- [123] E. P. Murray, M. Sever, and S. Barnett, "Electrochemical performance of (La,Sr)(Co,Fe)O₃-(Ce,Gd)O₃ composite cathodes," *Solid State Ionics*, vol. 148, no. 1-2, pp. 27–34, 2002.
- [124] H. J. Hwang, J. W. Moon, S. Lee, and E. a. Lee, "Electrochemical performance of LSCF-based composite cathodes for intermediate temperature SOFCs," *Journal of Power Sources*, vol. 145, no. 2, pp. 243–248, 2005.
- [125] Z. Shao and S. M. Haile, "A high-performance cathode for the next generation of solid-oxide fuel cells," *Nature*, vol. 431, no. 7005, pp. 170–173, 2004.
- [126] W. WANG and M. MOGENSEN, "High-performance lanthanum-ferrite-based cathode for SOFC," *Solid State Ionics*, vol. 176, no. 5-6, pp. 457–462, 2005.
- [127] A. De Groot, *Advanced energy analysis of high temperature fuel cell systems*. PhD thesis, TU Delft, Delft University of Technology, 2004.
- [128] S. Chan and Z. Xia, "Polarization effects in electrolyte/electrode-supported solid oxide fuel cells," *Journal of Applied Electrochemistry*, vol. 32, no. 3, pp. 339–347, 2002.

- [129] E. Achenbach, "Three-dimensional and time-dependent simulation of a planar solid oxide fuel cell stack," *Journal of Power Sources*, vol. 49, no. 1-3, pp. 333–348, 1994.
- [130] S. C. Singhal and K. Kendall, *High temperature solid oxide fuel cells: fundamentals, design, and applications*. Elsevier Science, 2003.
- [131] K. Choy, W. Bai, S. Charojrochkul, and B. C. H. Steele, "The development of intermediate-temperature solid oxide fuel cells for the next millennium," *Journal of Power Sources*, vol. 71, no. 1-2, pp. 361–369, 1998.
- [132] V. N. Nguyen, Q. Fang, U. Packbier, and L. Blum, "Long-term tests of a Jülich planar short stack with reversible solid oxide cells in both fuel cell and electrolysis modes," *International Journal of Hydrogen Energy*, vol. 38, no. 11, pp. 4281–4290, 2013.
- [133] L. Blum, U. Packbier, I. C. Vinke, and L. G. J. De Haart, "Long-Term Testing of SOFC Stacks at Forschungszentrum Jülich," *Fuel Cells*, vol. 13, no. 4, pp. 646–653, 2013.
- [134] S. P. Jiang, "Challenges in the development of reversible solid oxide cell technologies: a mini review," *Asia-Pacific Journal of Chemical Engineering*, vol. 11, no. 3, pp. 386–391, 2016.
- [135] X. Zhang, J. E. O'Brien, R. C. O'Brien, and G. K. Housley, "Durability evaluation of reversible solid oxide cells," *Journal of Power Sources*, vol. 242, pp. 566–574, nov 2013.
- [136] A. V. Virkar, "Mechanism of oxygen electrode delamination in solid oxide electrolyzer cells," *International Journal of Hydrogen Energy*, vol. 35, pp. 9527–9543, sep 2010.
- [137] C. Graves, S. D. Ebbesen, S. H. Jensen, S. B. Simonsen, and M. B. Mogensen, "Eliminating degradation in solid oxide electrochemical cells by reversible operation," *Nature Materials*, vol. 14, no. 2, pp. 239–244, 2014.
- [138] J. Hong, H. J. Kim, S. Y. Park, J. H. Lee, S. B. Park, J. H. Lee, B. K. Kim, H. J. Je, J. Y. Kim, and K. J. Yoon, "Electrochemical performance and long-term durability of

- a 200 W class solid oxide regenerative fuel cell stack,” *International Journal of Hydrogen Energy*, vol. 39, no. 35, pp. 20819–20828, 2014.
- [139] N. Minh, “Development of reversible solid oxide fuel cells (RSOFCs) and stacks,” *ECS Transactions*, vol. 35, no. 1, pp. 2897–2904, 2011.
- [140] S. Elangovan, J. J. Hartvigsen, and L. J. Frost, “Intermediate Temperature Reversible Fuel Cells,” *International Journal of Applied Ceramic Technology*, vol. 4, no. 2, pp. 109–118, 2007.
- [141] J. C. Ruiz-Morales, D. Marrero-López, J. Canales-Vázquez, and J. T. S. Irvine, “Symmetric and reversible solid oxide fuel cells,” *RSC Advances*, vol. 1, no. 8, p. 1403, 2011.
- [142] T. Cable and J. Setlock, “Regenerative performance of the NASA symmetrical solid oxide fuel cell design,” *International Journal of Applied Ceramic Technology*, vol. 12, pp. 1–12, 2011.
- [143] M. Mogensen and P. Hendriksen, “Chapter 10 - Testing of Electrodes, Cells and Short Stacks,” in *High Temperature and Solid Oxide Fuel Cells* (S. C. Singhal and K. Kendal, eds.), pp. 261–289, Amsterdam: Elsevier Science, 2003.
- [144] J. T. S. Irvine, D. C. Sinclair, and A. R. West, “Electroceramics: characterization by impedance spectroscopy,” *Advanced Materials*, vol. 2, no. 3, pp. 132–138, 1990.
- [145] M. E. Orazem and B. Tribollet, “Electrochemical Impedance Spectroscopy,” *Electrochemical Impedance Spectroscopy*, pp. 1–523, 2008.
- [146] N. Wagner, “Characterization of membrane electrode assemblies in polymer electrolyte fuel cells using a.c. impedance spectroscopy,” *Journal of Applied Electrochemistry*, vol. 32, no. 8, pp. 859–863, 2002.
- [147] Z. Stoyanov and D. Vladikova, “Measurement Methods Electrochemical: Impedance Spectroscopy,” *Encyclopedia of Electrochemical Power Sources*, vol. 3, pp. 632–642, 2009.
- [148] E. Barsoukov and J. R. Macdonald, *Impedance spectroscopy: theory, experiment, and applications*.
John Wiley & Sons, 2005.

- [149] M. Kusnezoff, W. Beckert, N. Trofimenko, B. Jacobs, C. Dosch, S. Megel, M. Rachau, C. Wieprecht, and D. Gipp, "Electrochemical mea characterization: Area specific resistance corrected to fuel utilization as universal characteristic for cell performance," *ECS Transactions*, vol. 68, no. 1, pp. 2555–2563, 2015.
- [150] S. Seidler, M. Henke, J. Kallo, W. G. Bessler, U. Maier, and K. A. Friedrich, "Pressurized solid oxide fuel cells: Experimental studies and modeling," *Journal of Power Sources*, vol. 196, no. 17, pp. 7195–7202, 2011.
- [151] M. Henke, C. Willich, C. Westner, F. Leucht, R. Leibinger, J. Kallo, and K. A. Friedrich, "Effect of pressure variation on power density and efficiency of solid oxide fuel cells," *Electrochimica Acta*, vol. 66, no. 0, pp. 158–163, 2012.
- [152] M. Riedel, R. Nitsche, M. Henke, M. P. Heddrich, and K. A. Friedrich, "Pressurized operation of a 10 layer solid oxide electrolysis stack," 2016.
- [153] W. G. Bessler, J. Warnatz, and D. G. Goodwin, "The influence of equilibrium potential on the hydrogen oxidation kinetics of SOFC anodes," *Solid State Ionics*, vol. 177, no. 39-40, pp. 3371–3383, 2007.
- [154] M. Vogler, A. Bieberle-Hütter, L. Gauckler, J. Warnatz, and W. G. Bessler, "Modelling study of surface reactions, diffusion, and spillover at a ni/ysz patterned anode," *Journal of The Electrochemical Society*, vol. 156, no. 5, pp. B663–B672, 2009.
- [155] M. Henke, J. Kallo, K. A. Friedrich, and W. G. Bessler, "Influence of pressurisation on SOFC performance and durability: A theoretical study," *Fuel Cells*, vol. 11, no. 4, pp. 581–591, 2011.
- [156] Y. Patcharavorachot, A. Arpornwichanop, and A. Chuachuensuk, "Electrochemical study of a planar solid oxide fuel cell: Role of support structures," *Journal of Power Sources*, vol. 177, no. 2, pp. 254–261, 2008.
- [157] M. Henke, C. Willich, J. Kallo, and K. A. Friedrich, "Theoretical study on pressurized operation of solid oxide electrolysis cells," *International Journal of Hydrogen Energy*, vol. 39, no. 24, pp. 12434–12439, 2014.
- [158] S. Chan, K. Khor, and Z. Xia, "A complete polarization model of a solid oxide fuel cell and its sensitivity to the change of cell component thickness," *Journal of Power Sources*, vol. 93, pp. 130–140, feb 2001.

- [159] M. Li, J. Brouwer, A. D. Rao, and G. S. Samuelsen, "Application of a detailed dimensional solid oxide fuel cell model in integrated gasification fuel cell system design and analysis," *Journal of Power Sources*, vol. 196, no. 14, pp. 5903–5912, 2011.
- [160] C. O. Colpan, I. Dincer, and F. Hamdullahpur, "Thermodynamic modeling of direct internal reforming solid oxide fuel cells operating with syngas," *International Journal of Hydrogen Energy*, vol. 32, pp. 787–795, 2007.
- [161] P. Iora, M. Taher, P. Chiesa, and N. Brandon, "A novel system for the production of pure hydrogen from natural gas based on solid oxide fuel cell –solid oxide electrolyzer," *International Journal of Hydrogen Energy*, vol. 35, no. 22, pp. 12680–12687, 2010.
- [162] P. Iora and P. Chiesa, "High efficiency process for the production of pure oxygen based on solid oxide fuel cell - solid oxide electrolyzer technology," *Journal of Power Sources*, vol. 190, no. 2, pp. 408–416, 2009.
- [163] P. Aguiar, C. Adjiman, and N. Brandon, "Anode-supported intermediate-temperature direct internal reforming solid oxide fuel cell," *Journal of Power Sources*, vol. 147, no. 1-2, pp. 136–147, 2005.
- [164] R. T. Leah, N. P. Brandon, and P. Aguiar, "Modelling of cells, stacks and systems based around metal-supported planar IT-SOFC cells with CGO electrolytes operating at 500–600 C," *Journal of power sources*, vol. 145, no. 2, pp. 336–352, 2005.
- [165] a. Salogni and P. Colonna, "Modeling of solid oxide fuel cells for dynamic simulations of integrated systems," *Applied Thermal Engineering*, vol. 30, no. 5, pp. 464–477, 2010.
- [166] P. Kazempoor and R. Braun, "Model validation and performance analysis of regenerative solid oxide cells: Electrolytic operation," *International Journal of Hydrogen Energy*, vol. 39, no. 6, pp. 2669–2684, 2014.
- [167] E. Lay-Grindler, J. Laurencin, G. Delette, J. Aicart, M. Petitjean, and L. Dessemond, "Micro modelling of solid oxide electrolysis cell: From performance to durability," *International Journal of Hydrogen Energy*, vol. 38, no. 17, pp. 6917–6929, 2013.

- [168] X. Jin and X. Xue, "Mathematical modeling analysis of regenerative solid oxide fuel cells in switching mode conditions," *Journal of Power Sources*, vol. 195, no. 19, pp. 6652–6658, 2010.
- [169] M. Ni, "2D thermal modeling of a solid oxide electrolyzer cell (SOEC) for syngas production by H₂O/CO₂ co-electrolysis," *International Journal of Hydrogen Energy*, vol. 37, no. 8, pp. 6389–6399, 2012.
- [170] D. Larrain, J. Van Herle, F. Maréchal, and D. Favrat, "Generalized model of planar SOFC repeat element for design optimization," *Journal of Power Sources*, vol. 131, no. 1-2, pp. 304–312, 2004.
- [171] M. Li, J. D. Powers, and J. Brouwer, "A Finite Volume SOFC Model for Coal-Based Integrated Gasification Fuel Cell Systems Analysis," *Journal of Fuel Cell Science and Technology*, vol. 7, no. 4, p. 041017, 2010.
- [172] A. Sciacovelli and V. Verda, "Entropy generation analysis in a monolithic-type solid oxide fuel cell (SOFC)," *Energy*, vol. 34, no. 7, pp. 850–865, 2009.
- [173] G. Hawkes, J. O'Brien, C. Stoots, and B. Hawkes, "3D CFD model of a multi-cell high-temperature electrolysis stack," *International Journal of Hydrogen Energy*, vol. 34, no. 9, pp. 4189–4197, 2009.
- [174] J. Herring, J. O'Brien, and C. Stoots, "Progress in high-temperature electrolysis for hydrogen production using planar SOFC technology," *International Journal of Hydrogen Energy*, vol. 32, no. 4, pp. 440–450, 2007.
- [175] Y. Xie and X. Xue, "Modeling of solid oxide electrolysis cell for syngas generation with detailed surface chemistry," *Solid State Ionics*, vol. 224, pp. 64–73, 2012.
- [176] W. G. Bessler, S. Gewies, and M. Vogler, "A new framework for physically based modeling of solid oxide fuel cells," *Electrochimica Acta*, vol. 53, pp. 1782–1800, dec 2007.
- [177] V. Menon, V. M. Janardhanan, and O. Deutschmann, "A mathematical model to analyze solid oxide electrolyzer cells (SOECs) for hydrogen production," *Chemical Engineering Science*, vol. 110, pp. 83–93, 2014.
- [178] H. Zhu, R. J. Kee, V. M. Janardhanan, O. Deutschmann, and D. G. Goodwin, "Modeling Elementary Heterogeneous Chemistry and Electrochemistry in Solid-

- Oxide Fuel Cells,” *Journal of The Electrochemical Society*, vol. 152, no. 12, pp. A2427–A2440, 2005.
- [179] P. Colonna and H. van Putten, “Dynamic modeling of steam power cycles,” *Applied Thermal Engineering*, vol. 27, no. 2-3, pp. 467–480, 2007.
- [180] F. Casella and A. Leva, “Object-oriented modelling & simulation of power plants with modelica,” in *Decision and Control, 2005 and 2005 European Control Conference. CDC-ECC’05. 44th IEEE Conference on*, pp. 7597–7602, IEEE, 2005.
- [181] F. Casella, J. G. van Putten, and P. Colonna, “Dynamic Simulation of a Biomass-Fired Steam Power Plant: A Comparison Between Causal and A-Causal Modular Modeling,” in *Volume 6: Energy Systems: Analysis, Thermodynamics and Sustainability*, pp. 205–216, ASME, 2007.
- [182] F. Casella and P. Colonna, “Dynamic modeling of IGCC power plants,” *Applied Thermal Engineering*, vol. 35, pp. 91–111, 2012.
- [183] S. A. Hajimolana, M. A. Hussain, W. A. W. Daud, M. Soroush, and a. Shamiri, “Mathematical modeling of solid oxide fuel cells: A review,” *Renewable and Sustainable Energy Reviews*, vol. 15, no. 4, pp. 1893–1917, 2011.
- [184] J. Xu and G. F. Froment, “Methane steam reforming, methanation and water-gas shift: I. Intrinsic kinetics,” *AIChE Journal*, vol. 35, no. 1, pp. 88–96, 1989.
- [185] E. Achenbach and E. Riensche, “Methane/steam reforming kinetics for solid oxide fuel cells,” *Journal of Power Sources*, vol. 52, no. 2, pp. 283–288, 1994.
- [186] Y. Wang, F. Yoshiba, M. Kawase, and T. Watanabe, “Performance and effective kinetic models of methane steam reforming over Ni/YSZ anode of planar SOFC,” *International Journal of Hydrogen Energy*, vol. 34, no. 9, pp. 3885–3893, 2009.
- [187] E. S. Hecht, G. K. Gupta, H. Zhu, A. M. Dean, R. J. Kee, L. Maier, and O. Deutschmann, “Methane reforming kinetics within a Ni-YSZ SOFC anode support,” *Applied Catalysis A: General*, vol. 295, pp. 40–51, 2005.
- [188] W. Lehnert, J. Meusinger, and F. Thom, “Modelling of gas transport phenomenon in SOFC anodes,” *Journal of Power Sources*, vol. 87, pp. 57–63, 2000.

- [189] H. Timmermann, W. Sawady, R. Reimert, and E. Ivers-Tiffée, “Kinetics of (reversible) internal reforming of methane in solid oxide fuel cells under stationary and APU conditions,” *Journal of Power Sources*, vol. 195, pp. 214–222, 2010.
- [190] P. Aguiar, D. Chadwick, and L. Kershenbaum, “Modelling of an indirect internal reforming solid oxide fuel cell,” *Chemical Engineering Science*, vol. 57, no. 10, pp. 1665–1677, 2002.
- [191] D. Ferrero, A. Lanzini, P. Leone, and M. Santarelli, “Reversible operation of solid oxide cells under electrolysis and fuel cell modes: Experimental study and model validation,” *Chemical Engineering Journal*, vol. 274, pp. 143–155, 2015.
- [192] M. García-Camprubí, S. Izquierdo, and N. Fueyo, “Challenges in the electrochemical modelling of solid oxide fuel and electrolyser cells,” *Renewable and Sustainable Energy Reviews*, vol. 33, pp. 701–718, 2014.
- [193] D. Noren and M. Hoffman, “Clarifying the Butler-Volmer equation and related approximations for calculating activation losses in solid oxide fuel cell models,” *Journal of Power Sources*, vol. 152, pp. 175–181, 2005.
- [194] R. Suwanwarangkul, E. Croiset, M. Fowler, P. Douglas, E. Entchev, and M. Douglas, “Performance comparison of Fick’s, dusty-gas and Stefan-Maxwell models to predict the concentration overpotential of a SOFC anode,” *Journal of Power Sources*, vol. 122, no. 1, pp. 9–18, 2003.
- [195] Y. Fu, Y. Jiang, S. Poizeau, A. Dutta, A. Mohanram, J. D. Pietras, and M. Z. Bazant, “Multicomponent Gas Diffusion in Porous Electrodes,” *Journal of The Electrochemical Society*, vol. 162, no. 6, pp. 613–621, 2015.
- [196] P. Aguiar, C. S. Adjiman, and N. P. Brandon, “Anode-supported intermediate temperature direct internal reforming solid oxide fuel cell. I: Model-based steady-state performance,” *Journal of Power Sources*, vol. 138, no. 1-2, pp. 120–136, 2004.
- [197] R. Bove, P. Lunghi, and N. Sammes, “SOFC mathematic model for systems simulations—Part 2: definition of an analytical model,” *International Journal of Hydrogen Energy*, vol. 30, no. 2, pp. 189–200, 2005.

- [198] R. Sioshansi and P. Denholm, "The Value of Concentrating Solar Power and Thermal Energy Storage," *IEEE Transactions on Sustainable Energy*, vol. 1, no. 3, pp. 173–183, 2010.
- [199] D. Laing, C. Bahl, T. Bauer, M. Fiß, N. Breidenbach, and M. Hempel, "High-Temperature Solid-Media Thermal Energy Storage for Solar Thermal Power Plants," *Proceedings of the IEEE*, vol. 100, no. 2, pp. 516–524, 2012.
- [200] A. Sharma, V. V. Tyagi, C. R. Chen, and D. Buddhi, "Review on thermal energy storage with phase change materials and applications," *Renewable and Sustainable Energy Reviews*, vol. 13, no. 2, pp. 318–345, 2009.
- [201] M. M. Farid, A. M. Khudhair, S. A. K. Razack, and S. Al-Hallaj, "A review on phase change energy storage: Materials and applications," *Energy Conversion and Management*, vol. 45, no. 9-10, pp. 1597–1615, 2004.
- [202] A. Gil, M. Medrano, I. Martorell, A. Lázaro, P. Dolado, B. Zalba, and L. F. Cabeza, "State of the art on high temperature thermal energy storage for power generation. part 1—concepts, materials and modellization," *Renewable and Sustainable Energy Reviews*, vol. 14, no. 1, pp. 31–55, 2010.
- [203] H. Michels and R. Pitz-Paal, "Cascaded latent heat storage for parabolic trough solar power plants," *Solar Energy*, vol. 81, no. 6, pp. 829–837, 2007.
- [204] M. Fang and G. Chen, "Effects of different multiple PCMs on the performance of a latent thermal energy storage system," *Applied Thermal Engineering*, vol. 27, no. 5-6, pp. 994–1000, 2007.
- [205] R. Bayón, E. Rojas, L. Valenzuela, E. Zarza, and J. León, "Analysis of the experimental behaviour of a 100 kWth latent heat storage system for direct steam generation in solar thermal power plants," *Applied Thermal Engineering*, vol. 30, no. 17-18, pp. 2643–2651, 2010.
- [206] H. Shabgard, C. W. Robak, T. L. Bergman, and A. Faghri, "Heat transfer and exergy analysis of cascaded latent heat storage with gravity-assisted heat pipes for concentrating solar power applications," *Solar Energy*, vol. 86, no. 3, pp. 816–830, 2012.

BIBLIOGRAPHY

- [207] D. MacPhee and I. Dincer, "Thermal modeling of a packed bed thermal energy storage system during charging," *Applied Thermal Engineering*, vol. 29, no. 4, pp. 695–705, 2009.
- [208] B. Zalba, J. M. Marin, L. F. Cabeza, and H. Mehling, "Review on thermal energy storage with phase change: materials, heat transfer analysis and applications," *Applied thermal engineering*, vol. 23, no. 3, pp. 251–283, 2003.
- [209] T. W. Kerslake and M. B. Ibrahim, "Analysis of Thermal Energy Storage Material With Change-of-Phase Volumetric Effects," *Journal of Solar Energy Engineering*, vol. 115, no. 1, p. 22, 1993.
- [210] M. M. Kenisarin, "High-temperature phase change materials for thermal energy storage," *Renewable and Sustainable Energy Reviews*, vol. 14, no. 3, pp. 955–970, 2010.
- [211] Hasnain S.M., "Review on sustainable thermal energy storage technologies, Part I: heat storage materials and techniques," *Energy Conversion and Management*, vol. 39, no. 11, pp. 1127–1138, 1998.
- [212] M. Medrano, A. Gil, I. Martorell, X. Potau, and L. F. Cabeza, "State of the art on high-temperature thermal energy storage for power generation. Part 2-Case studies," *Renewable and Sustainable Energy Reviews*, vol. 14, no. 1, pp. 56–72, 2010.
- [213] A. Hoshi, D. R. Mills, A. Bittar, and T. S. Saitoh, "Screening of high melting point phase change materials (PCM) in solar thermal concentrating technology based on CLFR," *Solar Energy*, vol. 79, no. 3, pp. 332–339, 2005.
- [214] A. K. Misra, "Fluoride salts as phase change materials for thermal energy storage in the temperature range 1000-1400 K. Thermal analysis and heat of fusion measurements," *Journal of the Electrochemical Society*, vol. 135, no. 4, pp. 850–854, 1988.
- [215] N. Gokon, D. Nakano, S. Inuta, and T. Kodama, "High-temperature carbonate/MgO composite materials as thermal storage media for double-walled solar reformer tubes," *Solar Energy*, vol. 82, no. 12, pp. 1145–1153, 2008.
- [216] A. Stückle, "Modelling of high temperature storage systems for latent heat," *7th Modelica Conference*, pp. 502–506, 2009.

- [217] W. Li, H. Wang, Y. Shi, and N. Cai, "Performance and methane production characteristics of H₂O–CO₂ co-electrolysis in solid oxide electrolysis cells," *International Journal of Hydrogen Energy*, vol. 38, no. 25, pp. 11104–11109, 2013.
- [218] C. Graves, S. D. Ebbesen, M. Mogensen, and K. S. Lackner, "Sustainable hydrocarbon fuels by recycling CO₂ and H₂O with renewable or nuclear energy," *Renewable and Sustainable Energy Reviews*, vol. 15, no. 1, pp. 1–23, 2011.
- [219] A. Lazzaretto and A. Toffolo, "A method to separate the problem of heat transfer interactions in the synthesis of thermal systems," *Energy*, vol. 33, no. 2, pp. 163–170, 2008.
- [220] A. Lazzaretto and F. Segato, "Thermodynamic Optimization of the HAT Cycle Plant Structure – Part II: Structure of the Heat Exchanger Network," *Journal of Engineering for Gas Turbines and Power*, vol. 123, no. 1, p. 8, 2001.
- [221] A. Lazzaretto and F. Segato, "Thermodynamic Optimization of the HAT Cycle Plant Structure – Part I: Optimization of the Basic Plant Configuration," *Journal of Engineering for Gas Turbines and Power*, vol. 123, no. 1, p. 1, 2001.
- [222] M. Morandin, F. Maréchal, M. Mercangöz, and F. Buchter, "Conceptual design of a thermo-electrical energy storage system based on heat integration of thermodynamic cycles – Part B: Alternative system configurations," *Energy*, vol. 45, no. 1, pp. 386–396, 2012.
- [223] P. Mottaghizadeh, S. Santhanam, M. P. Heddrich, K. A. Friedrich, and F. Rinaldi, "Process modeling of a reversible solid oxide cell (r-soc) energy storage system utilizing commercially available soc reactor," *Energy Conversion and Management*, vol. 142, pp. 477–493, 2017.
- [224] H. Er-rbib and C. Bouallou, "Modeling and simulation of CO methanation process for renewable electricity storage," *Energy*, vol. 75, pp. 81–88, 2014.
- [225] J. Jensen, J. Poulsen, and N. Andersen, "From Coal To Clean Energy," *Nitrogen+Syngas*, pp. 1–5, 2011.
- [226] R. R. Dickinson, D. L. Battye, V. M. Linton, P. J. Ashman, and G. G. J. Nathan, "Alternative carriers for remote renewable energy sources using existing CNG infrastructure," *International Journal of Hydrogen Energy*, vol. 35, no. 3, pp. 1321–1329, 2010.

BIBLIOGRAPHY

- [227] S. Heyne, M. C. Seemann, and S. Harvey, "Integration study for alternative methanation technologies for the production of synthetic natural gas from gasified biomass," *Chemical Engineering Transactions*, vol. 21, pp. 409–414, 2010.
- [228] M. Sudiro and a. Bertucco, "Synthetic Natural Gas (SNG) from coal and biomass: a survey of existing process technologies, open issues and perspectives," *Natural Gas*, pp. 105–127, 2010.
- [229] M. J. Moran, H. N. Shapiro, D. D. Boettner, and M. Bailey, *Fundamentals of engineering thermodynamics*. Wiley, 2010.
- [230] T. J. Kotas, *The exergy method of thermal plant analysis*. Elsevier, 2013.
- [231] R. C. Tolman and P. C. Fine, "On the irreversible production of entropy," *Reviews of Modern Physics*, vol. 20, no. 1, pp. 51–77, 1948.
- [232] S. Kjelstrup & D. Bedeaux, *Non-Equilibrium Thermodynamics of Heterogeneous Systems*. World Scientific Publishing Co. Pte. Ltd., 2008.
- [233] M. A. Rosen and I. Dincer, "Exergy as the confluence of energy, environment and sustainable development," *Exergy, An International Journal*, vol. 1, pp. 3–13, 2001.
- [234] R. L. Cornelissen, "Thermodynamics and sustainable development; the use of exergy analysis and the reduction of irreversibility," 1997.
- [235] N. Lior and N. Zhang, "Energy, exergy, and Second Law performance criteria," *Energy*, vol. 32, no. 4, pp. 281–296, 2007.
- [236] J. Szargut, A. Valero, W. Stanek, and A. V. D., "Towards an international legal reference environment," *Proceedings of ECOS 2005*, pp. 409–420, 2005.
- [237] A. Bejan, "Fundamentals of exergy analysis, entropy generation minimization, and the generation of flow architecture," *International Journal of Energy Research*, vol. 26, no. 7, pp. 545–565, 2002.

- [238] D. Bedeaux and S. Kjelstrup, "Irreversible thermodynamics-a tool to describe phase transitions far from global equilibrium," *Chemical Engineering Science*, vol. 59, no. 1, pp. 109–118, 2004.
- [239] S. Kjelstrup and T. Island, "The driving force distribution for minimum lost work in a chemical reactor close to and far from equilibrium. 2. Oxidation of SO₂," *Industrial & engineering chemistry research*, no. 6, pp. 3051–3055, 1999.
- [240] L. V. van der Ham, J. Gross, and S. Kjelstrup, "Two performance indicators for the characterization of the entropy production in a process unit," *Energy*, vol. 36, no. 6, pp. 3727–3732, 2011.
- [241] D. R. Morris and J. Szargut, "Standard chemical exergy of some elements and compounds on the planet earth," *Energy*, vol. 11, no. 8, pp. 733–755, 1986.
- [242] J. Szargut, "Chemical exergies of the elements," *Applied Energy*, vol. 32, no. 4, pp. 269–286, 1989.
- [243] P. Hinderink, H. J. van der Kooi, and J. Swaan Arons de, "On the efficiency and sustainability of the process industry," *Green Chemistry*, vol. 1, no. 6, pp. G176–G180, 1999.
- [244] K. Denbigh, "The second-law efficiency of chemical processes," *Chemical Engineering Science*, vol. 6, no. 1, pp. 1–9, 1956.
- [245] S. K. Ratkje and J. De Swaan Arons, "Denbigh revisited: Reducing lost work in chemical processes," *Chemical Engineering Science*, vol. 50, no. 10, pp. 1551–1560, 1995.
- [246] T. Førland and S. Kjelstrup Ratkje, "Entropy production by heat, mass, charge transfer and specific chemical reactions," *Electrochimica Acta*, vol. 25, no. 2, pp. 157–163, 1980.
- [247] N. Lior, "Thoughts about future power generation systems and the role of exergy analysis in their development," *Energy Conversion and Management*, vol. 43, no. 9-12, pp. 1187–1198, 2002.

**A**

Appendix A: Thermodynamic fundamentals

A.1 Thermodynamic fundamentals for chemical process systems

A thermodynamic system, either chemical or thermal, can be defined as a **closed** or an **open** system. An open system is one in which matter can flow through whereas in a closed system there is no exchange of matter with its surroundings. For analysis, a particular component or volume of interest is defined as control volume. A control volume can either be an open system or closed system. A system can be defined by a set of properties. A **property** is defined as a macroscopic quality that describes the system without considering the process it underwent to reach the current state. It is independent of the process. A **state** is the current condition of the system characterised by the properties. The thermodynamic properties can be further distinguished as **extensive** and **intensive**. Intensive properties are non-additive and are independent of the size of the system. They can vary with respect to both time and position. The extensive properties are additive, that is, the total value of the property is equal to the sum of the value of the property at each constituent when the system is divided into subsystems with real or imaginary boundaries. Temperature, pressure and specific volume are examples of intensive properties and energy, mass and momentum are examples of extensive properties.

Another important concept in the thermodynamic analysis of process systems is the

concept of **equilibrium**. To say a system is in equilibrium means that, no changes occur in the system such that all properties are constant when the system is isolated from its surroundings. Even though a system is isolated from its surroundings, state changes can occur as the intensive properties attain a uniform value triggering spontaneous internal changes. When no changes in intensive properties are observed, then the system is said to have achieved an equilibrium state. To satisfy condition of full equilibrium, thermal energy, mechanical energy, chemical energy and phase must independently be in equilibrium. In reality, all engineering processes take place under non-equilibrium conditions. For analysis, a process is assumed to be **quasi-static** when each state the system passes through during the process, is infinitesimally close to equilibrium. A system is undergoing a process when there is a change in the state of the system. The process is said to be **reversible** when the system and its surroundings are brought back to its initial state without any hysteresis. When a system undergoes a process it can interact with the surrounding by exchanging energy. Energy transfer can be in form of work or heat which is defined at system boundaries only when it interacts with its surrounding. Heat is a form of energy transfer due to the temperature difference between the system and surroundings. Work is an energy transfer to or from a system whose effect can be seen as equivalent to the lifting of weight to a certain height. As per standard sign convention, work done on the system is assumed to be negative and work done by the system is assumed to be positive.[229]

A.1.1 Laws of thermodynamics

A thermodynamic system is modelled based on the fundamental laws of thermodynamics. They lay the foundations of thermodynamic systems. Systems violating these fundamental laws are unrealistic. These fundamental laws are:

- Laws of conservation.
- First law of thermodynamics
- Second law of thermodynamics

In the following sections, the above laws will be explained with respect to chemical reaction systems.

Law of conservation of mass

Principle of mass conservation states that the rate of change of mass within a control volume is equal to sum of all the mass flow rates of matter entering and leaving the control volume.

$$\frac{dm_{cv}}{dt} = \sum_i \dot{m}' - \sum_i \dot{m}'' \quad (\text{A.1})$$

As per the standard convention of mass or volume flow entering a control volume is regarded as positive and the flows leaving the control volume are regarded as negative. Equation (A.1) is a generalised form. For steady state conditions, the rate of mass within the control volume is zero leading to the following form.

$$\sum_i \dot{m}' = \sum_i \dot{m}'' \quad (\text{A.2})$$

For chemical reaction systems, the law of mass conservation can be further extended to species conservation of every reactant and product in the inlet flow stream and outlet flow stream. A more conventional form of mass conservation or conservation of species in the chemical reaction system is given by equation (A.3). The stoichiometric coefficient, ν , takes a positive value for products and a negative value for reactants. The terms r_j and A stands for the rate of reaction flux and effective reactive area respectively.

$$\frac{dn_{i,cv}}{dt} = \sum_i \dot{n}'_i - \sum_i \dot{n}''_i + \nu_{ij} \cdot r_j \cdot A \quad (\text{A.3})$$

First Law of thermodynamics

The first law of thermodynamics stipulates energy conservation of a system and its surroundings. It states that when system and surroundings are considered together, then the total energy remains constant. A system and surroundings together are equivalent to an isolated system. Hence, by first law, the energy of an isolated system is constant.

$$\Delta E_{system} + \Delta E_{surrounding} = 0 \quad (\text{A.4})$$

Energy (E) of a system is comprised of three major macroscopic energy forms. The first being the kinetic energy due to the motion of the system as a whole. Potential energy associated with the position of the system in earth's gravity field. Final energy form is the internal energy which is due to the system itself. Internal energy is an extensive property of the system like kinetic and potential energy. One can relate to internal energy

as the energy possessed by the system due to internal makeup of the system such as the pressure, volume, molecular forces etc. Internal energy is denoted by U and specific internal energy is given by u . Generally, in engineering thermodynamics, change in kinetic energy and potential energy are negligible.

$$\Delta E = \Delta E_{KE} + \Delta E_{PE} + \Delta U \quad (\text{A.5})$$

When considering the system alone, the first law is defined as the rate of energy within the same system is equal to the sum of all energy transferred across system boundary as heat and work. For a system at rest, it relates the internal energy with heat and work transferred across its boundaries.

$$\Delta U = \sum Q_i + \sum W_i \quad (\text{A.6})$$

Second law of thermodynamics

The second law of thermodynamics relates the extensive property **Entropy** of the system and surroundings. To understand what entropy means, one must look at the microscopic aspects of the matter. Using the theory of statistical thermodynamics, entropy can be defined as a measure randomness of the kinetic energy of molecules in matter. This is, in turn, a measure of uncertainty of the microscopic state. In real engineering processes, only a small portion of internal energy is available for work due to the random distribution of the kinetic energy of molecules. Hence for engineering process, entropy can be seen a measure of unavailability of internal energy [230]. The second law postulates that the entropy of the system and its surroundings can never decrease. Considering the system and surrounding as one isolated system, then the entropy of an isolated system never decreases. The equality in equation A.7 corresponds to the case of reversible systems.

$$\Delta S_{system} + \Delta S_{surroundings} \geq 0 \quad (\text{A.7})$$

In order to apply the second law for thermodynamic analysis of engineering systems, a quantitative method to evaluate entropy as given in equation (A.8) is utilised.

$$dS \leq \frac{dQ}{dT} \quad (\text{A.8})$$

Unlike energy, entropy does not obey the conservation law. Therefore, the entropy change of the system should take into account not only the entropy exchanged across its boundaries but also the entropy generated within the system. An irreversible process occurring within the system will generate entropy whereas for a reversible process entropy is transferred within the system [231]. From a microscopic level entropy generation due to irreversible process means that during the process some amount of organised form of energy is transformed to one that has a higher degree of randomness. Irreversibility can be of two types. The first type is a process in which work is directly converted to internal energy of the system. Some examples of this process include friction, ohmic resistance, mechanical hysteresis etc. The second type involves a spontaneous non-equilibrium process where the system moves unrestrained towards equilibrium. Some process belonging to this category are spontaneous chemical reactions, unrestrained expansion of gases, heat transfer over finite temperature difference, diffusion etc. In actual engineering process, the irreversibility is caused by a combination of two types. The irreversible entropy generated can be evaluated by applying the second law postulate over a control region or system as given in (A.9). Alternatively, it can also be evaluated in detail using the theory of non-equilibrium thermodynamics [232].

$$\Pi = \Delta S + \Delta S_o + \sum_i \Delta S_j \geq 0 \quad (\text{A.9})$$

In equation (A.9), the first term on RHS, ΔS represents the entropy change due to the flow of matter in and out of the control region. The second term, ΔS_o is the entropy change of the surroundings given by $\frac{q_o}{T_o}$. The last term $\sum_j \Delta S_j$ is the entropy change of the heat reservoirs that exchange heat with the system.

The implication of second law in engineering thermodynamics is profound. The increase in entropy of an isolated system can be used in predicting the transformation of energy in the system, nature of process occurring in the system, provide information on heat transfers that can occur and those that are not possible and finally the spontaneity of chemical reactions. Additionally, using second law, it can be shown that the mechanical, thermal and chemical equilibrium corresponds to equalisation of their intensive properties such as pressure, temperature and chemical potential respectively. For a system of given energy and volume, equilibrium is achieved when the maximum entropy is attained for given energy and volume [94]. Finally, the second law determines the extent of energy conversion from one form to another and determines the quality of energy source.

A.1.2 Thermodynamic functions

In the previous sections, two important functions of a thermodynamic system, internal energy (U) and entropy (S), were introduced. U and S along with the intensive property, Temperature (T) are sufficient to describe and explain the functioning of thermodynamic systems. Additional functions are defined in relations of U , T , p , \mathbf{V} and S which enables an easier discussion. These auxiliary functions have more practical significance and can be easily visualised for real thermodynamic processes and systems.

Enthalpy

Very often in thermodynamics, the term $U + p\mathbf{V}$ is encountered. Hence it is convenient to define a new property called the enthalpy defined by equation (A.10). Like internal energy, enthalpy is an extensive property with unit joule. The term $p\mathbf{V}$ is the work of displacing the environment in placing a system of certain volume and pressure in an environment.

$$H = U + pV \quad (\text{A.10})$$

For a system undergoing a change in state from 1 to 2, from equation (A.10) and application of 1st law of thermodynamics for closed systems we get;

$$H_2 - H_1 = U_2 - U_1 + p_2\mathbf{V}_2 - p_1\mathbf{V}_1 \quad (\text{A.11a})$$

given that

$$U_2 - U_1 = Q + W \quad (\text{A.11b})$$

$$H_2 - H_1 = Q + W + p_2\mathbf{V}_2 - p_1\mathbf{V}_1 \quad (\text{A.11c})$$

In closed system, if the displacement work (last two terms in equation(A.11c)) is the only form of work, then the 2nd term on RHS of equation (A.11c) and the displacement work term cancels out. The difference in enthalpy function between the two states is given by (A.12).

$$H_2 - H_1 = Q \quad (\text{A.12})$$

For an open steady flow system, the enthalpy function is useful. The enthalpy function replaces the internal energy function in the conservation of energy for open steady flow systems assuming the kinetic energy and potential energy change are negligible.

$$H_2 - H_1 = Q + W \quad (\text{A.13})$$

In chemical reaction systems, enthalpy is used often in evaluating the energy released or consumed during chemical reactions. It is made up of two components as shown in equation (A.14)

$$h(T, p) = h_{ref}(T_{ref}, p^\circ) + \int_{T^\circ}^T c_p(T) dT \quad (\text{A.14})$$

The first term on the right of equation (A.14), $h_{ref}(T_{ref}, p^\circ)$, refers to the enthalpy of a substance at standard conditions. The standard conditions are chosen by convention as $p = 1 \text{ bar}$ and $T_{ref} = 298.15 \text{ K}$ or $25 \text{ }^\circ\text{C}$. The enthalpy at standard conditions is the datum and enthalpy at different conditions are calculated based on this datum. For elements occurring naturally in standard stable forms such as H_2 , N_2 , O_2 and C the value of standard enthalpy is zero. For chemical compounds, this term is commonly referred to as the **enthalpy of formation** in chemical process engineering. The enthalpy of formation is the heat released or absorbed when the chemical compounds are formed from its base elements at reference. The second term $\int_{T^\circ}^T c_p(T) dT$ is the function to calculate the value of the enthalpy at conditions different from the reference conditions. As one can notice, this term is only temperature dependant as the enthalpy varies negligibly with pressure. The term c_p is the specific heat of a substance and varies from one material to another and also with temperature. **Enthalpy of combustion** or heating value for chemical compounds is often used in chemical process engineering. It is the difference in value between the enthalpy of products and enthalpy of reactants when complete combustion takes place. If the water produced as a product of combustion is brought to liquid form, then the heating value obtained is the Higher Heating Value (HHV). If the water produced is maintained in vapour or gaseous form, then the heat value obtained is the LHV.

Gibbs Function

The Gibbs function is a thermodynamic function connecting the first and second law of thermodynamics. This relates the internal energy of the system with the entropy of the system. The Gibbs function is given by equation (A.15a) as a function of U and S ($f(U, S)$) or as a function of H and S ($f(H, S)$) as in equation (A.15b).

$$G = U + p\mathbf{V} - TS \quad (\text{A.15a})$$

$$G = H - TS \quad (\text{A.15b})$$

Like internal energy and enthalpy, the Gibbs function (G) is also an extensive property of the system. When a closed system undergoes a change of state from 1 to 2, then the change in Gibbs function is given by

$$G_2 - G_1 = U_2 - U_1 + p_2 \mathbf{V}_2 - p_1 \mathbf{V}_1 - (T_2 S_2 - T_1 S_1) \quad (\text{A.16a})$$

For closed system we have

$$U_2 - U_1 = Q + W$$

Hence we get

$$G_2 - G_1 = Q + W + p_2 \mathbf{V}_2 - p_1 \mathbf{V}_1 - (T_2 S_2 - T_1 S_1) \quad (\text{A.16b})$$

Assuming that the closed system exchange heat with a reservoir at a temperature (T) and initial and final state temperatures of the system are equal such that $T_1 = T_2 = T$. The system pressure (p) remains constant satisfying the condition $p_2 = p_1 = p$. From second law relation (A.8) we know $dS \leq \frac{dQ}{dT}$. Substituting the same in equation (A.16b) we attain

$$W + p(\mathbf{V}_2 - \mathbf{V}_1) \leq G_2 - G_1 \quad (\text{A.17})$$

The second term on the LHS of equation (A.17), $p(\mathbf{V}_2 - \mathbf{V}_1)$, corresponds to work done by the system with pressure (p) in displacing the surroundings. The actual total work done by the system is inclusive of the displacement work. Therefore one can define a new work term, as in (A.18a) representing the total work of the system. If the system in consideration is an electrochemical reactor producing an electrical work, then W' in (A.18a) represents the electrical work done by the electrochemical reactor system. Using (A.18a) in (A.17) we obtain (A.18b)

$$W' = W + p(\mathbf{V}_2 - \mathbf{V}_1) \quad (\text{A.18a})$$

$$W' \leq G_2 - G_1 \quad (\text{A.18b})$$

The maximum work that can be achieved by the system in moving from state 1 to state 2 is given by the difference in Gibbs function between the two states. The inequality in equation (A.18b) represents an irreversible process. Therefore, the work done by a real thermodynamic system is always less than reversible work. The equation (A.17) is valid **only for a closed system**. For the **closed system**, the change in Gibbs function between the two states represents work without **including** the displacement work [94].

For an open system, the change in Gibbs function between two states, the change in Gibbs function is given by applying equation (A.15b) for Gibbs function at two state points. The resultant formulation is given in (A.19a) For open systems:

$$G_2 - G_1 = H_2 - H_1 - (T_2 S_2 - T_1 S_1) \quad (\text{A.19a})$$

$$W \leq G_2 - G_1 \quad (\text{A.19b})$$

For an open system, the difference in Gibbs function between two state points represents the total work done on or by the system. In this regard, the Gibbs function already takes into account the displacement work term, $\Delta(p\mathbf{V})$. For an open steady flow system, the displacement work is '*non-useful work*' which occurs at the inlet and outlet of the system. Due to this reason, the gibbs function, G , is more relevant and significant for an open system as compared to Helmholtz function.

Chemical Potential

In the previous subsections, the intensive variables; Temperature and Pressure, were deemed sufficient to define a state of a thermodynamic system. Using temperature, pressure, internal energy and entropy as state parameters a set of equations for a closed system can be written as given in equation (A.20).

$$\begin{aligned} dU &= T dS - p dV \\ dH &= T dS + V dP \\ dG &= -S dT + V dP \end{aligned} \quad (\text{A.20})$$

Though this is valid, it is only partially right and valid for a system with fixed compositions matter systems of fixed size (moles of substance) only. In equation (A.20) if we assume the process to be isothermal and isobaric, then from the relation of dG , it would imply no work potential is possible. But an isothermal and isobaric process can still perform work if the size and composition of system changes. Hence a third variable that takes into account the effect of changes are composition and size is required.

Assume an open system is in homogenous phase with a mixture of different species of matter (say gases). If different species of matter can simultaneously enter and leave the system reversibly thereby changing the size and composition of the system, then the internal energy of the system varies with the composition and size of the system. Therefore, the internal energy is now defined as in equation (A.21a). Differentiating

equation (A.21a) would yield the (A.21b)

$$U = U(S, \mathbf{V}, n_1, \dots, n_i) \quad (\text{A.21a})$$

$$dU = \left(\frac{\partial U}{\partial S} \right)_{\mathbf{V}, n_i} dS + \left(\frac{\partial U}{\partial \mathbf{V}} \right)_{S, n_i} d\mathbf{V} + \sum_{i=1}^{i=k} \left(\frac{\partial U}{\partial n_i} \right)_{S, \mathbf{V}, n_j} dn_i \quad (\text{A.21b})$$

The partial derivative terms in the equation (A.21b) represents the three intensive variables. The last partial derivative term on the right side of equation (A.21b) is the definition of chemical potential.

$$\begin{aligned} T &= \left(\frac{\partial U}{\partial S} \right)_{\mathbf{V}, n_i} \\ p &= \left(\frac{\partial U}{\partial \mathbf{V}} \right)_{S, n_i} \\ \mu_i &= \left(\frac{\partial U}{\partial n_i} \right)_{S, \mathbf{V}, n_j} \end{aligned} \quad (\text{A.22})$$

The chemical potential of a substance can also be defined in terms of Gibbs function using similar methods followed above. The expression for chemical potential in terms of Gibbs function is as described in equation (A.23e).

$$G = G(T, p, n_1, \dots, n_i) \quad (\text{A.23a})$$

$$dG = \left(\frac{\partial G}{\partial T} \right)_{p, n_i} dT + \left(\frac{\partial G}{\partial p} \right)_{T, n_i} dp + \sum_{i=1}^{i=k} \left(\frac{\partial G}{\partial n_i} \right)_{T, p, n_j} dn_i \quad (\text{A.23b})$$

$$-S = \left(\frac{\partial G}{\partial T} \right)_{p, n_i} \quad (\text{A.23c})$$

$$V = \left(\frac{\partial G}{\partial p} \right)_{T, n_i} \quad (\text{A.23d})$$

$$\mu_i = \left(\frac{\partial G}{\partial n_i} \right)_{T, p, n_j} \quad (\text{A.23e})$$

From equations (A.22) and (A.23e) , chemical potential was defined by Gibbs as

"If to any homogenous mass we suppose an infinitesimal quantity of any substance to be added, mass remaining homogenous and its entropy and volume remain unchanged, the increase of energy of the mass divided by the quantity of the substance added is the potential for that substance in the mass considered."

Chemical potential is important in the study of thermodynamics of reaction systems and chemical engineering. The system of equations for state function defining a thermodynamic system are rewritten to include the chemical potential as shown in equation

(A.24a) - (A.24c) State function equations defining a system

$$dU = T dS - p dV + \sum_i n_i \mu_i \quad (\text{A.24a})$$

$$dG = -S dT - V dp + \sum_i n_i \mu_i \quad (\text{A.24b})$$

$$dH = T dS + V dp + \sum_i n_i \mu_i \quad (\text{A.24c})$$

On the right side of the equation (A.24a), TdS represents the effect of heat transfer, $p dV$ represents the work due to the volume change and finally $\sum_i n_i \mu_i$ is the effect of mass transfer and/or effect of a change in composition due to chemical reaction. If the equations are regarded as energy equation of an infinitesimal process, then the last term $\sum_i n_i \mu_i$ is the work potential of system owing to a change in its composition. This form of work is called the *chemical work*. Therefore, chemical potential is an intensive property of the system. Chemical potential, temperature and pressure together are generally referred to as driving forces in a thermodynamic process. Differences in chemical potential can lead to diffusion of a substance from a region of high chemical potential to lower chemical potential or can also give rise to chemical reactions. The difference in temperature will result in the transfer of heat and pressure difference can lead to volume change or flow of matter in open systems. If the driving forces are large, then the process is spontaneous and occurs irreversibly. Hence, the equalisation of driving forces is criteria for equilibrium. The system equations (A.24a) - (A.24c) are the fundamental equations of state functions.

A.2 Exergy Analysis in chemical reaction systems

In the previous sections, with the introduction of the 1st law, it was shown that energy is a conserved quantity and can be transformed to many forms. It can be broadly classified as ordered and disordered energy. Ordered energy are those forms of energy that can be completely transformed to work if it occurs reversibly. Reversible transformation of ordered energy does not involve entropy creation and can be assessed solely using the 1st law. Transfer of ordered energy from one system to another is work transfer with no heat involved. Therefore work is nothing but ordered energy moving from one system to another. An example of ordered form of energy are potential energy, kinetic energy (without turbulent flow). The second classification of energy is the disordered form of energy. It is generally the energy associated with the randomness of the molecules.

Thermal energy, chemical energy and turbulent flows are examples of disordered energy. In order to achieve maximum conversion of the disordered energy to maximum energy, the process must be completely reversible. The process of energy transfer and transformation is governed by both 1st and 2nd law of thermodynamics. Even if the process is reversible, the maximum conversion is limited and determined by the thermodynamic parameters at which the energy is available. The 2nd law of thermodynamics describes *the quality of energy*. It is the ability of the energy source to cause change. This quality of energy (for disordered energy form) depends on the entropy which in turn depends on the process, the form of energy and environment. To compare the quality of different forms of energy, a common definition of quality is required. Hence, the quality of energy is defined with respect to the environment. It is the maximum work that can be obtained from an energy source using the environment as the reference. This definition of "quality of energy" is referred to the *Exergy* of energy source. A more exact definition of exergy is; the maximum work that can be obtained when the energy source is brought into complete thermal, mechanical and chemical equilibrium with the environment [230, 233–235]. The environment is largely chosen to be similar to the earth's atmospheric conditions, but the actual definition of the environment can vary. A detailed discussion on the definition of environment is provided by Szargut et al in [236].

A.2.1 Exergy Analysis

Assume a thermodynamic system as shown in Figure A.1. The system is an open system, with a mass flow entering the system where it undergoes a thermodynamic process and exits the system. The system also interacts with thermal reservoirs, $\dot{Q}_1, \dots, \dot{Q}_n$ which are temperatures T_1, \dots, T_2 . The system also interacts with the environment by exchanging a heat, \dot{Q}_o at temperature, T_o . Work (\dot{W}) is done by the system and expansion work of $p_o \frac{dV}{dt}$ is enacted on the environment. Applying the 1st and 2nd laws of thermodynamics, we deduce

$$\frac{dE}{dt} = \sum_{i=0}^n \dot{Q}_i - \dot{W} + \sum \dot{m}' h' - \sum \dot{m}'' h'' \quad (\text{A.25a})$$

$$\Pi = \frac{dS}{dt} - \sum_{i=0}^n \frac{\dot{Q}_i}{T_i} - \sum \dot{m}' s' - \sum \dot{m}'' s'' \geq 0 \quad (\text{A.25b})$$

For engineering processes, the heat released or taken in from the atmosphere is negligible[237]. Eliminating the \dot{Q}_o from the equations we obtain equation (A.26).

$$\dot{W} = -\frac{d(E - T_o S)}{dt} + \sum_{i=0}^n \left(1 - \frac{T_o}{T_i}\right) \dot{Q}_i + \sum \dot{m}' (h' - T_o s') - \sum \dot{m}'' (h'' (h' - T_o s'')) - T_o \Pi \quad (\text{A.26})$$

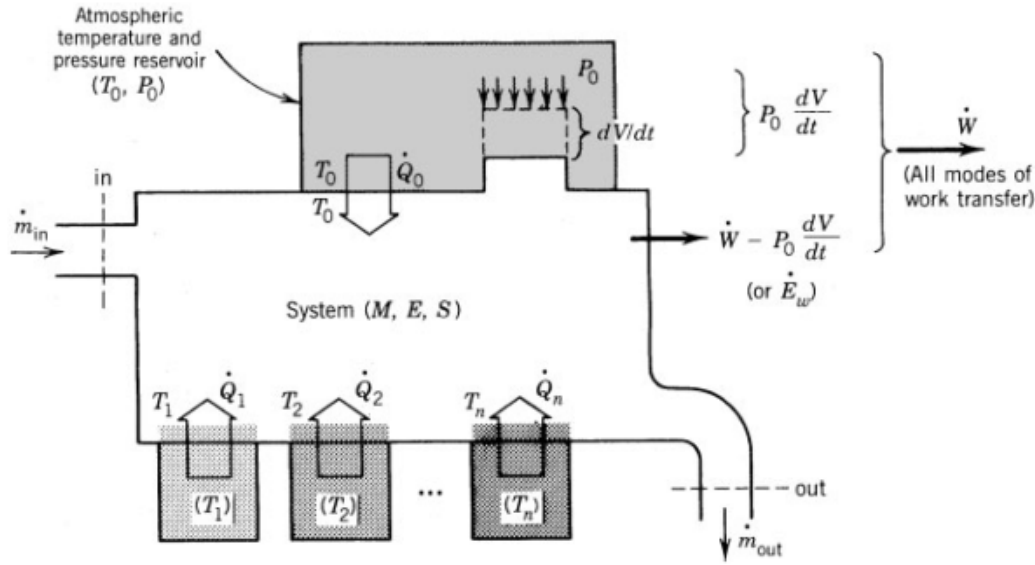


FIGURE A.1. Schematic representation of a open thermodynamic system with mass flow in and flow out. The system interacts with atmosphere and the thermal reservoirs. [237]

The equation (A.26) represents, the work produced by the system. The maximum work that can be obtained or minimum work to be supplied to the system to bring about a change in state is obtained for a reversible process when entropy generated (Π) is zero.

$$\dot{W}_{rev} = -\frac{d(E - T_o S)}{dt} + \sum_{i=0}^n \left(1 - \frac{T_o}{T_i}\right) \dot{Q}_i + \sum \dot{m}'(h' - T_o s') - \sum \dot{m}''(h'' - T_o s'') \quad (\text{A.27a})$$

$$\dot{W}_{rev} = -\frac{d(E - T_o S)}{dt} + \sum_{i=0}^n \left(1 - \frac{T_o}{T_i}\right) \dot{Q}_i + \sum \dot{m}' ex' - \sum \dot{m}'' ex'' \quad (\text{A.27b})$$

$$T_o \Pi = \dot{W}_{rev} - \dot{W} \quad (\text{A.27c})$$

Equations (A.27a) and (A.27c) represents the Gouy – Stodola theorem. The term $T_o \Pi$ in equation (A.27c) is the exergy destroyed during the irreversible process. The ratio of the actual work (\dot{W}) to the work of reversible process (\dot{W}_{rev}) is the defined as the second law efficiency of the process as shown in equation (A.28).

$$\eta_{II} = \frac{\dot{W}}{\dot{W}_{rev}} \quad (\text{A.28})$$

From (A.27c), it can be observed that the maximum work extracted from the system or minimum work supplied to the system, occurs for a completely reversible process. For all the processes that are not reversible, work is lost is destroyed due to the entropy

generation. This loss of work is commonly referred to as exergy destruction. Minimisation of entropy generation leads to highly efficient process. The exergy equation depends only on the initial and final states of the system within a process. It does not provide how the process occurred and how entropy evolved during the process, as it moved from initial to final states. Entropy generation or production can be analysed in more detailed by the framework of Non-Equilibrium Thermodynamics. For the purpose of process engineering, a global entropy balance between two states is sufficient to evaluate the entropy generation. For details on entropy generation and minimisation, refer to the following literature [232, 238–240].

Components of exergy

The equation (A.27b) represents a general exergy equation. The first term on the left of the equation represents the rate of change of exergy accumulation (non-flow exergy) within the system. For a steady state process, the first term is zero. The non-flow exergy is of significance for closed systems. The non-flow exergy component includes the changes due to thermal (Temperature), Mechanical (Pressure) and chemical (chemical potential) of the closed system during the process. The second term of equation (A.27b) is the exergy associated with heat transfer. The last two terms represents the steady flow exergy of the matter entering and leaving the system.

Exergy associated with heat transfer is the maximum work that can be obtained from thermal energy when using the environment as a thermal reservoir. For a thermal energy reservoir at a given temperature, the maximum work that can be produced by a reversible heat engine operating between the thermal reservoir and environment is provide by the Carnot relation. The term $\left(1 - \frac{T_o}{T}\right)$ in equation (A.29) is commonly referred to as the exergy factor of heat at a given temperature.

$$\dot{W} = \dot{Q} \left(1 - \frac{T_o}{T}\right) \quad (\text{A.29})$$

Flow Exergy is the exergy associated with the maximum work that can be obtained when a process stream with given composition, temperature and pressure is brought in complete thermo-mechanical and chemical equilibrium with the environment. The flow exergy of the process streams can be further resolved into two different components (i) Kinetic exergy, (ii) Potential exergy, (iii) Physical exergy and (iv) Chemical exergy. The kinetic and potential exergy are associated with the kinetic and potential

energy of the stream. Their exergetic values are same as the energy values as both Kinetic and Potential energy are ordered form of energy. For process flow systems in engineering, they are largely negligible. Physical and chemical exergy depends on the disordered energy forms.

$$ex = ex_{KE} + ex_{PE} + ex_{ph} + ex_{ch} \quad (A.30)$$

Physical Exergy is the maximum work obtained when a stream with temperature (T) and Pressure (p) is brought into equilibrium with the environment at temperature (T_o) and pressure (p_o) by a set of thermo-mechanical process interacting with the environment.

$$ex_{ph} = h - h_o - T(s - s_o) \quad (A.31)$$

Chemical Exergy is associated with the chemical energy of the stream. It is the work obtained when the stream is brought to a completely dead state. Dead state is a final equilibrium state with the environment, where all the substances in the stream are brought into chemical equilibrium (same compositions, partial pressures etc.) with the environment. In order to so, a reference chemical composition of the environment must be defined. The reference substances are usually taken to be as substances found in earth's environment (air, crust, water etc). A more detailed discussion on reference substance is found in [236, 241, 242]. For chemical engineering and process systems, chemical exergy of the mixtures is of utmost importance since in most process the working mediums are mixture of gases. If the gases and mixtures is assumed to be ideal. Then the exergy of chemical mixture is given by (A.32).

$$ex_{ch} = \sum_i x_i ex_{ch,i}^o + R T_o \sum_i x_i \ln x_i \quad (A.32)$$

The term $ex_{ch,i}^o$ is the chemical exergy of the substance in the pure state. A more detailed explanation of calculating the chemical exergy is explained in [230].

A.2.2 Maximum work and lost work in chemical processes

Application of exergy analysis and identification of sources of entropy generation in the chemical reaction system is essential in developing sustainable and efficiency process and reactors [243]. Consider a chemical reaction system occurring at certain temperature and pressure. Assume that the system can produce work which can be either in form of shaft work or electric work. From exergy analysis, it was shown that the maximum work

obtainable from a system undergoing a reversible process is equal to change in exergy between the final and initial state. If the chemical reaction occurs at environment conditions and assuming that reactants enter and leave the system at environment pressure and temperature. Then the exergy change of the process is equal to the Gibbs energy of the reaction as in equation (A.33). Consider the process is occurring at temperature a (T_1) and pressure (p_1) and at the end of the process, the system moves to pressure (p_2) and temperature (T_2), then the maximum work obtained from chemical reaction system is given by the relation (A.34). It is the sum of the change in Gibbs energy for the reaction plus the exergy difference due to the change in physical conditions [244, 245].

$$\dot{W}_{max}(p^\circ, T^\circ) = -\Delta_{rxn}Ex = -\Delta_{rxn}G(T^\circ, p^\circ) \quad (\text{A.33})$$

$$\dot{W}_{max}(p_1, T_1 \rightarrow p_2, T_2) = -\Delta_{rxn}Ex = -(\Delta H - T_o \Delta S) - \Delta_{rxn}G(T_o, p_o) \quad (\text{A.34})$$

Under practical engineering applications, chemical reactions processes are not reversible and thereby resulting in entropy generation. Hence an understanding of entropy generation process due to chemical reactions is crucial for minimising the lost work. Additionally, most of the chemical reaction systems are not designed to extract work potential of chemical reactions. Hence the total lost work includes the lost work due to entropy generation and the actual work that is not being extracted. Therefore the total lost work in chemical reaction process equals maximum work ($W_{lost} = \Delta Ex$) obtainable from the system.

Like heat transfer and volume expansion process, a chemical reaction is a process by which a system that is far from equilibrium moves towards equilibrium. As discussed earlier, minimisation of chemical potentials of the system is required for chemical equilibrium. Therefore, the driving force the reaction is the difference in chemical potential. The farther away the system is from equilibrium, greater is the driving force for the reaction to occur spontaneously in an unrestricted manner. This leads to irreversible process resulting in entropy generation and lost work. Therefore, entropy generation in chemical process can be related to driving force by the relation (A.35) [93, 245–247].

$$\dot{\Pi} = \frac{1}{T} \left(-\sum_i v_i \mu_i \right) d\xi \quad (\text{A.35})$$

In order to reduce or minimise the entropy production due to chemical reactions, the process must be carried out in a restrained manner. Based on the process, a chemical reactor can be described either as an unrestrained chemical engine or restrained chemical engine. In an unrestrained chemical engine, the process is spontaneous and it is not possible to extract work from the chemical reaction. In a restrained chemical engine, the chemical reaction rate is coupled to the work extraction (either in form of shaft work or electric work). Further, the pathway for the chemical reaction is open and the driving potential is zero (i.e. in the equilibrium state). When work is extracted, the equilibrium condition should be altered hence chemical reaction takes place to achieve a new equilibrium state. Therefore, the work extraction process should be coupled to changes in chemical potential. This can be achieved by applying an electric potential or change in pressure or temperature. When the work extraction process is slow enough in comparison to the rate of equilibrium achievement, then the process is restrained and operates close to the reversible limit. If the work extraction is fast in comparison to the time taken to achieve the equilibrium, leading to a high driving force to achieve equilibrium. Then the process becomes unrestrained leading to entropy generation [93, 245].



B Appendix B: Gas Diffusion model

B.1 Gas diffusion model

In order to evaluate the concentration and activation losses, the reactant concentrations at the reaction sites have to be computed. The reactant concentrations at the reaction sites are computed considering the diffusion transport process from the bulk through the porous electrodes. For the model to be valid at both low and high pressures it is important to consider Knudsen and molecular diffusion. An extended Fick's model is utilised to evaluate the concentrations at the triple phase boundary. The simple Fick's model accounts only for molecular diffusion and assumes the flux to be proportional to the concentration gradient. The extended form used in this model accounts for Knudsen diffusion by modifying the diffusion term accordingly. Likewise, the convective transport is considered via Darcy's equation. The transport term is given by equation (B.1).

$$N_i = \frac{1}{RT} \left(-D_i^{eff} \frac{\partial(x_i p)}{\partial z} + \frac{B_o x_i p}{\mu} \frac{dp}{dz} \right) \quad (B.1)$$

In the equation (B.1), N_i represents the mass transport of the gas component, B_o is the permeability, μ is viscosity, z represents the distance from the electrode surface to the electrode-electrolyte interface, x_i is the mole fraction of the species i and D_i^{eff} is the effective diffusion coefficient calculated from the Bosanquet formula [194]. The effective diffusion is given by equation (B.2).

$$D_i^{eff} = \left(\frac{1}{D_{im}^{eff}} + \frac{1}{D_{ik}^{eff}} \right)^{-1} \quad (\text{B.2})$$

The terms D_{im}^{eff} and D_{ik}^{eff} are the effective molecular and effective Knudsen diffusion of species i . The values are calculated by assuming an equi-molar counter diffusion of reactant and product species. The model is adopted by assuming constant pressure ($\frac{dp}{dz} = 0$). The equation (B.1) reduces to the form given in equation (B.3).

$$N_i = \frac{p}{RT} \left(-D_i^{eff} \frac{\partial x_i}{\partial z} \right) \quad (\text{B.3})$$

The effective diffusion of reactant component is evaluated based on the multicomponent diffusion. At the fuel electrode side, a ternary system is considered with H_2 , H_2O and N_2 . Only three gas components are considered on the fuel side since only H_2 , H_2O and N_2 are used for experimental analysis. Moreover, it is assumed that only H_2 - H_2O is the main electrochemical reaction. Hence, CO and CO_2 are not considered in here. The effective diffusion coefficient for hydrogen on the fuel side is given by equation (B.4).

$$\frac{1}{D_{\text{H}_2}^{eff}} = \frac{1}{D_{\text{H}_2,k}^{eff}} + \frac{1}{D_{\text{H}_2,\text{N}_2}^{eff}} + \left(\frac{1}{D_{\text{H}_2,\text{H}_2\text{O}}^{eff}} - \frac{1}{D_{\text{H}_2,\text{N}_2}^{eff}} \right) (1 - x_{\text{N}_2}) \quad (\text{B.4})$$

The mass transfer of the hydrogen is coupled to the current density via the Faraday's law (equation (B.5)). Substituting equation (B.5) in equation (B.3) and integrating the same with the boundary condition $x_{\text{H}_2}|_{z=0} = x_{\text{H}_2}^{bulk}$ results in equation (B.6) and (B.7) for H_2 and H_2O mole fractions respectively.

$$N_{\text{H}_2} = \frac{j}{2F} \quad (\text{B.5})$$

$$x_{\text{H}_2}^{tpb} = x_{\text{H}_2}^{bulk} - \frac{jRT}{2FD_{\text{H}_2}^{eff}p} z \quad (\text{B.6})$$

$$x_{\text{H}_2\text{O}}^{tpb} = x_{\text{H}_2\text{O}}^{bulk} + \frac{jRT}{2FD_{\text{H}_2\text{O}}^{eff}p} z \quad (\text{B.7})$$

To evaluate the oxygen diffusion on the cathode side, the binary diffusivity method is employed. The constant pressure is assumed. The oxygen mass transport is given by equation (B.8)

$$N_{\text{O}_2} = \frac{p}{RT} \left(-D_{\text{O}_2}^{eff} \frac{dx_{\text{O}_2}}{dz} + x_{\text{O}_2} \delta_{\text{O}_2} N_{\text{O}_2} \right) \quad (\text{B.8})$$

The effective diffusion coefficients for oxygen and δ_{O_2} are given by equation (B.9) and (B.10) respectively.

$$D_{O_2}^{eff} = \left(\frac{1}{D_{O_2, N_2}^{eff} + D_{O_2, k}^{eff}} \right)^{-1} \quad (B.9)$$

$$\delta_{O_2} = \frac{D_{O_2, k}^{eff}}{D_{O_2, N_2}^{eff} + D_{O_2, k}^{eff}} \quad (B.10)$$

Similar to the hydrogen, oxygen transport on the air side is coupled to the current density via Faraday's law ((B.11)). Substituting equation (B.11) in equation (B.8) and integrating with the limit $x_{O_2}|_{z=0} = x_{O_2}^{bulk}$ gives equation (B.12).

$$N_{O_2} = \frac{j}{4F} \quad (B.11)$$

$$x_{O_2}^{TPB} = \frac{1}{\delta_{O_2}} - \left(\frac{1}{\delta_{O_2}} - x_{O_2}^{bulk} \right) \exp \left(\frac{jR T \delta_{O_2}}{4F D_{O_2}^{eff} p} z \right) \quad (B.12)$$

B.1.1 Effective diffusion coefficients

TABLE B.1. The binary coefficients of different gas compositions at 310 K and atmospheric pressure

Parameter	Value	Units
$D_{H_2-H_2O}$	0.8684×10^{-4}	m^2/s
$D_{H_2-N_2}$	0.8114×10^{-4}	m^2/s
$D_{N_2-H_2O}$	0.2231×10^{-4}	m^2/s
$D_{O_2-N_2}$	0.2176×10^{-4}	m^2/s

The effective diffusion coefficients takes into account porosity (ϵ) and tortuosity (ψ) of the electrodes. It is calculate using the formula given in equation (B.13)

$$D^{eff} = D \left(\frac{\epsilon}{\psi} \right) \quad (B.13)$$

The Knudsen diffusion is evaluated from the kinetic theory of gases as given in equation (B.14)

$$D_{i,k} = \frac{d_p}{3} \sqrt{\frac{8RT}{\pi M_i}} \quad (B.14)$$

The binary diffusion coefficients are calculated based on the Lennard-Jones potential and Chapman-Enskog diffusion theory. The Chapman-Enskog theory utilises the molecular parameters of each species and collision integral data. The coefficient is calculated at a reference temperature of 310 K and atmospheric pressure. They are corrected for the required temperature and pressure using the equation (B.15)

$$D_{ij} = D_{ij}^{\circ} \left(\frac{T}{310} \right)^{1.75} \left(\frac{p^{\circ}}{p} \right) \quad (\text{B.15})$$

The values for the binary coefficients at the 310 K and atmospheric pressure is provided in the Table B.1

**C**

Appendix C: Aspen implementation of 0-D model

The commercial process engineer software Aspen Plus™ is used for the process system modelling and analysis. The software does not have an inbuilt rSOC model. Hence, the 0-D rSOC model was implemented in Aspen by combining certain inbuilt library component models to model the physical phenomenon. The 0-D rSOC model was implemented in Aspen as 2 sub models. One sub model simulates the SOFC operation mode and the other model simulates the SOEC operation mode. Both the sub models are enclosed inside an 'Hierarchy block'. The 'Hierarchy Block' represents the complete r-SOC model. The implementation of the SOFC and SOEC operation modes are discussed in the following sections.

C.1 SOFC operation mode

The SOFC sub model of the 0-D rSOC model as implemented in Aspen is shown in the Figure C.1. The various physical phenomenon occurring inside the rSOC reactor in SOFC mode is captured by inbuilt models available in Aspen library. The list of inbuilt Aspen library models used within the SOFC sub model is described in the Table C.1

TABLE C.1. List of inbuilt aspen library models used for SOFC model and their functions

Component ID	Component Type	Function
ANODE	RGIBBS	Models the fuel side chemical and electrochemical reactions assuming equilibrium at constant temperature and pressure
CATHODE	SEP	Models the cathode and electrolyte behaviour. Separates the oxygen molecules from air and supply to ANODE. Separation ratio is obtained from electrochemical block
B4	RGIBBS	Brings the inlet gas to equilibrium at reactor temperature and pressure.
HEATER	HEATER/COOLER	Models the energy balance at the reactor exit. Calculates outlet temperature
B1 and B2	HEATER/COOLER	Brings the inlet flows to the reactor temperature
SEP	SEP	Splits the anode streams and cathode streams at outlet after final energy balance
MIXER	MIXER	Combines anode and cathode streams to calculate outlet temperature. No reactions occur. No mixing effect is modelled.
SPLITER	SPLIT	Splits the total energy released by anode to electric work and thermal power
REQ-ION	CALCULATOR	Models the electrochemical behaviour; ideal voltage, cell voltage, ASR, oxygen mole transfer, etc.

C.2 SOEC operation mode

The SOEC sub model of the 0-D rSOC model as implemented in Aspen is shown in the Figure C.2. The various physical phenomenon occurring inside the rSOC reactor in SOEC mode is capture by inbuilt models available in Aspen library. The list of inbuilt Aspen library models used within the SOEC sub model is described in the Table C.2

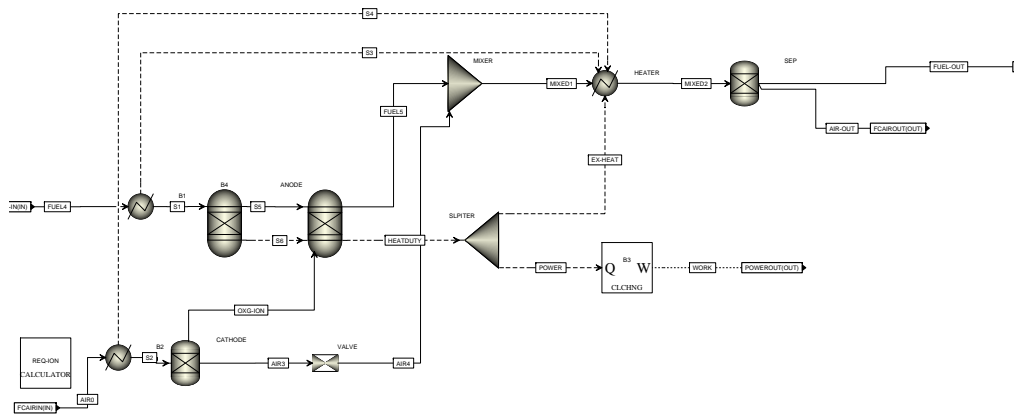


FIGURE C.1. Aspen implementation of 0-D rSOC model in SOFC mode

TABLE C.2. List of inbuilt aspen library models used for SOEC model and their functions

Component ID	Component Type	Function
RSTOIC	RSTOIC	Models the fuel side electrochemical reactions for give reactant utilisation value
AN-AIR	SEP	Models electrolyte behaviour. Separates the oxygen molecules from fuel side and sends to air side
RWGS	RGIBBS	Brings the inlet gas to equilibrium at reactor temperature and pressure.
HEATER	HEATER/COOLER	Models the energy balance at the reactor exit. Calculates outlet temperature
B1 and B2	HEATER/COOLER	Brings the inlet flows to the reactor temperature
AST-SEP	SEP	Splits the anode streams and cathode streams at outlet after final energy balance
MIXER	MIXER	Combines anode and cathode streams to calculate outlet temperature. No reactions occur. No mixing effect is modelled.
CA-FUEL	RGIBBS	Calculates the equilibrium at the outlet of the reactor at the reactor temperature and pressure
OXG-ION	CALCULATOR	Models the electrochemical behaviour; ideal voltage, cell voltage, ASR, oxygen mole transfer, etc.

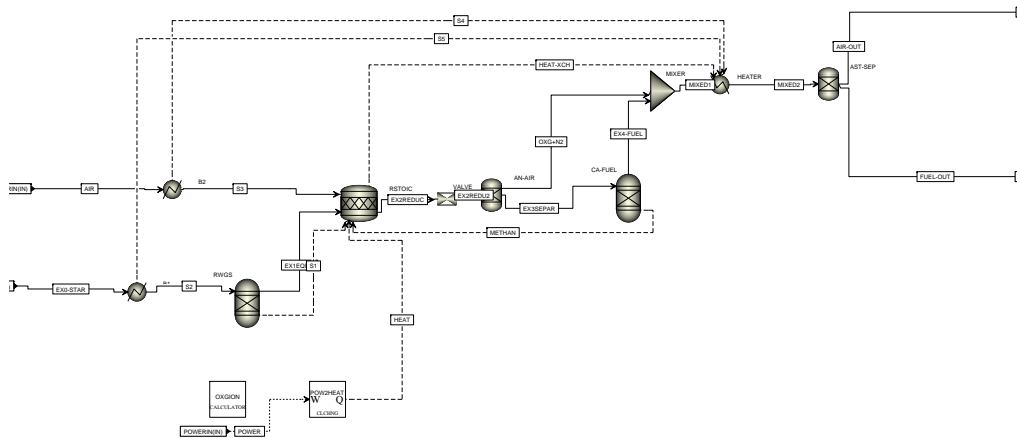
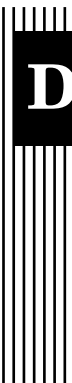


FIGURE C.2. Aspen implementation of 0-D rSOC model in SOEC mode



D Appendix D: Hydrogen based closed architecture rSOC system - performance and thermodynamic stream data

An expanded process flow diagram from the hydrogen based closed architecture system is presented here. System performance including the net electric power produced and consumed by the system in SOFC and SOEC mode respectively is presented here. The thermodynamic stream data of the process system modelling of the system at two different operation pressures is provided in this chapter.

D.1 Detailed process flow diagram

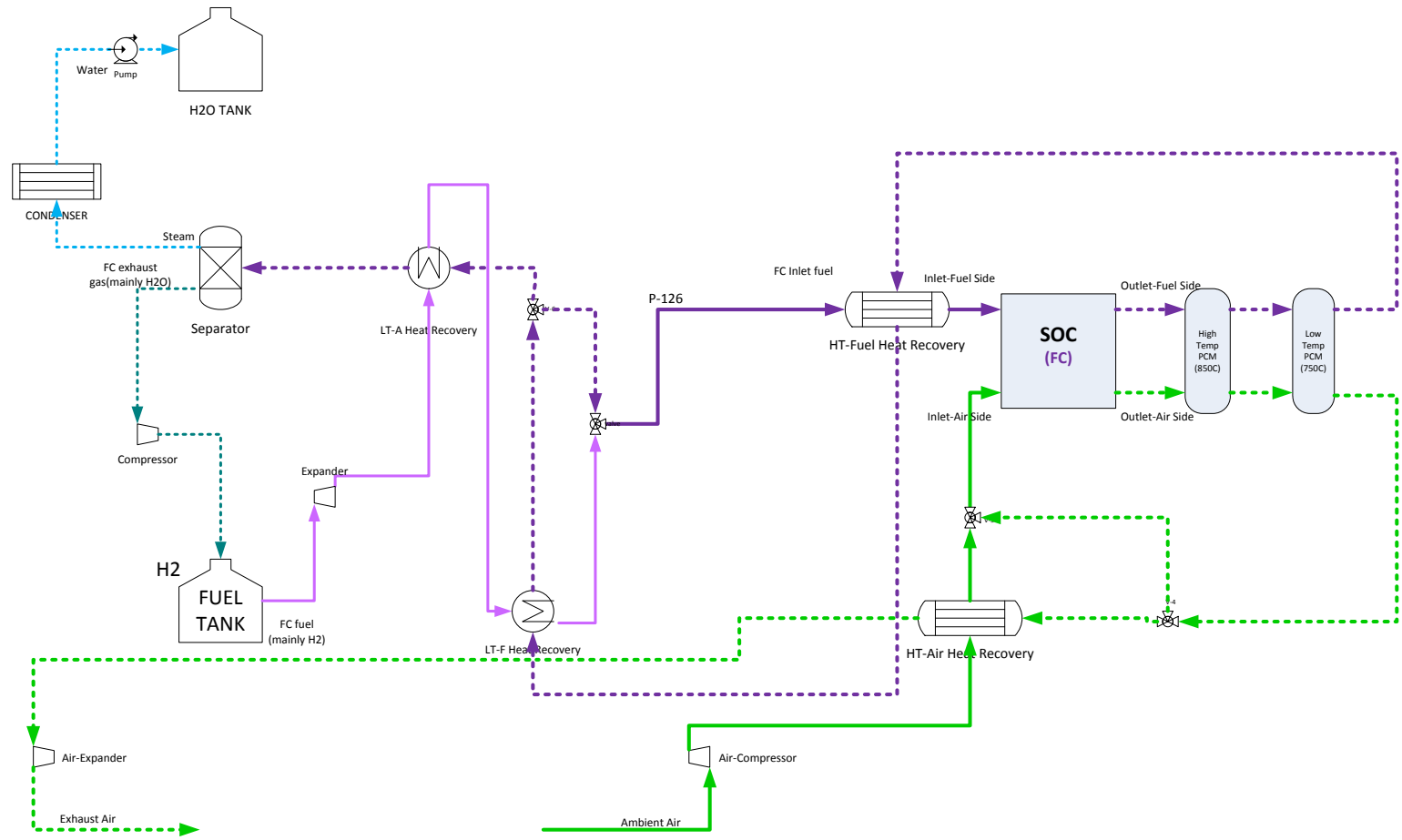


FIGURE D.1. Extended process flow diagram of Hydrogen based closed grid system in SOFC mode.

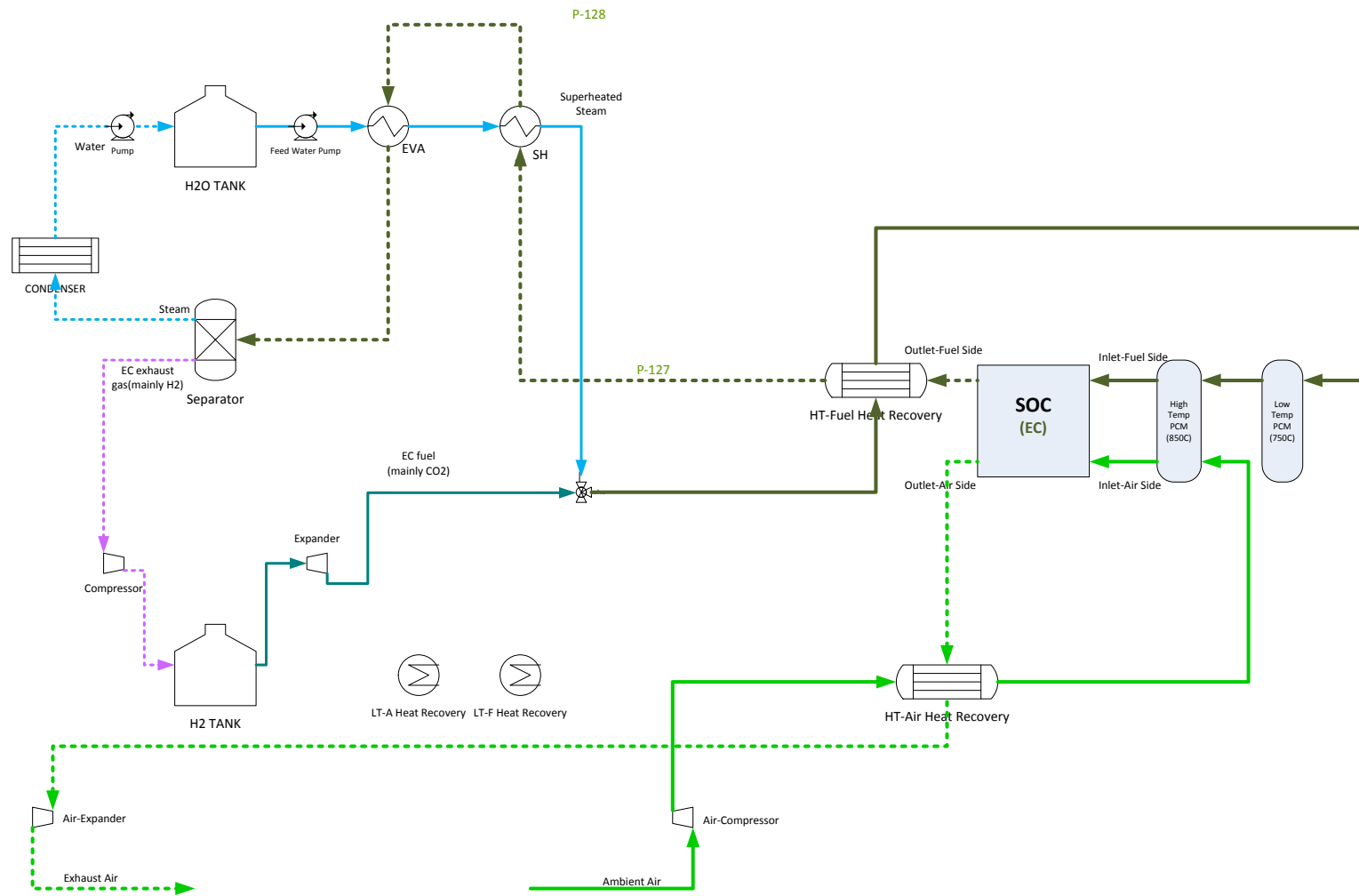


FIGURE D.2. Extended process flow diagram of Hydrogen based closed grid system in SOEC mode.

D.2 Performance data

TABLE D.1. rSOC system performance at 1 bar for the hydrogen based closed architecture rSOC system

Parameter	1 bar	25 bar
SOFC		
Effective reactor temperature	845 °C	845 °C
Cell voltage	0.731 V	0.803 V
Chemical power input	60 kW	60 kW
rSOC power output	30.4 kW	33.4 kW
BoP power consumption	0.710 kW	4.88 kW
Net power produced	29.6 kW	28.5 kW
Net efficiency in SOFC mode	49.4 %	47.5 %
SOEC		
Effective reactor temperature	809 °C	809 °C
Cell voltage	1.262 V	1.279 V
Chemical power produced	60 kW	60 kW
rSOC power input	52.5 kW	53 kW
BoP power consumption	3.51 kW	0.360 kW
Total electrical input	56.0 kW	53.5 kW
Net efficiency in SOEC mode	107.1 %	112.1 %
Roundtrip efficiency		
Reactor (Gross)	57.8 %	62.7 %
System (Net)	52.9	53.2 %

D.3 Thermodynamic stream data for non-pressurised hydrogen based closed system

The enthalpy, entropy, pressure, flow rate and exergy flows are presented in the Table D.2. The gas compositions, density and molecular weight of the streams are presented in the Table D.3.

Table D.2: Thermodynamic stream data for closed hydrogen based system at 1 bar

Streams	Total Flow	Pressure	Enthalpy	Entropy	Exergy		
					Thermomechanical	Chemical	Total
	kg/s	bar	J/kg	J/kg K	kJ/kmol	kJ/kmol	kW
E-TANK	6.79E-05	1.01	0.00	33.72	38909.18	236110.00	9.26
E-TANK1	6.79E-05	1.01	0.00	33.72	38909.18	236110.00	9.26
E-TANK2	6.79E-05	1.00	381175.00	1278.80	38929.26	236110.00	9.26
E-WATER	4.98E-04	0.98	-15885000.00	-9124.82	69528.47	900.00	1.95
E-WATER1	4.98E-04	0.98	-15885000.00	-9124.82	69528.47	900.00	1.95
E-WATER2	4.98E-04	1.00	-15885000.00	-9124.81	69528.47	900.00	1.95
EAIR-AMB	1.00E-02	1.00	0.00	151.91	57910.18	128.49	20.12
EAIR-IN1	1.00E-02	1.01	505.08	152.16	57922.55	128.49	20.12
EAIR-IN2	1.00E-02	1.00	505.08	152.45	57920.09	128.49	20.12
EAIR-IN3	1.00E-02	1.00	802647.00	1481.67	69820.97	128.49	24.25
EAIR-IN4	1.00E-02	1.00	860882.00	1536.20	70841.95	128.49	24.60
EAIROUT1	1.34E-02	1.00	207189.00	720.84	60100.85	346.31	27.46
EAIROUT2	1.34E-02	0.99	206581.00	721.05	60081.00	346.31	27.45
EC-IN	4.44E-03	1.00	-11406000.00	662.95	88573.01	28609.11	32.41
EC-IN-1	4.44E-03	1.00	-14236000.00	-4955.65	70366.46	28609.11	27.37
EC-IN-2	4.44E-03	1.00	-11898000.00	166.45	83675.14	28609.11	31.05
EC-IN-3	4.44E-03	1.00	-11898000.00	166.40	83674.31	28609.11	31.05
EC-OUT	1.00E-03	1.00	-349270.00	10067.45	53912.48	211792.57	73.48
EC-OUT1	1.00E-03	1.00	-1912300.00	8453.21	49877.52	211792.57	72.37

Table D.2: Thermodynamic stream data for closed hydrogen based system at 1 bar

Streams	Total Flow	Pressure	Enthalpy	Entropy	Exergy		
					Thermomechanical	Chemical	Total
	kg/s	bar	J/kg	J/kg K	kJ/kmol	kJ/kmol	kW
EC-OUT2	1.00E-03	0.99	-5994300.00	1617.93	42482.24	211792.57	70.32
EC-OUT3	1.00E-03	0.99	-6390400.00	524.68	42228.49	211792.57	70.25
EC-OUT4	1.00E-03	0.98	-6416300.00	458.75	42206.56	211792.57	70.25
EC-OUT5	1.00E-03	0.98	-7681400.00	-3631.03	41948.22	211792.57	70.18
EC-OUT6	5.02E-04	0.98	-71331.95	-103.66	38847.95	236110.00	68.44
EC-OUT7	5.02E-04	25.00	1639420.00	-8565.95	47382.76	236110.00	70.56
ECAIRIN	1.00E-02	1.00	860732.00	1536.06	70836.55	128.49	24.60
ECAIROUT	1.34E-02	1.00	803851.00	1513.14	70934.70	346.31	32.38
EHPCM1IA	2.45E-01	1.00	-11690000.00	249.76	94744.06	900.00	1300.71
EHPCM1IF	9.21E-01	1.00	-11690000.00	249.76	94744.06	900.00	4886.98
EHPCM1OA	2.45E-01	1.00	-11692000.00	247.65	94715.42	900.00	1300.32
EHPCM1OF	9.21E-01	1.00	-11692000.00	247.65	94715.42	900.00	4885.52
ELPCM1IF	4.51E+00	1.00	-11924000.00	31.59	91695.90	900.00	23155.04
ELPCM1OF	4.51E+00	1.00	-11927000.00	29.34	91668.00	900.00	23148.06
EW-TANK	4.38E-03	1.00	-15844000.00	-8987.23	69529.06	900.00	17.11
EW-TANK1	4.38E-03	1.03	-15844000.00	-8987.22	69529.06	900.00	17.11
EW-TANK2	4.38E-03	1.02	-15753000.00	-8700.03	69617.62	900.00	17.13
EW-TANK3	4.38E-03	1.02	-15753000.00	-8700.03	69617.62	900.00	17.13
EW-TANK4	4.38E-03	1.02	-14820000.00	-6167.19	72829.00	900.00	17.91

Table D.2: Thermodynamic stream data for closed hydrogen based system at 1 bar

Streams	Total Flow	Pressure	Enthalpy	Entropy	Exergy		
					Thermomechanical	Chemical	Total
	kg/s	bar	J/kg	J/kg K	kJ/kmol	kJ/kmol	kW
EW-TANK5	4.38E-03	1.01	-14463000.00	-5209.04	74506.83	900.00	18.32
F-RECYC	5.07E-04	0.99	-12081000.00	-44.46	82100.29	31725.59	3.64
F-TANK	5.02E-04	25.00	933549.00	-10389.86	47056.03	236110.00	70.48
F-TANK1	5.02E-04	25.00	1827240.00	-8116.36	47491.19	236110.00	70.59
F-TANK2	5.02E-04	1.10	1827240.00	4765.87	45724.65	236110.00	70.15
F-TANK3	5.02E-04	1.10	4787600.00	10476.61	44904.42	236110.00	69.95
F-TANK4	5.02E-04	1.09	7165540.00	13859.16	46441.14	236110.00	70.33
F-TANK5	5.02E-04	1.09	7165540.00	13878.13	46430.85	236110.00	70.33
F-WATER4	3.88E-03	0.99	-15864000.00	-9055.61	69525.78	900.00	15.16
F-WATER5	3.88E-03	0.98	-15864000.00	-9055.61	69525.78	900.00	15.16
F-WATER6	3.88E-03	0.98	-15864000.00	-9055.61	69525.78	900.00	15.16
FAIR-AMB	1.09E-01	1.00	0.00	151.91	57910.18	128.49	218.46
FAIR-IN	1.09E-01	1.01	1008.47	152.42	57934.89	128.49	218.55
FAIR-IN1	1.09E-01	1.01	58250.06	327.68	58020.72	128.49	218.88
FAIR-IN2	1.09E-01	1.01	722103.00	1400.03	70226.87	128.49	264.82
FAIR-IN3	1.09E-01	1.01	722103.00	1400.03	67717.76	183.54	255.58
FAIROUT1	1.05E-01	1.00	899883.00	1563.52	71194.87	226.56	261.15
FAIROUT2	1.05E-01	1.00	791797.00	1463.28	68964.48	226.56	252.99
FAIROUT3	1.05E-01	1.00	791797.00	1463.28	68964.48	226.56	252.99

Table D.2: Thermodynamic stream data for closed hydrogen based system at 1 bar

Streams	Total Flow	Pressure	Enthalpy	Entropy	Exergy		
					Thermomechanical	Chemical	Total
	kg/s	bar	J/kg	J/kg K	kJ/kmol	kJ/kmol	kW
FAIROUT4	1.05E-01	1.00	106202.00	449.82	54605.60	226.56	200.49
FAIROUT5	1.05E-01	0.99	106202.00	451.28	54593.11	226.56	200.44
FAIROUT6	1.05E-01	0.72	76081.38	465.63	53603.97	226.56	196.83
FAIRRECY	1.00E-10	0.00	0.00	0.00	46194.18	226.56	0.00
FC-FINAL	6.79E-05	25.00	1077980.00	-9997.35	47111.29	236110.00	9.53
FC-IN	1.01E-03	0.99	-525690.00	9913.91	53586.95	212154.16	74.64
FC-IN1	1.01E-03	0.99	-2507300.00	7709.50	50447.87	212154.16	73.76
FC-IN2	1.01E-03	0.99	-525690.00	9913.91	53586.95	212154.16	74.64
FC-OUT	4.45E-03	1.00	-11218000.00	843.06	89505.11	31725.59	34.05
FC-OUT1	4.45E-03	1.00	-11276000.00	791.41	88905.11	31725.59	33.88
FC-OUT2	4.45E-03	1.00	-11364000.00	711.97	87888.58	31725.59	33.60
FC-OUT3	4.45E-03	1.00	-11813000.00	265.85	84218.46	31725.59	32.57
FC-OUT4	4.45E-03	0.99	-12081000.00	-44.46	82097.69	31725.59	31.97
FC-OUT5	3.95E-03	0.99	-12081000.00	-44.46	82100.29	31725.59	28.33
FC-OUT6	3.95E-03	0.99	-12458000.00	-566.48	79922.93	31725.59	27.79
FC-OUT7	3.95E-03	0.99	-14033000.00	-4448.74	59825.50	31725.59	22.79
FC-OUT8	3.95E-03	0.99	-15579000.00	-8853.69	66354.10	31725.59	24.41
FC-OUT9	6.79E-05	0.99	0.00	116.62	38859.35	236110.00	9.26
FC-OUT10	6.79E-05	25.01	7686610.00	1581.82	53474.11	236110.00	9.75

Table D.2: Thermodynamic stream data for closed hydrogen based system at 1 bar

Streams	Total Flow	Pressure	Enthalpy	Entropy	Exergy		
					Thermomechanical	Chemical	Total
	kg/s	bar	J/kg	J/kg K	kJ/kmol	kJ/kmol	kW
FCAIRIN	1.09E-01	1.01	722103.00	1400.03	67717.76	183.54	255.58
FCAIROUT	1.05E-01	1.00	927009.00	1587.39	71695.79	226.56	262.98
FHPCMIA	1.20E+00	1.00	-11692000.00	247.65	94715.42	900.00	6368.95
FHPCMIF	1.10E-01	1.00	-11692000.00	247.65	94715.42	900.00	583.82
FHPCMOA	1.20E+00	1.00	-11690000.00	249.76	94744.06	900.00	6370.86
FHPCMOF	1.10E-01	1.00	-11690000.00	249.76	94744.06	900.00	584.00
FLPCMIA	4.93E+00	1.00	-11927000.00	29.34	91668.00	900.00	25316.43
FLPCMIF	1.70E-01	1.00	-11927000.00	29.34	91668.00	900.00	873.51
FLPCMOA	4.93E+00	1.00	-11924000.00	31.59	91695.90	900.00	25324.06
FLPCMOF	1.70E-01	1.00	-11924000.00	31.59	91695.90	900.00	873.77

Table D.3: Gas compositions of streams for closed hydrogen based system at 1 bar

Streams	Mole Fraction								Density	Mol.wt
	H ₂	H ₂ O	CO	CO ₂	CH ₄	O ₂	N ₂	C	kg/m ³	kg/kmol
E-TANK	1.00	0.00	0.00	0.00	0.00	0.00	0.00	0.00	0.08	2.02
E-TANK1	1.00	0.00	0.00	0.00	0.00	0.00	0.00	0.00	0.08	2.02
E-TANK2	1.00	0.00	0.00	0.00	0.00	0.00	0.00	0.00	0.07	2.02
E-WATER	0.00	1.00	0.00	0.00	0.00	0.00	0.00	0.00	998.77	18.02
E-WATER1	0.00	1.00	0.00	0.00	0.00	0.00	0.00	0.00	998.77	18.02
E-WATER2	0.00	1.00	0.00	0.00	0.00	0.00	0.00	0.00	998.77	18.02
EAIR-AMB	0.00	0.00	0.00	0.00	0.00	0.21	0.79	0.00	1.16	28.85
EAIR-IN1	0.00	0.00	0.00	0.00	0.00	0.21	0.79	0.00	1.17	28.85
EAIR-IN2	0.00	0.00	0.00	0.00	0.00	0.21	0.79	0.00	1.17	28.85
EAIR-IN3	0.00	0.00	0.00	0.00	0.00	0.21	0.79	0.00	0.33	28.85
EAIR-IN4	0.00	0.00	0.00	0.00	0.00	0.21	0.79	0.00	0.32	28.85
EAIROUT1	0.00	0.00	0.00	0.00	0.00	0.40	0.60	0.00	0.70	29.60
EAIROUT2	0.00	0.00	0.00	0.00	0.00	0.40	0.60	0.00	0.70	29.60
EC-IN	0.12	0.88	0.00	0.00	0.00	0.00	0.00	0.00	0.18	16.07
EC-IN-1	0.12	0.88	0.00	0.00	0.00	0.00	0.00	0.00	0.97	16.07
EC-IN-2	0.12	0.88	0.00	0.00	0.00	0.00	0.00	0.00	0.22	16.07
EC-IN-3	0.12	0.88	0.00	0.00	0.00	0.00	0.00	0.00	0.22	16.07
EC-OUT	0.90	0.10	0.00	0.00	0.00	0.00	0.00	0.00	0.04	3.62
EC-OUT1	0.90	0.10	0.00	0.00	0.00	0.00	0.00	0.00	0.05	3.62

Table D.3: Gas compositions of streams for closed hydrogen based system at 1 bar

Streams	Mole Fraction								Density	Mol.wt
	H ₂	H ₂ O	CO	CO ₂	CH ₄	O ₂	N ₂	C	kg/m ³	kg/kmol
EC-OUT2	0.90	0.10	0.00	0.00	0.00	0.00	0.00	0.00	0.11	3.62
EC-OUT3	0.90	0.10	0.00	0.00	0.00	0.00	0.00	0.00	0.13	3.62
EC-OUT4	0.90	0.10	0.00	0.00	0.00	0.00	0.00	0.00	0.13	3.62
EC-OUT5	0.90	0.10	0.00	0.00	0.00	0.00	0.00	0.00	0.16	3.62
EC-OUT6	1.00	0.00	0.00	0.00	0.00	0.00	0.00	0.00	0.08	2.02
EC-OUT7	1.00	0.00	0.00	0.00	0.00	0.00	0.00	0.00	1.47	2.02
ECAIRIN	0.00	0.00	0.00	0.00	0.00	0.21	0.79	0.00	0.32	28.85
ECAIROUT	0.00	0.00	0.00	0.00	0.00	0.40	0.60	0.00	0.34	29.60
EHPCM1IA	0.00	1.00	0.00	0.00	0.00	0.00	0.00	0.00	0.19	18.02
EHPCM1IF	0.00	1.00	0.00	0.00	0.00	0.00	0.00	0.00	0.19	18.02
EHPCM1OA	0.00	1.00	0.00	0.00	0.00	0.00	0.00	0.00	0.19	18.02
EHPCM1OF	0.00	1.00	0.00	0.00	0.00	0.00	0.00	0.00	0.19	18.02
ELPCM1IF	0.00	1.00	0.00	0.00	0.00	0.00	0.00	0.00	0.21	18.02
ELPCM1OF	0.00	1.00	0.00	0.00	0.00	0.00	0.00	0.00	0.21	18.02
EW-TANK	0.00	1.00	0.00	0.00	0.00	0.00	0.00	0.00	989.12	18.02
EW-TANK1	0.00	1.00	0.00	0.00	0.00	0.00	0.00	0.00	989.12	18.02
EW-TANK2	0.00	1.00	0.00	0.00	0.00	0.00	0.00	0.00	967.88	18.02
EW-TANK3	0.00	1.00	0.00	0.00	0.00	0.00	0.00	0.00	967.88	18.02
EW-TANK4	0.00	1.00	0.00	0.00	0.00	0.00	0.00	0.00	1.84	18.02

Table D.3: Gas compositions of streams for closed hydrogen based system at 1 bar

Streams	Mole Fraction								Density	Mol.wt
	H ₂	H ₂ O	CO	CO ₂	CH ₄	O ₂	N ₂	C	kg/m ³	kg/kmol
EW-TANK5	0.00	1.00	0.00	0.00	0.00	0.00	0.00	0.00	1.23	18.02
F-RECYC	0.14	0.86	0.00	0.00	0.00	0.00	0.00	0.00	0.24	15.85
F-TANK	1.00	0.00	0.00	0.00	0.00	0.00	0.00	0.00	1.67	2.02
F-TANK1	1.00	0.00	0.00	0.00	0.00	0.00	0.00	0.00	1.43	2.02
F-TANK2	1.00	0.00	0.00	0.00	0.00	0.00	0.00	0.00	0.06	2.02
F-TANK3	1.00	0.00	0.00	0.00	0.00	0.00	0.00	0.00	0.04	2.02
F-TANK4	1.00	0.00	0.00	0.00	0.00	0.00	0.00	0.00	0.03	2.02
F-TANK5	1.00	0.00	0.00	0.00	0.00	0.00	0.00	0.00	0.03	2.02
F-WATER4	0.00	1.00	0.00	0.00	0.00	0.00	0.00	0.00	993.96	18.02
F-WATER5	0.00	1.00	0.00	0.00	0.00	0.00	0.00	0.00	993.96	18.02
F-WATER6	0.00	1.00	0.00	0.00	0.00	0.00	0.00	0.00	993.96	18.02
FAIR-AMB	0.00	0.00	0.00	0.00	0.00	0.21	0.79	0.00	1.16	28.85
FAIR-IN	0.00	0.00	0.00	0.00	0.00	0.21	0.79	0.00	1.17	28.85
FAIR-IN1	0.00	0.00	0.00	0.00	0.00	0.21	0.79	0.00	0.99	28.85
FAIR-IN2	0.00	0.00	0.00	0.00	0.00	0.21	0.79	0.00	0.36	28.85
FAIR-IN3	0.00	0.00	0.00	0.00	0.00	0.21	0.79	0.00	0.36	28.85
FAIROUT1	0.00	0.00	0.00	0.00	0.00	0.19	0.81	0.00	0.31	28.76
FAIROUT2	0.00	0.00	0.00	0.00	0.00	0.19	0.81	0.00	0.34	28.76
FAIROUT3	0.00	0.00	0.00	0.00	0.00	0.19	0.81	0.00	0.34	28.76

Table D.3: Gas compositions of streams for closed hydrogen based system at 1 bar

Streams	Mole Fraction								Density	Mol.wt
	H ₂	H ₂ O	CO	CO ₂	CH ₄	O ₂	N ₂	C	kg/m ³	kg/kmol
FAIROUT4	0.00	0.00	0.00	0.00	0.00	0.19	0.81	0.00	0.86	28.76
FAIROUT5	0.00	0.00	0.00	0.00	0.00	0.19	0.81	0.00	0.85	28.76
FAIROUT6	0.00	0.00	0.00	0.00	0.00	0.19	0.81	0.00	0.67	28.76
FAIRRECY	0.00	0.00	0.00	0.00	0.00	0.00	0.00	0.00	0.00	0.00
FC-FINAL	1.00	0.00	0.00	0.00	0.00	0.00	0.00	0.00	1.62	2.02
FC-IN	0.90	0.10	0.00	0.00	0.00	0.00	0.00	0.00	0.04	3.59
FC-IN1	0.90	0.10	0.00	0.00	0.00	0.00	0.00	0.00	0.05	3.59
FC-IN2	0.90	0.10	0.00	0.00	0.00	0.00	0.00	0.00	0.04	3.59
FC-OUT	0.14	0.86	0.00	0.00	0.00	0.00	0.00	0.00	0.17	15.85
FC-OUT1	0.14	0.86	0.00	0.00	0.00	0.00	0.00	0.00	0.17	15.85
FC-OUT2	0.14	0.86	0.00	0.00	0.00	0.00	0.00	0.00	0.17	15.85
FC-OUT3	0.14	0.86	0.00	0.00	0.00	0.00	0.00	0.00	0.21	15.85
FC-OUT4	0.14	0.86	0.00	0.00	0.00	0.00	0.00	0.00	0.24	15.85
FC-OUT5	0.14	0.86	0.00	0.00	0.00	0.00	0.00	0.00	0.24	15.85
FC-OUT6	0.14	0.86	0.00	0.00	0.00	0.00	0.00	0.00	0.29	15.85
FC-OUT7	0.14	0.86	0.00	0.00	0.00	0.00	0.00	0.00	0.83	15.85
FC-OUT8	0.14	0.86	0.00	0.00	0.00	0.00	0.00	0.00	4.49	15.85
FC-OUT9	1.00	0.00	0.00	0.00	0.00	0.00	0.00	0.00	0.08	2.02
FC-OUT10	1.00	0.00	0.00	0.00	0.00	0.00	0.00	0.00	0.73	2.02

Table D.3: Gas compositions of streams for closed hydrogen based system at 1 bar

Streams	Mole Fraction								Density	Mol.wt
	H ₂	H ₂ O	CO	CO ₂	CH ₄	O ₂	N ₂	C	kg/m ³	kg/kmol
FCAIRIN	0.00	0.00	0.00	0.00	0.00	0.21	0.79	0.00	0.36	28.85
FCAIROUT	0.00	0.00	0.00	0.00	0.00	0.19	0.81	0.00	0.30	28.76
FHPCMIA	0.00	1.00	0.00	0.00	0.00	0.00	0.00	0.00	0.19	18.02
FHPCMIF	0.00	1.00	0.00	0.00	0.00	0.00	0.00	0.00	0.19	18.02
FHPCMOA	0.00	1.00	0.00	0.00	0.00	0.00	0.00	0.00	0.19	18.02
FHPCMOF	0.00	1.00	0.00	0.00	0.00	0.00	0.00	0.00	0.19	18.02
FLPCMIA	0.00	1.00	0.00	0.00	0.00	0.00	0.00	0.00	0.21	18.02
FLPCMIF	0.00	1.00	0.00	0.00	0.00	0.00	0.00	0.00	0.21	18.02
FLPCMOA	0.00	1.00	0.00	0.00	0.00	0.00	0.00	0.00	0.21	18.02
FLPCMOF	0.00	1.00	0.00	0.00	0.00	0.00	0.00	0.00	0.21	18.02

D.4 Thermodynamic stream data for pressurised hydrogen based closed system

The enthalpy, entropy, pressure, flow rate and exergy flows are presented in the Table D.4. The gas compositions, density and molecular weight of the streams are presented in the Table D.5.

Table D.4: Thermodynamic stream data for closed hydrogen based system at 25 bar

Streams	Total Flow	Pressure	Enthalpy	Entropy	Exergy		
					Thermomechanical	Chemical	Total
	kg/s	bar	J/kg	J/kg K	kJ/kmol	kJ/kmol	kW
E-TANK	6.79E-05	25.01	0.00	-13222.50	46876.64	236110.00	9.53
E-TANK1	6.79E-05	25.01	0.00	-13222.50	46876.64	236110.00	9.53
E-TANK2	6.79E-05	25.00	1657130.00	-8523.02	47392.66	236110.00	9.54
E-WATER	4.98E-04	24.98	-15885000.00	-9124.82	69528.47	900.00	1.95
E-WATER1	4.98E-04	24.98	-15885000.00	-9124.82	69528.47	900.00	1.95
E-WATER2	4.98E-04	1.00	-15887000.00	-9130.93	69531.27	900.00	1.95
EAIR-AMB	1.00E-02	1.00	0.00	151.91	57910.18	128.49	20.12
EAIR-IN1	1.00E-02	25.01	53045.40	-611.89	66010.57	128.49	22.92
EAIR-IN2	1.00E-02	25.00	53045.40	-611.88	66010.47	128.49	22.92
EAIR-IN3	1.00E-02	25.00	742724.00	494.83	76388.33	128.49	26.52
EAIR-IN4	1.00E-02	25.00	837445.00	586.64	78331.30	128.49	27.20
EAIROUT1	1.34E-02	25.00	298510.00	-18.23	69359.04	345.43	31.66
EAIROUT2	1.34E-02	1.00	-3294.02	181.33	58665.77	345.43	26.81
EC-IN	4.44E-03	25.00	-11457000.00	-1049.61	95963.71	28609.11	34.45
EC-IN-1	4.44E-03	25.00	-14069000.00	-5426.23	74950.71	28609.11	28.64
EC-IN-2	4.44E-03	25.00	-11697000.00	-1283.93	93226.25	28609.11	33.70
EC-IN-3	4.44E-03	25.00	-11697000.00	-1283.98	93226.52	28609.11	33.70
EC-OUT	1.00E-03	25.00	-290710.00	2721.30	62526.57	211782.62	75.86
EC-OUT1	1.00E-03	25.00	-4011000.00	-1789.26	53937.45	211782.62	73.49

Table D.4: Thermodynamic stream data for closed hydrogen based system at 25 bar

Streams	Total Flow	Pressure	Enthalpy	Entropy	Exergy		
					Thermomechanical	Chemical	Total
	kg/s	bar	J/kg	J/kg K	kJ/kmol	kJ/kmol	kW
EC-OUT2	1.00E-03	24.99	-4840400.00	-3239.55	52501.96	211782.62	73.09
EC-OUT3	1.00E-03	24.99	-5666200.00	-4990.77	51403.89	211782.62	72.79
EC-OUT4	1.00E-03	24.98	-5778600.00	-5260.42	51287.59	211782.62	72.76
EC-OUT5	1.00E-03	24.98	-7940000.00	-11262.40	49943.18	211782.62	72.38
EC-OUT6	5.02E-04	24.98	-71332.00	-13459.70	46875.38	236110.00	70.44
EC-OUT7	5.02E-04	25.00	-70135.30	-13459.10	46877.43	236110.00	70.44
ECAIRIN	1.00E-02	25.00	837445.00	586.64	78331.30	128.49	27.20
ECAIROUT	1.34E-02	25.00	811518.00	616.13	78944.53	345.43	36.02
EHPCM1IA	3.99E-01	1.00	-11690000.00	249.76	94744.06	900.00	2115.66
EHPCM1IF	4.49E-01	1.00	-11690000.00	249.76	94744.06	900.00	2383.76
EHPCM1OA	3.99E-01	1.00	-11692000.00	247.65	94715.42	900.00	2115.02
EHPCM1OF	4.49E-01	1.00	-11692000.00	247.65	94715.42	900.00	2383.04
ELPCM1IF	4.57E+00	1.00	-11924000.00	31.59	91695.90	900.00	23489.13
ELPCM1OF	4.57E+00	1.00	-11927000.00	29.34	91668.00	900.00	23482.05
EW-TANK	4.38E-03	25.00	-15541000.00	-8098.59	70205.68	900.00	17.27
EW-TANK1	4.38E-03	25.03	-15541000.00	-8098.58	70205.68	900.00	17.27
EW-TANK2	4.38E-03	25.02	-15352000.00	-7632.49	71101.22	900.00	17.49
EW-TANK3	4.38E-03	25.02	-15352000.00	-7632.49	71101.22	900.00	17.49
EW-TANK4	4.38E-03	25.02	-15163000.00	-7215.91	72285.09	900.00	17.78

Table D.4: Thermodynamic stream data for closed hydrogen based system at 25 bar

Streams	Total Flow	Pressure	Enthalpy	Entropy	Exergy		
					Thermomechanical	Chemical	Total
	kg/s	bar	J/kg	J/kg K	kJ/kmol	kJ/kmol	kW
EW-TANK5	4.38E-03	25.01	-14313000.00	-5525.90	78516.62	900.00	19.29
F-RECYC	5.07E-04	24.95	-12294000.00	-2018.10	86126.61	31725.59	3.77
F-TANK	5.02E-04	25.00	0.00	-13221.90	46876.24	236110.00	70.44
F-TANK1	5.02E-04	25.00	111831.00	-12850.80	46878.66	236110.00	70.44
F-TANK2	5.02E-04	25.03	113553.00	-12850.00	46881.62	236110.00	70.44
F-TANK3	5.02E-04	25.02	3251150.00	-5104.80	48551.53	236110.00	70.85
F-TANK4	5.02E-04	25.02	5835900.00	-848.42	51203.88	236110.00	71.52
F-TANK5	5.02E-04	25.01	5835900.00	-847.60	51203.38	236110.00	71.52
F-WATER4	3.88E-03	24.94	-15541000.00	-8098.59	70205.68	900.00	15.31
F-WATER5	3.88E-03	24.94	-15541000.00	-8098.59	70205.68	900.00	15.31
F-WATER6	3.88E-03	25.00	-15541000.00	-8098.58	70205.68	900.00	15.31
FAIR-AMB	2.28E-02	1.00	0.00	151.91	57910.18	128.49	45.95
FAIR-IN	2.28E-02	25.00	53023.00	-611.90	66009.97	128.49	52.37
FAIR-IN1	2.28E-02	25.00	67974.50	-570.11	66081.91	128.49	52.42
FAIR-IN2	2.28E-02	25.00	497604.00	215.83	71716.44	128.49	56.88
FAIR-IN3	9.67E-02	24.96	727785.00	428.56	75524.02	209.76	257.23
FAIROUT1	9.33E-02	24.96	907764.00	579.88	79004.07	273.48	260.73
FAIROUT2	9.33E-02	24.96	798977.00	479.04	76771.95	273.48	253.39
FAIROUT3	1.94E-02	24.96	798977.00	479.04	76771.95	273.48	52.71

Table D.4: Thermodynamic stream data for closed hydrogen based system at 25 bar

Streams	Total Flow	Pressure	Enthalpy	Entropy	Exergy		
					Thermomechanical	Chemical	Total
	kg/s	bar	J/kg	J/kg K	kJ/kmol	kJ/kmol	kW
FAIROUT4	1.94E-02	24.95	293075.00	-162.76	67852.83	273.48	46.61
FAIROUT5	1.94E-02	24.95	293075.00	-162.70	67852.33	273.48	46.61
FAIROUT6	1.94E-02	1.00	-12739.60	45.99	57416.59	273.48	39.47
FAIRRECY	7.39E-02	24.96	798977.00	479.04	76771.95	273.48	200.68
FC-FINAL	6.79E-05	25.00	254964.00	-12390.50	46890.53	236110.00	9.53
FC-IN	1.01E-03	24.94	-525690.00	2431.82	61598.04	212154.16	76.89
FC-IN1	1.01E-03	24.95	-3275400.00	-790.23	55172.81	212154.16	75.09
FC-IN2	1.01E-03	24.94	-525690.00	2431.82	61598.04	212154.16	76.89
FC-OUT	4.45E-03	24.96	-11233000.00	-857.88	97453.21	31725.59	36.28
FC-OUT1	4.45E-03	24.96	-11276000.00	-895.53	96951.17	31725.59	36.14
FC-OUT2	4.45E-03	24.96	-11379000.00	-989.23	95754.00	31725.59	35.81
FC-OUT3	4.45E-03	24.95	-12002000.00	-1640.53	88952.16	31725.59	33.90
FC-OUT4	4.45E-03	24.95	-12294000.00	-2018.10	86126.61	31725.59	33.10
FC-OUT5	3.95E-03	24.95	-12294000.00	-2018.10	86126.61	31725.59	29.33
FC-OUT6	3.95E-03	24.94	-12693000.00	-2663.48	82846.79	31725.59	28.52
FC-OUT7	3.95E-03	24.94	-12779000.00	-2832.28	82274.58	31725.59	28.38
FC-OUT8	3.95E-03	24.94	-15241000.00	-8088.51	68097.54	31725.59	24.85
FC-OUT9	6.79E-05	24.94	1077980.00	-9987.86	47105.59	236110.00	9.53
FC-OUT10	6.79E-05	25.00	1081930.00	-9986.95	47112.99	236110.00	9.53

Table D.4: Thermodynamic stream data for closed hydrogen based system at 25 bar

Streams	Total Flow	Pressure	Enthalpy	Entropy	Exergy		
					Thermomechanical	Chemical	Total
	kg/s	bar	J/kg	J/kg K	kJ/kmol	kJ/kmol	kW
FCAIRIN	9.67E-02	24.96	727799.00	428.58	75524.21	209.76	257.23
FCAIROUT	9.33E-02	24.96	927645.00	597.42	79419.55	273.48	262.10
FHPCMIA	7.80E-01	1.00	-11692000.00	247.65	94715.42	900.00	4139.81
FHPCMIF	8.00E-02	1.00	-11692000.00	247.65	94715.42	900.00	424.60
FHPCMOA	7.80E-01	1.00	-11690000.00	249.76	94744.06	900.00	4141.05
FHPCMOF	8.00E-02	1.00	-11690000.00	249.76	94744.06	900.00	424.72
FLPCMIA	4.40E+00	1.00	-11927000.00	29.34	91668.00	900.00	22598.27
FLPCMIF	2.00E-01	1.00	-11927000.00	29.34	91668.00	900.00	1027.65
FLPCMOA	4.40E+00	1.00	-11924000.00	31.59	91695.90	900.00	22605.08
FLPCMOF	2.00E-01	1.00	-11924000.00	31.59	91695.90	900.00	1027.96

Table D.5: Gas compositions of streams for closed hydrogen based system at 25 bar

Streams	Mole Fraction								Density	Mol.wt
	H ₂	H ₂ O	CO	CO ₂	CH ₄	O ₂	N ₂	C	kg/m ³	kg/kmol
E-TANK	1.00	0.00	0.00	0.00	0.00	0.00	0.00	0.00	2.03	2.02
E-TANK1	1.00	0.00	0.00	0.00	0.00	0.00	0.00	0.00	2.03	2.02
E-TANK2	1.00	0.00	0.00	0.00	0.00	0.00	0.00	0.00	1.47	2.02
E-WATER	0.00	1.00	0.00	0.00	0.00	0.00	0.00	0.00	998.77	18.02
E-WATER1	0.00	1.00	0.00	0.00	0.00	0.00	0.00	0.00	998.77	18.02
E-WATER2	0.00	1.00	0.00	0.00	0.00	0.00	0.00	0.00	999.19	18.02
EAIR-AMB	0.00	0.00	0.00	0.00	0.00	0.21	0.79	0.00	1.16	28.85
EAIR-IN1	0.00	0.00	0.00	0.00	0.00	0.21	0.79	0.00	24.75	28.85
EAIR-IN2	0.00	0.00	0.00	0.00	0.00	0.21	0.79	0.00	24.75	28.85
EAIR-IN3	0.00	0.00	0.00	0.00	0.00	0.21	0.79	0.00	8.75	28.85
EAIR-IN4	0.00	0.00	0.00	0.00	0.00	0.21	0.79	0.00	8.08	28.85
EAIROUT1	0.00	0.00	0.00	0.00	0.00	0.40	0.60	0.00	14.99	29.60
EAIROUT2	0.00	0.00	0.00	0.00	0.00	0.40	0.60	0.00	1.21	29.60
EC-IN	0.12	0.88	0.00	0.00	0.00	0.00	0.00	0.00	4.50	16.07
EC-IN-1	0.12	0.88	0.00	0.00	0.00	0.00	0.00	0.00	23.23	16.07
EC-IN-2	0.12	0.88	0.00	0.00	0.00	0.00	0.00	0.00	4.94	16.07
EC-IN-3	0.12	0.88	0.00	0.00	0.00	0.00	0.00	0.00	4.94	16.07
EC-OUT	0.90	0.10	0.00	0.00	0.00	0.00	0.00	0.00	1.02	3.62
EC-OUT1	0.90	0.10	0.00	0.00	0.00	0.00	0.00	0.00	1.74	3.62

Table D.5: Gas compositions of streams for closed hydrogen based system at 25 bar

Streams	Mole Fraction								Density	Mol.wt
	H ₂	H ₂ O	CO	CO ₂	CH ₄	O ₂	N ₂	C	kg/m ³	kg/kmol
EC-OUT2	0.90	0.10	0.00	0.00	0.00	0.00	0.00	0.00	2.08	3.62
EC-OUT3	0.90	0.10	0.00	0.00	0.00	0.00	0.00	0.00	2.57	3.62
EC-OUT4	0.90	0.10	0.00	0.00	0.00	0.00	0.00	0.00	2.65	3.62
EC-OUT5	0.90	0.10	0.00	0.00	0.00	0.00	0.00	0.00	4.11	3.62
EC-OUT6	1.00	0.00	0.00	0.00	0.00	0.00	0.00	0.00	2.07	2.02
EC-OUT7	1.00	0.00	0.00	0.00	0.00	0.00	0.00	0.00	2.07	2.02
ECAIRIN	0.00	0.00	0.00	0.00	0.00	0.21	0.79	0.00	8.08	28.85
ECAIROUT	0.00	0.00	0.00	0.00	0.00	0.40	0.60	0.00	8.39	29.60
EHPCM1IA	0.00	1.00	0.00	0.00	0.00	0.00	0.00	0.00	0.19	18.02
EHPCM1IF	0.00	1.00	0.00	0.00	0.00	0.00	0.00	0.00	0.19	18.02
EHPCM1OA	0.00	1.00	0.00	0.00	0.00	0.00	0.00	0.00	0.19	18.02
EHPCM1OF	0.00	1.00	0.00	0.00	0.00	0.00	0.00	0.00	0.19	18.02
ELPCM1IF	0.00	1.00	0.00	0.00	0.00	0.00	0.00	0.00	0.21	18.02
ELPCM1OF	0.00	1.00	0.00	0.00	0.00	0.00	0.00	0.00	0.21	18.02
EW-TANK	0.00	1.00	0.00	0.00	0.00	0.00	0.00	0.00	918.29	18.02
EW-TANK1	0.00	1.00	0.00	0.00	0.00	0.00	0.00	0.00	918.29	18.02
EW-TANK2	0.00	1.00	0.00	0.00	0.00	0.00	0.00	0.00	874.82	18.02
EW-TANK3	0.00	1.00	0.00	0.00	0.00	0.00	0.00	0.00	874.82	18.02
EW-TANK4	0.00	1.00	0.00	0.00	0.00	0.00	0.00	0.00	832.13	18.02

Table D.5: Gas compositions of streams for closed hydrogen based system at 25 bar

Streams	Mole Fraction								Density	Mol.wt
	H ₂	H ₂ O	CO	CO ₂	CH ₄	O ₂	N ₂	C	kg/m ³	kg/kmol
EW-TANK5	0.00	1.00	0.00	0.00	0.00	0.00	0.00	0.00	34.13	18.02
F-RECYC	0.14	0.86	0.00	0.00	0.00	0.00	0.00	0.00	6.69	15.85
F-TANK	1.00	0.00	0.00	0.00	0.00	0.00	0.00	0.00	2.03	2.02
F-TANK1	1.00	0.00	0.00	0.00	0.00	0.00	0.00	0.00	1.98	2.02
F-TANK2	1.00	0.00	0.00	0.00	0.00	0.00	0.00	0.00	1.98	2.02
F-TANK3	1.00	0.00	0.00	0.00	0.00	0.00	0.00	0.00	1.16	2.02
F-TANK4	1.00	0.00	0.00	0.00	0.00	0.00	0.00	0.00	0.87	2.02
F-TANK5	1.00	0.00	0.00	0.00	0.00	0.00	0.00	0.00	0.87	2.02
F-WATER4	0.00	1.00	0.00	0.00	0.00	0.00	0.00	0.00	918.29	18.02
F-WATER5	0.00	1.00	0.00	0.00	0.00	0.00	0.00	0.00	918.29	18.02
F-WATER6	0.00	1.00	0.00	0.00	0.00	0.00	0.00	0.00	918.29	18.02
FAIR-AMB	0.00	0.00	0.00	0.00	0.00	0.21	0.79	0.00	1.16	28.85
FAIR-IN	0.00	0.00	0.00	0.00	0.00	0.21	0.79	0.00	24.75	28.85
FAIR-IN1	0.00	0.00	0.00	0.00	0.00	0.21	0.79	0.00	23.75	28.85
FAIR-IN2	0.00	0.00	0.00	0.00	0.00	0.21	0.79	0.00	11.22	28.85
FAIR-IN3	0.00	0.00	0.00	0.00	0.00	0.11	0.89	0.00	8.78	28.47
FAIROUT1	0.00	0.00	0.00	0.00	0.00	0.09	0.91	0.00	7.56	28.36
FAIROUT2	0.00	0.00	0.00	0.00	0.00	0.09	0.91	0.00	8.24	28.36
FAIROUT3	0.00	0.00	0.00	0.00	0.00	0.09	0.91	0.00	8.24	28.36

Table D.5: Gas compositions of streams for closed hydrogen based system at 25 bar

Streams	Mole Fraction								Density	Mol.wt
	H ₂	H ₂ O	CO	CO ₂	CH ₄	O ₂	N ₂	C	kg/m ³	kg/kmol
FAIROUT4	0.00	0.00	0.00	0.00	0.00	0.09	0.91	0.00	14.68	28.36
FAIROUT5	0.00	0.00	0.00	0.00	0.00	0.09	0.91	0.00	14.68	28.36
FAIROUT6	0.00	0.00	0.00	0.00	0.00	0.09	0.91	0.00	1.19	28.36
FAIRRECY	0.00	0.00	0.00	0.00	0.00	0.09	0.91	0.00	8.24	28.36
FC-FINAL	1.00	0.00	0.00	0.00	0.00	0.00	0.00	0.00	1.92	2.02
FC-IN	0.90	0.10	0.00	0.00	0.00	0.00	0.00	0.00	1.05	3.59
FC-IN1	0.90	0.10	0.00	0.00	0.00	0.00	0.00	0.00	1.54	3.59
FC-IN2	0.90	0.10	0.00	0.00	0.00	0.00	0.00	0.00	1.05	3.59
FC-OUT	0.14	0.86	0.00	0.00	0.00	0.00	0.00	0.00	4.17	15.85
FC-OUT1	0.14	0.86	0.00	0.00	0.00	0.00	0.00	0.00	4.23	15.85
FC-OUT2	0.14	0.86	0.00	0.00	0.00	0.00	0.00	0.00	4.38	15.85
FC-OUT3	0.14	0.86	0.00	0.00	0.00	0.00	0.00	0.00	5.70	15.85
FC-OUT4	0.14	0.86	0.00	0.00	0.00	0.00	0.00	0.00	6.69	15.85
FC-OUT5	0.14	0.86	0.00	0.00	0.00	0.00	0.00	0.00	6.69	15.85
FC-OUT6	0.14	0.86	0.00	0.00	0.00	0.00	0.00	0.00	8.92	15.85
FC-OUT7	0.14	0.86	0.00	0.00	0.00	0.00	0.00	0.00	9.64	15.85
FC-OUT8	0.14	0.86	0.00	0.00	0.00	0.00	0.00	0.00	83.26	15.85
FC-OUT9	1.00	0.00	0.00	0.00	0.00	0.00	0.00	0.00	1.62	2.02
FC-OUT10	1.00	0.00	0.00	0.00	0.00	0.00	0.00	0.00	1.62	2.02

Table D.5: Gas compositions of streams for closed hydrogen based system at 25 bar

Streams	Mole Fraction								Density	Mol.wt
	H ₂	H ₂ O	CO	CO ₂	CH ₄	O ₂	N ₂	C	kg/m ³	kg/kmol
FCAIRIN	0.00	0.00	0.00	0.00	0.00	0.11	0.89	0.00	8.78	28.47
FCAIROUT	0.00	0.00	0.00	0.00	0.00	0.09	0.91	0.00	7.45	28.36
FHPCMIA	0.00	1.00	0.00	0.00	0.00	0.00	0.00	0.00	0.19	18.02
FHPCMIF	0.00	1.00	0.00	0.00	0.00	0.00	0.00	0.00	0.19	18.02
FHPCMOA	0.00	1.00	0.00	0.00	0.00	0.00	0.00	0.00	0.19	18.02
FHPCMOF	0.00	1.00	0.00	0.00	0.00	0.00	0.00	0.00	0.19	18.02
FLPCMIA	0.00	1.00	0.00	0.00	0.00	0.00	0.00	0.00	0.21	18.02
FLPCMIF	0.00	1.00	0.00	0.00	0.00	0.00	0.00	0.00	0.21	18.02
FLPCMOA	0.00	1.00	0.00	0.00	0.00	0.00	0.00	0.00	0.21	18.02
FLPCMOF	0.00	1.00	0.00	0.00	0.00	0.00	0.00	0.00	0.21	18.02

**E**

Appendix E: Methane based gas grid connected rSOC system- performance and thermodynamic stream data

An expanded process flow diagram from the methane based gas grid connected system is presented here. System performance including the net electric power produced and consumed by the system in SOFC and SOEC mode respectively is presented here. The thermodynamic stream data of the process system modelling of the system at two different current densities is provided in this chapter.

E.1 Detailed process flow diagram

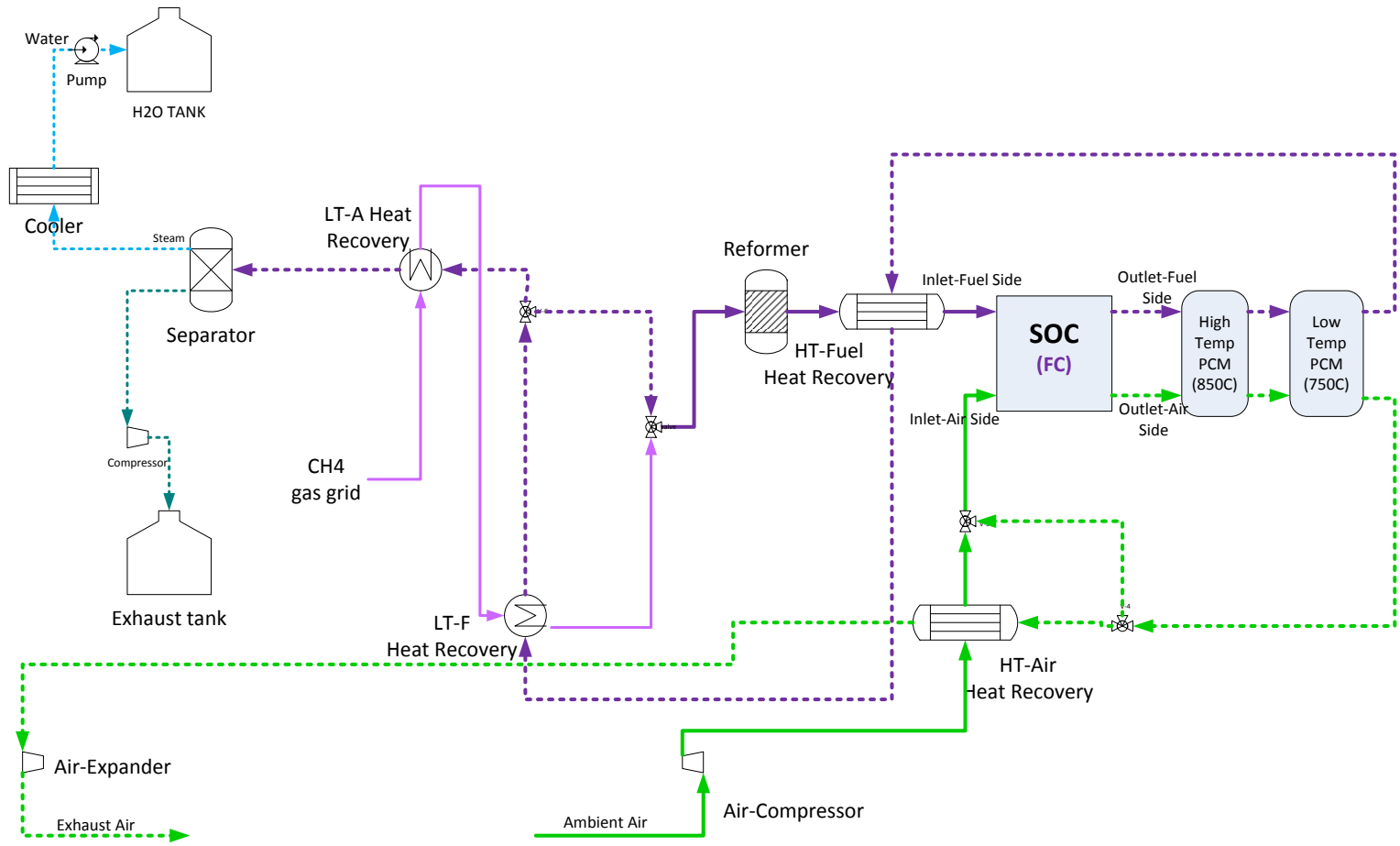


FIGURE E.1. Extended process flow diagram of methane based gas grid connected system in SOFC mode.

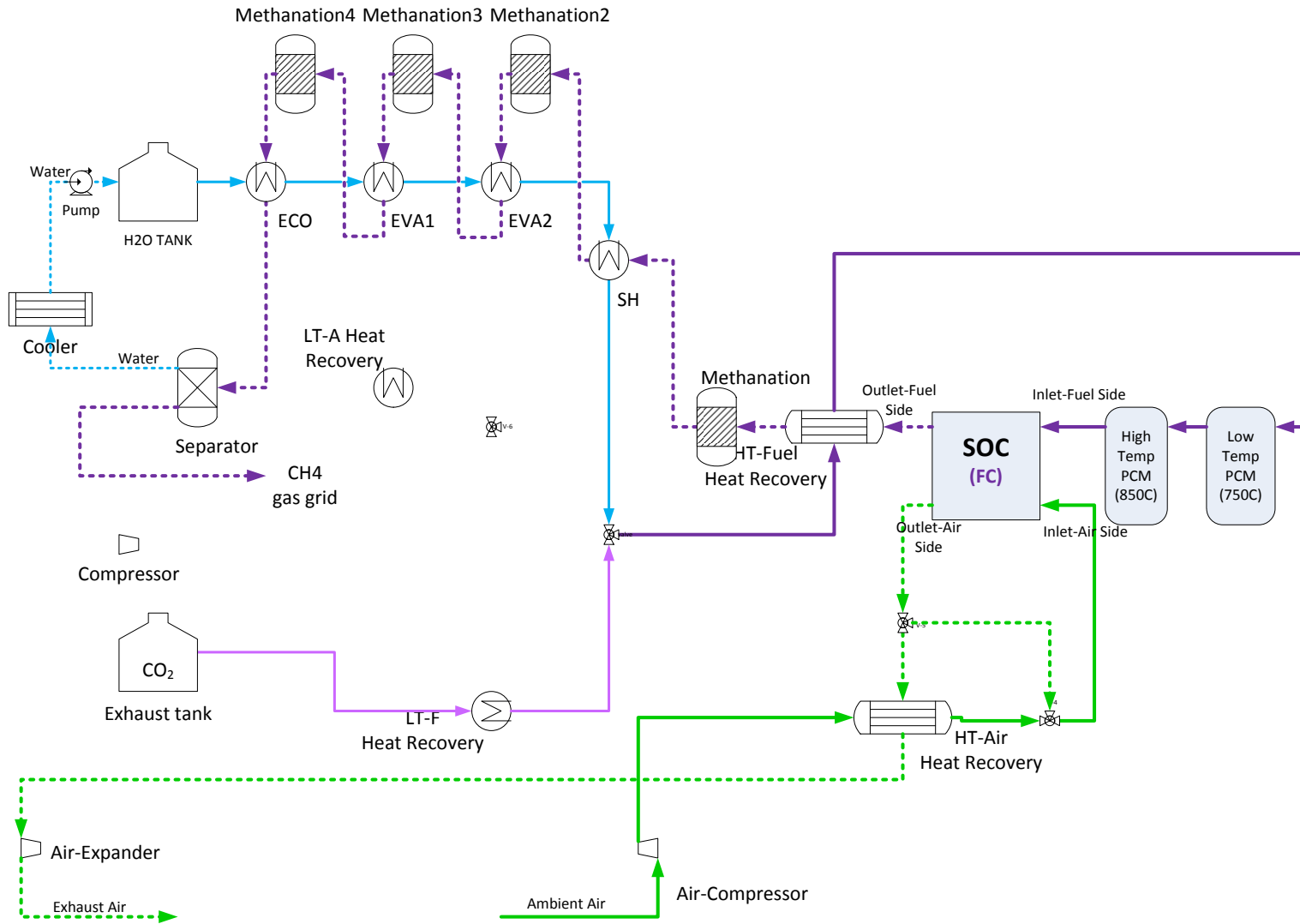


FIGURE E.2. Extended process flow diagram of methane based gas grid connected system in SOEC mode.

E.2 Performance data

TABLE E.1. Performance of the methane based gas grid connected rSOC system at a current density of 2500 A/m²

Parameter	Value	Unit
SOFC		
Effective reactor temperature	845	°C
Cell Voltage	0.772	V
Chemical power input	50	kW
rSOC power output	33.6	kW
BoP power consumption	5.07	kW
Net power produced	28.5	kW
Net efficiency in SOFC mode	57	%
SOEC		
Effective reactor temperature	800	°C
Cell voltage	1.235	V
Chemical power produced	50	kW
rSOC power input	53.9	kW
BoP power consumption	-0.13	kW
Total electrical input	53.8	kW
Net efficiency in SOEC mode	92.9	%
Roundtrip efficiency		
Reactor (gross)	62.2	%
System (net)	52.9	%

E.3 Thermodynamic stream data for gas grid connected methane based open system

The enthalpy, entropy, pressure, flow rate and exergy flows are presented in the Table E.2. The gas compositions, density and molecular weight of the streams are presented in the Table E.3.

Table E.2: Thermodynamic stream data for gas grid connected methane based system at 2500 A/m²

Streams	Total Flow	Pressure	Enthalpy	Entropy	Exergy		
					Thermomechanical	Chemical	Total
	kg/s	bar	J/kg	J/kg K	kJ/kmol	kJ/kmol	kW
E-TANK	2.64E-03	25.01	-8394600.00	-235.02	62966.68	86461.09	11.45
E-TANK2	2.64E-03	25.01	-8394600.00	-235.02	62966.68	86461.09	11.45
E-TANK3	2.64E-03	25.00	-8037700.00	573.04	67125.04	86461.09	11.77
E-WATER	1.62E-03	24.99	-15885000.00	-9124.82	69528.47	900.00	6.32
E-WATER1	1.62E-03	24.99	-15885000.00	-9124.82	69528.47	900.00	6.32
E-WATER3	1.62E-03	1.00	-15887000.00	-9130.94	69531.27	900.00	6.32
EAIR-AMB	1.20E-02	1.00	0.00	151.91	57910.18	128.49	24.14
EAIR-IN1	1.20E-02	25.01	53045.40	-611.89	66010.57	128.49	27.51
EAIR-IN2	1.20E-02	25.00	53045.40	-611.88	66010.47	128.49	27.51
EAIR-IN3	1.20E-02	25.00	791084.00	542.62	77469.08	128.49	32.28
EAIR-IN4	3.30E-02	25.00	805799.00	593.86	78271.36	201.55	88.50
EAIROUT	1.57E-02	25.00	814201.00	615.74	78745.22	307.06	41.91
EAIROUT1	1.57E-02	25.00	248433.00	-109.73	68165.33	307.06	36.30
EAIROUT3	1.57E-02	1.00	-28384.92	90.60	58228.83	307.06	31.03
EAIRRECY	2.10E-02	25.00	814201.00	615.74	78745.22	307.06	56.27
EC-IN	6.31E-03	25.00	-10009000.00	-47.38	94967.06	22826.03	33.04
EC-IN-1	6.31E-03	25.00	-10538000.00	-628.23	87394.84	22826.03	30.92
EC-IN-2	6.31E-03	25.00	-10085000.00	-120.07	93753.81	22826.03	32.70
EC-IN-3	6.31E-03	25.00	-10085000.00	-119.95	93763.59	22826.03	32.70

Table E.2: Thermodynamic stream data for gas grid connected methane based system at 2500 A/m²

Streams	Total Flow	Pressure	Enthalpy	Entropy	Exergy		
					Thermomechanical	Chemical	Total
	kg/s	bar	J/kg	J/kg K	kJ/kmol	kJ/kmol	kW
EC-OUT	2.66E-03	25.00	-5451000.00	1432.44	82476.20	252186.58	73.93
EC-OUT1	2.66E-03	25.00	-6982600.00	-483.50	71225.58	252186.58	71.44
EC-OUT2	2.66E-03	25.00	-6982600.00	-51.99	90133.74	280669.83	71.16
EC-OUT3	2.66E-03	25.00	-8175600.00	-1617.94	79906.61	280669.83	69.20
EC-OUT4	2.66E-03	25.00	-8175600.00	-1359.24	93579.22	307195.35	68.95
EC-OUT5	2.66E-03	25.00	-8930500.00	-2432.91	86564.56	307195.35	67.75
EC-OUT6	2.66E-03	25.00	-8930500.00	-2326.07	93219.28	324031.85	67.40
EC-OUT7	2.66E-03	25.00	-9295700.00	-2895.36	89701.61	324031.85	66.83
EC-OUT8	2.66E-03	25.00	-9295700.00	-2872.19	91735.15	330536.17	66.64
EC-OUT9	2.66E-03	25.00	-9650100.00	-3518.77	88954.23	330536.17	66.20
EC-OUT10	2.66E-03	24.99	-10713000.00	-5842.06	82836.58	330536.17	65.24
EC-OUT11	2.66E-03	24.99	-11540000.00	-8014.61	79802.15	330536.17	64.76
EC-OUT13	1.04E-03	24.99	-4784100.00	-6340.27	86577.84	768464.10	58.25
EC-OUT14	1.04E-03	25.00	-4784000.00	-6340.23	86578.65	768464.10	58.25
ECAIRIN	3.30E-02	25.00	813022.00	600.71	78482.75	201.55	88.74
ECAIROUT	3.67E-02	25.00	814201.00	615.74	78745.22	307.06	98.18
EHPCM1IF	2.00E-01	1.00	-11690000.00	249.76	94744.06	900.00	1061.80
EHPCM1OF	2.00E-01	1.00	-11692000.00	247.65	94715.42	900.00	1061.48
ELPCM1IF	1.24E+00	1.00	-11924000.00	31.59	91695.90	900.00	6373.41

Table E.2: Thermodynamic stream data for gas grid connected methane based system at 2500 A/m²

Streams	Total Flow	Pressure	Enthalpy	Entropy	Exergy		
					Thermomechanical	Chemical	Total
	kg/s	bar	J/kg	J/kg K	kJ/kmol	kJ/kmol	kW
ELPCM1OF	1.24E+00	1.00	-11927000.00	29.34	91668.00	900.00	6371.49
EW-TANK	3.67E-03	1.00	-15885000.00	-9124.82	69528.47	900.00	14.36
EW-TANK1	3.67E-03	25.03	-15882000.00	-9113.94	69528.84	900.00	14.36
EW-TANK2	3.67E-03	25.02	-15113000.00	-7114.22	72519.16	900.00	14.97
EW-TANK3	3.67E-03	25.02	-14849000.00	-6605.22	74883.96	900.00	15.45
EW-TANK4	3.67E-03	25.01	-14304000.00	-5507.43	79306.58	900.00	16.35
EW-TANK5	3.67E-03	25.01	-13441000.00	-3772.54	86008.66	900.00	17.72
EW-TANK6	3.67E-03	25.00	-12334000.00	-1893.64	95151.22	900.00	19.58
F-RECYC	3.51E-03	24.80	-9534700.00	179.56	88624.98	35190.96	17.58
F-TANK	1.00E-03	25.00	-4645100.00	-6685.30	87810.19	831650.00	57.31
F-TANK1	1.00E-03	25.00	-4493000.00	-6224.75	88071.60	831650.00	57.33
F-TANK2	1.00E-03	25.03	-4492700.00	-6224.66	88075.09	831650.00	57.33
F-TANK3	1.00E-03	25.02	-3188900.00	-3902.16	97866.59	831650.00	57.94
F-TANK4	1.00E-03	25.02	-2505500.00	-3106.15	105017.14	831650.00	58.39
F-TANK5	1.00E-03	25.01	-2505500.00	-3106.07	105016.65	831650.00	58.39
F-WATER4	1.98E-03	24.80	-15541000.00	-8098.59	70205.68	900.00	7.80
F-WATER5	1.98E-03	24.80	-15541000.00	-8098.59	70205.68	900.00	7.80
F-WATER6	1.98E-03	1.00	-15543000.00	-8103.70	70202.51	900.00	7.80
FAIR-AMB	1.87E-02	1.00	0.00	151.91	57910.18	128.49	37.64

Table E.2: Thermodynamic stream data for gas grid connected methane based system at 2500 A/m²

Streams	Total Flow	Pressure	Enthalpy	Entropy	Exergy		
					Thermomechanical	Chemical	Total
	kg/s	bar	J/kg	J/kg K	kJ/kmol	kJ/kmol	kW
FAIR-IN	1.87E-02	25.00	53022.96	-611.90	66009.97	128.49	42.89
FAIR-IN1	1.87E-02	25.00	298102.00	-78.92	68670.49	128.49	44.62
FAIR-IN2	1.87E-02	25.00	636890.00	382.77	74298.88	128.49	48.27
FAIR-IN3	3.64E-02	24.81	727016.00	437.79	75537.04	186.80	96.75
FAIROUT1	3.28E-02	24.81	911217.00	547.91	78756.22	371.07	92.13
FAIROUT2	3.28E-02	24.81	822154.00	466.03	77055.96	371.07	90.15
FAIROUT3	1.51E-02	24.81	822111.00	465.99	77054.76	371.07	41.44
FAIROUT4	1.51E-02	24.81	401871.00	-26.19	69509.05	371.07	37.40
FAIROUT5	1.51E-02	24.80	401871.00	-26.13	69508.55	371.07	37.40
FAIROUT6	1.51E-02	1.00	40276.47	182.94	57571.17	371.07	31.01
FAIRRECY	1.77E-02	24.81	822111.00	465.99	77054.76	371.07	48.71
FC-FINAL	2.65E-03	25.00	-8410700.00	-194.12	62776.51	88239.98	11.68
FC-IN	4.51E-03	25.00	-7613000.00	88.81	92320.78	267047.54	76.54
FC-IN1	4.51E-03	24.80	-7977000.00	-316.16	93379.22	276628.00	75.60
FC-IN2	4.51E-03	25.00	-7977000.00	-296.70	87033.58	267047.54	75.42
FC-IN3	4.51E-03	25.00	-7613000.00	88.81	92320.78	267047.54	76.54
FC-OUT	8.14E-03	24.81	-9186800.00	511.69	94613.80	35191.18	42.70
FC-OUT1	8.14E-03	24.81	-9224800.00	478.27	94086.33	35191.18	42.53
FC-OUT2	8.14E-03	24.81	-9248900.00	456.74	93655.63	35191.18	42.39

Table E.2: Thermodynamic stream data for gas grid connected methane based system at 2500 A/m²

Streams	Total Flow	Pressure	Enthalpy	Entropy	Exergy		
					Thermomechanical	Chemical	Total
	kg/s	bar	J/kg	J/kg K	kJ/kmol	kJ/kmol	kW
FC-OUT3	8.14E-03	24.81	-9450700.00	265.56	90057.57	35191.18	41.20
FC-OUT4	8.14E-03	24.80	-9534700.00	179.58	88624.26	35191.18	40.73
FC-OUT5	4.63E-03	24.80	-9534700.00	179.56	88624.26	35191.20	23.15
FC-OUT6	4.63E-03	24.80	-9816600.00	-145.19	84040.96	35191.20	22.29
FC-OUT7	4.63E-03	24.80	-10808000.00	-2012.68	73499.78	35191.20	20.32
FC-OUT8	4.63E-03	24.80	-11399000.00	-3390.75	68911.66	35190.94	19.46
FC-OUT9	2.65E-03	24.80	-8354200.00	-28.84	63025.83	88239.98	11.70
FC-OUT10	2.65E-03	25.00	-8353300.00	-28.49	63055.35	88239.98	11.70
FCAIRIN	3.64E-02	24.81	727016.00	437.79	75537.04	186.80	96.75
FCAIROUT	3.28E-02	24.81	935482.00	569.27	79153.66	371.07	92.59
FHPCMIA	3.35E-01	1.00	-11692000.00	247.65	94715.42	900.00	1778.00
FHPCMIF	1.30E-01	1.00	-11692000.00	247.65	94715.42	900.00	689.97
FHPCMOA	3.35E-01	1.00	-11690000.00	249.76	94744.06	900.00	1778.53
FHPCMOF	1.30E-01	1.00	-11690000.00	249.76	94744.06	900.00	690.18
FLPCMIA	1.27E+00	1.00	-11927000.00	29.34	91668.00	900.00	6510.22
FLPCMIF	8.50E-02	1.00	-11927000.00	29.34	91668.00	900.00	436.76
FLPCMOA	1.27E+00	1.00	-11924000.00	31.59	91695.90	900.00	6512.19
FLPCMOF	8.50E-02	1.00	-11924000.00	31.59	91695.90	900.00	436.89

Table E.3: Gas compositions of streams for gas grid connected methane based system at 2500 A/m²

Streams	Mole Fraction								Density	Mol.wt
	H ₂	H ₂ O	CO	CO ₂	CH ₄	O ₂	N ₂	C	kg/m ³	kg/kmol
E-TANK	0.19	0.00	0.11	0.70	0.00	0.00	0.00	0.00	34.70	34.40
E-TANK2	0.19	0.00	0.11	0.70	0.00	0.00	0.00	0.00	34.70	34.40
E-TANK3	0.19	0.00	0.11	0.70	0.00	0.00	0.00	0.00	16.88	34.40
E-WATER	0.00	1.00	0.00	0.00	0.00	0.00	0.00	0.00	998.77	18.02
E-WATER1	0.00	1.00	0.00	0.00	0.00	0.00	0.00	0.00	998.77	18.02
E-WATER3	0.00	1.00	0.00	0.00	0.00	0.00	0.00	0.00	999.19	18.02
EAIR-AMB	0.00	0.00	0.00	0.00	0.00	0.21	0.79	0.00	1.16	28.85
EAIR-IN1	0.00	0.00	0.00	0.00	0.00	0.21	0.79	0.00	24.75	28.85
EAIR-IN2	0.00	0.00	0.00	0.00	0.00	0.21	0.79	0.00	24.75	28.85
EAIR-IN3	0.00	0.00	0.00	0.00	0.00	0.21	0.79	0.00	8.40	28.85
EAIR-IN4	0.00	0.00	0.00	0.00	0.00	0.32	0.68	0.00	8.37	29.28
EAIROUT	0.00	0.00	0.00	0.00	0.00	0.38	0.62	0.00	8.36	29.53
EAIROUT1	0.00	0.00	0.00	0.00	0.00	0.38	0.62	0.00	16.29	29.53
EAIROUT3	0.00	0.00	0.00	0.00	0.00	0.38	0.62	0.00	1.32	29.53
EAIRRECY	0.00	0.00	0.00	0.00	0.00	0.38	0.62	0.00	8.36	29.53
EC-IN	0.05	0.73	0.03	0.19	0.00	0.00	0.00	0.00	6.39	22.49
EC-IN-1	0.05	0.73	0.03	0.19	0.00	0.00	0.00	0.00	8.74	22.49
EC-IN-2	0.05	0.73	0.03	0.19	0.00	0.00	0.00	0.00	6.64	22.49
EC-IN-3	0.05	0.73	0.03	0.19	0.00	0.00	0.00	0.00	6.64	22.49

Table E.3: Gas compositions of streams for gas grid connected methane based system at 2500 A/m²

Streams	Mole Fraction								Density	Mol.wt
	H ₂	H ₂ O	CO	CO ₂	CH ₄	O ₂	N ₂	C	kg/m ³	kg/kmol
EC-OUT	0.50	0.22	0.10	0.05	0.13	0.00	0.00	0.00	3.40	12.02
EC-OUT1	0.50	0.22	0.10	0.05	0.13	0.00	0.00	0.00	6.30	12.02
EC-OUT2	0.35	0.33	0.04	0.06	0.23	0.00	0.00	0.00	4.27	13.84
EC-OUT3	0.35	0.33	0.04	0.06	0.23	0.00	0.00	0.00	7.26	13.84
EC-OUT4	0.19	0.44	0.01	0.04	0.32	0.00	0.00	0.00	5.50	15.43
EC-OUT5	0.19	0.44	0.01	0.04	0.32	0.00	0.00	0.00	8.09	15.43
EC-OUT6	0.08	0.53	0.00	0.02	0.37	0.00	0.00	0.00	6.94	16.44
EC-OUT7	0.08	0.53	0.00	0.02	0.37	0.00	0.00	0.00	8.62	16.44
EC-OUT8	0.04	0.57	0.00	0.01	0.39	0.00	0.00	0.00	8.12	16.82
EC-OUT9	0.04	0.57	0.00	0.01	0.39	0.00	0.00	0.00	10.60	16.82
EC-OUT10	0.04	0.57	0.00	0.01	0.39	0.00	0.00	0.00	20.55	16.82
EC-OUT11	0.04	0.57	0.00	0.01	0.39	0.00	0.00	0.00	42.90	16.82
EC-OUT13	0.08	0.00	0.00	0.01	0.90	0.00	0.00	0.00	15.64	15.26
EC-OUT14	0.08	0.00	0.00	0.01	0.90	0.00	0.00	0.00	15.65	15.26
ECAIRIN	0.00	0.00	0.00	0.00	0.00	0.32	0.68	0.00	8.32	29.28
ECAIROUT	0.00	0.00	0.00	0.00	0.00	0.38	0.62	0.00	8.36	29.53
EHPCM1IF	0.00	1.00	0.00	0.00	0.00	0.00	0.00	0.00	0.19	18.02
EHPCM1OF	0.00	1.00	0.00	0.00	0.00	0.00	0.00	0.00	0.19	18.02
ELPCM1IF	0.00	1.00	0.00	0.00	0.00	0.00	0.00	0.00	0.21	18.02

Table E.3: Gas compositions of streams for gas grid connected methane based system at 2500 A/m²

Streams	Mole Fraction								Density	Mol.wt
	H ₂	H ₂ O	CO	CO ₂	CH ₄	O ₂	N ₂	C	kg/m ³	kg/kmol
ELPCM1OF	0.00	1.00	0.00	0.00	0.00	0.00	0.00	0.00	0.21	18.02
EW-TANK	0.00	1.00	0.00	0.00	0.00	0.00	0.00	0.00	998.77	18.02
EW-TANK1	0.00	1.00	0.00	0.00	0.00	0.00	0.00	0.00	998.02	18.02
EW-TANK2	0.00	1.00	0.00	0.00	0.00	0.00	0.00	0.00	821.16	18.02
EW-TANK3	0.00	1.00	0.00	0.00	0.00	0.00	0.00	0.00	346.87	18.02
EW-TANK4	0.00	1.00	0.00	0.00	0.00	0.00	0.00	0.00	33.61	18.02
EW-TANK5	0.00	1.00	0.00	0.00	0.00	0.00	0.00	0.00	13.84	18.02
EW-TANK6	0.00	1.00	0.00	0.00	0.00	0.00	0.00	0.00	6.44	18.02
F-RECYC	0.08	0.59	0.04	0.29	0.00	0.00	0.00	0.00	7.75	24.74
F-TANK	0.00	0.00	0.00	0.00	1.00	0.00	0.00	0.00	16.18	16.04
F-TANK1	0.00	0.00	0.00	0.00	1.00	0.00	0.00	0.00	13.25	16.04
F-TANK2	0.00	0.00	0.00	0.00	1.00	0.00	0.00	0.00	13.26	16.04
F-TANK3	0.00	0.00	0.00	0.00	1.00	0.00	0.00	0.00	6.21	16.04
F-TANK4	0.00	0.00	0.00	0.00	1.00	0.00	0.00	0.00	5.12	16.04
F-TANK5	0.00	0.00	0.00	0.00	1.00	0.00	0.00	0.00	5.12	16.04
F-WATER4	0.00	1.00	0.00	0.00	0.00	0.00	0.00	0.00	918.29	18.02
F-WATER5	0.00	1.00	0.00	0.00	0.00	0.00	0.00	0.00	918.29	18.02
F-WATER6	0.00	1.00	0.00	0.00	0.00	0.00	0.00	0.00	918.74	18.02
FAIR-AMB	0.00	0.00	0.00	0.00	0.00	0.21	0.79	0.00	1.16	28.85

Table E.3: Gas compositions of streams for gas grid connected methane based system at 2500 A/m²

Streams	Mole Fraction								Density	Mol.wt
	H ₂	H ₂ O	CO	CO ₂	CH ₄	O ₂	N ₂	C	kg/m ³	kg/kmol
FAIR-IN	0.00	0.00	0.00	0.00	0.00	0.21	0.79	0.00	24.75	28.85
FAIR-IN1	0.00	0.00	0.00	0.00	0.00	0.21	0.79	0.00	14.75	28.85
FAIR-IN2	0.00	0.00	0.00	0.00	0.00	0.21	0.79	0.00	9.66	28.85
FAIR-IN3	0.00	0.00	0.00	0.00	0.00	0.13	0.87	0.00	8.75	28.52
FAIROUT1	0.00	0.00	0.00	0.00	0.00	0.04	0.96	0.00	7.47	28.18
FAIROUT2	0.00	0.00	0.00	0.00	0.00	0.04	0.96	0.00	8.01	28.18
FAIROUT3	0.00	0.00	0.00	0.00	0.00	0.04	0.96	0.00	8.01	28.18
FAIROUT4	0.00	0.00	0.00	0.00	0.00	0.04	0.96	0.00	12.38	28.18
FAIROUT5	0.00	0.00	0.00	0.00	0.00	0.04	0.96	0.00	12.37	28.18
FAIROUT6	0.00	0.00	0.00	0.00	0.00	0.04	0.96	0.00	1.01	28.18
FAIRRECY	0.00	0.00	0.00	0.00	0.00	0.04	0.96	0.00	8.01	28.18
FC-FINAL	0.19	0.00	0.10	0.71	0.00	0.00	0.00	0.00	32.20	34.27
FC-IN	0.13	0.35	0.03	0.21	0.27	0.00	0.00	0.00	6.22	21.19
FC-IN1	0.06	0.41	0.03	0.20	0.31	0.00	0.00	0.00	6.95	22.09
FC-IN2	0.13	0.35	0.03	0.21	0.27	0.00	0.00	0.00	7.34	21.19
FC-IN3	0.13	0.35	0.03	0.21	0.27	0.00	0.00	0.00	6.22	21.19
FC-OUT	0.08	0.59	0.04	0.29	0.00	0.00	0.00	0.00	6.44	24.74
FC-OUT1	0.08	0.59	0.04	0.29	0.00	0.00	0.00	0.00	6.56	24.74
FC-OUT2	0.08	0.59	0.04	0.29	0.00	0.00	0.00	0.00	6.64	24.74

Table E.3: Gas compositions of streams for gas grid connected methane based system at 2500 A/m²

Streams	Mole Fraction								Density	Mol.wt
	H ₂	H ₂ O	CO	CO ₂	CH ₄	O ₂	N ₂	C	kg/m ³	kg/kmol
FC-OUT3	0.08	0.59	0.04	0.29	0.00	0.00	0.00	0.00	7.38	24.74
FC-OUT4	0.08	0.59	0.04	0.29	0.00	0.00	0.00	0.00	7.75	24.74
FC-OUT5	0.08	0.59	0.04	0.29	0.00	0.00	0.00	0.00	7.75	24.74
FC-OUT6	0.08	0.59	0.04	0.29	0.00	0.00	0.00	0.00	9.37	24.74
FC-OUT7	0.08	0.59	0.04	0.29	0.00	0.00	0.00	0.00	23.88	24.74
FC-OUT8	0.08	0.59	0.04	0.29	0.00	0.00	0.00	0.00	49.51	24.74
FC-OUT9	0.19	0.00	0.10	0.71	0.00	0.00	0.00	0.00	27.39	34.27
FC-OUT10	0.19	0.00	0.10	0.71	0.00	0.00	0.00	0.00	27.56	34.27
FCAIRIN	0.00	0.00	0.00	0.00	0.00	0.13	0.87	0.00	8.75	28.52
FCAIROUT	0.00	0.00	0.00	0.00	0.00	0.04	0.96	0.00	7.34	28.18
FHPCMIA	0.00	1.00	0.00	0.00	0.00	0.00	0.00	0.00	0.19	18.02
FHPCMIF	0.00	1.00	0.00	0.00	0.00	0.00	0.00	0.00	0.19	18.02
FHPCMOA	0.00	1.00	0.00	0.00	0.00	0.00	0.00	0.00	0.19	18.02
FHPCMOF	0.00	1.00	0.00	0.00	0.00	0.00	0.00	0.00	0.19	18.02
FLPCMIA	0.00	1.00	0.00	0.00	0.00	0.00	0.00	0.00	0.21	18.02
FLPCMIF	0.00	1.00	0.00	0.00	0.00	0.00	0.00	0.00	0.21	18.02
FLPCMOA	0.00	1.00	0.00	0.00	0.00	0.00	0.00	0.00	0.21	18.02
FLPCMOF	0.00	1.00	0.00	0.00	0.00	0.00	0.00	0.00	0.21	18.02

E.4 Thermodynamic stream data for gas grid connected methane based open system at 1500 A/m²

The enthalpy, entropy, pressure, flow rate and exergy flows are presented in the Table E.4. The gas compositions, density and molecular weight of the streams are presented in the Table E.5.

Table E.4: Thermodynamic stream data for gas grid connected methane based system at 1500 A/m²

Streams	Total Flow	Pressure	Enthalpy	Entropy	Exergy		
					Thermomechanical	Chemical	Total
	kg/s	bar	J/kg	J/kg K	kJ/kmol	kJ/kmol	kW
E-TANK	2.64E-03	25.01	-8394600.00	-235.02	62966.68	86461.09	11.45
E-TANK2	2.64E-03	25.01	-8394600.00	-235.02	62966.68	86461.09	11.45
E-TANK3	2.64E-03	25.00	-8055300.00	543.92	66647.33	86461.09	11.74
E-WATER	1.64E-03	24.99	-15885000.00	-9124.82	69528.47	900.00	6.42
E-WATER1	1.64E-03	24.99	-15885000.00	-9124.82	69528.47	900.00	6.42
E-WATER3	1.64E-03	1.00	-15887000.00	-9130.94	69531.27	900.00	6.42
EAIR-AMB	1.40E-02	1.00	0.00	151.91	57910.18	128.49	28.16
EAIR-IN1	1.40E-02	25.01	53045.40	-611.89	66010.57	128.49	32.09
EAIR-IN2	1.40E-02	25.00	53045.40	-611.88	66010.47	128.49	32.09
EAIR-IN3	1.40E-02	25.00	587457.00	326.29	73358.58	128.49	35.66
EAIR-IN4	1.47E-01	25.00	811264.00	605.79	78617.42	243.99	393.75
EAIROUT	1.76E-02	25.00	834870.00	631.01	79208.15	269.24	47.58
EAIROUT1	1.76E-02	25.00	410467.00	147.39	70957.08	269.24	42.64
EAIROUT3	1.76E-02	1.00	51458.41	347.26	58631.08	269.24	35.26
EAIRRECY	1.33E-01	25.00	834870.00	631.01	79208.15	269.24	358.26
EC-IN	6.31E-03	25.00	-10009000.00	-46.70	94986.94	22826.03	33.05
EC-IN-1	6.31E-03	25.00	-10654000.00	-784.81	85416.83	22826.03	30.36
EC-IN-2	6.31E-03	25.00	-10134000.00	-168.66	92994.80	22826.03	32.49
EC-IN-3	6.31E-03	25.00	-10134000.00	-168.68	92984.94	22826.03	32.48

Table E.4: Thermodynamic stream data for gas grid connected methane based system at 1500 A/m²

Streams	Total Flow	Pressure	Enthalpy	Entropy	Exergy		
					Thermomechanical	Chemical	Total
	kg/s	bar	J/kg	J/kg K	kJ/kmol	kJ/kmol	kW
EC-OUT	2.68E-03	25.00	-5845200.00	1124.13	79150.64	259725.59	72.14
EC-OUT1	2.68E-03	25.00	-7407900.00	-811.53	66721.50	259725.59	69.49
EC-OUT2	2.68E-03	25.00	-7407900.00	-432.07	84751.62	286592.98	69.19
EC-OUT3	2.68E-03	25.00	-8471600.00	-1857.05	75543.00	286592.98	67.47
EC-OUT4	2.68E-03	25.00	-8471600.00	-1646.14	88631.29	309513.50	67.30
EC-OUT5	2.68E-03	25.00	-9103600.00	-2568.19	82967.08	309513.50	66.34
EC-OUT6	2.68E-03	25.00	-9103600.00	-2493.17	89610.45	322682.03	66.28
EC-OUT7	2.68E-03	25.00	-9383800.00	-2940.09	87155.38	322682.03	65.89
EC-OUT8	2.68E-03	25.00	-9383800.00	-2926.91	89333.52	327280.81	65.88
EC-OUT9	2.68E-03	25.00	-9717100.00	-3547.37	86813.99	327280.81	65.48
EC-OUT10	2.68E-03	24.99	-10777000.00	-5863.58	80537.46	327280.81	64.49
EC-OUT11	2.68E-03	24.99	-11594000.00	-8010.58	77534.37	327280.81	64.01
EC-OUT13	1.04E-03	24.99	-4822800.00	-6304.45	84714.11	776129.37	57.61
EC-OUT14	1.04E-03	25.00	-4822700.00	-6304.40	84715.92	776129.37	57.61
ECAIRIN	1.47E-01	25.00	811262.00	605.79	78617.43	243.99	393.75
ECAIROUT	1.50E-01	25.00	834870.00	631.01	79208.15	269.24	405.84
EHPCM1IF	3.32E-01	1.00	-11690000.00	249.76	94744.06	900.00	1762.61
EHPCM1OF	3.32E-01	1.00	-11692000.00	247.65	94715.42	900.00	1762.08
ELPCM1IF	1.42E+00	1.00	-11924000.00	31.59	91695.90	900.00	7316.58

Table E.4: Thermodynamic stream data for gas grid connected methane based system at 1500 A/m²

Streams	Total Flow	Pressure	Enthalpy	Entropy	Exergy		
					Thermomechanical	Chemical	Total
	kg/s	bar	J/kg	J/kg K	kJ/kmol	kJ/kmol	kW
ELPCM1OF	1.42E+00	1.00	-11927000.00	29.34	91668.00	900.00	7314.37
EW-TANK	3.67E-03	1.00	-15885000.00	-9124.82	69528.47	900.00	14.36
EW-TANK1	3.67E-03	25.03	-15882000.00	-9113.94	69528.84	900.00	14.36
EW-TANK2	3.67E-03	25.02	-15107000.00	-7100.84	72674.94	900.00	15.00
EW-TANK3	3.67E-03	25.02	-14902000.00	-6707.19	74251.06	900.00	15.32
EW-TANK4	3.67E-03	25.01	-14440000.00	-5781.89	77600.90	900.00	16.00
EW-TANK5	3.67E-03	25.01	-13662000.00	-4217.99	83211.50	900.00	17.15
EW-TANK6	3.67E-03	25.00	-12520000.00	-2127.53	92563.12	900.00	19.05
F-RECYC	3.53E-03	24.90	-9542600.00	171.14	88854.70	33989.57	17.54
F-TANK	1.00E-03	25.00	-4645100.00	-6685.30	87810.19	831650.00	57.31
F-TANK1	1.00E-03	25.00	-4493900.00	-6227.44	88045.37	831650.00	57.33
F-TANK2	1.00E-03	25.03	-4493700.00	-6227.36	88048.99	831650.00	57.33
F-TANK3	1.00E-03	25.02	-3189600.00	-3903.10	97852.69	831650.00	57.94
F-TANK4	1.00E-03	25.02	-2506800.00	-3107.54	105001.45	831650.00	58.38
F-TANK5	1.00E-03	25.01	-2506800.00	-3107.47	105001.12	831650.00	58.38
F-WATER4	1.96E-03	24.90	-15541000.00	-8098.59	70205.68	900.00	7.75
F-WATER5	1.96E-03	24.90	-15541000.00	-8098.59	70205.68	900.00	7.75
F-WATER6	1.96E-03	1.00	-15543000.00	-8103.73	70202.51	900.00	7.75
FAIR-AMB	2.72E-02	1.00	0.00	151.91	57910.18	128.49	54.72

Table E.4: Thermodynamic stream data for gas grid connected methane based system at 1500 A/m²

Streams	Total Flow	Pressure	Enthalpy	Entropy	Exergy		
					Thermomechanical	Chemical	Total
	kg/s	bar	J/kg	J/kg K	kJ/kmol	kJ/kmol	kW
FAIR-IN	2.72E-02	25.00	53022.98	-611.90	66009.97	128.49	62.35
FAIR-IN1	2.72E-02	25.00	220736.00	-219.50	67473.30	128.49	63.73
FAIR-IN2	2.72E-02	25.00	636890.00	382.77	74298.88	128.49	70.17
FAIR-IN3	4.96E-02	24.91	725003.00	453.86	75735.38	149.39	131.29
FAIROUT1	4.59E-02	24.91	907268.00	591.77	79094.74	234.72	128.26
FAIROUT2	4.59E-02	24.91	832351.00	523.29	77545.85	234.72	125.75
FAIROUT3	2.36E-02	24.91	832103.00	523.06	77540.74	234.72	64.51
FAIROUT4	2.36E-02	24.91	351902.00	-52.93	68774.00	234.72	57.24
FAIROUT5	2.36E-02	24.90	351902.00	-52.87	68773.50	234.72	57.24
FAIROUT6	2.36E-02	1.00	16734.60	154.91	57487.31	234.72	47.87
FAIRRECY	2.24E-02	24.91	832103.00	523.06	77540.74	234.72	61.24
FC-FINAL	2.66E-03	25.00	-8446100.00	-222.43	63325.50	84325.64	11.50
FC-IN	4.53E-03	25.00	-7624900.00	86.60	92845.75	266130.45	76.72
FC-IN1	4.53E-03	24.90	-7990600.00	-320.93	93759.32	274884.85	75.61
FC-IN2	4.53E-03	25.00	-7990600.00	-300.88	87546.41	266130.45	75.58
FC-IN3	4.53E-03	25.00	-7624900.00	86.60	92845.75	266130.45	76.72
FC-OUT	8.16E-03	24.91	-9192100.00	505.66	95056.61	33989.31	42.55
FC-OUT1	8.16E-03	24.91	-9231400.00	471.06	94341.95	33989.31	42.31
FC-OUT2	8.16E-03	24.91	-9255700.00	449.33	93902.25	33989.31	42.17

Table E.4: Thermodynamic stream data for gas grid connected methane based system at 1500 A/m²

Streams	Total Flow	Pressure	Enthalpy	Entropy	Exergy		
					Thermomechanical	Chemical	Total
					kJ/kmol	kJ/kmol	kW
	kg/s	bar	J/kg	J/kg K			
FC-OUT3	8.16E-03	24.91	-9458900.00	256.86	90292.42	33989.31	40.98
FC-OUT4	8.16E-03	24.90	-9542600.00	171.15	88854.87	33989.31	40.50
FC-OUT5	4.63E-03	24.90	-9542500.00	171.14	88854.98	33989.28	22.96
FC-OUT6	4.63E-03	24.90	-9824400.00	-153.71	84271.96	33989.28	22.11
FC-OUT7	4.63E-03	24.90	-10810000.00	-2010.00	73569.00	33989.28	20.11
FC-OUT8	4.63E-03	24.90	-11401000.00	-3387.28	69111.20	33989.60	19.27
FC-OUT9	2.66E-03	24.90	-8389800.00	-58.78	63578.28	84325.64	11.52
FC-OUT10	2.66E-03	25.00	-8389300.00	-58.63	63596.82	84325.64	11.53
FCAIRIN	4.96E-02	24.91	725020.00	453.87	75735.73	149.39	131.29
FCAIROUT	4.59E-02	24.91	932098.00	613.61	79615.38	234.72	129.10
FHPCMIA	4.80E-01	1.00	-11692000.00	247.65	94715.42	900.00	2547.58
FHPCMIF	1.35E-01	1.00	-11692000.00	247.65	94715.42	900.00	716.51
FHPCMOA	4.80E-01	1.00	-11690000.00	249.76	94744.06	900.00	2548.34
FHPCMOF	1.35E-01	1.00	-11690000.00	249.76	94744.06	900.00	716.72
FLPCMIA	1.49E+00	1.00	-11927000.00	29.34	91668.00	900.00	7667.89
FLPCMIF	8.60E-02	1.00	-11927000.00	29.34	91668.00	900.00	441.89
FLPCMOA	1.49E+00	1.00	-11924000.00	31.59	91695.90	900.00	7670.20
FLPCMOF	8.60E-02	1.00	-11924000.00	31.59	91695.90	900.00	442.03

Table E.5: Gas compositions of streams for gas grid connected methane based system at 1500 A/m²

Streams	Mole Fraction								Density	Mol.wt
	H ₂	H ₂ O	CO	CO ₂	CH ₄	O ₂	N ₂	C	kg/m ³	kg/kmol
E-TANK	0.19	0.00	0.11	0.70	0.00	0.00	0.00	0.00	34.70	34.40
E-TANK2	0.19	0.00	0.11	0.70	0.00	0.00	0.00	0.00	34.70	34.40
E-TANK3	0.19	0.00	0.11	0.70	0.00	0.00	0.00	0.00	17.29	34.40
E-WATER	0.00	1.00	0.00	0.00	0.00	0.00	0.00	0.00	998.77	18.02
E-WATER1	0.00	1.00	0.00	0.00	0.00	0.00	0.00	0.00	998.77	18.02
E-WATER3	0.00	1.00	0.00	0.00	0.00	0.00	0.00	0.00	999.19	18.02
EAIR-AMB	0.00	0.00	0.00	0.00	0.00	0.21	0.79	0.00	1.16	28.85
EAIR-IN1	0.00	0.00	0.00	0.00	0.00	0.21	0.79	0.00	24.75	28.85
EAIR-IN2	0.00	0.00	0.00	0.00	0.00	0.21	0.79	0.00	24.75	28.85
EAIR-IN3	0.00	0.00	0.00	0.00	0.00	0.21	0.79	0.00	10.16	28.85
EAIR-IN4	0.00	0.00	0.00	0.00	0.00	0.34	0.66	0.00	8.35	29.39
EAIROUT	0.00	0.00	0.00	0.00	0.00	0.36	0.64	0.00	8.20	29.45
EAIROUT1	0.00	0.00	0.00	0.00	0.00	0.36	0.64	0.00	12.67	29.45
EAIROUT3	0.00	0.00	0.00	0.00	0.00	0.36	0.64	0.00	1.01	29.45
EAIRRECY	0.00	0.00	0.00	0.00	0.00	0.36	0.64	0.00	8.20	29.45
EC-IN	0.05	0.73	0.03	0.19	0.00	0.00	0.00	0.00	6.39	22.49
EC-IN-1	0.05	0.73	0.03	0.19	0.00	0.00	0.00	0.00	9.55	22.49
EC-IN-2	0.05	0.73	0.03	0.19	0.00	0.00	0.00	0.00	6.81	22.49
EC-IN-3	0.05	0.73	0.03	0.19	0.00	0.00	0.00	0.00	6.81	22.49

Table E.5: Gas compositions of streams for gas grid connected methane based system at 1500 A/m²

Streams	Mole Fraction								Density	Mol.wt
	H ₂	H ₂ O	CO	CO ₂	CH ₄	O ₂	N ₂	C	kg/m ³	kg/kmol
EC-OUT	0.45	0.25	0.08	0.05	0.16	0.00	0.00	0.00	3.51	12.61
EC-OUT1	0.45	0.25	0.08	0.05	0.16	0.00	0.00	0.00	6.61	12.61
EC-OUT2	0.30	0.36	0.02	0.06	0.25	0.00	0.00	0.00	4.61	14.41
EC-OUT3	0.30	0.36	0.02	0.06	0.25	0.00	0.00	0.00	7.56	14.41
EC-OUT4	0.15	0.48	0.00	0.04	0.33	0.00	0.00	0.00	5.93	15.88
EC-OUT5	0.15	0.48	0.00	0.04	0.33	0.00	0.00	0.00	8.33	15.88
EC-OUT6	0.06	0.55	0.00	0.02	0.37	0.00	0.00	0.00	7.36	16.70
EC-OUT7	0.06	0.55	0.00	0.02	0.37	0.00	0.00	0.00	8.76	16.70
EC-OUT8	0.03	0.58	0.00	0.01	0.39	0.00	0.00	0.00	8.39	16.98
EC-OUT9	0.03	0.58	0.00	0.01	0.39	0.00	0.00	0.00	10.87	16.98
EC-OUT10	0.03	0.58	0.00	0.01	0.39	0.00	0.00	0.00	21.17	16.98
EC-OUT11	0.03	0.58	0.00	0.01	0.39	0.00	0.00	0.00	44.40	16.98
EC-OUT13	0.07	0.00	0.00	0.02	0.91	0.00	0.00	0.00	15.95	15.56
EC-OUT14	0.07	0.00	0.00	0.02	0.91	0.00	0.00	0.00	15.96	15.56
ECAIRIN	0.00	0.00	0.00	0.00	0.00	0.34	0.66	0.00	8.35	29.39
ECAIROUT	0.00	0.00	0.00	0.00	0.00	0.36	0.64	0.00	8.20	29.45
EHPCM1IF	0.00	1.00	0.00	0.00	0.00	0.00	0.00	0.00	0.19	18.02
EHPCM1OF	0.00	1.00	0.00	0.00	0.00	0.00	0.00	0.00	0.19	18.02
ELPCM1IF	0.00	1.00	0.00	0.00	0.00	0.00	0.00	0.00	0.21	18.02

Table E.5: Gas compositions of streams for gas grid connected methane based system at 1500 A/m²

Streams	Mole Fraction								Density	Mol.wt
	H ₂	H ₂ O	CO	CO ₂	CH ₄	O ₂	N ₂	C	kg/m ³	kg/kmol
ELPCM1OF	0.00	1.00	0.00	0.00	0.00	0.00	0.00	0.00	0.21	18.02
EW-TANK	0.00	1.00	0.00	0.00	0.00	0.00	0.00	0.00	998.77	18.02
EW-TANK1	0.00	1.00	0.00	0.00	0.00	0.00	0.00	0.00	998.02	18.02
EW-TANK2	0.00	1.00	0.00	0.00	0.00	0.00	0.00	0.00	819.70	18.02
EW-TANK3	0.00	1.00	0.00	0.00	0.00	0.00	0.00	0.00	775.16	18.02
EW-TANK4	0.00	1.00	0.00	0.00	0.00	0.00	0.00	0.00	43.41	18.02
EW-TANK5	0.00	1.00	0.00	0.00	0.00	0.00	0.00	0.00	16.31	18.02
EW-TANK6	0.00	1.00	0.00	0.00	0.00	0.00	0.00	0.00	7.18	18.02
F-RECYC	0.08	0.58	0.04	0.30	0.00	0.00	0.00	0.00	7.79	24.75
F-TANK	0.00	0.00	0.00	0.00	1.00	0.00	0.00	0.00	16.18	16.04
F-TANK1	0.00	0.00	0.00	0.00	1.00	0.00	0.00	0.00	13.27	16.04
F-TANK2	0.00	0.00	0.00	0.00	1.00	0.00	0.00	0.00	13.28	16.04
F-TANK3	0.00	0.00	0.00	0.00	1.00	0.00	0.00	0.00	6.21	16.04
F-TANK4	0.00	0.00	0.00	0.00	1.00	0.00	0.00	0.00	5.12	16.04
F-TANK5	0.00	0.00	0.00	0.00	1.00	0.00	0.00	0.00	5.12	16.04
F-WATER4	0.00	1.00	0.00	0.00	0.00	0.00	0.00	0.00	918.29	18.02
F-WATER5	0.00	1.00	0.00	0.00	0.00	0.00	0.00	0.00	918.29	18.02
F-WATER6	0.00	1.00	0.00	0.00	0.00	0.00	0.00	0.00	918.75	18.02
FAIR-AMB	0.00	0.00	0.00	0.00	0.00	0.21	0.79	0.00	1.16	28.85

Table E.5: Gas compositions of streams for gas grid connected methane based system at 1500 A/m²

Streams	Mole Fraction								Density	Mol.wt
	H ₂	H ₂ O	CO	CO ₂	CH ₄	O ₂	N ₂	C	kg/m ³	kg/kmol
FAIR-IN	0.00	0.00	0.00	0.00	0.00	0.21	0.79	0.00	24.75	28.85
FAIR-IN1	0.00	0.00	0.00	0.00	0.00	0.21	0.79	0.00	16.87	28.85
FAIR-IN2	0.00	0.00	0.00	0.00	0.00	0.21	0.79	0.00	9.66	28.85
FAIR-IN3	0.00	0.00	0.00	0.00	0.00	0.16	0.84	0.00	8.82	28.65
FAIROUT1	0.00	0.00	0.00	0.00	0.00	0.10	0.90	0.00	7.56	28.42
FAIROUT2	0.00	0.00	0.00	0.00	0.00	0.10	0.90	0.00	8.01	28.42
FAIROUT3	0.00	0.00	0.00	0.00	0.00	0.10	0.90	0.00	8.02	28.42
FAIROUT4	0.00	0.00	0.00	0.00	0.00	0.10	0.90	0.00	13.40	28.42
FAIROUT5	0.00	0.00	0.00	0.00	0.00	0.10	0.90	0.00	13.40	28.42
FAIROUT6	0.00	0.00	0.00	0.00	0.00	0.10	0.90	0.00	1.09	28.42
FAIRRECY	0.00	0.00	0.00	0.00	0.00	0.10	0.90	0.00	8.02	28.42
FC-FINAL	0.20	0.00	0.09	0.71	0.00	0.00	0.00	0.00	32.06	34.17
FC-IN	0.13	0.35	0.03	0.21	0.27	0.00	0.00	0.00	6.23	21.21
FC-IN1	0.06	0.41	0.03	0.21	0.30	0.00	0.00	0.00	6.98	22.10
FC-IN2	0.13	0.35	0.03	0.21	0.27	0.00	0.00	0.00	7.35	21.21
FC-IN3	0.13	0.35	0.03	0.21	0.27	0.00	0.00	0.00	6.23	21.21
FC-OUT	0.08	0.58	0.04	0.30	0.00	0.00	0.00	0.00	6.46	24.75
FC-OUT1	0.08	0.58	0.04	0.30	0.00	0.00	0.00	0.00	6.59	24.75
FC-OUT2	0.08	0.58	0.04	0.30	0.00	0.00	0.00	0.00	6.67	24.75

Table E.5: Gas compositions of streams for gas grid connected methane based system at 1500 A/m²

Streams	Mole Fraction								Density	Mol.wt
	H ₂	H ₂ O	CO	CO ₂	CH ₄	O ₂	N ₂	C	kg/m ³	kg/kmol
FC-OUT3	0.08	0.58	0.04	0.30	0.00	0.00	0.00	0.00	7.42	24.75
FC-OUT4	0.08	0.58	0.04	0.30	0.00	0.00	0.00	0.00	7.79	24.75
FC-OUT5	0.08	0.58	0.04	0.30	0.00	0.00	0.00	0.00	7.79	24.75
FC-OUT6	0.08	0.58	0.04	0.30	0.00	0.00	0.00	0.00	9.42	24.75
FC-OUT7	0.08	0.58	0.04	0.30	0.00	0.00	0.00	0.00	23.86	24.75
FC-OUT8	0.08	0.58	0.04	0.30	0.00	0.00	0.00	0.00	49.33	24.75
FC-OUT9	0.20	0.00	0.09	0.71	0.00	0.00	0.00	0.00	27.42	34.17
FC-OUT10	0.20	0.00	0.09	0.71	0.00	0.00	0.00	0.00	27.51	34.17
FCAIRIN	0.00	0.00	0.00	0.00	0.00	0.16	0.84	0.00	8.82	28.65
FCAIROUT	0.00	0.00	0.00	0.00	0.00	0.10	0.90	0.00	7.42	28.42
FHPCMIA	0.00	1.00	0.00	0.00	0.00	0.00	0.00	0.00	0.19	18.02
FHPCMIF	0.00	1.00	0.00	0.00	0.00	0.00	0.00	0.00	0.19	18.02
FHPCMOA	0.00	1.00	0.00	0.00	0.00	0.00	0.00	0.00	0.19	18.02
FHPCMOF	0.00	1.00	0.00	0.00	0.00	0.00	0.00	0.00	0.19	18.02
FLPCMIA	0.00	1.00	0.00	0.00	0.00	0.00	0.00	0.00	0.21	18.02
FLPCMIF	0.00	1.00	0.00	0.00	0.00	0.00	0.00	0.00	0.21	18.02
FLPCMOA	0.00	1.00	0.00	0.00	0.00	0.00	0.00	0.00	0.21	18.02
FLPCMOF	0.00	1.00	0.00	0.00	0.00	0.00	0.00	0.00	0.21	18.02

